BULLETIN OF THE EARTHQUAKE RESEARCH INSTITUTE,
UNIVERSITY OF TOKYO. Vol. 37, Part 2. June, 1959.

# 東京大學
# 地震研究所彙報

第 37 號　第 2 册

昭和 34 年 6 月

## 目　次

論文及報告


| | | | 頁 |
|---|---|---|---|
| 14. | 近地地震波動の相関法による研究（英文） | 安芸敬一・辻浦賢 | 207 |
| 15. | 地球熱学（第2報）岩漿貫入と地表の熱の流れ（英文） | 力武常次 | 233 |
| 16. | 地磁気ダイナモの強制振動（英文） | 力武常次 | 245 |
| 17. | 地震波のスペクトル構造 —そのマグニチユード決定におよぼす影響—（英文） | 松本利松 | 265 |
| 18. | 爆破地震動観測によつて得られた$S$波の走時について（英文） | 浅野周三・田三雲健・嶋悦三・宇佐美竜夫 | 279 |
| 19. | 多くの観測点の資料による脈動の研究（其の一） —脈動源について—（英文） | 三東哲夫 | 307 |
| 20. | 電磁水平動脈動計（英文） | 岸上冬彦・渡辺義夫 | 327 |
| 21. | 震源決定の精度について（第3報）（邦文） | 浅野周三 | 337 |
| 22. | 紀伊半島の局地地震（第1報） —和歌山県御坊における小地震の観測—（邦文） | 宮村摂三 | 347 |
| 23. | 近地地震初動の到来方向とみかけの速度（邦文） | 宮村摂三・辻浦賢 | 359 |
| 24. | 全商用交流電源簡易電子地震計（邦文） | 松本英照 | 375 |
| 25. | 対数特性広振幅範囲電子地震計（邦文） | 松本英照 | 381 |


所　報

(The titles in occidental languages are given on the back cover.)

地震研究所彙報は，年4回定期に（ただし，第1号より第6号までは不定期に，第7号は3冊として刊行された），彙報別冊は不定期に刊行される．

この彙報に載せられた論文及び報告についての責任は，すべてその著者のみにある．

この彙報についての照会通信は，すべて東京大学地震研究所長にあてられたい．

*The Bulletin is published quarterly. (Vols. 1–6 were published at irregular intervals and Vol. 7 consisted of three parts.)*
*Supplementary Volume is published at irregular interval.*

*The authors of the papers alone are responsible for the statements and opinions contained in their respective papers.*

*All communications relating to this Bulletin should be addressed to the Director of the Earthquake Research Institute, University of Tokyo, Japan.*

Earthquake Research Institute, University of Tokyo
Address:
No. 1, Motofuji-cho, Bunkyo-ku,
Tokyo Metropolis, Japan.
Telephone: 92-3161-Extension 6506
Cable address: ZISINKEN, TOKYO.

東京大学地震研究所
所在地
東京都文京区本富士町一番地
電話 小石川 92—3161 (代) 構内 6506
電略 ブンケウ トウダイ ヂシン

BULLETIN OF THE EARTHQUAKE
RESEARCH INSTITUTE
Vol. 37 (1959), pp. 207-232

# 14. *Correlational Study of Near Earthquake Waves.*

By Keiiti AKI and Masaru TSUJIURA,

Earthquake Research Institute.

(Read Sept. 16, 1958.—Received March 28, 1959.)

## 1. Introduction

This paper is the second report on the study of near earthquake waves by a correlational method. In the first report (1958)[1], we gave the result of a preliminary investigation which was made by means of a temporary tripartite net at Kamakura in southern Kanto. This tripartite net was a very small one having an average span of about 100 m, and the seismometers were placed on sandstone which is not very hard. The length of span was appropriate for waves having a velocity less than 3 km per sec, but too small for waves of higher velocity. In the present study, the length of span was elongated to about 500 m, and the temporary tripartite net was set up on granitic rocks exposed near Mt. Tukuba in eastern Kanto.

By the preliminary investigation at Kamakura, it was found that spatially random waves coexist with high velocity waves having the direction of propagation pointing to the origin of the earthquake and also with low velocity waves which have different directions not dependent upon the origin and sometimes are not plane waves within the network. Earthquake waves were divided into consecutive portions each of 2 to 3 seconds time interval for the analysis, and it was found that the fraction of average power (average power here means time average of the square of the amplitude.) carried by the regular plane waves is largest in the initial portion, that it gradually decreases with the time, again becomes large at the arrival of the $S$ wave, and later tends to become almost negligible.

The knowledge of this kind of facts is essential, if one wants to make use of the whole seismogram instead of few particular phases for purposes such as locating small earthquakes and estimating earthquake energy. Also to study them for different frequency ranges and at vari-

1) K. AKI, M. TSUJIURA, M. HORI and K. GOTO, *Bull. Earthq. Res. Inst.*, **36** (1958), 71-98.

ous places will help the understanding of complicated phenomena such as the scattering of waves due to local heterogeneity and local vibrations of the ground induced by the incidence of primary waves coming from the origin of earthquake.

The present writers are especially interested in locating very small earthquakes which have the frequency range of vibration from 1 cps to 50 cps. As well known the frequency of occurrence of earthquakes increases with decreasing magnitude according to Gutenberg-Richter's formula (1949)[2], or an equivalent one called Ishimoto-Iida's formula in Japan. It was revealed by Asada (1958)[3] that very small earthquakes are recorded at a frequency as high as 200 per day at Mt. Tukuba in eastern Kanto during a normal period in accordance with the above formulas. Therefore if we can determine the hypocentres of these earthquakes, we shall have more reliable and continuous information about the seismic activity at a particular place under the ground. This information may be important in connection with the occurrence of larger earthquakes.

For the purpose of locating small earthquakes, the use of a single station having a small tripartite net of seismometers has greater advantages than that of separate stations each having a single seismometer: first because a considerable number of earthquakes recorded at one station are not recorded at other stations even if the sensitivity of the seismometers is very high; secondly, it is not easy in any sense to maintain many separate stations having highly sensitive seismometers with amplifiers and accurate clocks; and thirdly, it will take much more time at the central station to gather and process the data in the separate station system than in the single station system. But the accuracy of determination of hypocentre is certainly better for separate stations than for a single tripartite station using the times of the initial motions of $P$ and $S$ waves. It is intended, therefore, to make use of the whole seismogram instead of initial motions of a few phases.

The details of the method used in the present study were given in previous papers (1957, 1958)[4),5], so only a brief description of it will be given here in comparison with other methods that can be applied for the same purpose.

2) B. GUTENBERG and C. F. RICHTER, "*Seismicity of the Earth*", Princeton, N. J., 1949.

3) T. ASADA, *Jour. Phys. Earth.*, **5** (1957), 83–113.

4) K. AKI, *Bull. Earthq. Res. Inst.*, **35** (1957), 415–456.

5) K. AKI *et al.*, *loc. cit.*, 1).

If the correlation function of two signals, coming from two seismometers placed at a certain distance, is computed, shifting one with respect to the other in time, a curve will be obtained in which the shift time giving the maximum correlation is equal to $r/V$, where $r$ is the distance between seismometers and $V$ is the apparent velocity of the wave through the two points. This method will give a very accurate determination of local velocity, if the wave in question has a flat frequency spectrum and a single definite velocity which is independent of frequency. In this case, the correlation curve will take the form of a $\delta$-function. But, if the frequency spectrum of the wave is not flat, not only will the sharpness of the peak in the correlation curve be lost, but also secondary peaks will appear at different shift times depending on the shape of the spectrum. Further, if the wave is composed of more than two partial waves of different velocities which may depend on frequency, it will be very difficult to interpret the obtained correlation curve in order to learn the value of velocity and the fraction of average power for each component wave.

Therefore it is at least desirable to eliminate approximately the influence of frequency spectrum upon the final correlation curve. This is possible if one observes the wave in a limited frequency range by filtering it with a band pass filter. Then the correlation coefficient may be computed (the use of the "coefficient" removes the amplitude effect) shifting the seismometer signal in space instead of time, in other words, the autocorrelation of the wave in space, particularly for a limited frequency range, may be computed instead of the crosscorrelation of vibrations at two points. If the band width of the frequency range is taken very small, a correlation coefficient curve of the following form for the wave having a single velocity $V$ will be obtained.

$$\rho(f, r)=\cos\left(\frac{fr}{V}\right) \qquad (1)$$

where $f$ is the frequency of centre in the band.

This type of correlation curve is no longer influenced by the spectral distribution of wave, besides it has a greater advantage that we can easily find its theoretical form for various models of complicated waves.

For instance, if the wave in question is a dispersive wave, it can be shown that Eq. 1 holds also in this case without any modification except the substitution of the function $V(f)$ of frequency $f$ for the constant velocity $V$. If the wave is composed of two partial waves

having different velocities $V_1$ and $V_2$, and fractions of average power $P_1$ and $P_2$, then the correlation curve will take the following form

$$\rho(f, r)=\frac{P_1 \cos\left(\frac{fr}{V_1}\right)+P_2 \cos\left(\frac{fr}{V_2}\right)}{P_1+P_2} \qquad (2)$$

under the condition that the partial waves are independent of each other. This formula is useful to separate waves propagating in different directions through the same place at the same time, and can be generalized to the case of an arbitrary number of partial waves. On the other hand, if the wave in question is purely random in space, we may express the correlation curve in the following form,

$$\left.\begin{aligned}\rho(f, r)=\frac{\delta(fr)}{\delta(0)}&=1\,, \quad fr=0\\ &=0\,, \quad \neq 0\end{aligned}\right\} \qquad (3)$$

And if a regular wave of velocity $V$ is mixed with this type of random noise we may express this in the following formula

$$\rho(f, r)=\frac{P_0\frac{\delta(fr)}{\delta(0)}+P_1 \cos\left(\frac{fr}{V_1}\right)}{P_0+P_1} \qquad (4)$$

where $P_0$ and $P_1$ are the fractions of average power carried by the random noise and the regular wave respectively.

The above method of analysis, however, requires a great number of seismometers, amplifiers, and channels in the recorder which should have a recording time of more than one minute, when the correlation curve is to be plotted against spacial distance, $r$. Therefore the curve is plotted against the pass frequency, $f$, of the filter in our investigation. By this conversion the least number of seismometers required for the analysis of earthquake waves is reduced to three.

## 2. Observation and analysis

We observed local earthquakes at the foot of Mt. Tukuba which is located about at the centre of eastern Kanto. The reason why we chose this place as our field of experiment is as follows: first, this is one of the places where the noise level is the lowest throughout Kanto;

secondly, we can find there granitic rocks exposed on the surface; thirdly, there is a permanent observatory, which belongs to the Earthquake Research Institute, Tokyo University, provided with various kinds of modern equipment and power supplies.

We selected six sites for seismometer locations around the observatory. Fig. 1 shows the map of sites and the distances among them measured by a precise triangulation. At each site, a house for the seismometer made of concrete blocks is cemented to exposed granitic rock which is cut and smoothed to fit the house.

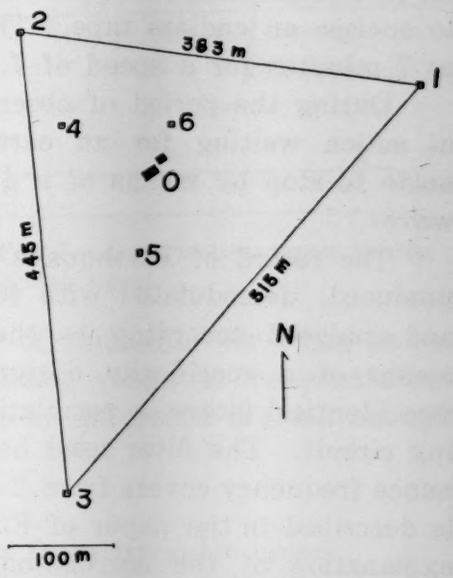


Fig. 1. Map of seismometer location. No. 6 is the Tukuba Observatory seismometer vault and O is its office building.

Seismometers used are moving coil type transducers sensitive to vertical motion, and have a free frequency of 3 cps. We used in the present observation, as in the preliminary one at Kamakura, the U.H.F. radio telerecording seismograph, RTS–II, made by S. Miyamura and M. Tsujiura (1957)[6] of our Institute. This apparatus transmitted the seismometer signals from Mt. Tukuba to the receiving station which was set up in the ninth story of a house of the medical department of Tokyo University at Hongo, Tokyo. The use of this radio telerecorder is not essential for the purpose of the present study, but remarkably increased the efficiency of study by making our field observation a kind of laboratory experiment.

We used two sets of RTS–II in the present observation. In each set, three seismometer signals are amplified, and modulate the frequency of three carriers of audiofrequency, 800, 2670 and 8900 cps respectively. The modulated signals are mixed together and again modulate the frequency of a carrier of 417.7 Mc/s, which is sent from the transmitter as radio waves to the receiver. At the receiving station the received signals are demodulated with respect to the carrier of 417.7 Mc/s and recorded on a magnetic tape, being still modulated by the signals of seismic frequency. Since our magnetic recorder has two channels, we

6) S. MIYAMURA and M. TSUJIURA, *Bull. Earthq. Res. Inst.*, **35** (1957), 381–394.

are able to make a simultaneous recording of six seismometer signals with the two sets of RTS-II.

The recording was made by using a special reel which was designed to enclose an endless tape. The tape enclosed in the reel works as long as 7 minutes for a speed of 7.5 inches per sec.

During the period of observation, the tape recorder is continuously in action waiting for an earthquake, and when one takes place, it is made to stop by means of a delayed trigger circuit after recording of waves.

The record of earthquake motions stored in the endless tape is reproduced, demodulated with respect to the carriers of audiofrequency, and analysed according to the method stated in the introduction by means of a specifically designed computer. This computer consists of two identical filters, a correlation computer, a gate circuit, and a checking circuit. The filter used here is of phase shift type and its resonance frequency covers from 2 cps to 18 cps. The function of this filter is described in the paper of K. Aki (1957)[7] referred to before, with the explanation of the correlation computer in which decatron tubes are used as an integrator and an indicator. The gate circuit controls the computer to make a separate computation for each consecutive portion into which the record of the earthquake is divided. The time interval of the portion is taken as 2.5 seconds which was found to be appropriate for the present purpose in the preliminary experiment.

A checking circuit is provided to check whether the computer is in order. This circuit generates two checking signals, each of which is a series of pulses recurring every 2.5 seconds, one of which is shifted 1/7.5 sec from the other. If we put these two signals, through a pair of identical filters having the resonance frequency $f$ and sufficiently high $Q$ value, into the correlation computer and observe the variation of correlation coefficient by changing the frequency of filters, we shall get a curve of the following form,

$$\rho(f)=\cos\left(2\pi\frac{f}{7.5}\right).$$

Each time before the computation this check was made by the comparison of the result with the above theoretical value; the deviation in terms of the correlation coefficient was usually less than 10%. An example of the correlation curve for the checking signals is shown in

7) K. AKI, *loc. cit.*, 5).

Fig. 2.

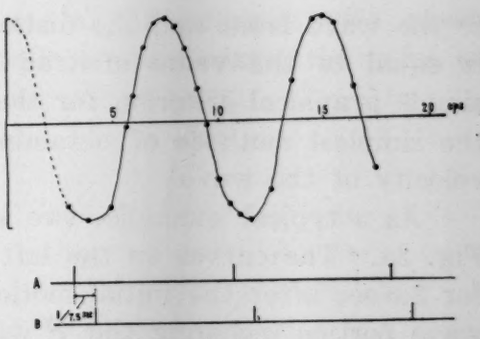


Fig. 2. A correlation curves for the checking signal.

In the present investigation, if the phase characteristic of one channel differs from the phase characteristics of the others the result will be seriously distorted. Therefore the phase characteristics of seismometers, amplifiers, modulators and de-modulators were carefully examined, and it was found that the phase differences among the responses of different channels to an input of sinusoidal form can be reduced to about 10 degrees over the frequency range to be studied in the present experiment[8]. This magnitude of difference is small enough for the present purpose.

### 3. Discrimination of plane waves from irregular noises

As far as the noises in earthquake waves are purely random in space, the discrimination of a plane wave from the noises is not difficult. As stated in the introduction, the correlation curve takes the cosine form for a regular plane wave and the form of a $\delta$-function for a purely random noise. One can easily learn the velocity and fraction of average power for the plane wave when it coexists with the purely random noise in the earthquake waves.

But, sometimes we find a correlation curve of intermediate nature between the above two, suggesting the existence of a group of waves which are neither purely random nor perfectly regular. In some of these cases, the form of the correlation curve appears to involve a cosine form and lead us to make a misinterpretation that a plane wave exists in that wave. But, one can decide whether the plane wave really exists in the wave or not, by comparing the values of velocity obtained from every correlation curve for different pairs of seismometers. For instance, if lines are drawn on a map parallel to the lines connecting seismometer pairs and intersect at a point 0, and a point is marked on each line at the distance equal to the value of the apparent velocity along the line from the point 0, then all of the points should lie on a straight line in the case of the plane wave. And this straight line is parallel

8) M. TSUJIURA and S. MIYAMURA, *Bull. Earthq. Res. Inst.*, **37** (1959), 193–206.

to the wave front and the distance between this line and the point 0 is equal to the value of true velocity of the plane wave. This is a simple graphical criterion for the regularity of waves as well as one of the simplest methods of obtaining the direction of propagation and the velocity of the wave.

As a typical example, two sets of correlation curves are shown in Fig. 3a. The curves on the left are obtained from the wave portion for 2.5 sec after the initial motion, and those on the right are from the wave portion including the $S$ wave, both of an earthquake wave recorded on Aug. 22, 1958. The pair of numbers shown on the upper left of each curve indicates the pair of seismometers which are located at the places having the same numbers in Fig. 1 and between which the correlation curve is computed.

In any of these curves a cosine form is discernible though it is more or less distorted by the presence of irregular noise. The dotted curves in the same figure are drawn in order to show how we find the

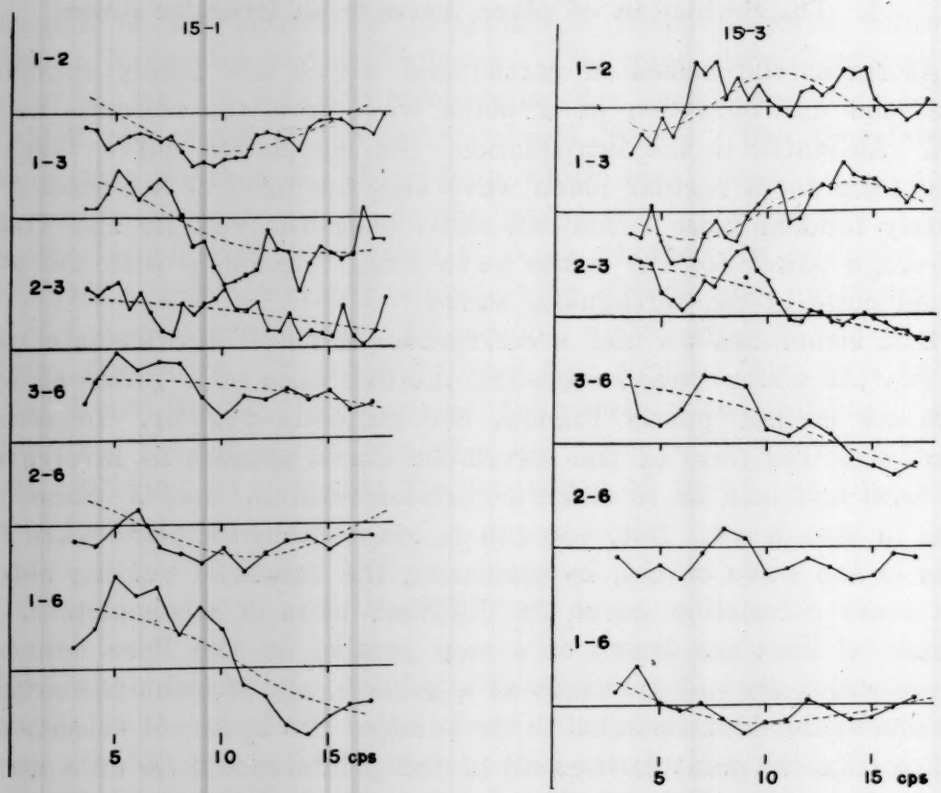


Fig. 3a. Correlation curves for the $P$ and $S$ wave portions of the earthquake No. 15 recorded on Aug. 22, 07 h 09 m.

smoothed curves of nearly cosine form in the original. To check whether these cosine forms are truly from a plane wave, the value of apparent velocity obtained from each of the smoothed curves is plotted in Fig. 3b in the way described above. The points lie fairly well on a straight line, and we can be sure that a plane wave exists in this wave portion. In this case, the velocity of the wave portion after the *P* phase is 7.9 km/s and that of the portion including the *S* phase is 4.1 km/s. Their directions of propagation are slightly different.

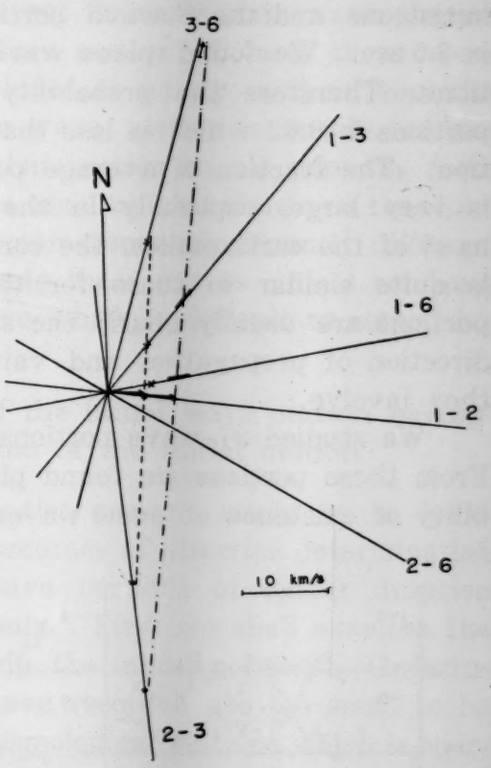


Fig. 3b. Graph to check the regularity of waves.

In this way, plane waves are sought in every portion, having a 2.5 sec interval, of 18 earthquake waves recorded at Mt. Tukuba. These earthquakes are local ones and their *P*–*S* times are in the range from about 5 sec to 20 sec. We found well established plane waves in the first wave portion of all the earthquakes but one. In this exceptional one, the direction of initial motion at one place is found to be reverse to those at the other places, therefore an accidental noise at the place can be probably considered as the cause of irregularity of that wave portion. The fraction of average power carried by these plane waves in the initial wave portions varies considerably among earthquakes, it was 80% in the largest case and about 40% on the average. This value of the fraction is not strictly independent of the frequency, and usually large in low frequencies and smaller in higher frequencies. The value given above is obtained by a rough estimation averaging with respect to the frequency.

In the wave portion including the *S* phase, it is less easy to find plane waves than in the case of the initial portion, and the fraction of average power carried by the plane waves is smaller. We found plane waves in the *S* portions of 14 earthquakes and failed in 4 earthquakes. The fraction of average power carried by these plane waves was 60%

in the largest case, and roughly 20 to 30% in most cases.

The 18 earthquakes studied contain 76 wave portions between the initial one and the $S$ wave portion. The time interval of each portion is 2.5 sec. We found plane waves in 47 portions out of these 76 portions. Therefore the probability of existence of plane waves in these portions is 0.62 which is less than 0.78 in the case of the $S$ wave portion. The fraction of average power carried by plane waves sometimes is very large, especially in the portions next to the initial ones. In most of the earthquakes, the correlation curves for the initial portion is quite similar to those for the next one. So these successive two portions are usually nearly the same in the fraction of average power, direction of propagation and value of velocity of plane waves which they involve.

We studied 97 wave portions which came after the $S$ wave portions. From these portions we found plane waves in 29 portions. The probability of existence of plane waves is about 0.30 which is much less than

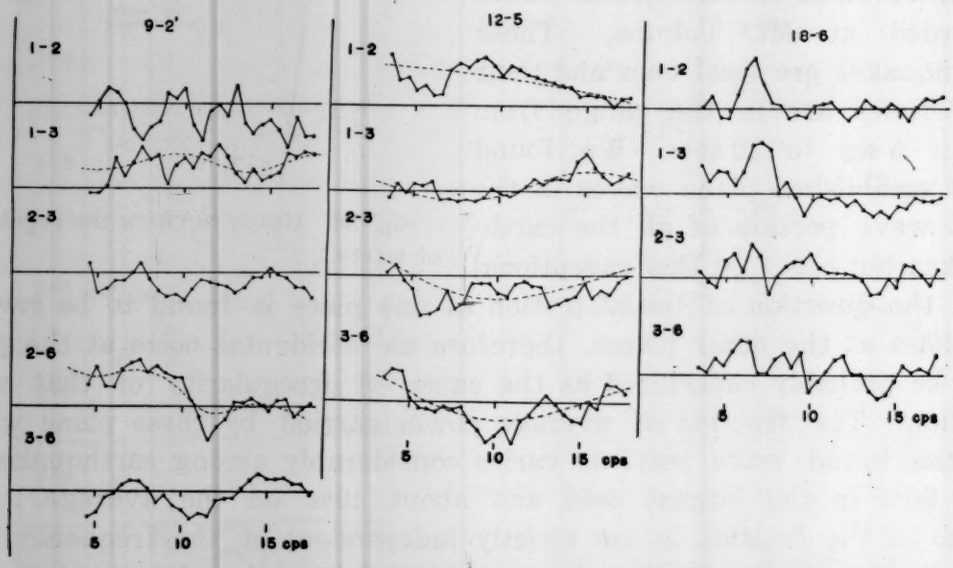


Fig. 4. Typical examples of correlation curves for the coda wave portions.

that for the portions between $P$ and $S$. The fraction of average power carried by them is very small and never exceeds 30%. Typical examples of the correlation curves for these portions are shown in Fig. 4. The set of curves on the left in the figure refers to low velocity waves, and the curves in the middle refer to high velocity waves. In both cases, the amplitude of cosine forms discernible in these curves is small,

that is, the fraction average power carried by the plane wave involved in the portions is small.

The wave portions where we could not find any plane wave are not necessarily purely random in space. As a matter of fact, there were no wave portions which can be concluded as purely random from the point of their correlation curves. If a wave portion is purely random in space, every correlation curve for that portion should take the form of a $\delta$-function. But the actual curves are like that shown on the right of Fig. 4. The value of correlation is sometimes significantly different from zero. It is impossible to interprete these curves unless we have a detailed theoretical model of the wave which is difficult to establish.

## 4. Comparison of the propagation of the initial wave portion having the duration of 2.5 sec with that of the initial motion

One of the principal purpose of the present study is to learn whether it is possible to increase the accuracy of direction determination of wave propagation by the use of wave portions of longer duration instead of the use of initial motion only. First we shall examine the propagation of the plane waves found in the initial portions. Unfortunately, most of the earthquakes we have recorded are too small to be recorded by the routine network of seismological stations which is operated by the Meteorological Agency in Japan. So, we have no information from this source about the true hypocentres of these earthquakes with one exception, for which an estimation is given. As an alternative procedure to study the problem we can take the following method[9].

As we have earthquake records stored in magnetic tapes, it is very easy to reproduce them on a paper which runs at a speed as high as 10 cm per sec. Therefore, if the wave form at the commencement of the initial motion is sharp enough, we can determine its direction of propagation with a good accuracy. We found that the initial motion is quite sharp for about half of the earthquakes observed. For the rest of them the initial motion is not very sharp but we could determine the apparent velocity and direction of propagation[9]. We compared the direction of propagation of the initial wave portion with that of the initial motion in the case of sharp commencement and in that of vague commencement separately. In each case the mean value of the absolute value of the difference in angle between the two directions is computed.

9) S. MIYAMURA and M. TSUJIURA, *Bull. Earthq. Res. Inst.*, **37** (1959), 359-374.

It was 2.8 degrees in the case of sharp commencement and 12.3 degrees in the case of vague commencement. The difference is apparently significant, and should be attributed to the difference in sharpness of the waveform of initial motion. So, it is a reasonable conclusion that at least for the case of vague commencement the direction determination by the use of the initial wave portion of 2.5 sec duration is much more accurate than that by the use of the initial motion only.

Besides, in the exceptional case in which the epicentre is determined by the network of routine stations, the direction pointing to this epicentre, the direction of propagation of the initial motion and that of the initial wave portion coincide within 5 degrees. And the last one was between two others. This fact perhaps allows us to extend our conclusion.

On the other hand, the value of velocity of the initial wave portion does not coincide very well with that of the initial motion even when the coincidence between their directions is very good. This was expected because the initial wave potion involves partial waves which travelled along different paths from that of the initial motion and have different velocities along the horizon. Therefore, the velocity we obtained from that wave portion is an averaged one over those partial waves and may represent the velocity of the most prevailing partial wave in that portion.

If the velocity and thickness of the layers under the surface are known, the minimum value of the apparent velocity of initial motion along the horizon for an earthquake of a given epicentral distance can be obtained very easily. Fig. 5 (dotted lines) shows this minimum value of velocity for the area in question obtained from the result of seismic explosion experiment (1958)[10]. In the same figure are plotted the velocities of initial motions of earthquake waves investigated in the concurrent study by S. Miyamura and M. Tsujiura[11] against the *P–S* duration. The good agree-

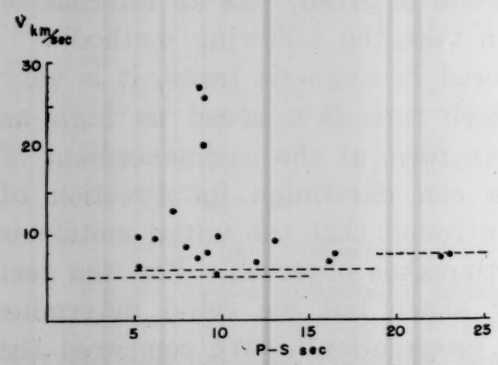


Fig. 5. Apparent velocity of propagation of initial motion plotted against *P–S* time. (After S. Miyamura and Tsujiura, *loc. cit.*, 9).).

10) RESEARCH GROUP FOR EXPLOSION SEISMOLOGY, *Zisin, Ser.* [ii], **11** (1958), 102–113.
11) S. MIYAMURA and M. TSUJIURA, *loc. cit.*, 9).

ment of theory and fact assures that the values of velocity of initial motion obtained for these earthquakes are reliable.

On the other hand, the velocity of the initial wave portion differs from that of the initial motion, being sometimes twice as large as the latter and sometimes one half, though most of them coincide within a relative error of 20%. The ratio of the velocity for the initial wave portion to that for the initial motion is plotted against the *P–S* time in Fig. 6. The ratio is not systematic with respect to the epicentral distance as shown in the figure. Therefore it is reasonable to think that the wave which prevails in the initial wave portion of 2.5 sec duration varies in a way depending mostly on the condition at which the earthquake starts and generates waves. On the average this prevailing wave is similar to the initial motion.

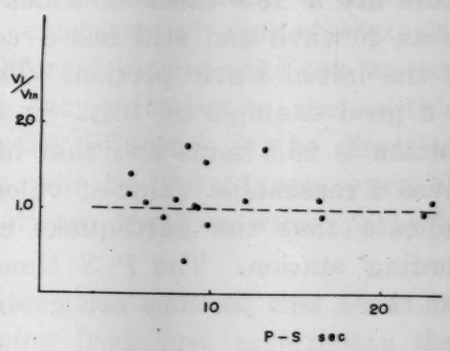


Fig. 6. The ratio of the velocity of the initial wave portion to that of initial motion plotted against *P–S* time.

For each individual earthquake the velocity and direction of propagation are given as a vector in Fig. 8 to Fig. 25 for every wave portion (1, 1′, 2, ....), wherever a plane wave is found, with the velocity vector for the initial motion (In) as well as the seismogram.

### 5. The nature of the wave portion including the S wave

As can be seen in Figs. 8 to 25, the wave portion, in which the *S* wave is considered to be prevailing from the inspection of seismograms, has a velocity sometimes too high and sometimes too low for the *S* wave. This is partly owing to our procedure in which the wave portions are picked up consecutively with a given time interval and they may involve partial waves having the nature of *P* waves and the surface waves. But if we shorten the interval of wave portion to eliminate the influence of the other waves than the *S* wave, the result will be less reliable because of the smaller size of samples. This kind of difficulty is inherent in the correlational study of waves.

The direction of propagation of this wave portion generally differs from that of the initial wave portion of the same earthquake. The discrepancy in angle is as small as 2 degrees in one case and as large

as 60 degrees in another, and 25 degrees on the average. This discrepancy is quite natural if the wave portion is of the nature of the surface waves, because we are dealing with the waves having wave lengths of several hundred meters and the horizontal heterogeneity in topography and geology near the surface may easily cause this discrepancy. But there are a few cases in which the wave portion should be considered as an $S$ wave and still has a considerably different direction from that of the initial wave portion. The earthquake recorded on Aug. 8, 1958 is a good example of this. In this case the velocity of the initial wave portion is 26.6 kmps and that of the $S$ wave portion is 14.9 kmps which gives a reasonable value of velocity ratio $P$ to $S$. These high velocities indicate that the earthquake occurred nearly right underneath the recording station. The $P$–$S$ time is about 9 sec. The correlation curves for these two portions are given in Fig. 7 in order to show that the

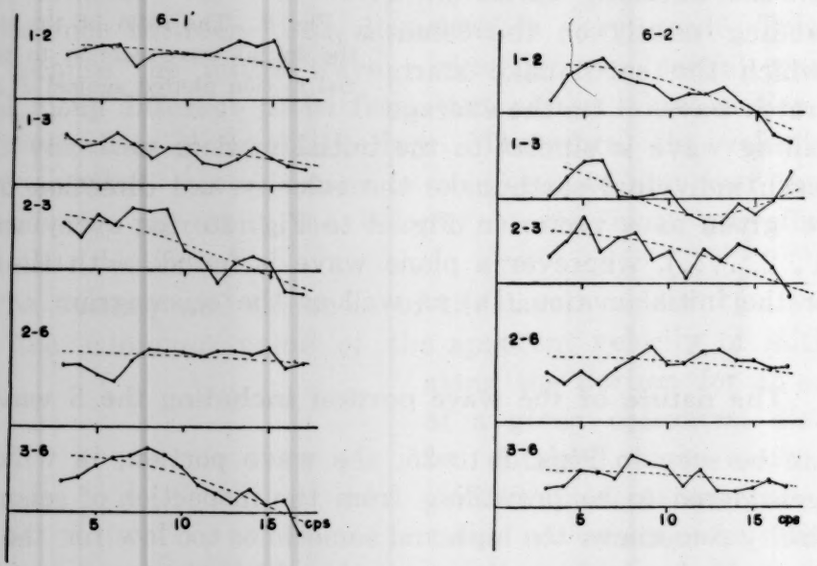


Fig. 7. Correlation curves for the $P$ and $S$ wave portions of the earthquake No. 8 recorded on Aug. 8, 04 h 35 m.

difference between the directions of propagation of these portions is quite significant. Form the ratio of the characteristic frequencies (by characteristic frequency we mean the wave length of the cosine correlation curve) for $P$ and $S$ wave portions for each pair of seismometers. If these two wave portions differ only in velocity and not in direction of propagation, then these ratios should all be the same. But in the present case, this ratio differs among the seismometer pairs, more for

the pairs 2–3, 2–6 and 3–6 and less for the rest. This gives rise to a difference in angle of about 60 degrees between the directions of propagation of $P$ and $S$ wave portions.

This can be explained as follows; if the distribution of velocity of the $P$ wave under the ground differs from that of the $S$ wave in some way due to, for instance, the heterogeneity in distribution of material having a different Poisson's ratio or the existence of melted material at some places, the wave path will be different between the two waves. Further, if their wave paths are almost perpendicular to the earth's surface, as they are in the present case, the difference in the direction of propagation along the horizontal plane will be very large, even if the net amount of difference in angle between the two wave paths is small.

If we make, therefore, a more systematic study of this direction difference for the earthquake waves coming from just underneath the recording station, we shall be able to learn very precisely the difference between the distributions of velocity of $P$ and $S$ waves under the ground. This study can be done successfully only by the application of the present method, because it is very difficult to determine accurately the time of the commencement of the $S$ wave on the seismogram.

## 6. Some remarks on the wave portions other than those including P and S wave

Figs. 8 to 25 show the velocity vectors of all the plane waves found in the records of 18 earthquakes. The following facts are worth noting here.

As can be seen in the figures, for the second 2.5 sec wave portion we find almost the same direction of propagation and value of velocity as for the initial wave portion in most of the cases. But after this, the velocity vector becomes variable and sometimes differs considerably from that of the initial wave portion. Therefore for the purpose of locating the earthquake epicentre the wave portion for the first 5 sec can be safely used.

The value of velocity of the wave portions located between $P$ and $S$ waves is usually very large. But in three earthquakes out of the eighteen, plane waves having a velocity of 3.5 to 3.8 kmps are found to exist. These may be surface waves generated, not near the origin of the earthquake, but near the recording station.

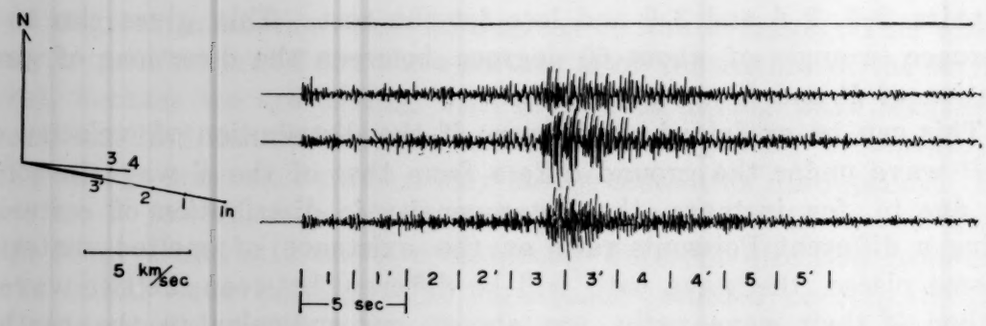


Fig. 8. Velocity vectors for the earthquake of Aug. 22, 07 h 09 m, No. 15.

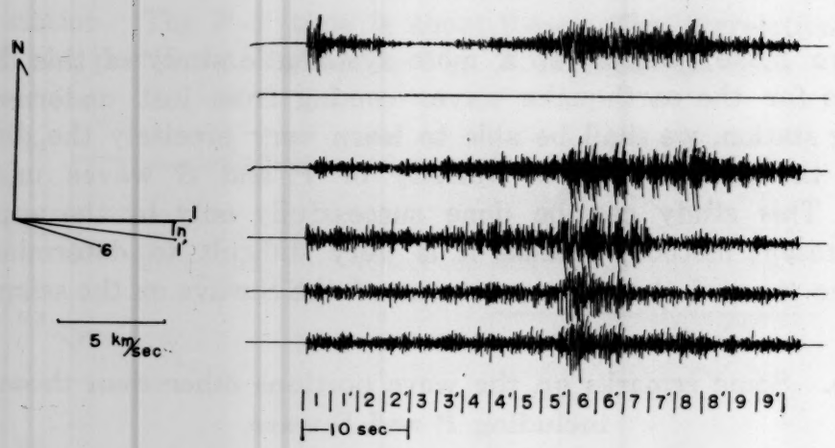


Fig. 9. Velocity vectors for the earthquake of Aug. 7, 14 h 13 m, No. 7.

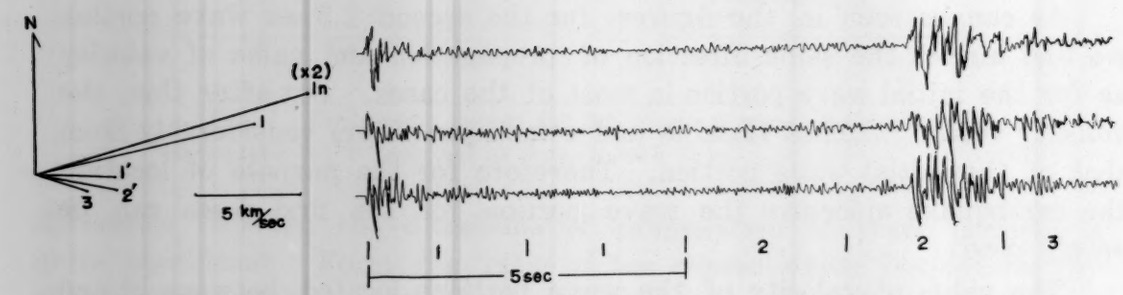


Fig. 10. Velocity vectors for the earthquake of Aug. 29, 04 h 35 m, No. 21.

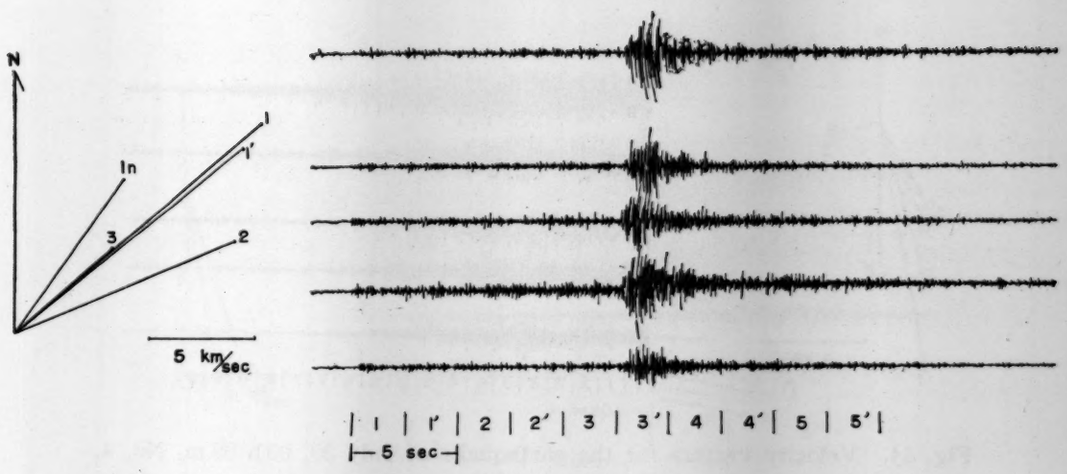


Fig. 11. Velocity vectors for the earthquake of Aug. 25, 19 h 38 m, No. 18.

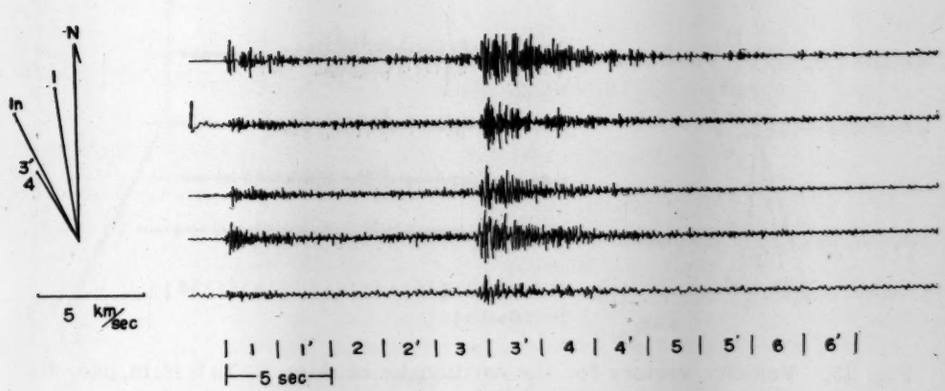


Fig. 12. Velocity vectors for the earthquake of July 29, 02 h 03 m, No. 2.

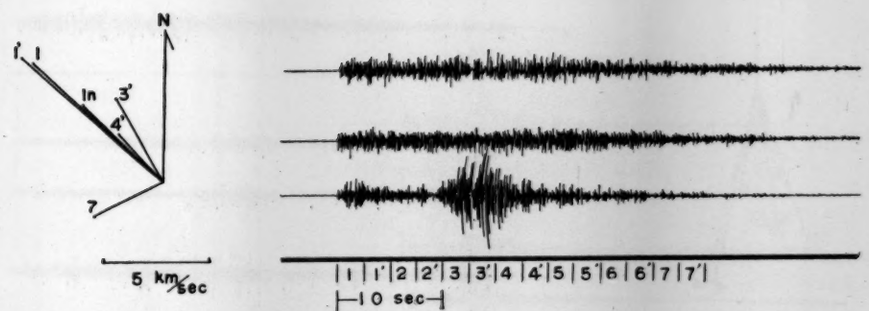


Fig. 13. Velocity vectors for the earthquake of July 29, 13 h 53 m, No. 3.

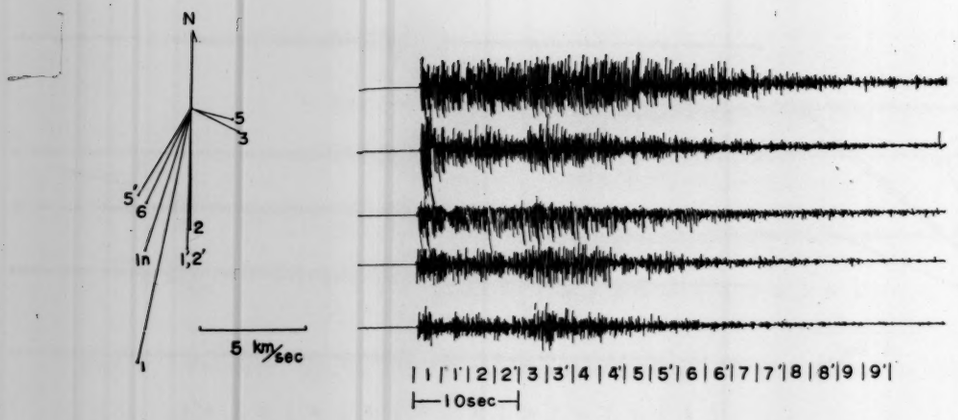


Fig. 14. Velocity vectors for the earthquake of July 30, 00 h 05 m, No. 4.

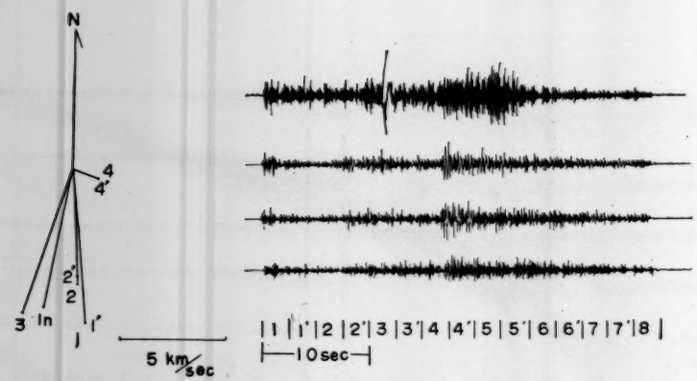


Fig. 15. Velocity vectors for the earthquake of Aug. 9, 13 h 02 m, No. 10.

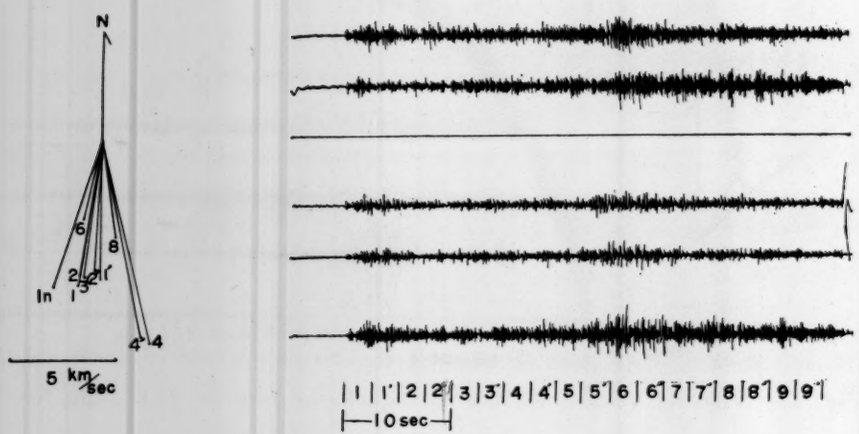


Fig. 16. Velocity vectors for the earthquake of Aug. 15, 18 h 49 m, No. 11.

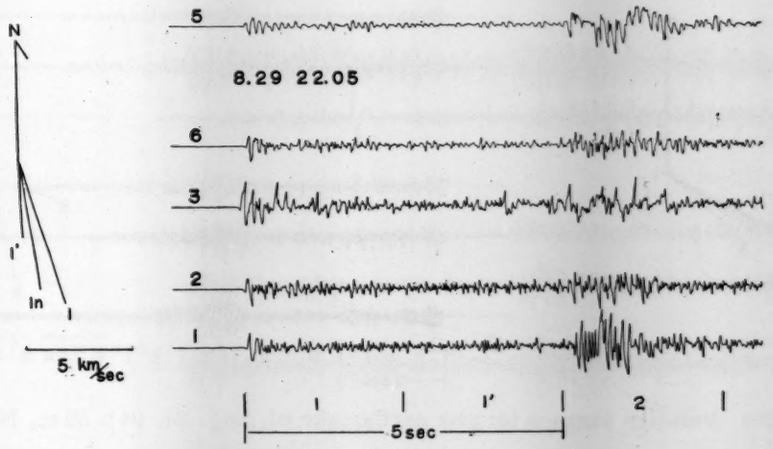


Fig. 17. Velocity vectors for the earthquake of Aug. 29, 22 h 03 m, No. 22.

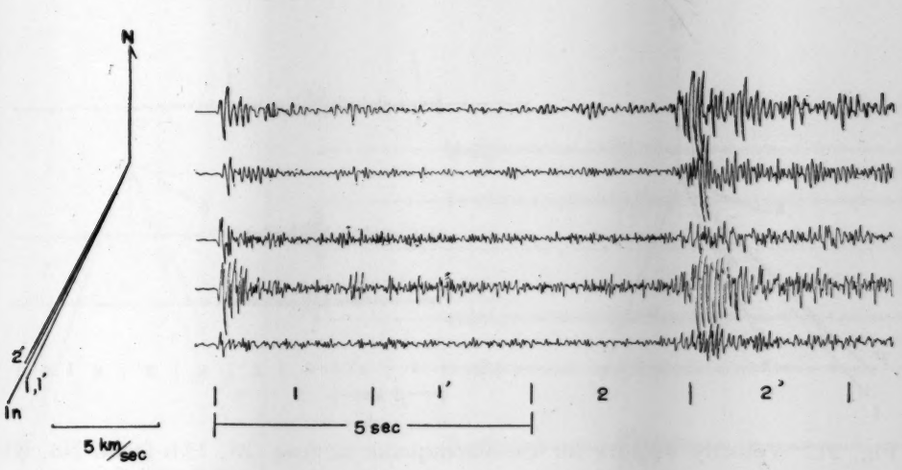


Fig. 18. Velocity vectors for the earthquake of July 30, 19 h 50 m, No. 5.

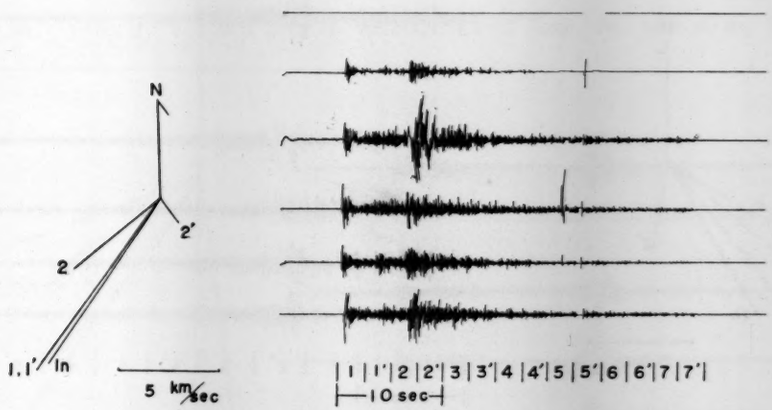


Fig. 19. Velocity vectors for the earthquake of Aug. 9, 10 h 37 m, No. 9.

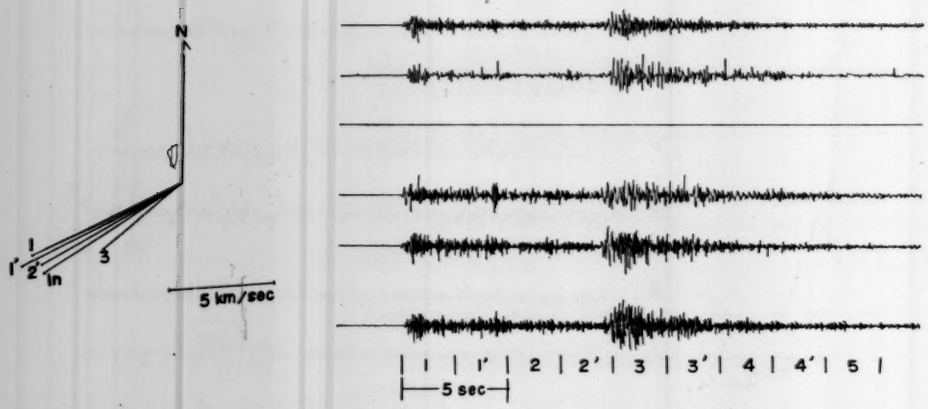


Fig. 20. Velocity vectors for the earthquake of Aug. 24, 04 h 55 m, No. 16.

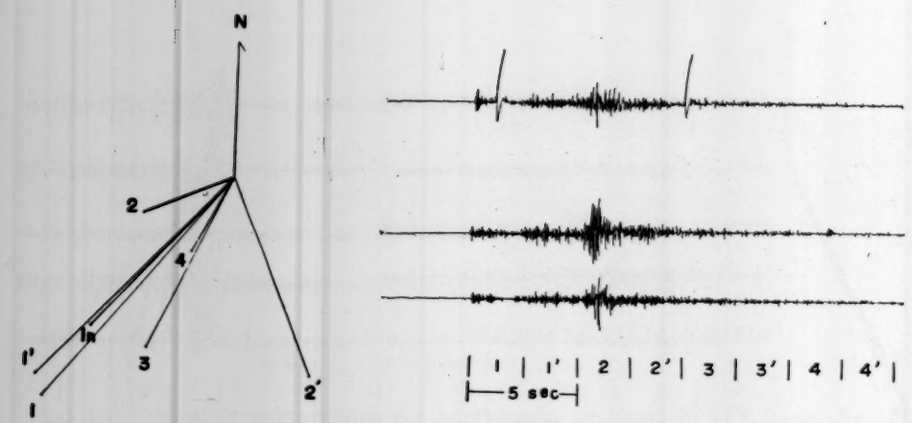


Fig. 21. Velocity vectors for the earthquake of Aug. 28, 13 h 06 m, No. 20.

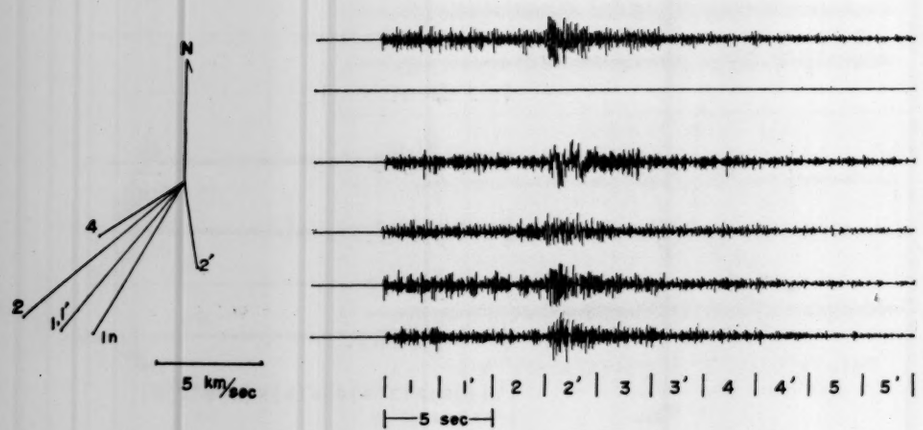


Fig. 22. Velocity vectors for the earthquake of Aug. 8, 04 h 35 m, No. 8.

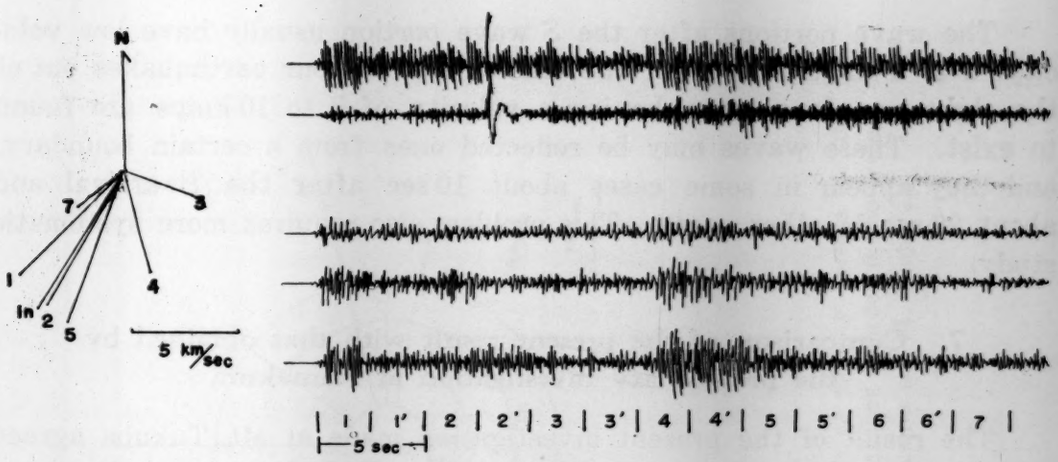


Fig. 23. Velocity vectors for the earthquake of Aug. 15, 15 h 34 m, No. 13.

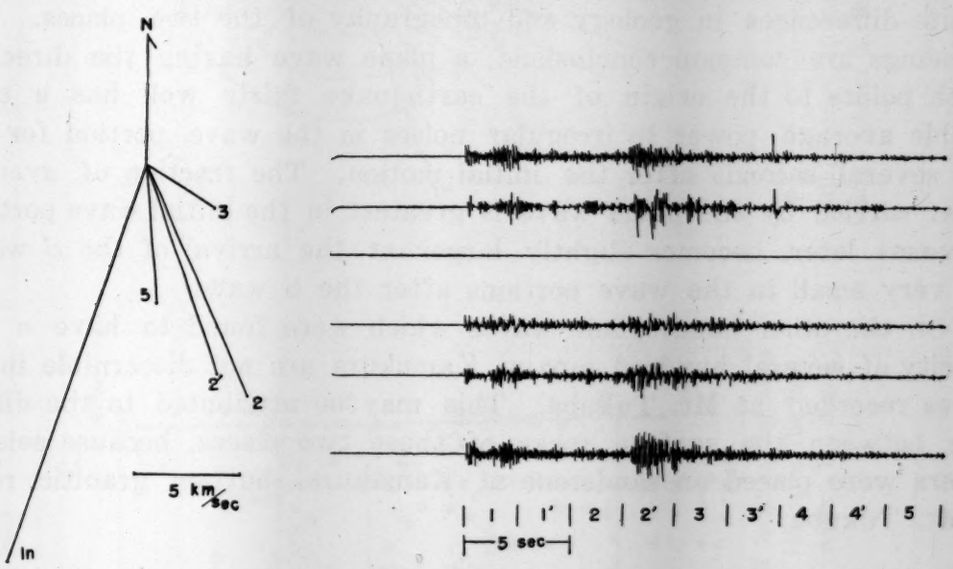


Fig. 24. Velocity vectors for the earthquake of Aug. 24, 14 h 40 m, No. 17.

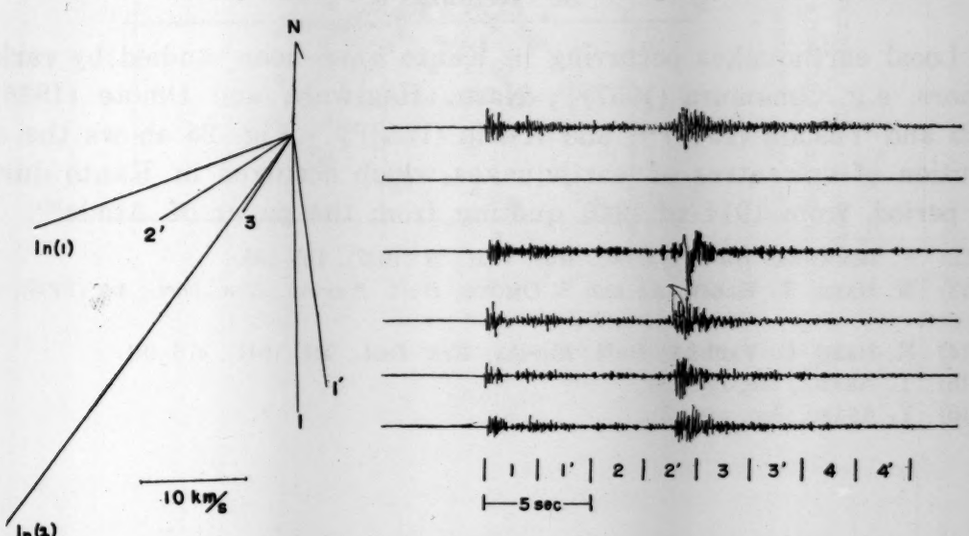


Fig. 25. Velocity vectors for the earthquake of Aug. 6, 23 h 22 m, No. 6.

The wave portions after the $S$ wave portion usually have low velocity, 2 to 4 kmps in most of the cases. But in four earthquakes out of the eighteen, plane wave having a velocity of 7 to 10 kmps are found to exist. These waves may be reflected ones from a certain boundary, and they appear in some cases about 10 sec after the $P$ arrival and about 20 sec in other cases. This problem also requires more systematic study.

## 7. Comparison of the present result with that obtained by the preliminary investigation at Kamakura

The result of the present investigation made at Mt. Tukuba agreed with that of the preliminary study made at Kamakura in most aspects despite differences in geology and topography of the two places. The followings are common conclusions; a plane wave having the direction which points to the origin of the earthquake fairly well has a comparable average power to irregular noises in the wave portion for the first several seconds after the initial motion. The fraction of average power carried by the plane wave is greatest in the initial wave portion, decreases later, becomes slightly larger at the arrival of the $S$ wave, and very small in the wave portions after the $S$ wave.

On the other hand, plane waves which were found to have a low velocity of several hundred mps at Kamakura are not discernible in the waves recorded at Mt. Tukuba. This may be attributed to the difference between the surface rocks of these two places, because seismometers were placed on sandstone at Kamakura, but on granitic rocks at Mt. Tukuba.

## 8. Remarks

Local earthquakes occurring in Kanto have been studied by various authors, e.g., Imamura (1957)[12], Nasu, Hagiwara and Omote (1936)[13], Nasu and Yasuda (1941)[14], and Asada (1958)[15]. Fig. 26 shows the distribution of epicentres of earthquakes which occurred in Kanto during the period from 1914 to 1940 quoting from the paper of Asada[16]. On

12) A. IMAMURA, *Bull. Earthq. Res. Inst.*, **3** (1927), 165–185.

13) N. NASU, T. HAGIWARA and S. OMOTE, *Bull. Earthq. Res. Inst.*, **14** (1936), 427–437.

14) N. NASU, C. YASUDA, *Bull. Earthq. Res. Inst.*, **18** (1941), 476–491.

15) T. ASADA, *loc. cit.*, 3).

16) T. ASADA, *loc. cit.*, 3).

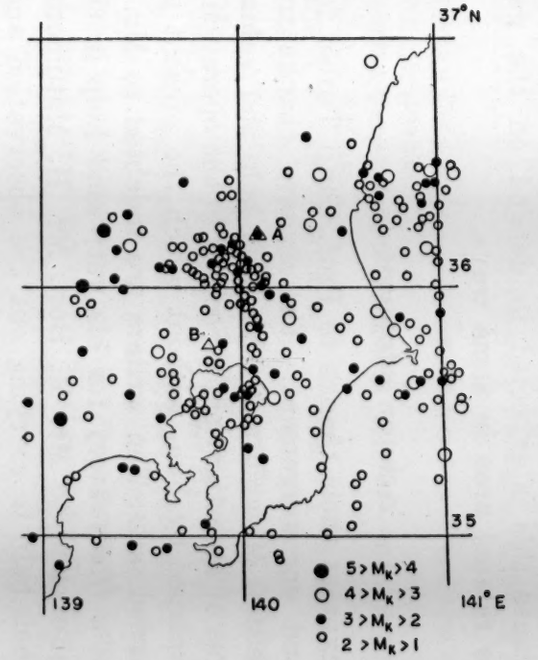


Fig. 26. Epicenters of local earthquakes in Kanto. The mark A indicates the location of Mt. Tukuba. (After T. Asada, *Loc. cit.*, 3).)

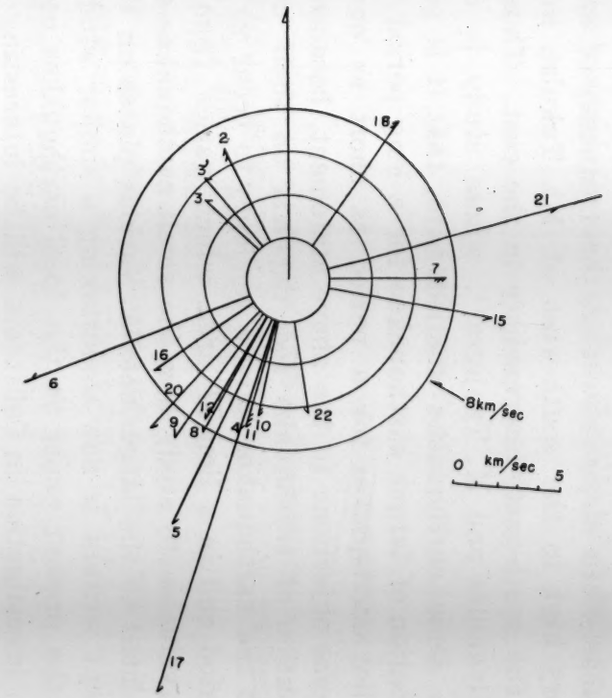


Fig. 27. Distribution of velocity vectors for the initial motion of earthquakes recorded in the present study. (After S. Miyamura and M. Tsujiura).

the other hand, the distribution of the velocity vectors for the propagation of initial motion of earthquakes which we recorded in the present investigation is shown in Fig. 27. The coincidence between these two maps is remarkable; Both maps show that the frequency of earthquake occurrence is very high in the south-west of Mt. Tukuba, low in the north-west and the south-east, intermediate in the east. Thus we conclude with S. Miyamura and M. Tsujiura[17], whose study is concerned partly with the same earthquakes studied here, that it is possible to guess the distribution of larger earthquakes for a long period by learning that of smaller earthquakes for a period as short as one month. There may be some objections to the above statement, because in some cases the distribution of earthquake foci depends on their magnitude and also because the earthquakes have a tendency to occur as a swarm for a limited period and in a limited area which varies from time to time. But it is valuable to study how the small earthquakes occur and how they are related to the larger ones at various places on the earth. One of the present writers is now undertaking a similar study by the method used in the present paper on the local earthquakes occuring in California. This investigation in California will be interesting also with respect to the question of the fraction of average power carried separately by the plane waves and irregular noises which coexist in earthquake waves, because this is expected to depend on the geology and topography of the related area in some ways.

**Acknowledgement**

The writers express their thanks to Prof. Chuji Tsuboi for his constant guidance and encouragement. The writers' thanks are also due to Assist. Prof. Setumi Miyamura for his kind help and valuable advice given in the course of investigation, especially in the operation of seismograph systems developed hy him, without which the present work could not have been carried out. The writers are indebted to Mr. M. Watanabe of Mt. Tukuba Observatory for his very kind help in the location of seismometer sites and to Mr. M. Hori, Mr. H. Matumoto and Miss H. Kanehira for their help in carrying out the observation and analysis. We owe to Mr. A. Okada the determination of the position of seismometers, and to Mr. A. Jitsukawa his help in making a temporary receiving station.

17) S. MIYAMURA and M. TSUJIURA, *loc. cit.*, 10).

This manuscript was partly prepared, while one of the writers was working in the California Institute of Technology as a visiting research fellow. The writers thank Prof. C. Hewitt Dix for his kindness in reading the manuscript and giving them helpful discussion and criticism.

---

## 14. 近地地震波動の相関法による研究

地震研究所 {安芸敬一 / 辻浦賢}

この研究は，表題はちがうが，著者らによる既報「近地地震波動のスペクトル的研究 (1)」の続報である．表題をかえた理由は，スペクトル的研究ということばが，地震波の時間的スペクトルのみの研究という意味に誤解されやすいからである．

われわれの目的は，地震波の空間スペクトルをしらべることによつて，これまでのように，ただ特別な相の初動にのみ注目するかわりに，地震波動の任意の部分の性質を，統計的にあきらかにすることである．この種の知識はちいさい地震の震源をきめたり，地震のエネルギーを評価するなどの問題で，地震波のはじめからおわりまで全部を利用しようとするばあい是非とも必要なことである．

前報では鎌倉における予備的な研究結果を報告したが，本研究では，つぎの 4 つの点で改良をくわえた．

1. 地震計を鎌倉の砂岩のかわりに，筑波山近隣の花崗岩の露出しているところに設置し，台数を3台から6台にまし，各地震計間の距離を平均約 100 m から，約 500 m にのばした．
2. 観測には，6 台の上下動地震計，2 台の無線地震波記録装置 RTS-II, 2 軌道のテープレコーダーがもちいられたが，これらの位相特性を各チャンネル間で，位相差 10 度内外におさえることができた．
3. 解析装置に検算回路を附設した結果，相関係数のあたいにして 10% の誤差で計算できる状態に装置を維持することができた．
4. 受信点を東京大学の病院新館 9 階に設置し，記録解析一切を，そこでおこなつたので，研究の能率がいちぢるしく増進した．

約1個月の観測で，約 20 個の地震を磁気テープに記録した．第1報でのべたのとおなじ方法，装置で解析した結果えられたおもな結論はつぎのようなものである．

1. 地震波には，どの部分にも，複雑な雑音がまじつている．この研究では，各部分のながさを共通に 2.5秒にとつたが，初動からはじまる最初の部分では，ほとんど，つねに規則ただしい平面波がみいだされる．この平面波がうけもつ Power のわりあいは，最大 80%，平均 40% である．$S$ 波をふくむ部分に平面波がみいだされる確率は，約 80% で，そのうけもつ Power のわりあいは，大体 20～30% である．$P$ と $S$ のあいだの部分では，平面波が約 60% の確率でみいだされ，そのうけもつ Power のわりあいは，$P$ の部分のすぐあとでは，しばしばおおきく，その他では，おおきいばあいもあり，ちいさいばあいもあつて，まちまちである．$S$ の部分のあとでは，一般に平面波をみとめることは困難で，その確率は 30% 程度であり，そのうけもつ Power のわりあいもきわめてちいさく，30% をこえることはない．平面波をみいだしえなかつた部分の性質はきわめて複雑であつて，空間的白色雑音と断ずることはできない．
2. われわれは記録をテープにとつているので，それを非常にはやいおくりの記録紙上に再生することが容易である．したがつて，$P$ 波のたちあがりを精度よくよみとることができる．ただし $P$ 波の立上りの波形がするどいときには信頼できるが，にぶいときには，信頼できない．そこで，たちあがりのするどい地震ばかり（全体の約半数）をあつめて，それらについて，初動の

到来方向と最初の 2.5 秒間の波動部分にみいだされた平面波の進行方向とをくらべてみると，角度差の絶対値の平均が 2.8 度であつた．するどくないばあいには，おなじ平均が 12.3 度であつたので，このちがいは，あきらかに初動の方に責任がある．したがつて伝播方向の精度に関しては，初動だけよりも，初動から 2.5 秒間の波動全部をつかつた方がよいことがわかる．われわれのしらべた地震のうち，ひとつだけ気象庁の観測網で震源がもとめられたが，この震源への方向，初動の伝播方向，初動部分の伝播方向の三者とも 5 度くらいの範囲におさまり，最後のものが他のふたつの中間をさしていた．初動の到来方向とみかけの速度については，宮村・辻浦[9]により別にくわしく報告されている．

3. $S$ 波をふくむ部分の波動としての性質は一般に複雑であつて，えられた速度も表面波にちかいばあいや，$P$ 波にちかいばあいなど，いろいろである．その伝播方向も $P$ 波部分と一般に一致せず，その差の絶対値の平均は 25 度もある．この差は，もし，この部分に表面波が卓越しているとすれば，表面波は地表のあさいところの不一様性によつて，(われわれは，波長数百米の波動を対象としているので) 屈折しやすいから，当然期待されてよいとおもう．しかし，一方あきらかに，$S$ 波がおもに卓越しているとみられる地震のばあいに，非常にはつきりしたくいちがいがみいだされた．このばあいには $P$ 波部分の速度 26.6 km/s に対して，$S$ 波部分が 14.9 km/s の速度をもつていて，たしかに表面波ではない．速度がおおきいからこの地震は観測点のほとんど直下でおこつたとおもわれる．したがつて，$P$ 波と $S$ 波にわずかな伝播方向の差があつても，地表面にそうみかけの方向には，おおきな差を生じうる．$P$ 波と $S$ 波のわずかな方向の差というものは，Poisson 比のちがう物質の分布とか，とけている物質部分の存在によつて，容易に説明される．いいかえれば，観測点のほとんど直下におこる地震をつかえば，地下における $P$ と $S$ の速度分布のくいちがいを非常に精密にしらべることが可能である．この問題には，もつと系統的な研究が必要である．

4. 筑波山と鎌倉での結果は，ほとんどの点で，大差なかつたが，ただ鎌倉でみいだされた数百米毎秒のおそい速度をもつ波動は，筑波ではみとめられかつた．あさいところの地質がちがうためであろう．

5. この観測でえられた地震の震源の筑波山からの方向分布をつくると，宮村・辻浦[9]ものべているように 1914 年から 1940 年にかけて生じた地震分布図と微細な点まで一致している．1 個月程度の観測で約 30 年間の地震分布図を推測できるということは，興味深い．

このような研究は，いろいろな場所でおこなうことが重要である．著者の 1 人は，現在カリフォルニアの局地地震をしらべるべく，現地においてこのための装置をつくり，観測をはじめている．

BULLETIN OF THE EARTHQUAKE
RESEARCH INSTITUTE
Vol. 37 (1959), pp. 233-243

# 15. *Studies of the Thermal State of the Earth. The Second Paper: Heat Flow associated with Magma Intrusion.*

By Tsuneji RIKITAKE,

Earthquake Research Institute.

(Read Jan. 27, 1959.–Received Jan. 27, 1959.)

## Summary

On the assumption that hot magma intrudes suddenly in a spherical cavity in the earth's crust, the conduction of heat inside and outside the magma is discussed. The changes in the geothermal gradient and consequently the heat flow at the earth's surface right up the magma are then calculated. It is assumed 1) that the initial temperatures are constant and zero respectively inside and outside the sphere and 2) that the temperature at the earth's surface is always kept at zero.

It turns out that the geothermal gradient at the surface gradually increases reaching a maximum and then slowly diminishes. The maximum of the gradient is largely dependent on both the size of the sphere and the depth. If the radius and the depth of the centre are assumed respectively as 2 and 5 *km*, the gradient corresponding to an initial temperature, which is assumed as 1300°*C*, takes the maximum around 40°*C*/*km* for a usual thermal diffusivity of rocks some $6\times10^4$ *years* past after the intrusion. This value amounts to only double the gradient due to the general heat flow of crustal origin, so that it would not be easy to detect the magma mass of the size by measuring the geothermal gradient anomaly provided the intrusion has occurred at the depth considered or deeper. Large geothermal gradients observed at some volcanic areas are likely to be caused by a high temperature mass permeated by hot gases at a depth of 1 *km* or less.

## 1. Introduction

One of the aims of the geothermal studies[1] which we have recently started is to bring out geothermal anomalies which may be associated

1) S. UYEDA, T. YUKUTAKE and I. TANAOKA, *Bull. Earthq. Res. Inst.*, **36** (1958), 251.

with geological and geophysical activities. On Volcano Sirane, an active volcano, we actually found a geothermal gradient as large as $242°C/km$. The heat flow is estimated at $10.8\times10^{-6}\,cal/sec\,cm^2$ there. These values would be one of the most straightforward examples of a large thermal anomaly which may be caused by underground high temperatures.

We then come to a question. How deep and how large will the hot region be? Since it is not practicable to conduct measurements of geothermal gradient at many points over the area, however, we can answer practically nothing from observation. In order to have a rough idea, we had better investigate theoretically a few typical models relevant to possible geothermal anomaly at the present state of investigation.

In this paper, account will be taken of heat conduction in the earth's crust when an underground spherical region is heated up quickly. When a volcano becomes active, the interior of the volcano would become hot as was inferred from the geomagnetic studies[2] on Volcano Mihara at the time of its 1950 eruption. Although some parts of the heat thus stored in the volcano are sent out from the crater together with lava, ashes, water-vapour and other gases, there should be some heat diffusing through the crust. It is intended here to examine quantitatively the geothermal gradient at the earth's surface or heat flow associated with such heat conduction by assuming depth, size and initial temperature of the magma mass.

This sort of study will be also useful for examining the possibility of detecting underground magma intrusion which is supposed to be the cause of earthquake swarms. Since a long time is required in order to observe an appreciable heat flow at the earth's surface, however, the underground activity for this case must occur continually over a long period.

Heat conduction within a volcano has been a topic of geophysics[3]. Cooling of a laccolith or intrusive magma mass is also a good exercise of mathematical theory of heat conduction in solids[4]. To the writer's knowledge, however, no study on cooling of magma has been published with adequate considerations of the boundary condition at the earth's surface. Since the geothermal gradient near the surface is the main interest in order to discuss the possibility of detecting magma mass by geothermal method, the boundary condition, on which the geothermal

2) T. RIKITAKE, *Bull. Earthq. Res. Inst.*, **29** (1951), 161.
3) Y. KODAIRA, *Geophys. Mag.*, **1** (1926), 14.
4) For example, H. S. CARSLAW and J. G. JAEGER, *Conduction of heat in solids*, Oxford (1948), 200.

gradient is largely dependent, should be taken into account.

In the light of the above, the cooling of a hot spherical mass, of which the initial temperature is assumed as constant, embedded in the cool earth having a plane boundary, where the temperature is kept zero, will be solved in this paper.

## 2. Theory

Let us suppose a semi-infinite earth in which a sphere is embedded as can be seen in Fig. 1. If we denote the temperature and thermal diffusivity outside the sphere respectively by $u_1$ and $\kappa_1$, the equation of heat conduction, which satisfies the initial condition that $u_1=0$ at $t=0$, can be written as

$$pu_1=\kappa_1\nabla^2u_1\,, \qquad (1)$$

where $p$ denotes the time-operator $\partial/\partial t$.

Inside the sphere, the equation is given by

$$pu_2=\kappa_2\nabla^2u_2+p\Theta\,, \qquad (2)$$

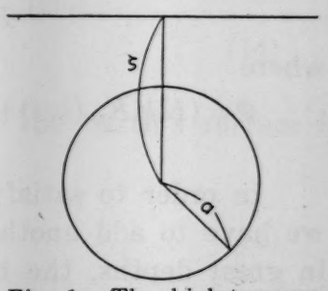


Fig. 1. The high-temperature spherical mass embedded in the earth.

where $u_2$ and $\kappa_2$ denote respectively the temperature and thermal diffusivity in the region. The second term of the righthand-side is added to the equation in order to satisfy the initial condition that $u_2=\Theta$ throughout the sphere at $t=0$, $\Theta$ being assumed to be a constant here.

If we put

$$k_1=\kappa_1^{-1/2}p^{1/2},\quad k_2=\kappa_2^{-1/2}p^{1/2}, \qquad (3)$$

the solutions of (1) and (2), which do not become infinitely large respectively at $r\to\infty$ and $r\to0$, where $r$ denotes the radial distance from the origin taken at the centre of the sphere, can be given as

$$u_1=A(k_1r)^{-1/2}K_{1/2}(k_1r)\,, \qquad (4)$$

$$u_2=\Theta+B(k_2r)^{-1/2}I_{1/2}(k_2r)\,, \qquad (5)$$

in which $A$ and $B$ are functions of $p$, while $I_{1/2}$ and $K_{1/2}$ are modified Bessel functions of degree 1/2.

In general, the conditions to be satisfied at the boundary of the

sphere or $r=a$ are 1) the continuity of heat flow and 2) the proportionality of the heat flow to the temperature difference; they can be written as

$$K_1\frac{\partial u_1}{\partial r}=K_2\frac{\partial u_2}{\partial r}=g(u_1-u_2)\ , \tag{6}$$

where $K_1$ and $K_2$ denote the thermal conductivity outside and inside the sphere.

If we put (4) and (5) into (6) and solve the equations with respect to $A$ and $B$, we obtain

$$A=\Phi^{-1}g\Theta K_2k_2(k_1a)^{1/2}I_{3/2}(k_2a)\ , \tag{7}$$

$$B=-\Phi^{-1}g\Theta K_1k_1(k_2a)^{1/2}K_{3/2}(k_1a)\ , \tag{8}$$

where

$$\Phi=\{K_1k_1K_{3/2}(k_1a)+gK_{1/2}(k_1a)\}K_2k_2I_{3/2}(k_2a)+gK_1k_1I_{1/2}(k_2a)K_{3/2}(k\,a)\ . \tag{9}$$

In order to satisfy the boundary condition at the earth's surface, we have to add another solution $u'$ to $u_1$. Since $u'$ would become small in great depths, the thermal property inside the sphere may be assumed as the same as that outside it, for the first approximation, in obtaining $u'$. If we assume, for the sake of simplicity, that $K_1=K_2$ and $\kappa_1=\kappa_2$, the solution, which will be obtained in the above way, will be exact.

It is well known that

$$\left.\begin{aligned}
K_{1/2}(x)&=\left(\frac{\pi}{2x}\right)^{1/2}e^{-x}\ ,\\
K_{3/2}(x)&=\left(\frac{\pi}{2x}\right)^{1/2}(1+x^{-1})e^{-x}\ ,\\
I_{1/2}(x)&=\left(\frac{2}{\pi x}\right)^{1/2}\sinh x\ ,\\
I_{3/2}(x)&=\left(\frac{2}{\pi x}\right)^{1/2}(\cosh x-x^{-1}\sinh x)\ .
\end{aligned}\right\} \tag{10}$$

From (4), therefore, we have

$$u_1=\sqrt{\frac{\pi}{2}}A\frac{e^{-k_1r}}{k_1r}\ . \tag{11}$$

Meanwhile, if we take a cylindrical coordinate $(\rho, \phi, z)$ having its origin at the centre of the sphere and taking the $z$-axis upwards, we have a well known relation

$$\frac{e^{-kr}}{r}=\int_0^\infty e^{-z\sqrt{\lambda^2+k^2}}J_0(\lambda\rho)\frac{\lambda d\lambda}{\sqrt{\lambda^2+k^2}} \qquad (z>0), \quad (12)$$

which can be found in a number of text-books of mathematical physics, so that (11) is transformed to

$$u_1=\sqrt{\frac{\pi}{2}}Ak_1^{-1}\int_0^\infty e^{-z\sqrt{\lambda^2+k_1^2}}J_0(\lambda\rho)\frac{\lambda d\lambda}{\sqrt{\lambda^2+k_1^2}}\,. \quad (13)$$

We then take an additional solution of the following form

$$u'=\int_0^\infty C(\lambda)e^{z\sqrt{\lambda^2+k_1^2}}J_0(\lambda\rho)d\lambda\,. \quad (14)$$

The general form of boundary condition at the earth's surface is written as

$$\left(K_1\frac{\partial}{\partial z}+h\right)(u_1+u'-u_a)=0 \quad (15)$$

where $u_a$ is the air temperature and $h$ is a constant. For the earth's surface, where the air is always moving about, $h$ is considered to be fairly large, so that, if we simply assume $u_a=0$, the relation

$$u_1+u'=0 \quad (16)$$

is a good approximation of (15).

Let us designate the depth of the centre of the sphere by $\zeta$. Putting both (13) and (14) into (16) which is to be satisfied at $z=\zeta$, we obtain

$$C(\lambda)=-\sqrt{\frac{\pi}{2}}Ak_1^{-1}e^{-2\zeta\sqrt{\lambda^2+k_1^2}}\frac{\lambda}{\sqrt{\lambda^2+k_1^2}}\,. \quad (17)$$

Substituting (17) into (14), it follows that

$$u'=-\sqrt{\frac{\pi}{2}}Ak_1^{-1}\int_0^\infty e^{-(2\zeta-z)\sqrt{\lambda^2+k_1^2}}J_0(\lambda\rho)\frac{\lambda d\lambda}{\sqrt{\lambda^2+k_1^2}}\,, \quad (18)$$

which, if we denote the distance from the point $z=2\zeta$ on the $z$-axis by $r'$, can be written as

$$u' = -\sqrt{\frac{\pi}{2}}\, A \frac{e^{-k_1 r'}}{k_1 r'} , \tag{19}$$

so that we see that $u'$ is derived from the image source which is placed at the symmetrical position in regard to the earth's surface.

Now we are in a position to interpret the operational equations (11), (19) and (5) in order to obtain expressions which are explicit with respect to $t$. Since the general forms of $A$ and $B$ are so complicated, as given in (7) and (8), that no exact solutions can be deduced, however, some simplifications of the boundary condition and parameters are to be considered here. First of all, we regard $K_1/g$ and $K_2/g$ as infinitesimally small, the interface drop of temperature being ignored in that case. We further assume that the thermal properties inside and outside the sphere are the same. Putting then $K_1=K_2=K$, $\kappa_1=\kappa_2=\kappa$ and consequently $k_1=k_2=k$, it is found, with the aid of the formulas of modified Bessel functions, that (7) and (8) can be written as

$$A=\Theta(ka)^{3/2} I_{3/2}(ka) , \tag{20}$$

$$B=-\Theta(ka)^{3/2} K_{3/2}(ka) . \tag{21}$$

With these expressions, (11), (19) and (5) are reduced to the forms;

$$u_1 = \frac{\Theta}{2r}[a(e^{-\kappa^{-1/2}(r-a)p^{1/2}} + e^{-\kappa^{-1/2}(r+a)p^{1/2}}) - \kappa^{1/2}p^{-1/2}(e^{-\kappa^{-1/2}(r-a)p^{1/2}} - e^{-\kappa^{-1/2}(r+a)p^{1/2}})] , \tag{22}$$

$$u' = -\frac{\Theta}{2r'}[a(e^{-\kappa^{-1/2}(r'-a)p^{1/2}} + e^{-\kappa^{-1/2}(r'+a)p^{1/2}}) - \kappa^{1/2}p^{-1/2}(e^{-\kappa^{-1/2}(r'-a)p^{1/2}} - e^{-\kappa^{-1/2}(r'+a)p^{1/2}})] , \tag{23}$$

$$u_2 = \Theta - \frac{\Theta}{2r}[a(e^{-\kappa^{-1/2}(a-r)p^{1/2}} - e^{-\kappa^{-1/2}(a+r)p^{1/2}}) + \kappa^{1/2}p^{-1/2}(e^{-\kappa^{-1/2}(a-r)p^{1/2}} - e^{-\kappa^{-1/2}(a+r)p^{1/2}})] . \tag{24}$$

On interpreting the above operational equations term by term, we arrive at the solutions which can be written as

$$u_1 = \Theta\left[\frac{1}{2}\left(\text{erf.}\frac{r+a}{2\kappa^{1/2}t^{1/2}} - \text{erf.}\frac{r-a}{2\kappa^{1/2}t^{1/2}}\right) + \frac{1}{r}\left(\frac{\kappa t}{\pi}\right)^{1/2}(e^{-(r+a)^2/4\kappa t} - e^{-(r-a)^2/4\kappa t})\right] , \tag{25}$$

$$u'=-\Theta\left[\frac{1}{2}\left(\text{erf. }\frac{r'+a}{2\kappa^{1/2}t^{1/2}}-\text{erf. }\frac{r'-a}{2\kappa^{1/2}t^{1/2}}\right)+\frac{1}{r'}\left(\frac{\kappa t}{\pi}\right)^{1/2}\left(e^{-(r'+a)^2/4\kappa t}-e^{-(r'-a)^2/4\kappa t}\right)\right], \tag{26}$$

$$u_2=\Theta\left[\frac{1}{2}\left(\text{erf. }\frac{a+r}{2\kappa^{1/2}t^{1/2}}+\text{erf. }\frac{a-r}{2\kappa^{1/2}t^{1/2}}\right)+\frac{1}{r}\left(\frac{\kappa t}{\pi}\right)^{1/2}\left(e^{-(a+r)^2/4\kappa t}-e^{-(a-r)^2/4\kappa t}\right)\right]. \tag{27}$$

## 3. Temperature distribution

By making $u_1+u'$ $(r>a)$ and $u_2+u'$ $(r<a)$, the temperature at any place and any time can be calculated with the aid of (25), (26) and (27). For example, let us take $\kappa=0.01\,c.g.s.$, which may be regarded as usual for rocks, $a=2s\,km$ ($s$ may take any positive value), while $\zeta$, depth of the centre of the sphere, takes three values, $5s$, $4s$ and $3s\,km$. Corresponding to $\zeta=5s\,km$, the distributions of the temperature on the vertical line passing through the centre can be calculated for various epochs as are shown in Fig. 2. Since lengths always appear in (25), (26) and (27) as ratio to square root of time, it is noticed that, if we multiply the depth as well as the radius of the sphere by $s$, the corresponding curves of temperature distribution may be regarded as those for the epochs at

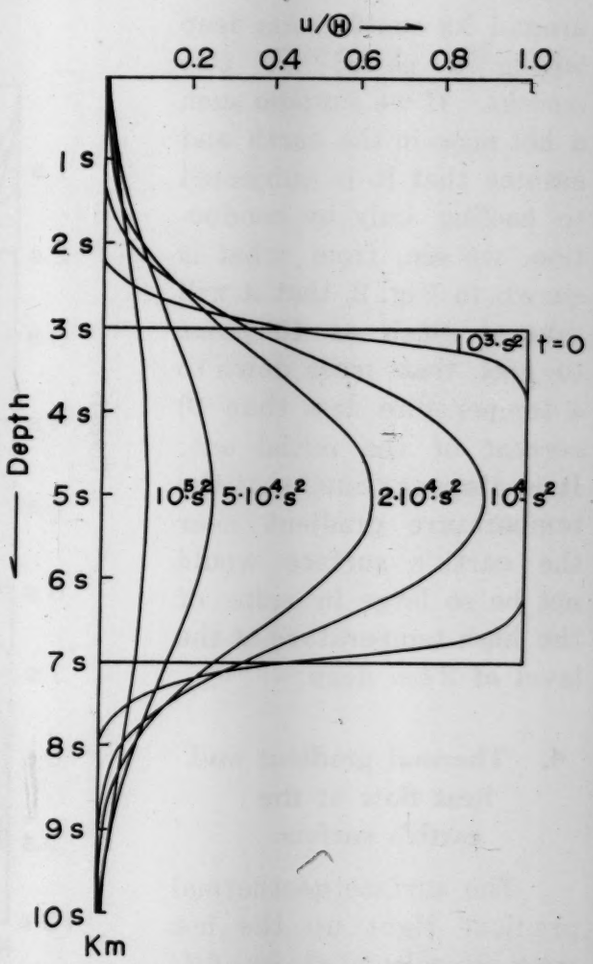


Fig. 2. The distribution of the temperature on the vertical line passing the centre of the sphere for $a=2s\,km$ and $\zeta=5s\,km$.

which the times are multiplied by $s^2$.

As can be seen in Fig. 2, the conduction of heat outside the sphere is extremely slow. The influence of the earth's surface is not remarkable for this case, the distribution of temperature is practically symmetric about the centre of the sphere.

In Figs. 3 and 4, however, the depths of the centre are taken respectively as $4s$ and $3s$ *km*. In these cases, the influence of the earth's surface becomes considerable, the asymmetry of temperature distribution being enlarged as the sphere approaches the surface.

At the time of the 1950 eruption of Volcano Mihara, the writer has presumed, by analysing the results of repeated geomagnetic surveys, that a roughly spherical hot region of 2 *km* in radius appeared around its centre 5 *km* deep within a period of two *months*. If we suppose such a hot mass in the earth and assume that it is subjected to cooling only by conduction, we see, from what is shown in Fig. 2, that it will take as much as $10^5$ *years* to cool that mass down to a temperature less than 10 *percent* of the initial one. It is also suggested that the temperature gradient near the earth's surface would not be so large in spite of the high temperature at the level of 3 *km* deep.

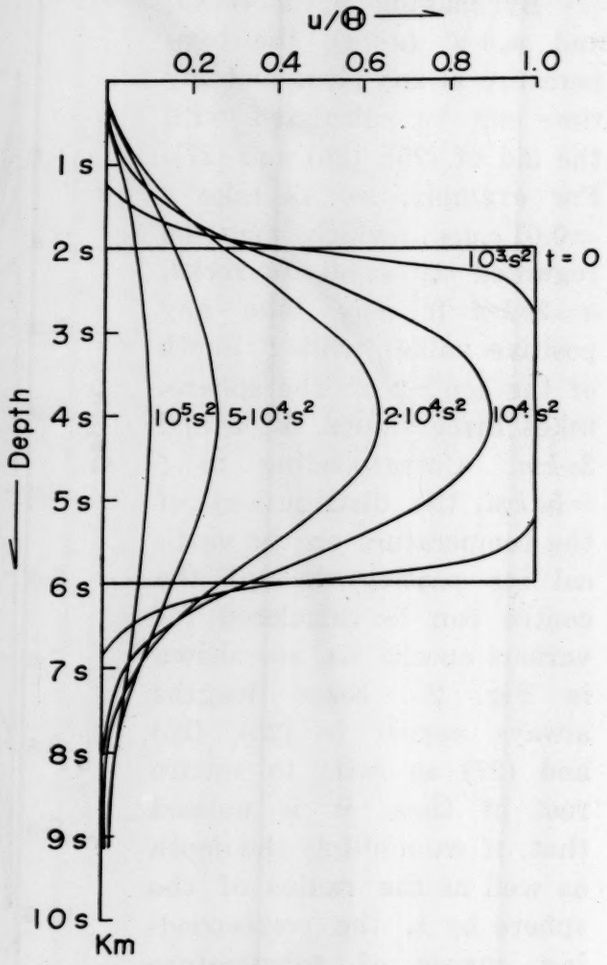


Fig. 3. The distribution of the temperature on the vertical line passing the centre of the sphere for $a=2s$ *km* and $\zeta=4s$ *km*.

## 4. Thermal gradient and heat flow at the earth's surface

The surface geothermal gradient right up the hot mass is calculated by differentiating $u_1+u'$ with respect to $z$. We obtain

$$-\left[\frac{\partial(u_1+u')}{\partial z}\right]_{\rho=0,z=\zeta}=\Theta\frac{a}{\zeta}\left(\frac{1}{\pi\kappa t}\right)^{1/2}\left[\left(1+\frac{2\kappa t}{a\zeta}\right)e^{-\frac{(\zeta+a)^2}{4\kappa t}}+\left(1-\frac{2\kappa t}{a\zeta}\right)e^{-\frac{(\zeta-a)^2}{4\kappa t}}\right]. \tag{28}$$

Corresponding to the three cases calculated in the last section, the changes in the surface temperature gradient with time is calculated and shown in Fig. 5 for $\zeta=5s$, $4s$ and $3s\,km$, while $a$ is assumed to be always equal to $2s\,km$. If we assume that $\Theta$ amounts to $1300°C$, the peaks of the gradient become roughly 40, 100 and $350°C/km$ for $\zeta=5$, 4 and $3\,km$. If the thermal conductivity is assumed to take a usual value for rocks, $5\times10^{-3}\,cal/cm\,sec\,°C$ say, these gradients give heat flows amounting to 2, 5 and $17.5\times10^{-6}\,cal/cm^2\,sec$ respectively.

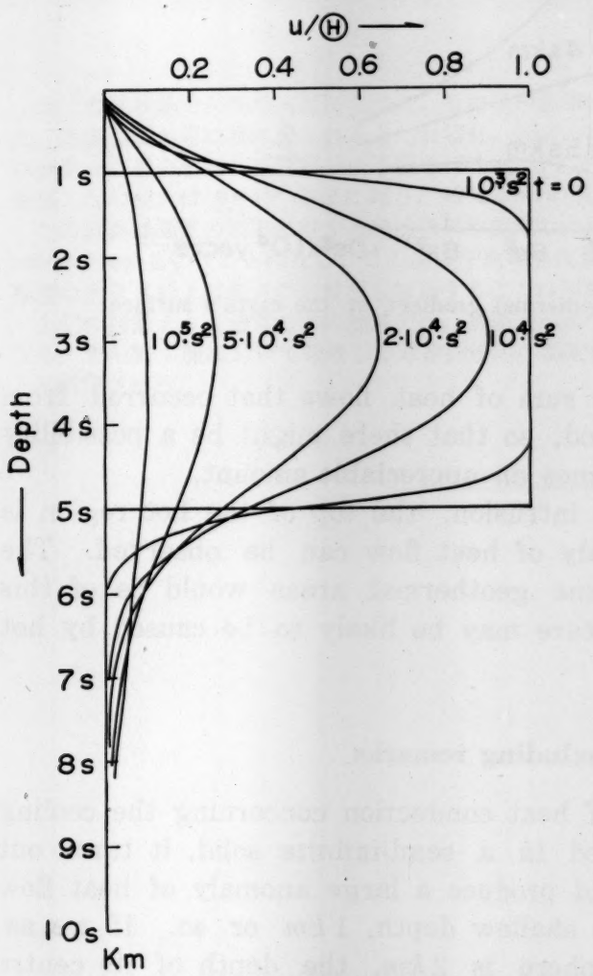


Fig. 4. The distribution of the temperature on the vertical line passing the centre of the sphere for $a=2s\,km$ and $\zeta=3s\,km$.

We see from the above results that the heat flow due to an underground hot magma mass is not so large except for shallow one. For instance, the $1300°C$ magma of $2\,km$ in radius, the depth of its top being $3\,km$, gives rise to a heat flow as small as $2\times10^{-6}\,cal/cm^2\,sec$, that is, only double the mean heat flow of crustal origin. If a magma of the same mass intrudes in a farther depth, no marked anomaly in heat flow can be observed.

We should pay attention to the fact, however, that the changes in the gradient are extremely slow. Since the heat flow, which is not greatly different from its maximum, continues over a long period, $10^5$ *years* say, we may well expect repeated intrusions of a similar sort. In that case,

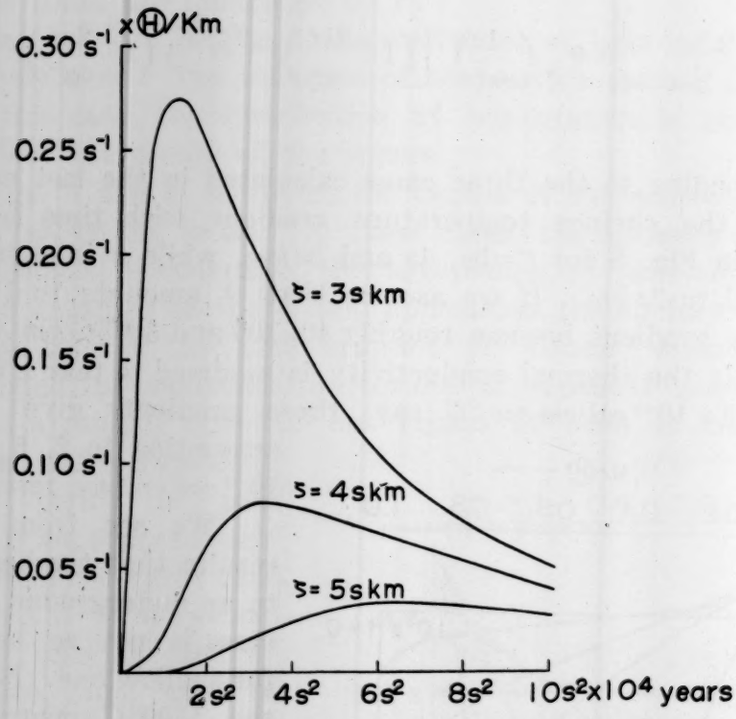


Fig. 5. The changes in the geothermal gradient at the earth's surface right up the magma.

it happens that we observe the sum of heat flows that occurred from time to time during a long period, so that there might be a possibility that the present heat flow becomes an appreciable amount.

In the case of a shallow intrusion, the top of the hot region is 1 *km* deep say, a marked anomaly of heat flow can be observed. The large heat flows observed in some geothermal areas would be of this origin though the high temperature may be likely to be caused by hot gases coming from below.

## 5. Concluding remarks

On the basis of a theory of heat conduction concerning the cooling of a spherical region embedded in a semi-infinite solid, it turns out that a magma intrusion does not produce a large anomaly of heat flow unless the intrusion occurs in a shallow depth, 1 *km* or so. If we assume that the radius of the sphere is 2 *km*, the depth of its centre 5 *km*, we can expect a heat flow right up the sphere amounting to $2 \times 10^{-6}$ *cal/cm sec* which is only double the general heat flow from within

the earth. It would be of difficulty to detect a high temperature mass of that size by measuring heat flow at the earth's surface provided the depth exceeds 5 *km*.

There is no doubt, however, that, if the top of hot region reaches somehow a depth of 1 *km* or thereabout, we can observe a large anomaly of heat flow, 10 times or more of the general one.

---

## 15. 地球熱学 (第 2 報) 岩漿貫入と地表の熱の流れ

地震研究所　力　武　常　次

地下の球状部分が突然高温になつて，その後熱伝導によりどのように冷却するかを理論的に調べた．地表温度が常に零に保たれるとした場合，地表の地温勾配はだんだんと増加して極大に達し，以後徐々に減少する．高温部分の半径を 2 *km*，中心の深さを 5 *km*，初期温度を 1300°*C* とすれば，地温勾配の極大は $6\times10^4$ 年後に起り，40°*C*/*km* の値をとる．

この計算は通常の岩石に対する熱拡散率を仮定した結果で，地表の熱流量に換算すれば $2\times10^{-6}$ *cal*/*cm*$^2$ *sec* ということになる．この値は平均の熱流量の倍にすぎないので，熱流量の測定からこの程度の大きさおよび深さの岩漿溜を検出することは困難であると予想される．

上記の結果より，通常の火山地域では，熱流量が必ずしも異常に大きいとは考えられないことになる．また第 1 報において報告した草津白根山の測定例は，熱源がずつと地表に近い場合であることが推定される．

---

BULLETIN OF THE EARTHQUAKE
RESEARCH INSTITUTE
Vol. 37 (1959), pp. 245-264

# 16. *Forced Oscillations of the Earth's Dynamo.*

By Tsuneji RIKITAKE,

Earthquake Research Institute.

(Read Feb. 24, 1959.—Received Feb. 24, 1959.)

## Summary

A theory, based on magneto-hydrodynamics, that the geomagnetic secular variations are caused by forced oscillations of small amplitude superposing on the steady state of the earth's dynamo is tried. With drastic simplifications, the driving force due to buoyancy is obtained for hypothetical variations of a 100-*year* period. The time-dependent thermal field responsible for such a force field is also obtained. It is shown that the amplitude of the field would be $10^{-4}°C$ in order to account for the $S_1^0$ field whose amplitude is assumed as 1000 *gammas* at the pole.

## 1. Introduction

It has become widely believed that geomagnetic secular variations are caused by fluid motions in the earth's core wherein magnetic fields are maintained by the dynamo action. Although it is not known whether or not the earth's dynamo is steady or non-steady, it is possible to study secular variations as small disturbances given to the dynamo which is regarded as nearly steady during a period longer than those of secular variations.

The first study in this line has been published by the present writer[1] by taking Bullard's dynamo[2] as the steady state. As far as the influence of the Coriolis force due to the earth's rotation is disregarded, the study led to a conclusion that the dynamo, whose toroidal magnetic fields are as large as those estimated by Bullard, would not be stable for small disturbances. It is also suggested that geomagnetic secular variations might be explained by the free magneto-hydrodynamic oscillations of the system.

1) T. RIKITAKE, *Bull. Earthq. Res. Inst.*, **33** (1955), 1.

2) E. C. BULLARD and H. GELLMAN, *Phil. Trans. Roy. Soc. London A*, **247** (1954), 213.

The above study would not be adequately applied to the earth's dynamo because the Coriolis force, which usually plays an important role in studies of rotating fluid mass of large dimension, is completely ignored. The present writer[3] extended his study to the case in which the core is subjected to a uniform rotation. It has then turned out that the influence of the Coriolis force is so strong that the dynamo considered is stable for small disturbances unless the steady magnetic fields are as large as $10^5$ *gauss* or more. We therefore see that the previous view that the secular variations might be caused by free magneto-hydrodynamic oscillations in the core is not acceptable when we take into account the effect of the Coriolis force.

In the light of the above, it is naturally required to suppose some time-dependent driving force in order that we can account for the secular variation as a result of magneto-hydrodynamic processes prevailing in the earth's core. The most likely cause of such a force would be the buoyancy force of thermal origin. The purpose of this paper is to study forced oscillations of the dynamo, of which the steady state has been studied by Bullard and others, and also to investigate the force field which gives rise to the dipole part of geomagnetic secular variation. Owing to the mathematical complexity, however, only fluid motion, driving force and thermal field which are related to secular variation of the $S_1^0$ type will be taken into account.

## 2. Equations to be solved

Maxwell's equations can be written as

$$\vec{I}=\sigma(\vec{E}+\vec{V}\wedge\vec{H})\,, \tag{1}$$

$$\mathrm{curl}\,\vec{E}=-\partial\vec{H}/\partial t\,, \tag{2}$$

$$\mathrm{curl}\,\vec{H}=4\pi\vec{I}\,, \tag{3}$$

where $\vec{I}$, $\vec{E}$, $\vec{H}$, $\sigma$ and $\vec{V}$ denote respectively the electric current density, electric field, magnetic field, electrical conductivity and velocity of fluid motion. The magnetic permeability is assumed as unity in electromagnetic unit.

Meanwhile the equation of motion can be written as

$$\rho\partial\vec{V}/\partial t+\rho(\vec{V}\cdot\mathrm{grad})\vec{V}+2\rho(\vec{\omega}_0\wedge\vec{V})=\vec{I}\wedge\vec{H}-\mathrm{grad}\,\vec{P}+\vec{G} \tag{4}$$

3) T. RIKITAKE, *Bull. Earthq. Res. Inst.*, **34** (1956), 283.

where $\rho$, $\vec{\omega}_0$, $P$ and $\vec{G}$ denote respectively the density, rotation vector of uniform rotation about $\theta=0$ axis, pressure and non-electromagnetic force.

Let us put

$$\left.\begin{aligned} &\vec{I}=\vec{I}_0+\vec{i},\ \vec{E}=\vec{E}_0+\vec{e},\ \vec{H}=\vec{H}_0+\vec{h}, \\ &\vec{V}=\vec{V}_0+\vec{v},\ P=P_0+p,\ \vec{G}=\vec{G}_0+\vec{g}, \end{aligned}\right\} \qquad (5)$$

in which the quantities with subscript 0 specify the steady state, while those denoted by small letters are the departures from the steady state and are regarded as the first order small quantities. Putting (5) into the equations from (1) to (4), we have a system of linear differential equations such as

$$\vec{i}=\sigma(\vec{e}+\vec{v}\wedge\vec{H}_0+\vec{V}_0\wedge\vec{h})\ , \qquad (6)$$

$$\operatorname{curl}\vec{e}=-\partial\vec{h}/\partial t\ , \qquad (7)$$

$$\operatorname{curl}\vec{h}=4\pi\vec{i}\ , \qquad (8)$$

$$\rho\partial\vec{v}/\partial t+2\rho(\vec{\omega}_0\wedge\vec{v})=\vec{i}\wedge\vec{H}_0+\vec{I}_0\wedge\vec{h}-\operatorname{grad}p+\vec{g}\ , \qquad (9)$$

provided the second order small quantities are ignored.

On the assumption that $\vec{H}_0$, $\vec{V}_0$, $\vec{I}_0$ and $\vec{\omega}_0$ are known, we are going to solve these equations under suitable boundary conditions. The only difference of these equations from those treated in the previous paper[3] is the point that the non-electromagnetic force $\vec{g}$ is not ignored here.

We may further assume that the fluid is incompressible, so that

$$\operatorname{div}\vec{v}=0\ . \qquad (10)$$

By taking curl of (6) and eliminating $\vec{e}$ with the aid of (7), we obtain

$$\operatorname{curl}\vec{i}=\sigma\{-D\vec{h}+\operatorname{curl}(\vec{v}\wedge\vec{H}_0)+\operatorname{curl}(\vec{V}_0\wedge\vec{h})\}\ , \qquad (11)$$

where we write $D$ in place of $\partial/\partial t$. On the other hand we have from (8)

$$4\pi\operatorname{curl}\vec{i}=\operatorname{curl}\operatorname{curl}\vec{h}=-\nabla^2\vec{h}\ , \qquad (12)$$

because $\operatorname{div}\vec{h}=0$.

From (11) and (12), we can eliminate $\vec{i}$ getting

$$\{D-(4\pi\sigma)^{-1}\nabla^2\}\vec{h}=\mathrm{curl}\,(\vec{V}_0\wedge\vec{h})+\mathrm{curl}\,(\vec{v}\wedge\vec{H}_0)\,. \tag{13}$$

We also have from (9)

$$\rho D\vec{v}+2\rho(\vec{\omega}_0\wedge\vec{v})=(4\pi)^{-1}\{(\mathrm{curl}\,\vec{h}\wedge\vec{H}_0)+(\mathrm{curl}\,\vec{H}_0\wedge\vec{h})\}-\mathrm{grad}\,p+\vec{g}\,. \tag{14}$$

(13) and (14) are regarded as the simultaneous equations for $\vec{h}$ and $\vec{v}$.

### 3. Solution for pressure

Let us assume that $\vec{g}$ is the buoyancy force. In that case it is obvious that its $\theta$ and $\phi$ components are to be zero, the radial component of $\vec{g}$ being written as $g$ hereafter.

If we make div of (14) we obtain

$$\nabla^2 p=-(4\pi)^{-1}(\vec{H}_0\cdot\nabla^2\vec{h}+\vec{h}\cdot\nabla^2\vec{H}_0+2\mathrm{curl}\,\vec{h}\cdot\mathrm{curl}\,\vec{H}_0)+2\rho\vec{\omega}_0\cdot\mathrm{curl}\,\vec{v}+r^{-2}\frac{d(r^2g)}{dr} \tag{15}$$

because of (10). $\mathrm{curl}\,\vec{\omega}_0=0$ which is derived from the condition of uniform rotation is also taken into account.

In general, $\vec{h}$ is to be expressed with the sum of poloidal and toroidal magnetic fields of various degree. As has been done in the previous papers[1),3)], however, we shall assume $\vec{h}$ is of the $S_1^0$ type and ignore the fields of other type which will appear in the righthand-side of (13), otherwise the problem becomes far from tractable because many fields of various type come out through the induction processes.

If we take only the $S_1^0$ field, we may write as

$$\left.\begin{aligned}
\vec{h}&=\begin{cases}-2s(r)P_1\\ -\left(r\dfrac{ds}{dr}+2s\right)\dfrac{dP_1}{d\theta}\\ 0\,,\end{cases}\\
\mathrm{curl}\,\vec{h}&=\begin{cases}0\\ 0\\ -\left(r\dfrac{d^2s}{dr^2}+4\dfrac{ds}{dr}\right)\dfrac{dP_1}{d\theta}\,,\end{cases}\\
\nabla^2\vec{h}&=\begin{cases}-2\left(\dfrac{d^2s}{dr^2}+\dfrac{4}{r}\dfrac{ds}{dr}\right)P_1\\ -\left(r\dfrac{d^3s}{dr^3}+6\dfrac{d^2s}{dr^2}+\dfrac{4ds}{rdr}\right)\dfrac{dP_1}{d\theta}\\ 0\,.\end{cases}
\end{aligned}\right\} \tag{16}$$

As for the steady magnetic fields and fluid motions, we take the simplest combination of Bullard's dynamo[2], so that the motion consists of the $T_1^0$ and $S_2^{2c}$ types while the magnetic fields contain the $S_1^0$, $T_2^0$, $T_2^{2c}$ and $T_2^{2s}$ types. It then follows that

$$\left.\begin{aligned}\vec{H}_0&=\vec{H}_1+\vec{H}_2+\vec{H}_3+\vec{H}_4\,,\\ \vec{V}_0&=\vec{V}_1+\vec{V}_2\,,\end{aligned}\right\} \tag{17}$$

where

$$\left.\begin{aligned}\vec{H}_1&=\begin{cases}-2S_1(r)P_1\\ -\left(r\dfrac{dS_1}{dr}+2S_1\right)\dfrac{dP_1}{d\theta}\\ 0\,,\end{cases}\\ \operatorname{curl}\vec{H}_1&=\begin{cases}0\\ 0\\ -\left(r\dfrac{d^2S_1}{dr^2}+4\dfrac{dS_1}{dr}\right)\dfrac{dP_1}{d\theta}\end{cases}\\ \nabla^2\vec{H}_1&=\begin{cases}-2\left(\dfrac{d^2S_1}{dr^2}+\dfrac{4}{r}\dfrac{dS_1}{dr}\right)P_1\\ -\left(r\dfrac{d^3S_1}{dr^3}+6\dfrac{d^2S_1}{dr^2}+\dfrac{4}{r}\dfrac{dS_1}{dr}\right)\dfrac{dP_1}{d\theta}\\ 0\,,\end{cases}\end{aligned}\right\} \tag{18}$$

$$\left.\begin{aligned}\vec{H}_2&=\begin{cases}0\\ 0\\ (r/a)^2T_2(r)\dfrac{dP_2}{d\theta}\,,\end{cases}\\ \operatorname{curl}\vec{H}_2&=\begin{cases}-6a^{-2}rT_2P_2\\ -a^{-2}\left(r\dfrac{dT_2}{dr}+3T_2\right)r\dfrac{dP_2}{d\theta}\\ 0\,,\end{cases}\\ \nabla^2\vec{H}_2&=\begin{cases}0\\ 0\\ a^{-2}\left(\dfrac{d^2T_2}{dr^2}+\dfrac{6}{r}\dfrac{dT_2}{dr}\right)r^2\dfrac{dP_2}{d\theta}\,,\end{cases}\end{aligned}\right\} \tag{19}$$

$$\vec{H}_3=\begin{cases}0\\ -(r/a)^2 T_3(r)\dfrac{\partial(P_2^2\cos 2\phi)}{\sin\theta\partial\phi}\\ (r/a)^2 T_3(r)\dfrac{\partial(P_2^2\cos 2\phi)}{\partial\theta}\end{cases},$$

$$\operatorname{curl}\vec{H}_3=\begin{cases}-6a^{-2}rT_3P_2^2\cos 2\phi\\ -a^{-2}\left(r\dfrac{dT_3}{dr}+3T_3\right)r\dfrac{\partial(P_2^2\cos 2\phi)}{\partial\theta}\\ -a^{-2}\left(r\dfrac{dT_3}{dr}+3T_3\right)r\dfrac{\partial(P_2^2\cos 2\phi)}{\sin\theta\partial\phi}\end{cases},$$

$$\nabla^2\vec{H}_3=\begin{cases}0\\ -a^{-2}\left(\dfrac{d^2T_3}{dr^2}+\dfrac{6}{r}\dfrac{dT_3}{dr}\right)r^2\dfrac{\partial(P_2^2\cos 2\phi)}{\sin\theta\partial\phi}\\ a^{-2}\left(\dfrac{d^2T_3}{dr^2}+\dfrac{6}{r}\dfrac{dT_3}{dr}\right)r^2\dfrac{\partial(P_2^2\cos 2\phi)}{\partial\theta}\end{cases}, \tag{20}$$

$$\vec{H}_4=\begin{cases}0\\ -(r/a)^2 T_4(r)\dfrac{\partial(P_2^2\sin 2\phi)}{\sin\theta\partial\phi}\\ (r/a)^2 T_4(r)\dfrac{\partial(P_2^2\sin 2\phi)}{\partial\theta}\end{cases},$$

$$\operatorname{curl}\vec{H}_4=\begin{cases}-6a^{-2}rT_4P_2^2\sin 2\phi\\ -a^{-2}\left(r\dfrac{dT_4}{dr}+3T_4\right)r\dfrac{\partial(P_2^2\sin 2\phi)}{\partial\theta}\\ -a^{-2}\left(r\dfrac{dT_4}{dr}+3T_4\right)r\dfrac{\partial(P_2^2\sin 2\phi)}{\sin\theta\partial\phi}\end{cases},$$

$$\nabla^2\vec{H}_4=\begin{cases}0\\ -a^{-2}\left(\dfrac{d^2T_4}{dr^2}+\dfrac{6}{r}\dfrac{dT_4}{dr}\right)r^2\dfrac{\partial(P_2^2\sin 2\phi)}{\sin\theta\partial\phi}\\ a^{-2}\left(\dfrac{d^2T_4}{dr^2}+\dfrac{6}{r}\dfrac{dT_4}{dr}\right)r^2\dfrac{\partial(P_2^2\sin 2\phi)}{\partial\theta}\end{cases}, \tag{21}$$

$$\vec{V}_1=\begin{cases}0\\ 0\\ (r/a)V_1(r)\dfrac{dP_1}{d\theta}\end{cases}, \tag{22}$$

$$\vec{V}_2=\begin{cases}-6(r/a)V_2P_2^2\cos 2\phi\\ -(r/a)\left(r\dfrac{dV_2}{dr}+3V_2\right)\dfrac{\partial(P_2^2\cos 2\phi)}{\partial\theta}\\ -(r/a)\left(r\dfrac{dV_2}{dr}+3V_2\right)\dfrac{\partial(P_2^2\cos 2\phi)}{\sin\theta\partial\phi}\end{cases}. \tag{23}$$

With the above expressions, the first three terms of the righthand-side of (15) are calculated as follows;

$$\begin{aligned}\vec{H}_0\cdot\nabla^2\vec{h}=&\frac{2}{3}\left\{2S_1\left(\frac{d^2s}{dr^2}+\frac{4}{r}\frac{ds}{dr}\right)+\left(r\frac{dS_1}{dr}+2S_1\right)\left(r\frac{d^3s}{dr^3}+6\frac{d^2s}{dr^2}+\frac{4}{r}\frac{ds}{dr}\right)\right\}\\ &+\frac{2}{3}\left\{4S_1\left(\frac{d^2s}{dr^2}+\frac{4}{r}\frac{ds}{dr}\right)-\left(r\frac{dS_1}{dr}+2S_1\right)\left(r\frac{d^3s}{dr^3}+6\frac{d^2s}{dr^2}+\frac{4}{r}\frac{ds}{dr}\right)\right\}P_2\\ &+2a^{-2}T_3r^2\left(r\frac{d^3s}{dr^3}+6\frac{d^2s}{dr^2}+\frac{4}{r}\frac{ds}{dr}\right)P_2^2\sin 2\phi\\ &-2a^{-2}T_4r^2\left(r\frac{d^3s}{dr^3}+6\frac{d^2s}{dr^2}+\frac{4}{r}\frac{ds}{dr}\right)P_2^2\cos 2\phi\,,\end{aligned} \tag{24}$$

$$\begin{aligned}\vec{h}\cdot\nabla^2\vec{H}_0=&\frac{2}{3}\left\{2\left(\frac{d^2S_1}{dr^2}+\frac{4}{r}\frac{dS_1}{dr}\right)s+\left(r\frac{d^3S_1}{dr^3}+6\frac{d^2S_1}{dr^2}+\frac{4}{r}\frac{dS_1}{dr}\right)\left(r\frac{ds}{dr}+2s\right)\right\}\\ &+\frac{2}{3}\left\{4\left(\frac{d^2S_1}{dr^2}+\frac{4}{r}\frac{dS_1}{dr}\right)s-\left(r\frac{d^3S_1}{dr^3}+6\frac{d^2S_1}{dr^2}+\frac{4}{r}\frac{dS_1}{dr}\right)\left(r\frac{ds}{dr}+2s\right)\right\}P_2\\ &+2a^{-2}\left(r^2\frac{d^2T_3}{dr^2}+6r\frac{dT_3}{dr}\right)\left(r\frac{ds}{dr}+2s\right)P_2^2\sin 2\phi\\ &-2a^{-2}\left(r^2\frac{d^2T_4}{dr^2}+6r\frac{dT_4}{dr}\right)\left(r\frac{ds}{dr}+2s\right)P_2^2\cos 2\phi\,,\end{aligned} \tag{25}$$

$$\begin{aligned}\operatorname{curl}\vec{h}\cdot\operatorname{curl}\vec{H}_0=&\frac{2}{3}\left(r\frac{d^2S_1}{dr^2}+4\frac{dS_1}{dr}\right)\left(r\frac{d^2s}{dr^2}+4\frac{ds}{dr}\right)\\ &-\frac{2}{3}\left(r\frac{d^2S_1}{dr^2}+4\frac{dS_1}{dr}\right)\left(r\frac{d^2s}{dr^2}+4\frac{ds}{dr}\right)P_2\\ &+2a^{-2}\left(r^2\frac{dT_3}{dr}+3rT_3\right)\left(r\frac{d^2s}{dr^2}+4\frac{ds}{dr}\right)P_2^2\sin 2\phi\\ &-2a^{-2}\left(r^2\frac{dT_4}{dr}+3rT_4\right)\left(r\frac{d^2s}{dr^2}+4\frac{ds}{dr}\right)P_2^2\cos 2\phi\,.\end{aligned} \tag{26}$$

We thus see that the electromagnetic force considered gives rise to pressure of which the distribution is described with spherical surface harmonics $P_0$, $P_2$, $P_2^2\cos 2\phi$ and $P_2^2\sin 2\phi$.

In the next place, we have to examine the role of $\vec{\omega}_0\cdot\mathrm{curl}\,\vec{v}$. Since the velocities that give rise to the $S_1^0$ magnetic field through curl $(\vec{v}\wedge\vec{H}_0)$ in (13) are only the $S_2^0$, $S_2^{2c}$ and $S_2^{2s}$ types, it is sufficient to consider the following velocities;

$$\vec{v}=\vec{v}_1+\vec{v}_2+\vec{v}_3\,, \tag{27}$$

where

$$\vec{v}_1=\begin{cases}-6\xi_2(r)rP_2\\ -\left(r\dfrac{d\xi_2}{dr}+3\xi_2\right)r\dfrac{dP_2}{d\theta}\\ 0\,,\end{cases} \tag{28}$$

$$\vec{v}_2=\begin{cases}-6\xi_2^{2c}(r)rP_2^2\cos 2\phi\\ -\left(r\dfrac{d\xi_2^{2c}}{dr}+3\xi_2^{2c}\right)r\dfrac{\partial(P_2^2\cos 2\phi)}{\partial\theta}\\ -\left(r\dfrac{d\xi_2^{2c}}{dr}+3\xi_2^{2c}\right)r\dfrac{\partial(P_2^2\cos 2\phi)}{\sin\theta\partial\phi}\,,\end{cases} \tag{29}$$

$$\vec{v}_3=\begin{cases}-6\xi_2^{2s}(r)rP_2^2\sin 2\phi\\ -\left(r\dfrac{d\xi_2^{2s}}{dr}+3\xi_2^{2s}\right)r\dfrac{\partial(P_2^2\sin 2\phi)}{\partial\theta}\\ -\left(r\dfrac{d\xi_2^{2s}}{dr}+3\xi_2^{2s}\right)r\dfrac{\partial(P_2^2\sin 2\phi)}{\sin\theta\partial\phi}\,.\end{cases} \tag{30}$$

In that case, we obtain

$$\left.\begin{aligned}&\vec{\omega}_0\cdot\mathrm{curl}\,\vec{v}_1=0\,,\\ &\vec{\omega}_0\cdot\mathrm{curl}\,\vec{v}_2=2\omega r^2\left(\frac{d^2\xi_2^{2c}}{dr^2}+\frac{6}{r}\,\frac{d\xi_2^{2c}}{dr}\right)P_2^2\sin 2\phi\,,\\ &\vec{\omega}_0\cdot\mathrm{curl}\,\vec{v}_3=-2\omega r^2\left(\frac{d^2\xi_2^{2s}}{dr^2}+\frac{6}{r}\,\frac{d\xi_2^{2s}}{dr}\right)P_2^2\cos 2\phi\,.\end{aligned}\right\} \tag{31}$$

Finally, $\vec{g}$ may be assumed as

$$\vec{g}=\vec{g}_1+\vec{g}_2+\vec{g}_3\,, \tag{32}$$

where

$$\left.\begin{aligned}
\vec{g}_1 &= \begin{cases} F_2(r)P_2 \\ 0 \\ 0, \end{cases} \\
\vec{g}_2 &= \begin{cases} F_2^{2c}(r)P_2^2\cos 2\phi \\ 0 \\ 0, \end{cases} \\
\vec{g}_3 &= \begin{cases} F_2^{2s}(r)P_2^2\sin 2\phi \\ 0 \\ 0, \end{cases}
\end{aligned}\right\} \tag{33}$$

while forces of other types have nothing to do with the present problem.

Introducing (24), (25), (26), (31) and (33) to the righthand-side of (15), we obtain the differential equation for the pressure as follows;

$$\nabla^2 p = f_0 + f_2 P_2 + f_2^{2c} P_2^2 \cos 2\phi + f_2^{2s} P_2^2 \sin 2\phi \tag{34}$$

where

$$\left.\begin{aligned}
f_0 &= -(4\pi)^{-1}\frac{4}{3}S_1\left(r\frac{d^3s}{dr^3}+7\frac{d^2s}{dr^2}+\frac{8}{r}\frac{ds}{dr}\right), \\
f_2 &= -(4\pi)^{-1}\frac{4}{3}S_1\left(r\frac{d^3s}{dr^3}+4\frac{d^2s}{dr^2}-\frac{4}{r}\frac{ds}{dr}\right)+\frac{d(r^2F_2)}{r^2dr}, \\
\begin{pmatrix} f_2^{2c} \\ f_2^{2s} \end{pmatrix} &= \pm(4\pi)^{-1}2(r/a)^2\begin{pmatrix} T_4 \\ T_3 \end{pmatrix}\left(r\frac{d^3s}{dr^3}+12\frac{d^2s}{dr^2}+\frac{28}{r}\frac{ds}{dr}\right) \\
&\quad \mp 4\rho\omega\begin{pmatrix} \dfrac{d^2\xi_2^{2s}}{dr^2}+\dfrac{6}{r}\dfrac{d\xi_2^{2s}}{dr} \\ \dfrac{d^2\xi_2^{2c}}{dr^2}+\dfrac{6}{r}\dfrac{d\xi_2^{2c}}{dr} \end{pmatrix}+\begin{pmatrix} \dfrac{d(r^2F_2^{2c})}{r^2dr} \\ \dfrac{d(r^2F_2^{2s})}{r^2dr} \end{pmatrix},
\end{aligned}\right\} \tag{35}$$

in which it is assumed, for the sake of simplicity, that $S_1$, $T_3$, and $T_4$ are independent of $r$.

The solution of (34) can be expressed as

$$p = \sum_{n,m} q_n^m(r) Y_n^m , \tag{36}$$

where

$$Y_n^m = P_n^m(\cos\theta)\begin{matrix}\cos \\ \sin\end{matrix} m\phi .$$

Since $\nabla^2 p$ can be written as

$$\nabla^2 p=\sum_{n,m}\left\{\frac{1}{r^2}\frac{d}{dr}\left(r^2\frac{d}{dr}\right)-\frac{n(n+1)}{r^2}\right\}q_n^m(r)Y_n^m\,,$$

we have a set of ordinary differential equations such as

$$\left.\begin{aligned}&\frac{1}{r}\frac{d}{dr}\left(r^2\frac{d}{dr}\right)q_0^0=f_0\,,\\&\left\{\frac{1}{r^2}\frac{d}{dr}\left(r^2\frac{d}{dr}\right)-\frac{6}{r^2}\right\}\begin{pmatrix}q_2^0\\q_2^{2c}\\q_2^{2c}\end{pmatrix}=\begin{pmatrix}f_2\\f_2^{2c}\\f_2^{2s}\end{pmatrix}.\end{aligned}\right\}\tag{37}$$

The solutions of (37) which remain finite at $r=0$ are given as

$$\left.\begin{aligned}q_0^0&=(4\pi)^{-1}\left\{L_0^0-\frac{4}{3}S_1\left(r\frac{ds}{dr}+3s\right)\right\}\,,\\q_2^0&=(4\pi)^{-1}\left\{(r/a)^2L_2^0+\frac{4}{3}S_1 r\frac{ds}{dr}\right\}\\&\quad+\frac{1}{5}\left\{3r^2\int_0^r r^{-2}F_2dr+2r^{-3}\int_0^r r^3F_2dr\right\}\,,\\\begin{pmatrix}q_2^{2c}\\q_2^{2s}\end{pmatrix}&=(4\pi)^{-1}\left\{(r/a)^2\begin{pmatrix}L_2^{2c}\\L_2^{2s}\end{pmatrix}\pm\begin{pmatrix}T_4\\T_3\end{pmatrix}\left(r^3\frac{ds}{dr}+4r^2s-2r^{-3}\int_0^r r^4s\,dr\right)\right\}\\&\quad\mp 4\rho\omega r^2\begin{pmatrix}\xi_2^{2s}\\\xi_2^{2c}\end{pmatrix}+\frac{1}{5}\left\{3r^2\int_0^r r^{-2}\begin{pmatrix}F_2^{2c}\\F_2^{2s}\end{pmatrix}dr+2r^{-3}\int_0^r r^3\begin{pmatrix}F_2^{2c}\\F_2^{2s}\end{pmatrix}dr\right\}\,,\end{aligned}\right\}\tag{38}$$

where $L_0^0$, $L_2^0$, $L_2^{2c}$ and $L_2^{2s}$ are constants which shall be determined by the boundary conditions.

## 4. Velocity and magnetic field

Since we can obtain the solution for pressure, we go back to (14) in which grad $p$ is calculated from (36) together with (38).

If we ignore the $T_1^0$, $T_3^0$, $T_3^{2c}$ and $T_3^{2s}$ velocities which are derived from curl $\vec{H}_0\wedge\vec{h}$, (14) leads to the equations for the $T_2^0$, $T_2^{2c}$ and $T_2^{2s}$ velocities which are readily obtained as follows;

$$D\rho\xi_2=(4\pi a^2)^{-1}\left(\frac{1}{3}L_2^0-\frac{2}{3}a^2S_1r^{-1}\frac{ds}{dr}\right)+\frac{1}{5}\left(\int_0^r r^{-2}F_2dr-r^{-5}\int_0^r r^3F_2\,dr\right)\,,\tag{39}$$

$$D\rho\xi_2^{2c}=(4\pi a^2)^{-1}\left(\frac{1}{3}L_2^{2c}+2T_4r^{-5}\int_0^r r^4sdr\right)-\frac{2}{3}\rho\omega\left(r\frac{d\xi_2^{2s}}{dr}+3\xi_2^{2s}\right)$$
$$+\frac{1}{5}\left(\int_0^r r^{-2}F_2^{2c}dr-r^{-5}\int_0^r r^3F_2^{2c}dr\right), \tag{40}$$

$$D\rho\xi_2^{2s}=(4\pi a^2)^{-1}\left(\frac{1}{3}L_2^{2s}-2T_3r^{-5}\int_0^r r^4sdr\right)+\frac{2}{3}\rho\omega\left(r\frac{d\xi_2^{2c}}{dr}+3\xi_2^{2c}\right)$$
$$+\frac{1}{5}\left(\int_0^r r^{-2}F_2^{2s}dr-r^{-5}\int_0^r r^3F_2^{2s}dr\right). \tag{41}$$

It is also easily seen that the pressure gradient which does not depend on $\theta$ and $\phi$ is cancelled by the electromagnetic force derived from curl $\vec{h}\wedge\vec{H}_1$. $L_2^0$, $L_2^{2c}$ and $L_2^{2s}$ are to be determined by the conditions that the normal component of the velocities should vanish at $r=0$.

If we calculate curl $(\vec{V}_0\wedge\vec{h})$ and curl $(\vec{v}\wedge\vec{H}_0)$ and pick up only the $S_1^0$ magnetic field, (13) gives

$$Ds-(4\pi\sigma)^{-1}\left(\frac{d^2s}{dr^2}+\frac{4}{r}\frac{ds}{dr}\right)=-\frac{6}{5}S_1\left(r\frac{d\xi_2}{dr}+5\xi_2\right)-\frac{216}{5}a^{-2}r^2(T_4\xi_2^{2c}-T_3\xi_2^{2s}). \tag{42}$$

The equations (39), (40), (41) and (42) can be regarded as the simultaneous integro-differential equations for $\xi_2$, $\xi_2^{2c}$, $\xi_2^{2s}$ and $s$.

## 5. Approximate solution of the integro-differential equations

Since the integro-differential equations are complicated, it seems unlikely that exact solutions can be obtained. As has been done in the previous papers[1),3)], let us assume

$$s=\sum_n a_n(r/a)^n,\quad \xi_2^{2c}=\sum_n A_n(r/a)^n,\quad \xi_2^{2s}=\sum_n B_n(r/a)^n. \tag{43}$$

We shall further assume $F_2=F_2^{2s}=0$. Since the steady state includes the $S_2^{2c}$ motion, the assumption may be justified if we emphasize small fluctuations of the force which drives only the $S_2^{2c}$ motion. $F_2^{2c}$ is also assumed to be expressed as

$$F_2^{2c}=\sum_n \zeta_n(r/a)^{n+1}. \tag{44}$$

When we introduce (43) into (42) from which $\xi_2$ has been eliminated by use of (39), we obtain

$$4\pi\rho D^2a^2\sum_n a_n\left(\frac{r}{a}\right)^n-\rho D\sigma^{-1}\sum_n n(n+3)a_n\left(\frac{r}{a}\right)^{n-2}$$
$$=-\frac{6}{5}S_1\left(\frac{5}{3}L_2^0-\frac{2}{3}S_1\sum_n n(n+3)\left(\frac{r}{a}\right)^{n-2}\right)$$
$$-\frac{216}{5}(4\pi\rho Da^2)\left(T_4\sum_n A_n\left(\frac{r}{a}\right)^{n+2}-T_3\sum_n B_n\left(\frac{r}{a}\right)^{n+2}\right). \tag{45}$$

From (40) and (41), we also have

$$D\rho\sum_n A_n\left(\frac{r}{a}\right)^n=(4\pi a^2)^{-1}\left(\frac{1}{3}L_2^{2c}+2T_4\sum_n\frac{a_n}{n+5}\left(\frac{r}{a}\right)^n\right)$$
$$-\frac{2}{3}\rho\omega\sum_n(n+3)B_n\left(\frac{r}{a}\right)^n+a^{-1}\sum_n\frac{\zeta_n}{n(n+5)}\left(\frac{r}{a}\right)^n, \tag{46}$$

$$D\rho\sum_n B_n\left(\frac{r}{a}\right)^n=(4\pi a^2)^{-1}\left(\frac{1}{3}L_2^{2s}-2T_3\sum_n\frac{a_n}{n+5}\left(\frac{r}{a}\right)^n\right)$$
$$+\frac{2}{3}\rho\omega\sum_n(n+3)A_n\left(\frac{r}{a}\right)^n, \tag{47}$$

in which we can write $L_2^0$, $L_2^{2c}$ and $L_2^{2s}$ in a form of series with respect to $a_n$ by applying the boundary conditions. Eliminating $L_2^0$, $L_2^{2c}$ and $L_2^{2s}$, the above three equations become

$$4\pi\rho D^2a^2\sum_n a_n\left(\frac{r}{a}\right)^n-\rho D\sigma^{-1}\sum_n n(n+3)a_n\left(\frac{r}{a}\right)^{n-2}$$
$$=-\frac{4}{5}S_1^2\sum_n a_n\left\{5-(n+3)\left(\frac{r}{a}\right)^{n-2}\right\}n$$
$$-\frac{216}{5}(4\pi\rho Da^2)\sum_n(T_4A_n-T_3B_n)\left(\frac{r}{a}\right)^{n+2}, \tag{48}$$

$$4\pi\rho Da^2\sum_n A_n\left(\frac{r}{a}\right)^n=2T_4\sum_n\frac{a_n}{n+5}\left\{\left(\frac{r}{a}\right)^n-1\right\}$$
$$-\frac{2}{3}(4\pi\rho\omega a^2)\sum_n B_n\left\{(n+3)\left(\frac{r}{a}\right)^n-n\right\}$$
$$+4\pi a\sum_n\frac{\zeta_n}{n(n+5)}\left\{\left(\frac{r}{a}\right)^n-1\right\}, \tag{49}$$

$$4\pi\rho Da^2\sum_n B_n\left(\frac{r}{a}\right)^n=-2T_3\sum_n\frac{a_n}{n+5}\left\{\left(\frac{r}{a}\right)^n-1\right\}$$

$$+\frac{2}{3}(4\pi\rho\omega a^2)\sum_n A_n\left\{(n+3)\left(\frac{r}{a}\right)^n-n\right\}. \qquad (50)$$

By equating the coefficients of the corresponding terms of both the sides of these equations, we obtain

$$\left.\begin{aligned}
&4\pi\rho D^2a^2a_0-10\rho D\sigma^{-1}a_2=-16S_1^2a_4\,,\\
&4\pi\rho D^2a^2a_2-28\rho D\sigma^{-1}a_4=\frac{112}{5}S_1^2a_4-\frac{216}{5}(4\pi\rho a^2D)(T_4A_0-T_3B_0)\,,\\
&4\pi\rho Da^2A_0=-2T_4\left(\frac{a_2}{7}+\frac{a_4}{9}\right)-\frac{2}{3}(4\pi\rho\omega a^2)(3B_0-2B_2-4B_4)\\
&\qquad\qquad -4\pi a\left(\frac{\zeta_2}{14}+\frac{\zeta_4}{36}\right),\\
&4\pi\rho Da^2A_2=2T_4\frac{a_2}{7}-\frac{10}{3}(4\pi\rho\omega a^2)B_2+4\pi a\frac{\zeta_2}{14}\,,\\
&4\pi\rho Da^2A_4=2T_4\frac{a_4}{9}-\frac{14}{3}(4\pi\rho\omega a^2)B_4+4\pi a\frac{\zeta_4}{36}\,,\\
&4\pi\rho Da^2B_0=2T_3\left(\frac{a_2}{7}+\frac{a_4}{9}\right)+\frac{2}{3}(4\pi\rho\omega a^2)(3A_0-2A_2-4A_4)\,,\\
&4\pi\rho Da^2B_2=-2T_3\frac{a_2}{7}+\frac{10}{3}(4\pi\rho\omega a^2)A_2\,,\\
&4\pi\rho Da^2B_4=-2T_3\frac{a_4}{9}+\frac{14}{3}(4\pi\rho\omega a^2)A_4\,,
\end{aligned}\right\} \qquad (51)$$

where $a_n$'s, $A_n$'s, $B_n$'s and $\zeta_n$'s for $n>4$ are ignored. It is easily seen that $a_n$'s, $A_n$'s, $B_n$'s and $\zeta_n$'s for odd $n$ vanish. It should be also noted that $\zeta_0$ is taken to be zero in order to avoid the term for $n=0$ which otherwise becomes indeterminate.

We have one more equation

$$3a_0+5a_2+7a_4=0\,, \qquad (52)$$

which is deduced from the condition that the magnetic field is continuous at $r=a$.

Since the force is regarded as that caused by buoyancy, it must

be zero at the boundary of the core. This implies $\zeta_2+\zeta_4=0$ for the present approximation, so that

$$F_2^{2c}=\zeta_2\left(\frac{r}{a}\right)^3\left\{1-\left(\frac{r}{a}\right)^2\right\}. \tag{53}$$

Now we are in a position to solve (51) together with (52) in regard to $a_0$, $a_2$, $a_4$, $A_0$, $A_2$, $A_4$, $B_0$, $B_2$ and $B_4$. After some calculations we obtain

$$\left.\begin{aligned} a\rho\Phi(D)a_0 &=\kappa\left[\frac{54}{7}\left(DT_4-\frac{10}{3}\omega T_3\right)\left(D^2+\left(\frac{14}{3}\omega\right)^2\right)\right. \\ &\quad \left.-3\left(DT_4-\frac{14}{3}\omega T_3\right)\left(D^2+\left(\frac{10}{3}\omega\right)^2\right)\right]\zeta_2, \\ a_2 &=\frac{2}{5}\kappa^{-1}Da_0, \\ a_4 &=-\left(\frac{3}{7}+\frac{2}{7}\kappa^{-1}D\right)a_0, \end{aligned}\right\} \tag{54}$$

where

$$\begin{aligned} \Phi(D)=D^6&+5\kappa D^5+\left(\frac{296}{9}\omega^2-\frac{48}{35}\frac{T_3^2+T_4^2}{\pi\rho a^2}+\frac{15}{2}\kappa^2\right)D^4 \\ &+\kappa\left(\frac{1480}{9}\omega^2+\frac{18}{7}\frac{T_3^2+T_4^2}{\pi\rho a^2}\right)D^3 \\ &+\left(\frac{19600}{81}\omega^2-\frac{15168}{315}\frac{T_3^2+T_4^2}{\pi\rho a^2}+\frac{740}{3}\kappa^2\right)\omega^2D^2 \\ &+\kappa\left(\frac{98000}{81}\omega^2+\frac{200}{7}\frac{T_3^2+T_4^2}{\pi\rho a^2}\right)\omega^2D+\frac{16000}{9}\kappa^2\omega^4 \end{aligned} \tag{55}$$

and

$$\kappa=(\pi\sigma a^2)^{-1}. \tag{56}$$

In the calculation, $S_1$ is assumed as zero, because, in the earth's dynamo, the toroidal fields are believed to be larger than the poloidal one.

The equations (54) seem still complicated. We shall make further simplifications on the basis of physical consideration. We may first put

$$T_3=T_4=T \tag{57}$$

for the order-of-magnitude estimate. Taking $\omega=7.5\times10^{-5}\,sec^{-1}$, $a=3.5$

$\times 10^8\,cm$ and $\rho=10\,g/cm^3$, we see that the relation

$$\omega^2 \gg \frac{T^2}{\pi\rho a^2} \tag{58}$$

holds for $T<10^5\,gauss$. Since $T$ is thought to amount to the order of $10\,gauss$ in the core, (58) is safely assumed.

If $\sigma=10^{-6}\,e.m.u.$, which is usually believed for the core, we have

$$\kappa=2.6\times10^{-12}\,sec^{-1}\,,$$

hence

$$\omega \gg \kappa\,. \tag{59}$$

Let us consider a variation of a 100-*year* period. In that case, we may put

$$D=i\alpha \quad \alpha=2.0\times10^{-9}\,sec^{-1}\,, \tag{60}$$

whence we see that

$$\alpha \gg \kappa\,. \tag{61}$$

Taking into account (57), (58), (59) and (61), the solutions can be simplified as

$$\left.\begin{aligned} a_0&=0\,,\\ a_2&=\frac{6T}{5a\rho}\frac{\frac{11}{7}D^3-\frac{82}{21}\omega D^2+\frac{404}{9}\omega^2 D-\frac{3640}{27}\omega^3}{D\left(D^4+\frac{296}{9}\omega^2D^2+\frac{19600}{81}\omega^4\right)}\zeta_2\,,\\ a_4&=-\frac{5}{7}a_2\,. \end{aligned}\right\} \tag{62}$$

If $\zeta_2$ is given as a function of time, the second equation of (62) is the differential equation of forced oscillation for $a_2$. As is well known in the case of forced oscillation of a simple pendulum, $a_2$ is obtained by putting $D=i\alpha$ when the free oscillations are damped out. Assuming a 100-*year* period, we obtain

$$|a_2|=1.3\times10^3\,T\zeta_2 \tag{63}$$

where $|a_2|$ denotes the modulus of $a_2$, while $a$ and $\rho$ are taken as before.

## 6. Driving force and thermal field

Now it is possible from (63) to obtain the coefficients of the driving force which causes the 100-*year* period secular variation of the $S_1^0$ magnetic field. (63) leads to

$$\zeta_2 = 7.9 \times 10^{-4} \frac{|a_2|}{T} . \tag{64}$$

In the following, let us estimate the order of $\zeta_2$. First of all, $|a_2|$ should be estimated. According to the repeated analyses of the earth's magnetic field, it is well known that the strength of the earth's dipole underwent a decrease amounting to $0.5 \times 10^{25}$ *e.m.u.* during the past 100 *years*. Although it is not known whether or not the change is periodic, we may, for a rough estimate, suppose that there is a 100-*year* period secular variation of which the amplitude is 0.01 *gauss* at the pole. In order to have this order of magnetic field at the earth's surface, an amplitude of 0.07 *gauss* should take place at the core-mantle boundary. This figure must become slightly larger if we take the shielding effect of the mantle into account. Accordingly, $s$ in (16) takes a value around 0.09 *gauss*. From the third relation of (62), $a_2$ is then estimated at 0.3 *gauss*.

As for the steady magnetic fields of the earth's dynamo, Bullard[2] estimated that the $T_2^0$ field amounts to 480 *gauss*. On the other hand the $S_1^0$ field would be only a few *gauss*. The $T_2^{2c}$ and $T_2^{2s}$ fields would take intermediate intensities. From these considerations, a probable estimate of $|a_2|/T$ would be

$$|a_2|/T \sim 10^{-2} , \tag{65}$$

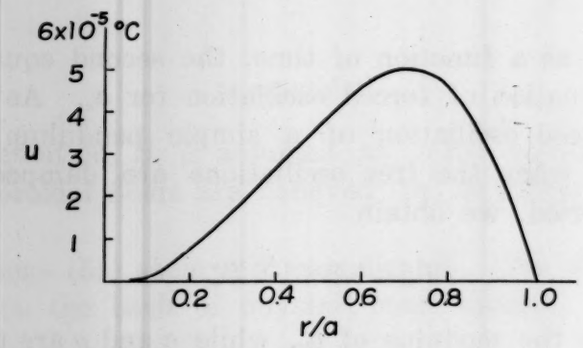


Fig. 1. The distribution of $u$.

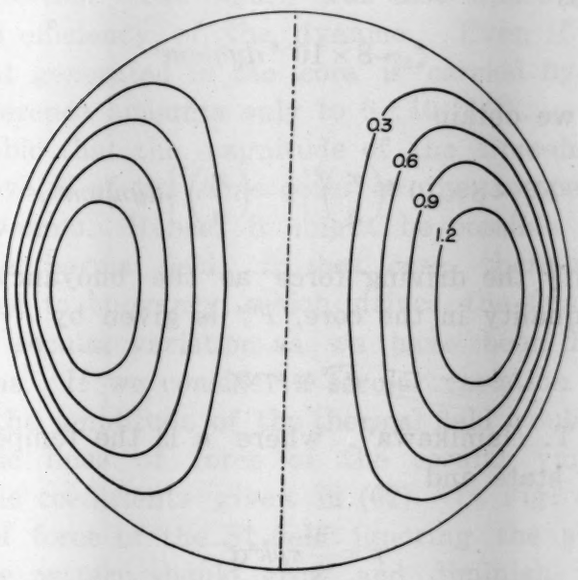


Fig. 2. The distribution pattern of temperature departure in the $\phi=0$ meridian plane in units of $10^{-4}°C$.

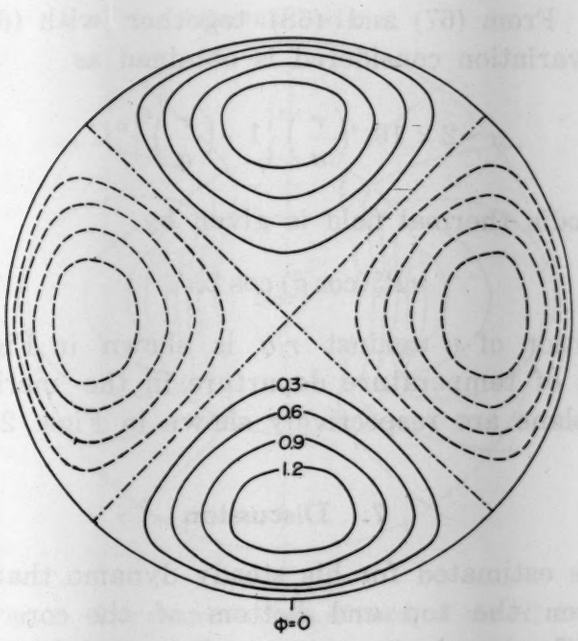


Fig. 3. The distribution pattern of temperature departure in the equatorial plane in units of $10^{-4}°C$.

so that (64) gives

$$\zeta_2 \sim 8\times 10^{-6}\, dyn/cm^3 \tag{66}$$

and, from (53), we obtain

$$F_2^{2c} \sim 8\times 10^{-6}\left(\frac{r}{a}\right)^3\left\{1-\left(\frac{r}{a}\right)^2\right\} dyn/cm^3 . \tag{67}$$

If we identify the driving force as the buoyancy one due to the temperature inequality in the core, $F_2^{2c}$ is given by

$$F_2^{2c}=\rho\gamma u r \tag{68}$$

as discussed by T. Namikawa[4], where $u$ is the temperature departure from the steady state and

$$\gamma=\frac{4}{3}\pi\rho k^2\alpha' . \tag{69}$$

$k^2$ and $\alpha'$ denote respectively the universal constant of gravitation and coefficient of cubical expansion, the latter being estimated by Bullard[2] at $4.5\times 10^{-6}{}^\circ/C$. From (67) and (68) together with (69), $u$ responsible for the secular variation considered is obtained as

$$u \sim 2\times 10^{-4}\left(\frac{r}{a}\right)^2\left\{1-\left(\frac{r}{a}\right)^2\right\}{}^\circ C , \tag{70}$$

so that the periodic thermal field is given by

$$u P_2^2(\cos\theta)\cos 2\phi .$$

The distribution of $u$ against $r/a$ is shown in Fig. 1. Meanwhile the distributions of temperature departure in the meridian plane $\phi=0$ and equatorial plane are respectively shown in Figs. 2 and 3.

## 7. Discussion

Bullard[2] has estimated for his steady dynamo that the temperature difference between the top and bottom of the core would be $450^\circ C$. However, the difference in temperature between rising and falling convective currents has been also estimated by him at $3\times 10^{-4}{}^\circ C$ from the consideration that the buoyancy forces must be comparable with the

4) T. NAMIKAWA, *Journ. Geomagn. Geoelectr.*, **9** (1957), 182.

electromagnetic forces. The figure was also approved by examining thermodynamical efficiency of the dynamo. Even if we assume that most of the heat generated in the core is carried by convection, the temperature difference amounts only to $6\times10^{-3}°C$[5].

It is noticeable that the magnitude of the time-dependent thermal field studied above is of the same order as the temperature difference of the steady dynamo. Hence, it might be possible to expect such a fluctuation in the thermal field. In that case, there arises a time-dependent force due to buoyancy, which drives the fluid motion causing the geomagnetic secular variation as we have been discussing in the foregoing sections. If we consider a secular variation of longer period, 1000 *years* say, the amplitude of the thermal field would become smaller.

The magnetic lines of force of the secular variation are easily obtained with the coefficients given in (62). In Fig. 4 are shown the magnetic lines of force of the $S_1^0$ field ignoring the shielding effect in the mantle. The pattern should grow and diminish with a 100-*year* period. It is also possible to obtain the fluid motions though no attempts of that sort have been made.

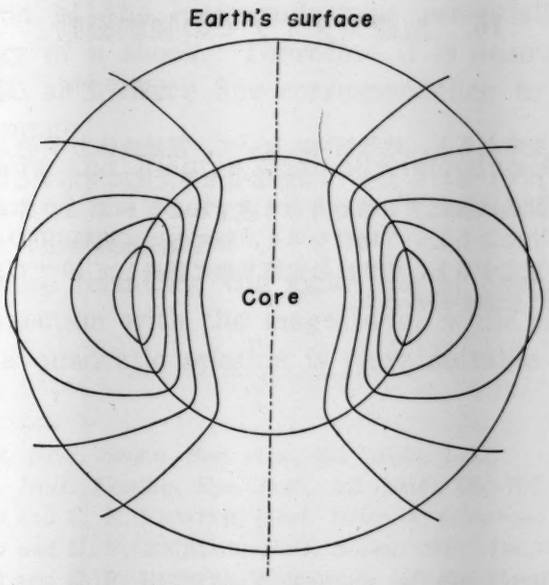


Fig. 4. The magnetic lines of force of the $S_1^0$ field.

No account is taken of the cause of the time-dependent thermal field supposed here. It might be due to oscillations caused by couplings

5) E. C. BULLARD, *Proc. Roy. Soc. London A*, **197** (1949), 433.

between magnetic fields, fluid motions and heat conduction. This point should be studied later.

## 8. Concluding remarks

A theory that the geomagnetic secular variations might be caused by forced oscillations of magneto-hydrodynamical nature is tried in this paper. The oscillations are treated as small perturbations superposing on the steady state of the earth's dynamo which is at work in the core. From an extremely simplified treatment, the buoyancy force which gives rise to the hypothetical 100-*year* period secular variation of the $S_1^0$ field is obtained. If the amplitude of the $S_1^0$ field is assumed as 1000 *gammas* at the pole, the corresponding temperature departure from the steady state must amount to the order of $10^{-4}°C$ at its maximum. This figure may be acceptable if we take into account the thermal state of the steady dynamo as has been discussed by Bullard.

---

## 16. 地磁気ダイナモの強制振動

地震研究所　力　武　常　次

地球回転のコリオリ力を考えると，地球核内において，電磁流体力学的自由振動は起りにくいことが筆者によつて指摘されている．したがつて地磁気永年変化に対応する核内の電磁流体力学的過程を考えるためには，時間的に変化する駆動力を考慮する必要がある．本報においては，その駆動力は温度差に起因する浮力によるという場合を考え，極において振幅 1000 ガンマ，周期 100 年の双極子磁場の永年変化を想定すると，核内には定常状態に重畳して $10^{-4}°C$ 程度の振幅をもつ温度差の分布があればよいという結論が得られた．

---

BULLETIN OF THE EARTHQUAKE
RESEARCH INSTITUTE
Vol. 37 (1959), pp. 265-277

# 17. On the Spectral Structure of Earthquake Waves.

## —Its Influence on Magnitude Scale—

By Tosimatu MATUMOTO,

Earthquake Research Institute.

(Read Nov. 25, 1958.—Received Mar. 31, 1959.)

## 1. Introduction

To express the scale of an earthquake, the quantity " magnitude " is defined, which was originary proposed by C. F. Richter[1] in such a way as the logarithm of the maximum trace amplitude, expressed in micron, with which the standard torsion seismometer ($T_0=0.8$ sec., $V=2800$, $h=0.8$) would register that shock at an epicentral distance of 100 km.

H. Kawasumi[2] proposed another way to express the magnitude of a shock. His magnitude scale $M_k$ is determined by the intensity (in Japanses scale) at an epicentral distance of 100 km.

The conception of the magnitude was essentially connected with that of the energy of a shock. Therefore it is desireable to define the magnitude scale so as to have fine correspondence to the energy scale covering a wide range.

Since Gutenberg and Richter originally introduced the formula relating the magnitude and the energy of a shock, not a few formulas have been proposed for this relation[3)-9)].

In most of these formulas, the logarithm of energy is considered to have a linear connection with the magnitude, while Gutenberg recently pointed out that a quadratic relation is more suitable than a linear one.

---

1) C. F. RICHTER, *Bull. Seism. Soc. Am.*, **25** (1935), 1-32.
2) H. KAWASUMI, *Bull. Earthq. Res. Inst.*, **12** (1934), 660-705.
3) B. GUTENBERG and C. F. RICHTER, *Gerl. Beitr. z. Geophys.*, **47** (1936), 73-131.
4) B. GUTENBERG and C. F. RICHTER, *Bull. Seism. Soc. Am.*, **32** (1942), 163-191.
5) B. GUTENBERG and C. F. RICHTER, *Seismicity of the Earth. 1st Ed.* (Princeton, 1949).
6) D. FILIPPO and L. MARCELL, *Ann. di Geofisica*, **3** (1950), 3337-348.
7) B. GUTENBERG and C. F. RICHTER, *Seismicity of the Earth. 2nd Ed.* (Princeton, 1954).
8) M. BÅTH, *Trans. Am. Geophys. Union*, **36** (1955), 861-765.
9) B. GUTENBERG and C. F. RICHTER, *Bull. Seism. Soc. Am.*, **46** (1956), 105-145.

It is an interesting problem what is the most applicable equation about the energy-magnitude relation, and whether or no any warp of the magnitude scale exist refering to the energy scale.

Though the method of the magnitude determination above mentioned is brief and convenient, the nature of earthquake waves are very complicated. The spectral structure of earthquake waves are greatly affected by magnitude, eipcentral distance, mechanism of occurrence, ray paths, characteristics of the seismometers and other reasons. Owing to this complicated character of the earthquake waves, the nature of the maximum trace amplitude is not so simple. Therefore it looks worth further investigating how the maximum amplitude connected with the spectral structure of the earthquake waves.

In this paper, the definition of the magnitude is reexamined, and the preliminary step of the consideration on the spectral structure has involved.

## Notation

$a(\Delta)$ =the maximum trace amplitude (expressed in micron) registered by the standard torsion seismometer at an epicentral distance of $\Delta$ km.

$a_0(\Delta)$ =the maximum trace amplitude caused by a shock of magnitude 0.

$a_M^{(j)}(\Delta)$ =the maximum trace amplitude caused by a shock of magnitude $M$, and registered by the j-th seismometer.

$A(\Delta)$ =the maximum ground motion observed at the distance of $\Delta$ km.

$\Delta$ =the epicentral distance.

$f^{(j)}(T)$ =the dynamical characteristics of the j-th seismometer.

$g(T, \Delta)$ =the factor of diminution of an earthquake wave.

$h^{(j)}$ =the damping constant of the j-th seismometer.

$M$ or $M_G$ =the earthquake magnitude defined by Gutenberg and Richter.

$M_{ch}$ =the earthquake magnitude derived by Tsuboi.

$M_k$ =the earthquake magnitude defined by Kawasumi.

$S_M(T)$ =the spectrum of the earthquake wave caused by a shock of magnitude $M$ and measured at the origin.

$s_M(T, \Delta)$ =the spectrum of the earthquake wave measured at the distance of $\Delta$ km.

$s_M^{(j)}(T, \Delta)$ =the spectrum of the observed earthquake wave recorded by the j-th seismometer at the distance of $\Delta$ km.

$T$ =the period of the wave.
$T_0$ =the period of the maximum ground motion.
$T^{(j)}$ =the natural period of j-th seismometer.
$V^{(j)}$ =the statical magnification of j-th seismometer.

## 2. Richter's Assumption

From Richter's definition, the magnitude $M$ is expressed as:

$$M=\log a(100)\ . \tag{1}$$

To expand this definition for arbitrary distances, the reduction of the amplitude measured at the distance of $\Delta$ km is needed. Richter set up an important assumption that the diminution of the amplitude is only the function of the distance and that the ratio of the diminution has no connection with the size of a shock.

Standing on this assumption, he determined the diminished amplitude $a_0(\Delta)$ caused by a shock of magnitude zero for the range of the distance from 25 to 600 km.
Using $a_0(\Delta)$, the magnitude is expressed as:

$$M=\log a(\Delta)-\log a_0(\Delta)\ . \tag{2}$$

However, it is known that the predominant period of the earthquake wave is affected by the size of the earthquake, and also the diminution is the function of the period of the waves as well as of the distance. These facts disagree with Richter's assumption.

To make this problem clear, we want to consider the spectrum of observed seismic waves $s_M(T, \Delta)$, which is derived from the spectrum of radiated seismic wave $S_M(T)$ as follows:

$$s_M(T, \Delta)=g(T, \Delta)S_M(T)\ . \tag{3}$$

We put an assumption on the spectral structure $s_M(T, \Delta)$, in which the period of the maximum intensity of this spectrum is given by the period corresponding to that of maximum amplitude of the wave. Even when this assumption is not satisfied in the whole duration of the wave, it is satisfactory in the neighbouring part of the maximum amplitude.

The maximum trace amplitude $a_i(\Delta)$, which originated by a shock of magnitude $M=i$, is thus

$$a_i(\Delta)=k[V\cdot g(T, \Delta)S_i(T)]_{\max}\ , \tag{4}$$

where $k$ is the constant relating the interval of the analysed time series. From the equation (1),

$$M_{i+1}=\log k[V\cdot g(T,\ \Delta)S_{i+1}(T)]_{\max}\ ,$$

and

$$M_i=\log k[V\cdot g(T,\ \Delta)S_i(T)]_{\max}\ .$$

Therefore

$$\log\frac{[g(T,\ 100)S_{i+1}(T)]_{\max}}{[g(T,\ 100)S_i(T)]_{\max}}=1\ . \qquad (5)$$

Equation (5) indicate the condition which derived from Richter's definition at the epicentral distance of 100 km.
Similarly following relation is hold at the arbitray distance:

$$\log\frac{[g(T,\ \Delta)S_{i+1}(T)]_{\max}}{[g(T,\ \Delta)\ S_i(T)]_{\max}}=1\ . \qquad (6)$$

In the following, we want to try schematic consideration about some simplified models. In each model, the assumptions are set up as follows:

*Model A*

At the origin, the spectra $S_i(T)$ of the respective shocks have quite similar forms and only differ in their intensity according to the magnitude of the shock. In each case, the specrral structure is derived by the equation such as:

$$S_i(T)=10^iS_0(T)\ , \qquad (7)$$

where $S_0(T)$ means the spectrum of the waves caused by the shock of magnitude $M=0$.

The factor of the diminution is the function of both the distance and the period.

*Model B*

The spectra $S_i(T)$ change their forms according to the magnitude, and also the predominant periods $T_0$ corresponding to the maximum intensity are varied by the magnitude. In this model, the diminution factor is assumed to be the function of the distance only.

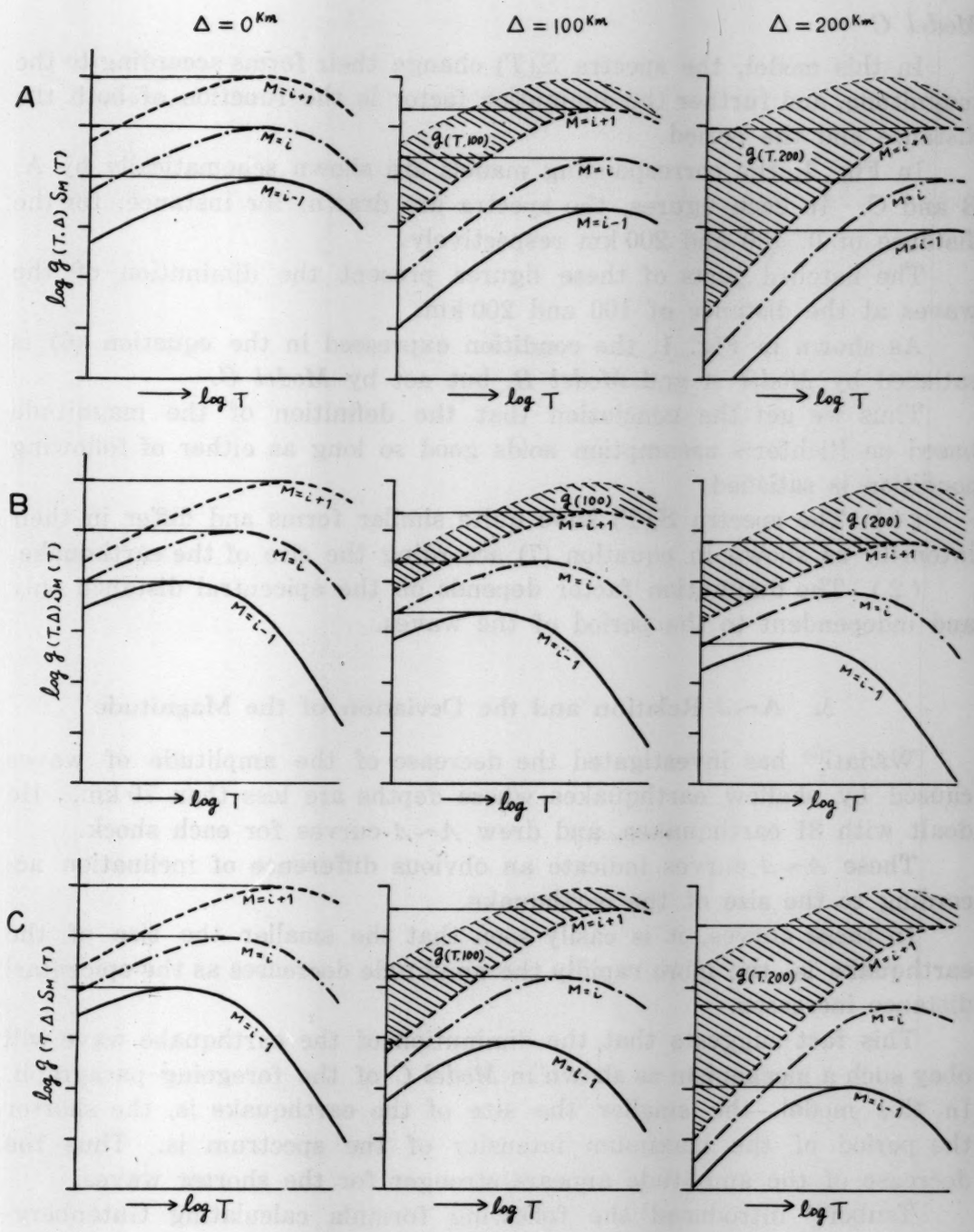


Fig. 1. Schematic models of the spectral transformation.

*Model C*

In this model, the spectra $S_i(T)$ change their forms according to the magnitude, and further the diminution factor is the function of both the distance and the period.

In Fig. 1, the corresponding madels are shown schematically by A, B and C. In each figures, the spectra are drawn, for instance, for the distance of 0, 100 and 200 km respectively.

The hatched parts of these figures present the diminution of the waves at the distance of 100 and 200 km.

As shown in Fig. 1, the condition expressed in the equation (6) is satisfied by *Model A* and *Model B*, but not by *Model C*.

Thus we get the conclusion that the definition of the magnitude based on Richter's assumption holds good so long as either of following condition is satisfied:

(1) The spectra $S_i(T)$ have quite similar forms and differ in their intensity as shown in equation (7) according the size of the earthquake.

(2) The diminution factor depends on the epicentral distance only and independent to the period of the waves.

### 3. $A\sim\Delta$ Relation and the Deviation of the Magnitude

Wadati[10] has investigated the decrease of the amplitude of waves caused by shallow earthquakes whose depths are less than 70 km. He dealt with 31 earthquakes, and drew $A\sim\Delta$ curves for each shock.

These $A\sim\Delta$ curves indicate an obvious difference of inclination according to the size of the earthquake.

In these curves, it is easily seen that the smaller the size of the earthquake is, the more rapidly the amplitude decreases as the epicentarl distance increases.

This fact suggests that the diminution of the earthquake wave will obey such a mechanism as shown in *Model C* of the foregoing paragraph. In this model, the smaller the size of the earthquake is, the shorter the period of the maximum intensity of the spectrum is. Thus the decrease of the amplitude appears stronger for the shorter waves.

Tsuboi[11] introduced the following formula calculating Gutenberg-Richter's magnitude for the earthquakes occurring in or near Japan:

$$M_{c\lambda}=1.73\log\Delta+\log A-0.83 \qquad (8)$$

10) K. WADATI, *Geophys. Mag.*, **4** (1931), 231–283.
11) C. TSUBOI, *Zisin, II*, **7** (1954), 185–193.

Tsuboi indicated $M_{ch}$ shows good agreement with $M_G$.

It is interesting for us to know the discrepancy between Wadati's $A \sim \Delta$ curves and $A \sim \Delta$ curves derived by the equation (8) which based on Richter's assumption.

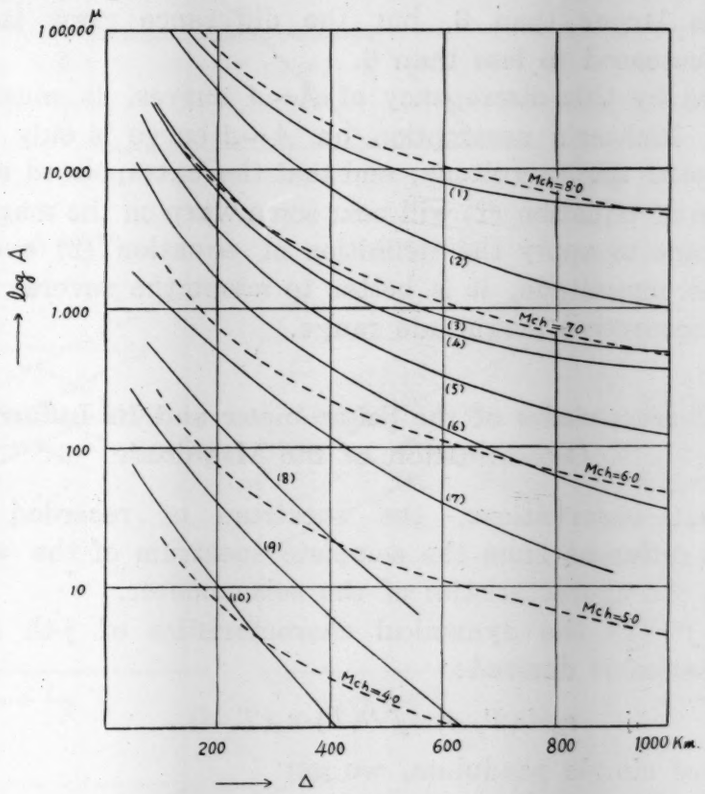


Fig. 2. $A \sim \Delta$ curves of the earthquake waves.

Table 1.

| No. | Time of Occurrence | Depth | $M_{ch}$ | |
|---|---|---|---|---|
| | h m | km. | | |
| 1 | 1923, Sept. 01 11 58 | | (7.9) | Great Kwanto Earthq. |
| 2 | 1927, Mar. 07 18 28 | 10 | 7.5 | North Tango Earthq. |
| 3 | 1925, May. 23 11 09 | | (7.0) | North Tazima Earthq. |
| 4 | 1930, Nov. 26 04 03 | 0—5 | 7.9 | North Izu Earthq. |
| 5 | 1929, May, 22 01 35 | 30 | 6.8 | |
| 6 | 1930, June, 01 02 58 | 30 | 6.6 | |
| 7 | 1931, Jnne, 09 14 07 | 20 | 6.1 | |
| 8 | 1931, Mar. 07 01 53 | | 5.4 | |
| 9 | 1930, Mar. 22 17 50 | 20 | 5.8 | |
| 10 | 1930, Mar. 09 19 54 | 20—30 | 5.0 | |

In Fig. 2, some of the $A\sim\Delta$ curves derived by Wadati is shown. The earthquakes drawn in Fig. 2 are listed in Table 1. In Fig. 2, also the $A\sim\Delta$ curves derived by the equation (8) are shown by the dotted lines.

Comparing both curves, good agreement will be found unless the magnitude is larger than 6, but the difference grew larger as the magnitude decreased to less than 6.

As shown by this discrepancy of $A\sim\Delta$ curves, it must be deeply noticed that Richter's assumption on $A\sim\Delta$ curve is only fitted to the limited range of the magnitude, and that the extrapolated application of the definition of equation (2) will bear some warp on the magnitude scale.

If we want to apply the definition of equation (2) over the wide range of the magnitude, it is better to adopt the several $A\sim\Delta$ curves against the respective magnitude range.

## 4. The Characteristics of the Seismometer and Its Influence on the Determination of the Magnitude

In actual observations, the spectrum of recorded seismogram $s_M^{(j)}(T, \Delta)$ is different from the complete spectrum of the wave $s_M(T, \Delta)$ according to the characteristics of the seismometer.

Putting $f^{(j)}(T)$ the dynamical characteristics of j-th seismometer, following relation is derived:

$$s_M^{(j)}(T, \Delta)=f^{(j)}(T)\cdot s_M(T, \Delta)\ . \qquad (9)$$

In the case of simple pendulum, we get

$$f^{(j)}(T)=\frac{1}{\sqrt{\{(T/T^{(j)})^2-1\}^2+4h^{(j)2}(T/T^{(j)})^2}}\ . \qquad (10)$$

If the value of the damping constant is a little less than unity, the magnification curve of the seismometer is approximated by the curves shown in Fig. 3-D.

The observed maximum trace amplitude recorded by the j-th seismometer $a_M^{(j)}(\Delta)$ is expressed as follows:

$$a_M^{(j)}(\Delta)=k[V^{(j)}\cdot s_M^{(j)}(T, \Delta)]_{\max}=k[V^{(j)}f^{(j)}(T)\cdot g(T, \Delta)\cdot s_M(T)]_{\max}\ . \qquad (11)$$

For the simplicity, we put the assumptions for the spectral structure at origin such as:

(1) $\log S_M(T)$ versus $\log T$ has linear relation over the whole range in which $S_M(T)$ exist.

(2) the upper limit of the period of the earthquake wave $T_0$ is confined by the following equation as:

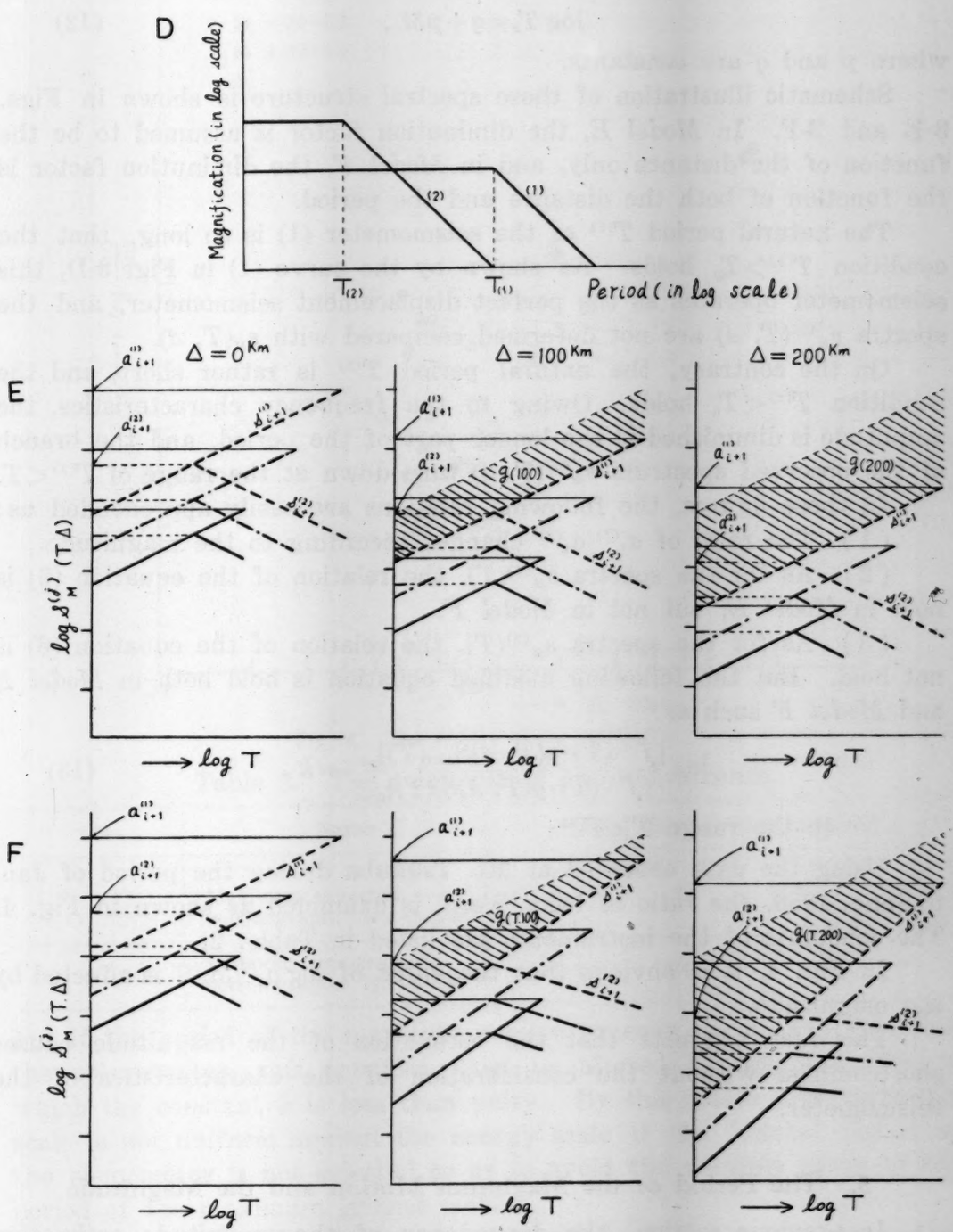


Fig. 3. D: the frequency characteristics of the seismometer.
E and F: schematic models of observed spectra $s_M^{(j)}(T, \Delta)$.

$$\log T_0 = q + pM \,, \tag{12}$$

where $p$ and $q$ are constants.

Schematic illustration of these spectral structure is shown in Figs. 3-E and 3-F. In *Model E*, the diminution factor is assumed to be the function of the distance only, and in *Model F*, the diminution factor is the function of both the distance and the period.

The natural period $T^{(1)}$ of the seismometer (1) is so long, that the condition $T^{(1)} > T_0$ holds. As shown by the curve (1) in Fig. 3-D, this seismometer operates as the perfect displacement seismometer, and the spectra $s_M{}^{(1)}(T, \Delta)$ are not deformed compared with $s_M(T, \Delta)$.

On the contrary, the natural period $T^{(2)}$ is rather short, and the condition $T^{(2)} < T_0$ holds. Owing to the frequency characteristics, the amplitude is diminished at the longer part of the period, and the branch of the observed spectrum $s_M{}^{(2)}(T, \Delta)$ turn down at the range of $T^{(2)} < T$.

In these figures, the following relations are easily apprehended as:

(1) The ratio of $a_i{}^{(1)}/a_i{}^{(2)}$ changes according to the magnitude.

(2) As for the spectra $s_M{}^{(1)}(T)$, the relation of the equation (6) is hold in *Model E*, but not in *Model F*.

(3) As for the spectra $s_M{}^{(2)}(T)$, the relation of the equation (6) is not hold. But the following modified equation is hold both in *Model E* and *Model F* such as:

$$\log \frac{[f^{(2)}(T) \cdot g(T, \Delta) S_{i+1}(T)]_{\max}}{[f^{(2)}(T) \cdot g(T, \Delta) S_i(T)]_{\max}} = k \,. \tag{13}$$

in the range $T \geqq T^{(2)}$

Using the data observed at Mt. Tsukuba during the period of Jan. to June, 1956, the ratio of $\log a_i{}^{(1)}/a_i{}^{(2)}$ is examined as shown in Fig. 4. The constants of the instruments are listed in Table. 2.

In Fig. 4, it is obvious that the value of $\log a_i{}^{(1)}/a_i{}^{(2)}$ is affected by the magnitude.

This fact suggests that the estimation of the magnitude causes shortcomings without the consideration of the characteristics of the seismometer.

## 5. The Period of the Maximum Motion and the Magnitude

In previous section, the dependency of the magnitude estimation on the characteristics of the seismometer is considered. If the natural period of the seismometer is longer than the predominant period of the maximum ground motion, the magnitude is estimated by equation (2),

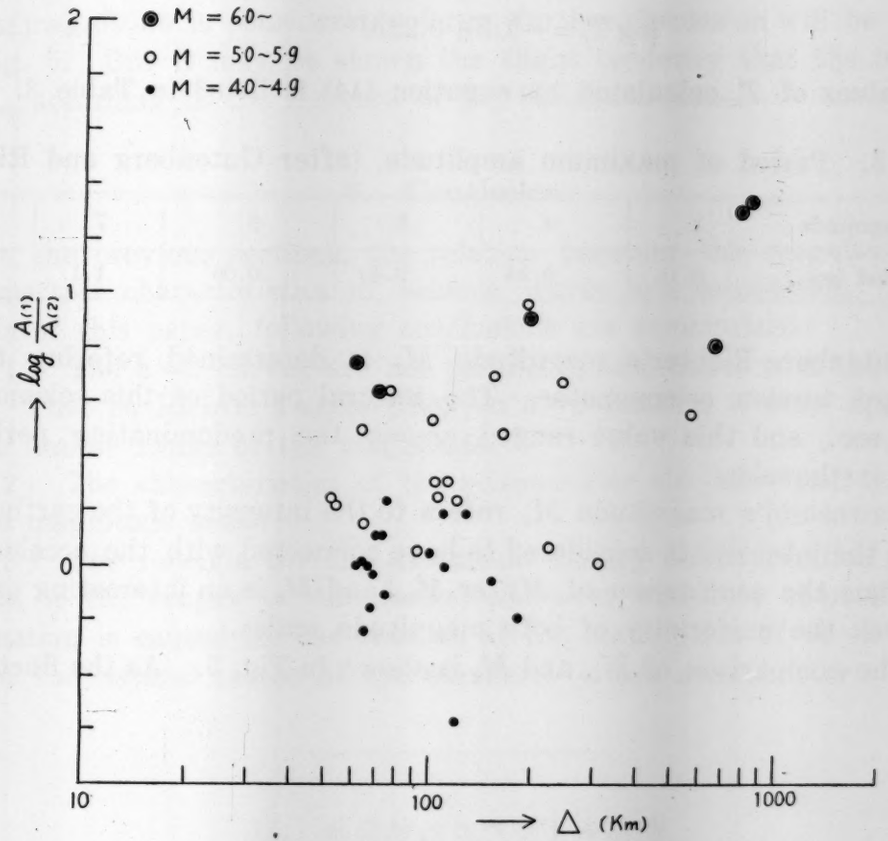


Fig. 4. The values of log $a_i^{(1)}/a_i^{(i)}$.

Table 2. The constants of the instruments.

| No. | Name | Period | Magnification | Damping |
|---|---|---|---|---|
| | | sec. | | |
| (1) | Hagiwara inverted seismograph. NS & EW | 6.0 | 40 | $h$=0.7 |
| (2) | Ishimoto acceleration seismograph. NS & EW | 0.10 | 240 | 0.7 |

but if the period of the maximum motion exceeds the natural period of the seismometer, this equation must be altered by equation (13), in which the constant $k$ is less than unity. By this reason, the magnitude scale is not uniform against the energy scale if the natural period of the sismometer is not selected so as to avoid the variable range of the period of the maximum ground motion.

Gutenberg and Richter[12] gave the period of the maximum motion as follows:

12) *loc. cit.* (4).

$$\log T_0 = -1.5 + 0.22M \tag{14}$$

The values of $T_0$ calculated by equation (14) is listed in Table 3.

Table 3. Period of maximum amplitude. (after Gutenberg and Richter)

| Magnitude | 3 | 4 | 5 | 6 | 7 | 8 |
|---|---|---|---|---|---|---|
| Period (sec.) | 0.15 | 0.24 | 0.40 | 0.66 | 1.1 | 1.6 |

Gutenberg-Richter's magnitude $M_G$ is determined refering to the standard torsion seismometer. The natural period of this seismometer is 0.8 sec., and this value ranged among the predominating period of usual earthquakes.

Kawasumi's magnitude $M_k$ refers to the intensity of the earthquake, where the intensity is considered to have connected with the acceleration.

Thus the comparison of $M_G$ (or $M_{ch}$) and $M_k$ is an interesting problem to check the uniformity of both magnitude scales.

The comparison of $M_{ch}$ and $M_k$ is shown in Fig. 5. As the fluctuation

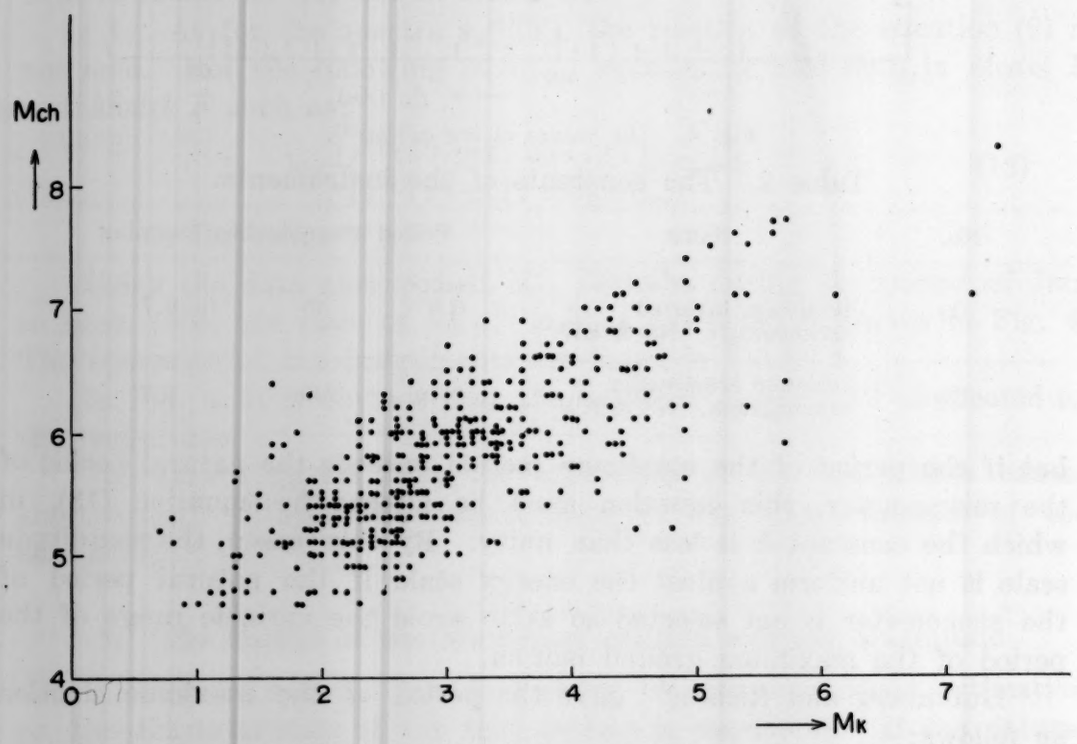


Fig. 5. Comparison of $M_{ch}$ and $M_k$. The values of $M_k$ refer to the catalogue issued by Japan Meteorological Agency on 1952, and $M_{ch}$ refer to the new catalogue of 1958.

of the magnitude is considerably large, further discussion will be invalid in Fig. 5. But it may be shown the slight tendency that the increase of $M_{ch}$ according to the increase of $M_k$ become smaller.

## 6. Conclusion

In the previous sections, the relation between the magnitude and the spectral characteristics of seismic waves are considered. As the results of this paper, following conclusions are summarized:

(1) The $a \sim \Delta$ curves are not parallel in accordance with the magnitude. That is, Richter's assumption on $a \sim \Delta$ relation is only applicable in the limited range of the magnitude.

(2) The characteristics of the seismometer also affects on the warp of the magnitude scale.

(3) The formula for the magnitude-energy transformation may be altered to the ranges of the magnitude over and less than 6. This alternation is caused by the reasons of the assumption of $A \sim \Delta$ curves and of the natural period of the standard torsion seismometer.

---

## 17. 地震波のスペクトル構造

### —そのマグニチュード決定におよぼす影響—

地震研究所　松　本　利　松

リヒターや河角によつて定義されたマグニチュードは地震の規模を表現するためにははなはだ便利な量である．このマグニチュードも終局的には地震波のエネルギーと関連を持つことにその意味があるのであるから，マグニチュード-エネルギー変換において，系統的なひずみを生じないように，マグニチュードという物指自体が均一性を保つていることが望ましい．

しかし，地震波のスペクトル構造は一般にはなはだ複雑であり，簡単なマグニチュードの定義からみて，このような均一性が，大地震から微小地震までの広い帯域に対して成り立つているかどうか検討する必要があるように思われる．

本論文では地震波のスペクトル構造についての概念的な模型を考え，このような構造がマグニチュード決定に対してどのような関連性を持つかを二三の観測材料をまじえて調べてみた．

もちろん地震波のスペクトル構造については多くの未知の領域が残されてをり，今後更に研究する必要があることは言を俟たない．

---

BULLETIN OF THE EARTHQUAKE
RESEARCH INSTITUTE
Vol. 37 (1959), pp. 279-306

# 18. *On the Travel-Times of S-Waves, Derived from the Explosion Seismic Observations.*

By Shūzō ASANO,* Nozomu DEN,** Takeshi MIKUMO,***
Etsuzo SHIMA* and Tatsuo USAMI.****

(Read Dec. 23, 1958.—Received March 28, 1959.)

## 1. Introduction

The first large scale observation of tremors caused by a blast of a big amount of explosives was carried out on October 25, 1950, in north-eastern Japan, to study the structure of the earth's crust[1]. This blast took place near Isibuti, in order to get a large amount of rocks for construction of a rock-fill dam. Since then, for engineering purposes, many blasts have been carried out in Tōhoku and Kwantō areas. The Research Group for Explosion Seismology†, the present authors being members, observed eleven sets of tremors caused by these explosions. R. G. E. S. observed also two other large blasts, which were intended exclusively for our research purposes. Blasts are tabulated in Table 1. The results of observations were reported in each case[2].

The main object of R. G. E. S. is to study the structure of the earth's crust. Therefore, although the seismograms contain a lot of other interesting information, R. G. E. S. used mainly the arrival-times of the initial motions, as they are most reliable. Thus R. G. E. S. did

* Earthquake Research Institute, University of Tokyo.
** Geophysical Institute, University of Tokyo.
*** Geophysical Institute, University of Kyoto.
**** Japan Meteorological Agency.
† abbreviated to R. G. E. S. in this paper.

1) R. G. E. S., *Bull. Earthq. Res. Inst.*, **29** (1951), 97.

2) R. G. E. S., *Bull. Earthq. Res. Inst.*, **30** (1952), 279.
R. G. E. S., *Bull. Earthq. Res. Inst.*, **31** (1953), 281.
R. G. E. S., *Bull. Earthq. Res. Inst.*, **32** (1954), 79.
R. G. E. S., *Bull. Earthq. Res. Inst.*, **33** (1955), 699.
R. G. E. S., *Pub. Bureau Central Séism. Int., Serié A, Trav. Sci.*, **19** (1956).
R. G. E. S., *Bull. Earthq. Res. Inst.*, **36** (1958), 329.
T. USAMI, T. MIKUMO, E. SHIMA, I. TAMAKI, S. ASANO, T. ASADA and T. MATUZAWA, *Bull. Earthq. Res. Inst.*, **36** (1958), 349.
R. G. E. S., *Bull. Earthq. Res. Inst.*, **37** (1959), 89.
T. MATUZAWA., *Bull. Earthq. Res. Inst.*, **37** (1959), 123.

Table 1. Table of Explosions.

| Name of Explosion | | Origin Time, J. S. T. |
|---|---|---|
| Isibuti | I * | Oct. 25, 1950, 12h 06m 07.97s |
| 〃 | II | Dec. 27, 1951, 12 05 59.8 |
| 〃 | III | July 25, 1952, 12 04 59.42 |
| Kamaisi | I ** | Dec. 7, 1952, 03 34 59.91 |
| 〃 | II | Sept. 13, 1953, 03 04 57.07 |
| Dōsen | | May 1, 1954, 01 35 00.28 |
| Sin'yama | | May 1, 1954, 03 35 00.51 |
| Daidō | | May 3, 1954, 01 35 00.17 |
| Takinosawa | | May 3, 1954, 03 35 00.51 |
| Nozori | I *** | Nov. 14, 1954, 01 05 00.87 |
| 〃 | II | Aug. 15, 1955, 01 05 00.29 |
| Hokota | I **** | Dec. 5, 1956, 01 05 00.21 |
| 〃 | II | Aug. 26, 1957, 01 05 00.00 |

* abbreviated to I–I.
** abbreviated to K–I.
*** abbreviated to N–I.
**** abbreviated to H–I.

not pay much attention to the arrival-times of other late phases for interpreting the earth's crust, and the data were left unpublished, except in some of the papers.

In this paper we study the arrival-times of late phases, especially about the *S*-phases, which were recorded in the above mentioned thirteen observations.

## 2. Used data

Number of available seismograms obtained from thirteen observations were 196 in total. First, the supposed arrival-times of *S*-waves were read quite independently by each author, and the values were adopted only when the agreement was found satisfactorily. On some records, we could read only the arrival-times of the initial motions, but not of the late phases because of the scale-out owing to the high sensitivity of the instruments. After all, we could read 120 seismograms.

Adopted values are tabulated in Table 2 and 3. For convenience' sake, the read values were classified into five classes—$a_1$, $a_2$, b, c and d. These classes indicate the accuracy of reading, and the limits of errors are listed respectively at the end of Table 2. For the case of four observations, which were carried out near the Kamaisi Mine, we used the classes p, q, r, s and t. Because these blasts were rather on

Table 2.

| Name of Explosion | Station | $\Delta$ km | $S$ sec | Class | $S-O$ sec |
|---|---|---|---|---|---|
| I - I | Isibuti | 1.8 | 8.52 | $a_1$ | 0.55 |
| | | | 8.61 | $a_2$ | 0.64 |
| | | | 9.27 | $a_1$ | 1.30 |
| 〃 | Sendai | 98.24 | 37.2 | d | 29.2 |
| I - II | Isibuti | 1.69 | | | 0.34 |
| 〃 | Orose | 1.08 | 0.77 | $a_1$ | 0.97 |
| 〃 | Hondera | 15.29 | 5.08 | c | 5.28 |
| 〃 | Wakayanagi | 14.62 | 5.14 | b | 5.34 |
| 〃 | Dobasi | 12.09 | 4.76 | $a_1$ | 4.96 |
| 〃 | Atago | 8.65 | 3.12 | $a_1$ | 3.32 |
| 〃 | Kawatabi | 41.92 | 14.1 | c | 14.3 |
| 〃 | Katurazawa | 21.10 | 6.8 | b | 7.0 |
| 〃 | Kamaisi | 87.54 | 26.42 | $a_2$ | 26.62 |
| 〃 | Kurikoma | 22.52 | 7.12 | b | 7.32 |
| | | | 7.6 | c | 7.8 |
| I - III | Hondera | 15.3 | 4.78 | d | 5.36 |
| 〃 | Mamurogawa | 58.7 | 17.77 | c | 18.35 |
| 〃 | Innai | 46.0 | 14.42 | $a_2$ | 15.00 |
| | | | 14.9 | $a_1$ | 15.48 |
| 〃 | Kawatabi | 41.9 | 11.57 | c | 12.15 |
| | | | 13.33 | c | 13.91 |
| 〃 | Nenosiroisi | 87.8 | 26.46 | $a_2$ | 27.04 |
| 〃 | Yuzawa | 33.8 | 10.61 | $a_1$ | 11.19 |
| 〃 | Motegi | 290.7 | 80.72 | d | 81.30 |
| | | | 82.61 | b | 83.19 |
| | | | 83.39 | $a_2$ | 83.97 |
| K - I | Setamai | 20.4 | 6.32 | c | 6.41 |
| 〃 | Kesenuma | 45.5 | 13.18 | b | 13.27 |
| | | | 13.54 | b | 13.63 |
| 〃 | Mizusawa | 51.4 | | c | 16.6 |
| 〃 | Onagawa | 97.3 | 28.69 | c | 28.78 |
| | | | 29.65 | b | 29.74 |
| 〃 | Kaneyama | 173.7 | 49.47 | $a_2$ | 49.56 |
| | | | 49.98 | $a_2$ | 50.07 |
| 〃 | Kawamata | 202.3 | 58.85 | d | 58.94 |
| | | | 59.75 | d | 59.84 |
| | | | 60.13 | d | 60.22 |

(to be continued)

Table 2. (continued)

| Name of Explosion | Station | $\Delta$ km | $S$ sec | Class | $S-O$ sec |
|---|---|---|---|---|---|
| K-I | Nogisawa | 261.1 | 71.39 | d | 71.48 |
| | | | 72.34 | d | 72.43 |
| 〃 | Ide | 36.9 | 11.00 | $a_2$ | 11.09 |
| 〃 | Yuzawa | 103.3 | 30.46 | b | 30.55 |
| | | | 29.00 | c | 29.09 |
| 〃 | Mamurogawa | 130.5 | 39.68 | d | 39.77 |
| K-II | Nakasone | 11.2 | 0.63 | $a_1$ | 3.56 |
| 〃 | Sakari | 23.92 | 4.48 | b | 7.41 |
| 〃 | Kesennuma | 45.04 | 10.78 | $a_2$ | 13.71 |
| 〃 | Sizugawa | 72.25 | 17.20 | b | 20.13 |
| 〃 | Onagawa | 97.32 | 25.24 | b | 28.17 |
| | | | 27.59 | b | 30.52 |
| 〃 | Mukaiyama | 137.38 | 37.47 | $a_1$ | 40.40 |
| 〃 | Funaoka | 159.6 | 44.55 | d | 47.48 |
| | | | 46.20 | d | 49.13 |
| 〃 | Kaneyama | 173.7 | 47.38 | b | 50.30 |
| 〃 | Kawamata | 202.46 | 54.11 | $a_2$ | 57.04 |
| 〃 | Nogisawa | 261.04 | 67.31 | c | 70.24 |
| N-I | Sawatariguti | 18.22 | 7.10 | c | 6.23 |
| 〃 | Takayama | 30.19 | 11.39 | $a_2$ | 10.52 |
| 〃 | Ōgo | 56.43 | 19.67 | c | 18.80 |
| 〃 | Asikaga | 88.86 | 27.96 | c | 27.09 |
| 〃 | Totigi | 103.34 | 31.46 | c | 30.59 |
| 〃 | Tukuba | 142.99 | 41.93 | $a_1$ | 41.06 |
| N-II | Sima | 17.21 | 5.68 | $a_2$ | 5.39 |
| 〃 | Nakanozyō | 24.05 | 7.64 | c | 7.35 |
| 〃 | Ikaho | 35.29 | 12.05 | b | 11.76 |
| 〃 | Ōmama | 65.75 | 19.86 | $a_2$ | 19.57 |
| 〃 | Kiryū | 73.29 | 22.92 | d | 22.63 |
| 〃 | Ōya | 107.37 | 31.97 | b | 31.68 |
| 〃 | Kakioka | 149.56 | 42.42 | b | 42.13 |
| | | | 43.61 | b | 43.32 |
| H-I | Tomoegawa | 7.24 | 4.52 | $a_1$ | 4.31 |
| 〃 | Tamari | 20.26 | 8.23 | $a_1$ | 8.02 |

(to be continued)

Table 2. (continued)

| Name of Explosion | Station | $\Delta$ km | $S$ scc | Class | $S-O$ sec |
|---|---|---|---|---|---|
| H-I | Tukuba | 41.26 | 13.72 | $a_1$ | 13.51 |
| 〃 | Yūki | 63.73 | 22.56 | $a_1$ | 22.35 |
| 〃 | Asikaga | 97.10 | 28.87 | d | 28.66 |
| | | | 32.36 | d | 32.15 |
| 〃 | Ōgo | 129.64 | 40.56 | b | 40.35 |
| | | | 44.83 | b | 44.62 |
| 〃 | Sibukawa | 146.06 | 44.24 | $a_2$ | 44.03 |
| | | | 44.68 | $a_2$ | 44.47 |
| | | | 48.95 | b | 48.74 |
| 〃 | Agatuma | 163.63 | 48.43 | $a_1$ | 48.22 |
| | | | 53.6 | b | 53.4 |
| 〃 | Hanasiki | 180.91 | 51.18 | $a_2$ | 50.97 |
| | | | 53.02 | $a_2$ | 52.81 |
| 〃 | Matusiro | 215.94 | 61.00 | $a_2$ | 60.79 |
| H-II | Ōya | 11.50 | 4.85 | $a_1$ | 4.85 |
| 〃 | Mito A | 21.82 | 8.83 | $a_2$ | 8.83 |
| 〃 | Mito B | 24.84 | 9.13 | b | 9.13 |
| 〃 | Hitati | 55.16 | 15.89 | $a_2$ | 15.89 |
| | | | 17.83 | $a_1$ | 17.83 |
| 〃 | Daigo | 73.03 | 23.95 | b | 23.95 |
| 〃 | Tanakura | 98.94 | 30.51 | c | 30.51 |
| | | | 31.05 | c | 31.05 |
| 〃 | Tamagawa | 119.47 | 35.25 | b | 35.25 |
| 〃 | Tamura | 131.79 | 40.16 | $a_2$ | 40.16 |
| 〃 | Siroiwa | 150.33 | 43.10 | $a_2$ | 43.10 |
| | | | 44.30 | $a_2$ | 44.30 |
| 〃 | Kawamata | 171.72 | 48.49 | $a_2$ | 48.49 |
| 〃 | Isida | 181.05 | 52.92 | $a_2$ | 52.92 |
| 〃 | Kaneyama | 196.25 | 56.06 | b | 56.06 |
| | | | 57.77 | b | 57.77 |
| 〃 | Watari | 211.06 | 59.0 | d | 59.0 |
| 〃 | Miyatoko | 252.37 | 70.5 | d | 70.5 |

$S$: Arrival time of $S$-wave;
$O$: Origin Time;
Class: Accuracy of reading;

| | sec | sec |
|---|---|---|
| $a_1$ | $0.0 < t \leq 0.1$ | |
| $a_2$ | $0.1 < t \leq 0.3$ | |
| b | $0.3 < t \leq 0.6$ | |
| c | $0.6 < t \leq 1.0$ | |
| d | $1.0 < t$ | |

Table 3.

| Name of Explosion | Station | $\Delta$ km | $S$ sec | Class | $S-O$ sec |
|---|---|---|---|---|---|
| Dōsen | Ōhasi | 5.615 | 2.07 | q | 1.79 |
| 〃 | Ōmatu | 2.437 | 1.55 | p | 1.27 |
| 〃 | Noda | 4.920 | 1.87 | q | 1.59 |
| 〃 | Kosano | 6.618 | 2.52 | p | 2.24 |
| 〃 | Nakatuma | 8.513 | 3.04 | p | 2.76 |
| | | | 3.19 | p | 2.91 |
| 〃 | Takinosawa | 12.895 | 4.2 | s | 3.92 |
| 〃 | Uresi | 10.943 | 3.81 | t | 3.53 |
| 〃 | Tōni | 11.414 | 4.33 | s | 4.05 |
| | | | 4.00 | s | 3.72 |
| 〃 | Okirai | 14.509 | 4.52 | s | 4.24 |
| | | | 4.74 | p | 4.46 |
| 〃 | Hikoroiti | 15.108 | 5.03 | p | 4.75 |
| 〃 | Tōno | 20.962 | 6.91 | p | 6.63 |
| 〃 | Matusiro | 3.177 | 1.33 | t | 1.06 |
| Sin'yama | Ōhasi | 3.500 | 1.60 | t | 1.09 |
| 〃 | Matukura | 10.235 | 3.75 | t | 3.24 |
| 〃 | Noda | 11.822 | 4.78 | p | 4.27 |
| 〃 | Kosano | 13.247 | 4.49 | p | 3.98 |
| | | 13.097 | 4.80 | p | 4.29 |
| 〃 | Nakatuma | 14.590 | 5.18 | q | 4.67 |
| | | | 4.93 | r | 4.42 |
| 〃 | Takinosawa | 19.355 | 6.46 | q | 5.95 |
| 〃 | Uresi | 17.565 | 6.00 | t | 5.49 |
| 〃 | Okirai | 22.590 | 7.25 | s | 6.74 |
| 〃 | Hikoroiti | 18.971 | 6.08 | r | 5.57 |
| 〃 | Asigase | 4.447 | 1.98 | t | 1.47 |
| 〃 | Tōno | 13.294 | 4.76 | p | 4.25 |
| Daidō | Ōmatu | 4.943 | 1.90 | q | 1.73 |
| 〃 | Dōsen | 6.898 | 2.50 | p | 2.33 |
| 〃 | Noda | 11.458 | 3.87 | q | 3.70 |
| 〃 | Kosano | 13.111 | 4.51 | t | 4.34 |
| 〃 | Takinosawa | 19.498 | 6.38 | q | 6.21 |
| 〃 | Uresi | 17.729 | 5.84 | r | 5.57 |
| 〃 | Okirai | 17.857 | 5.60 | p | 5.43 |

(to be continued)

Table 3. (continued)

| Name of Explosion | Station | $\Delta$ ōm | $S$ sec | Class | $S-O$ sec |
|---|---|---|---|---|---|
| Daidō | Hikoroiti | 13.244 | 4.14 | p | 3.97 |
| 〃 | Asigase | 3.026 | 1.20 | q | 1.03 |
| 〃 | Tōno | 14.638 | 4.79 | p | 4.62 |
| Takinosawa | Ōhasi | 16.729 | 5.65 | p | 5.14 |
| | | | 5.86 | p | 5.35 |
| 〃 | Ōmatu | 14.698 | 5.30 | q | 4.79 |
| 〃 | Dōsen | 12.730 | 4.67 | t | 4.16 |
| | | | 5.03 | t | 4.52 |
| 〃 | Noda | 8.154 | 3.28 | q | 2.77 |
| 〃 | Kosano | 6.381 | 2.26 | r | 1.75 |
| | | | 2.67 | s | 2.16 |
| 〃 | Nakatuma | 4.887 | 2.18 | q | 1.74 |
| | | | 2.32 | q | 1.81 |
| 〃 | Uresi | 1.999 | 1.39 | p | 0.88 |
| 〃 | Tōni | 6.737 | 2.75 | q | 2.24 |
| 〃 | Okirai | 18.679 | 6.28 | s | 5.77 |
| 〃 | Hikoroiti | 25.801 | 8.40 | p | 7.89 |
| 〃 | Tōno | 32.718 | 10.51 | p | 10.00 |

$S$: Arrival time of $S$-wave,
$O$: Origin Time;
Class: Accuracy of reading;

| | sec | sec |
|---|---|---|
| p | $0.00 < t \leq 0.02$ | |
| q | $0.02 < t \leq 0.06$ | |
| r | $0.06 < t \leq 0.10$ | |
| s | $0.10 < t \leq 0.20$ | |
| t | $0.20 < t$ | |

a small scale and the distance from the origin to the farthest observation-point was 32.7 km, the paper-speed of seismograms was regulated faster and the accuracy of read values was better than the other cases. The limits of errors in the above stated cases are listed at the end of Table 3. The examples of these classes are shown in Figs. 6–15.

### 3. Travel-times

Fig. 1 shows the travel-time graph of the $S$-waves from the four explosions, which were blasted near the Kamaisi Mine. The ordinate

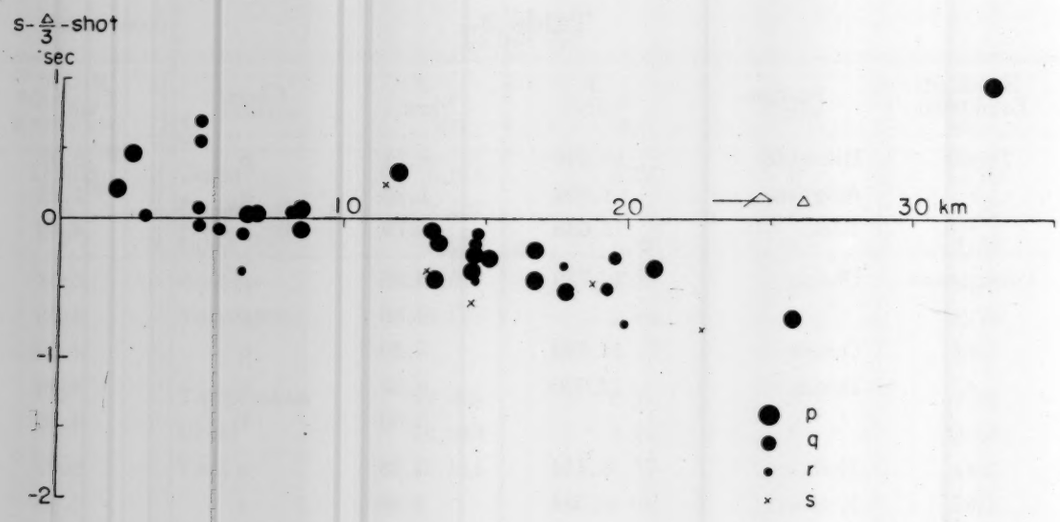


Fig. 1.

of this graph is $S-O-\frac{\Delta}{3}$(sec). We determined, by the method of least squares, the velocities of $S$-waves from this graph as follows:

$$t=(0.03\pm0.02)+\frac{\Delta}{(3.04\pm0.01)} \quad \text{sec} \qquad (1)$$

derived from 9 data for $\Delta<10$ km.

$$t=(0.26\pm0.06)+\frac{\Delta}{(3.36\pm0.04)} \quad \text{sec} \qquad (2)$$

derived from 16 data for $\Delta>10$ km.

In these calculations, we used the values of the classes p and q. Fig. 2 is the ordinary travel-time graph, showing the two velocities mentioned above. From equations (1) and (2), using the intercept time, we could calculate easily the depth of one of the velocity-discontinuities existing in the upper part of the earth's crust. We got 0.67 km as a value of the depth, assuming a structure of horizontal parallel layers. And the value is not so inconsistent with the one which was calculated from the data of $P$-waves.

Fig. 3 shows the travel-time graph of the $S$-waves from the blasts in Kwantō and Tōhoku areas. Observed values, concerning the Tōhoku area, are shown in this graph by the solid circles. We can see easily that the intercept time for Kwantō area is larger than that for Tōhoku area. So we determined the velocities of $S$-waves in each area and

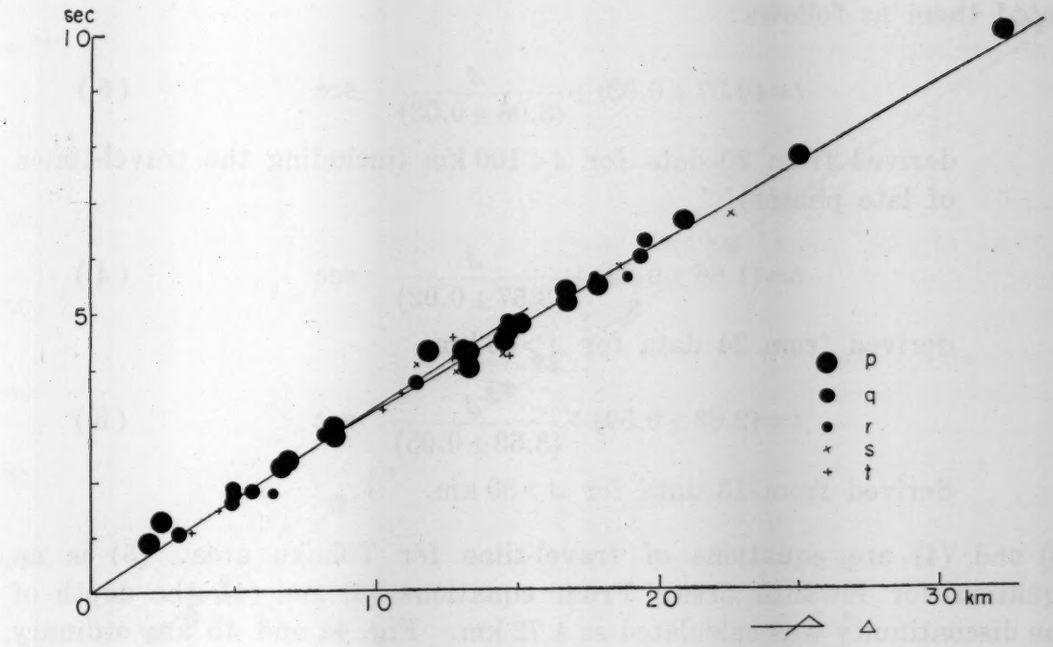
sec
10
5
0
10
20
30 km
p
q
r
s
t
Δ

Fig. 2.

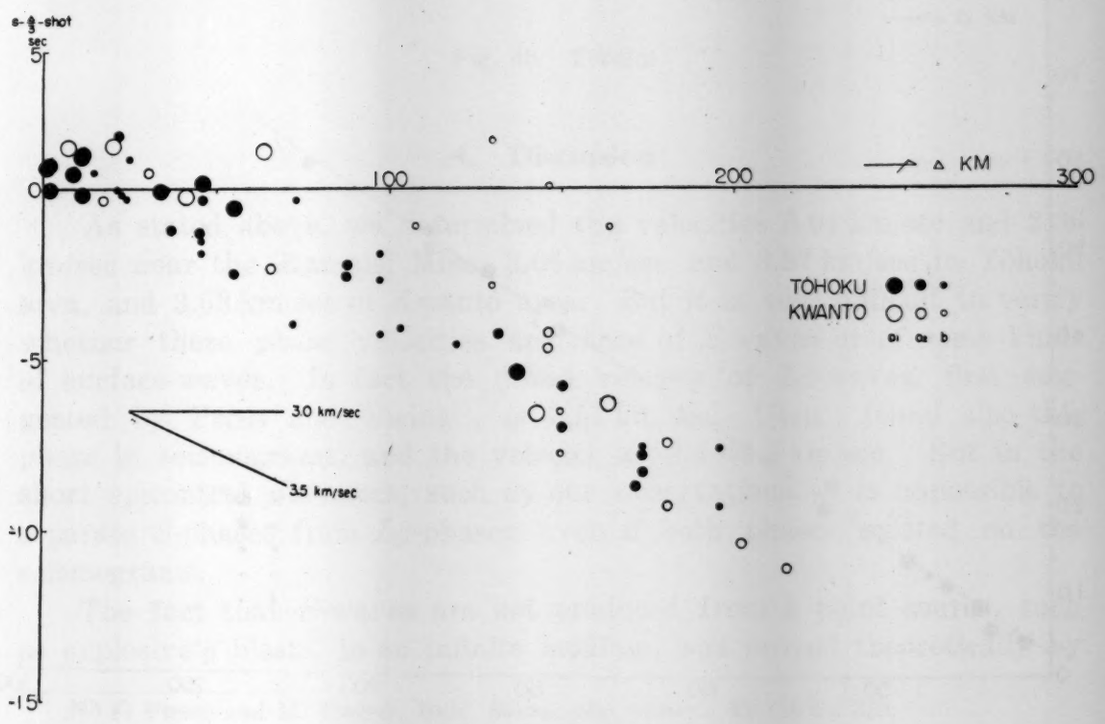
s-p-shot
sec
5
0
-5
-10
-15
100
200
300
Δ KM
TOHOKU
KWANTO
3.0 km/sec
3.5 km/sec

Fig. 3.

stated them as follows:

$$t=(0.07\pm0.03)+\frac{\Delta}{(3.06\pm0.03)} \quad \text{sec} \qquad (3)$$

derived from 20 data for $\Delta<100$ km (including the travel-times of late phases).

$$t=(1.66\pm0.29)+\frac{\Delta}{(3.57\pm0.02)} \quad \text{sec} \qquad (4)$$

derived from 24 data for $\Delta>30$ km.

$$t=(2.63\pm0.50)+\frac{\Delta}{(3.63\pm0.05)} \quad \text{sec} \qquad (5)$$

derived from 13 data for $\Delta>30$ km.

(3) and (4) are equations of travel-time for Tōhoku area. (5) is an equation for Kwantō area. From equations (3) and (4), the depth of the discontinuity was calculated as 4.72 km. Fig. 4a and 4b are ordinary travel-time graphs.

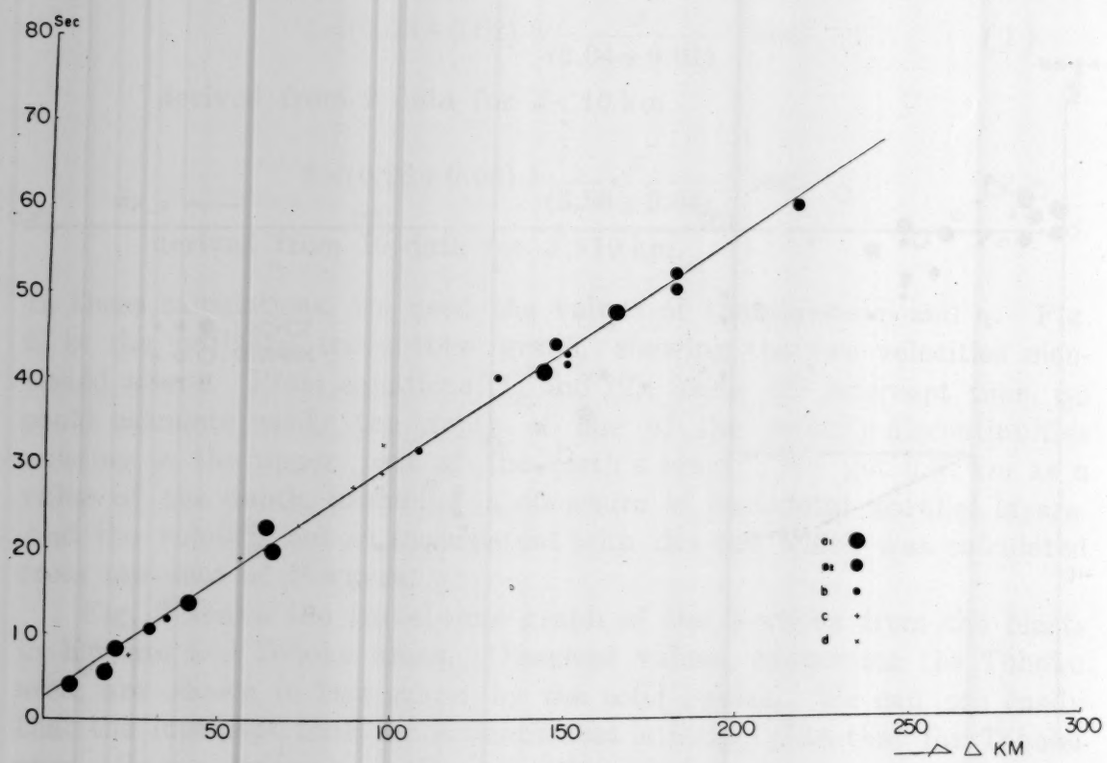


Fig. 4a. Kwantō.

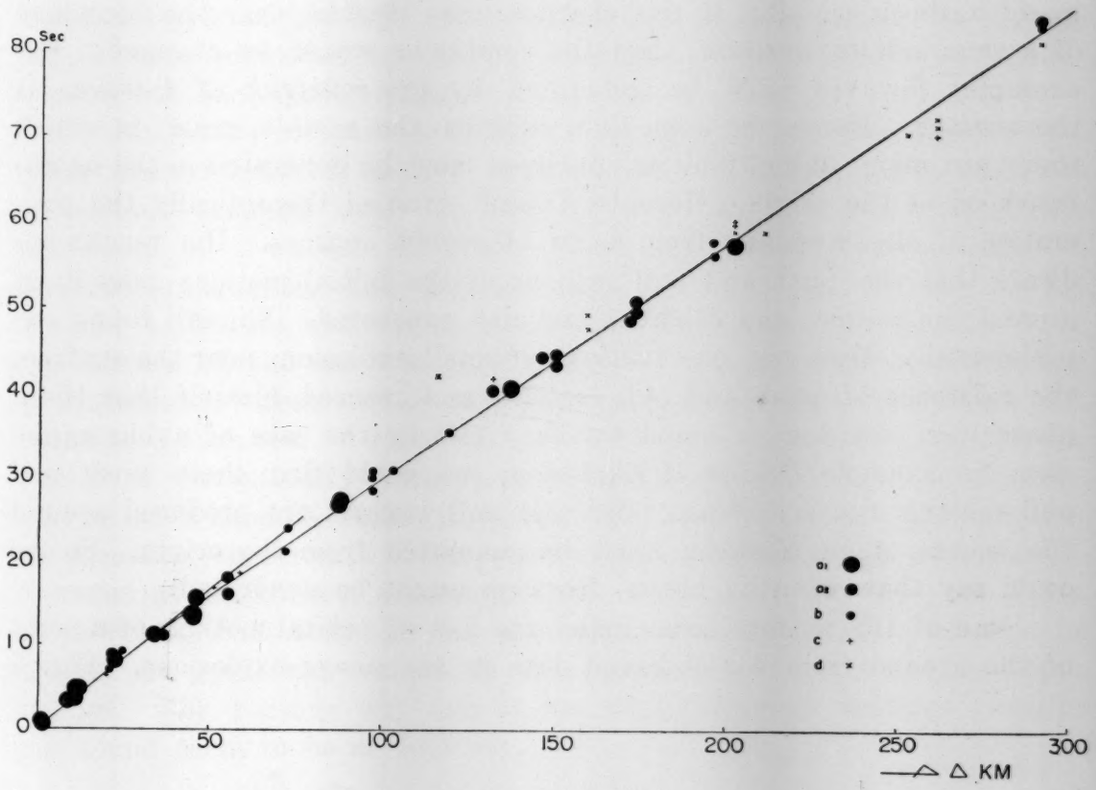


Fig. 4b. Tōhoku

## 4. Discussion

As stated above, we determined the velocities 3.04 km/sec and 3.36 km/sec near the Kamaisi Mine, 3.06 km/sec and 3.57 km/sec in Tōhoku area, and 3.63 km/sec in Kwantō area. But it is very difficult to verify whether these phase velocities are those of *S*-waves or of some kinds of surface-waves. In fact the phase velocity of *Lg*-waves, first suggested by Press and Ewing[3], is 3.51 km/sec. Utsu[4] found also this phase in seismograms, and the velocity as 3.4~3.6 km/sec. But in the short epicentral distances, such as our observations, it is impossible to separate *S*-phases from *Lg*-phases, even if both phases existed on the seismograms.

The fact that *S*-waves are not produced from a point source, such as explosive's blasts, in an infinite medium, was proved theoretically by

3) F. PRESS and M. EWING, *Bull. Seism. Soc. Amer.*, **42** (1952), 219.
4) T. UTSU, *Quart. Journ. Seism.*, **23** (1958), (in Japanese).

many authorities. But if the charges were blasted near the boundary of a semi-infinite medium, then the conditions would be changed. For example, *S*-waves must be generated by the reflection of *P*-waves at the surface. Hence, in a medium such as the earth's crust, in which there are many discontinuities, *S*-waves must be generated in the neighbourhood of the origin. Recently Usami[5] studied theoretically the generation of elastic waves from some ellipsoidal sources. His results indicate that the push and pull regions of the initial motions may exist around the source, and *S*-waves are also generated. Shima[6] found experimentally, from the observations of small explosions near the surface, the existence of push and pull regions, and assured himself that these phase were not due to sound waves. Also in the case of a big explosion, for example Hokota II Explosion, we could find these push and pull regions clearly. When push and pull regions are produced around the source, then *S*-waves must be generated from the origin. So we could say that, even by blasts, *S*-waves might be generated.

One of the writers constructed the loci of orbital motions of a point of the ground from his observed data in the above explosions. Fig. 5

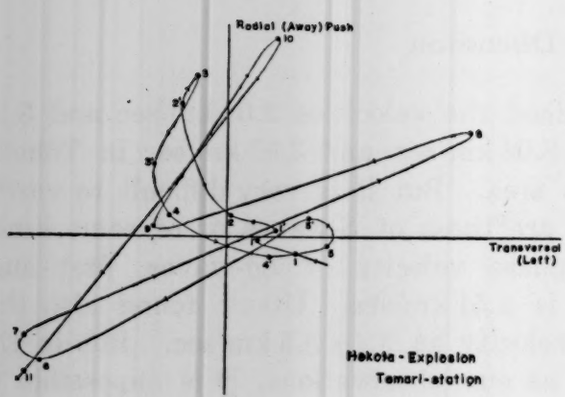


Fig. 5a.

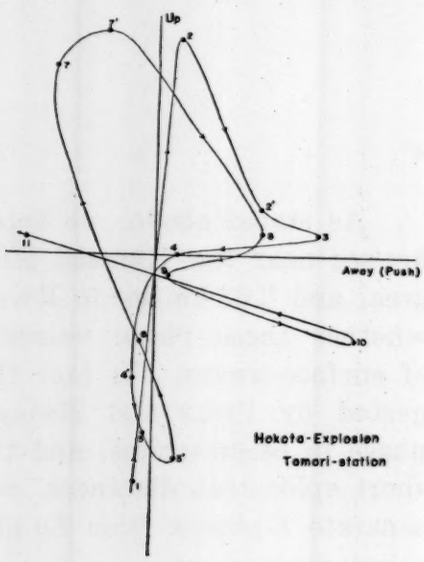


Fig. 5b.

5) U. USAMI, *Geophys. Mag.*, **29** (1958), 11.
6) E. SHIMA., *Monthly Meeting of the Earthq. Res. Inst.*, (SePt. 1954).

is an example of the loci. From these loci he found that the phases, which were identified by us as *S*-waves, did not behave as surface waves, but as *S*-type waves.

Now, let us compare our results with the *S*-wave velocities derived from observations of natural earthquakes. If there exists sufficient agreement between them, it may be said that the observed phases are these of *S*-waves. Professor Matuzawa[7] studied travel-times of shallow-earthquakes, and obtained the velocities of *S*-waves as 3.0 km/sec, 4.0 km/sec and 4.5 km/sec, and the depths of discontinuities from the surface of the earth as 20 km and 50 km respectively. According to Kishimoto's[8] results, the velocities of *S*-waves were derived as 3.1 km/sec, 3.4 km/sec, 4.0 km/sec and 4.7 km/sec, corresponding to the depths of discontinuity surfaces of 6 km, 20 km and 30 km respectively. On the other hand, Koshikawa[9] studied the travel-times of eight natural earthquakes, occurred in Kwantō area, and determined the velocities of *S*-waves as 3.1 km/sec, 3.3 km/sec and 3.6 km/sec. We can see from these results that although the agreement of these results with ours is not always good, the values in this paper are often found in these studies. The reasons why one to one correspondence between them is not found seem to be as follows:

(1) The accuracy of our results is much higher than those of natural earthquakes.

(2) The misidentification of the *S*-phase.

(3) The difference of the underground structure of the regions studied, and so on.

Now let us see Table 4, in which the representative velocities of *P*-waves and *S*-waves in some regions of the world, obtained from seismic observations of blasts, are tabulated. Values of $S_2$ show good agreement with each other. So does $S_1$ which was also found in Western Transvaal. It seems that the corresponding layers in these areas are seismically similar. Suffixes of *S* were put by the authors for convenience' sake of comparison, and other suffixes were used in each original paper.

7) T. MATUZAWA, *Bull. Earthq. Res. Inst.*, **5** (1928) 1.
T. MATUZAWA, *Bull. Earthq. Res. Inst.*, **6** (1929), 177, 205, 213.
8) Y. KISHIMOTO, *Mem. Coll. Sci. Kyoto Univ., Ser. A*, **27** (1955), 243.
9) Y. KOSHIKAWA, *Bull. Utsunomiya Univ.*, **6** (1956) 31.

(1)

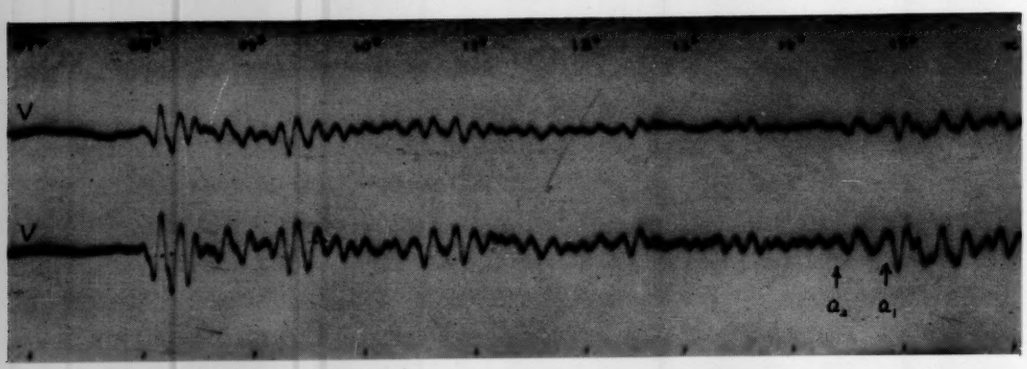


(2)

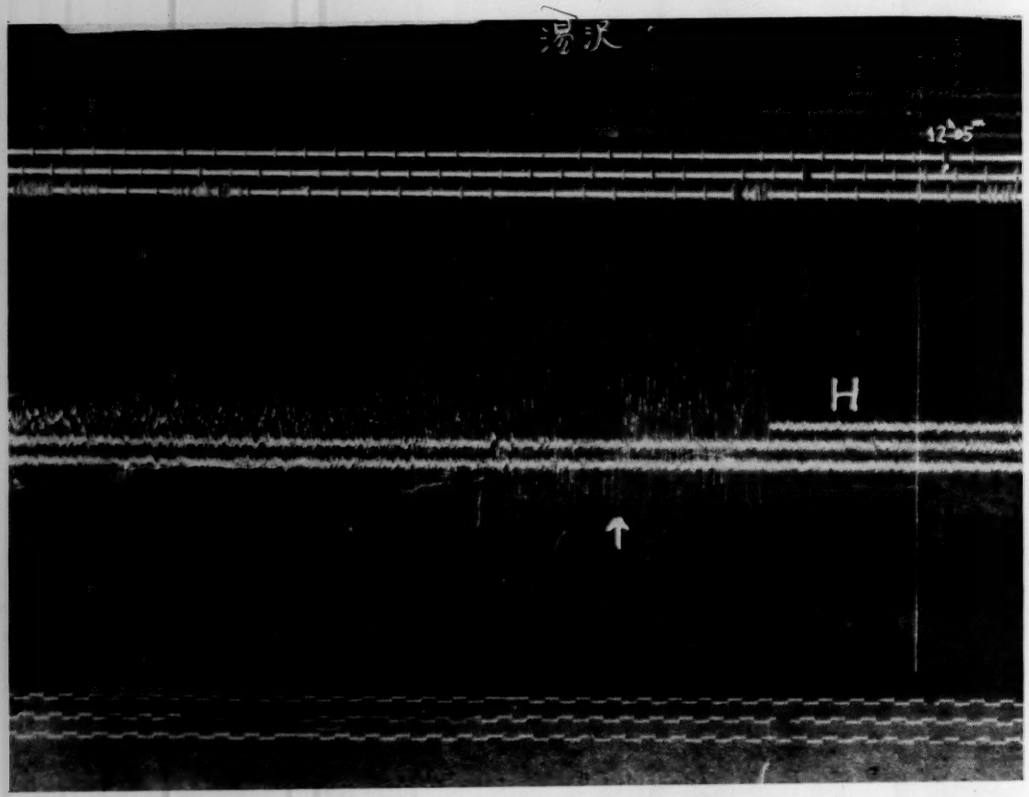


Fig. 6. Examples of records with class $a_1$.
(1) Seismogram at Innai in I–III ($\Delta$=46.0 km).
(2) Seismogram at Yuzawa in I–III ($\Delta$=33.8 km).

(3)

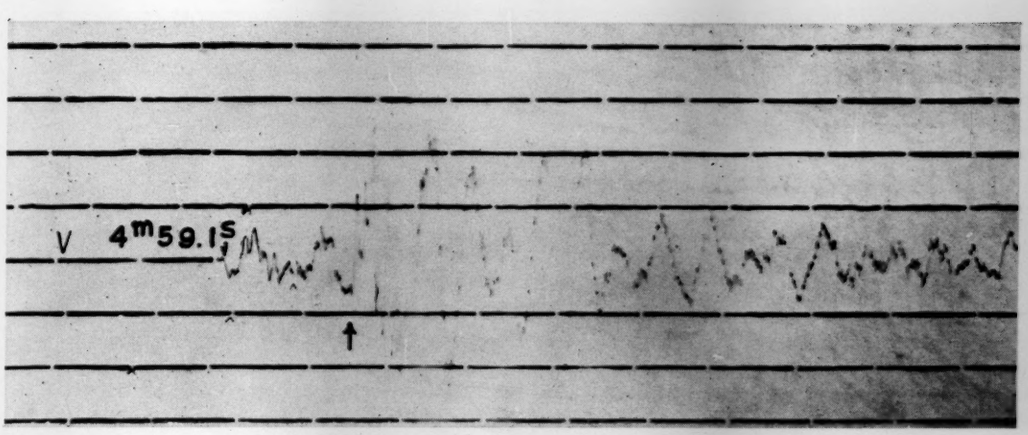


(4)

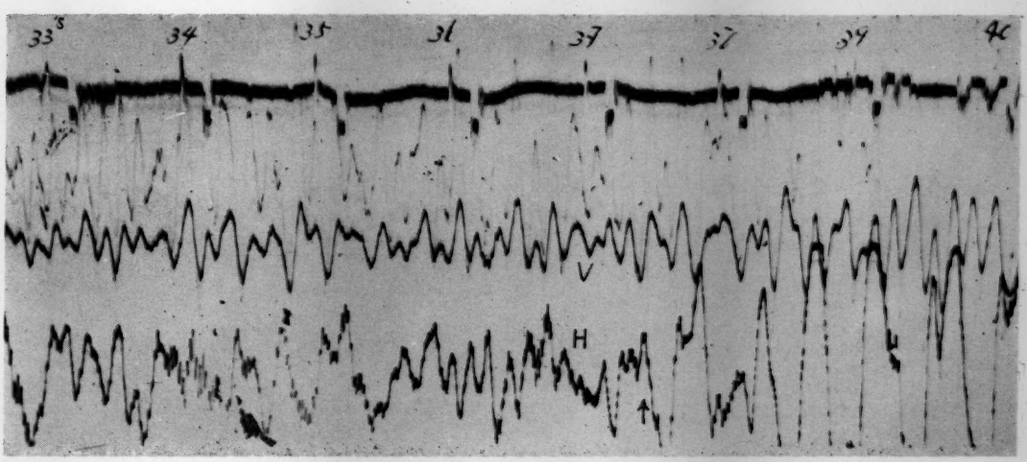


(5)

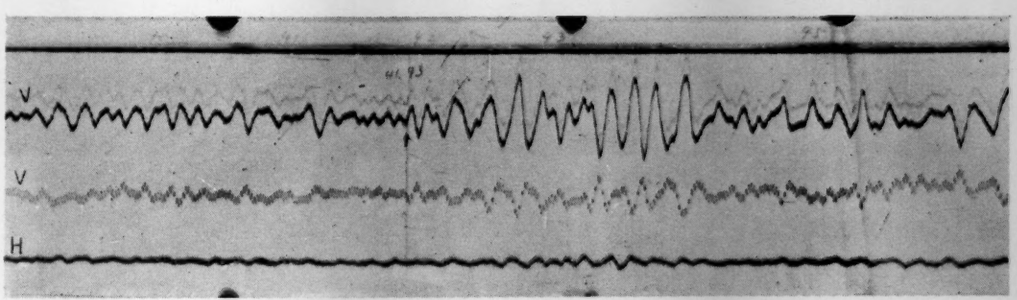


(3) Seismogram at Nakasone in K–II ($\Delta$=11.2 km).
(4) Seismogram at Mukaiyama in K–II ($\Delta$=137.4 km).
(5) Seismogram at Tukuba in N–I ($\Delta$=143.0 km).

(6)

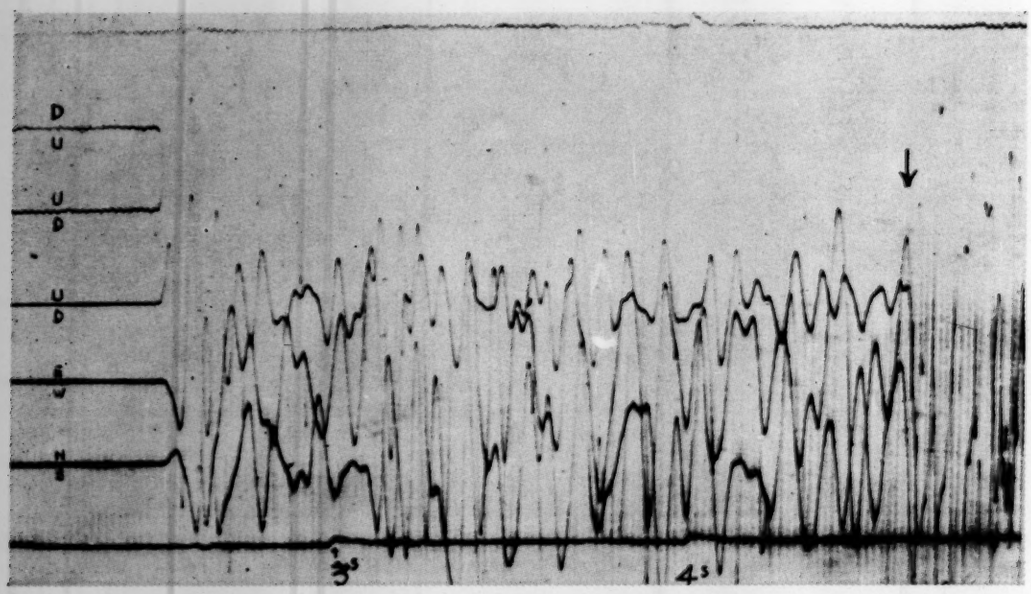


(7)

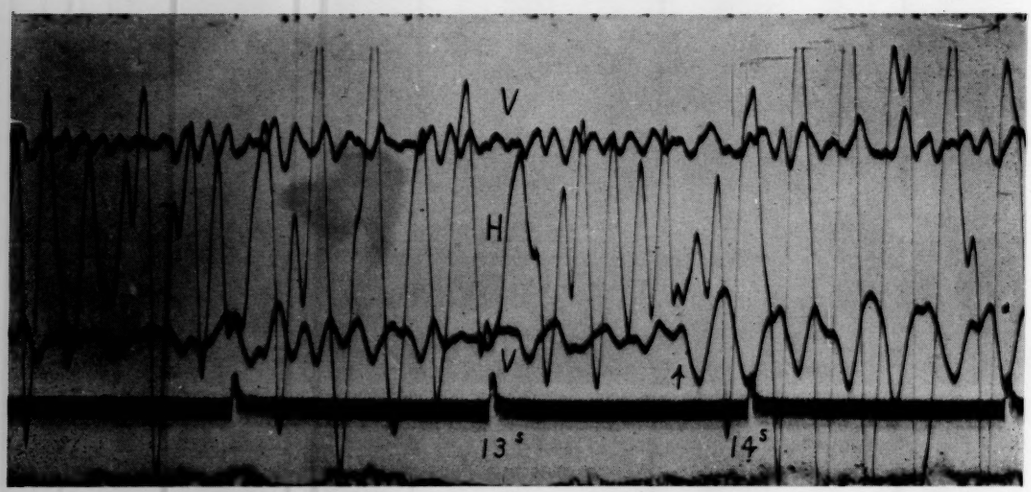


(6) Seismogram at Tomoegawa in H-I ($\Delta$=7.24 km).
(7) Seismogram at Tukuba in H-I ($\Delta$=41.3 km).

(1)

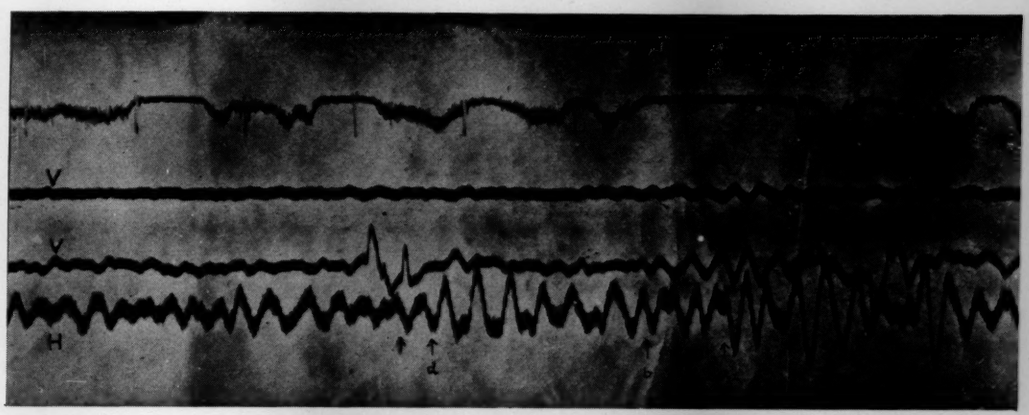


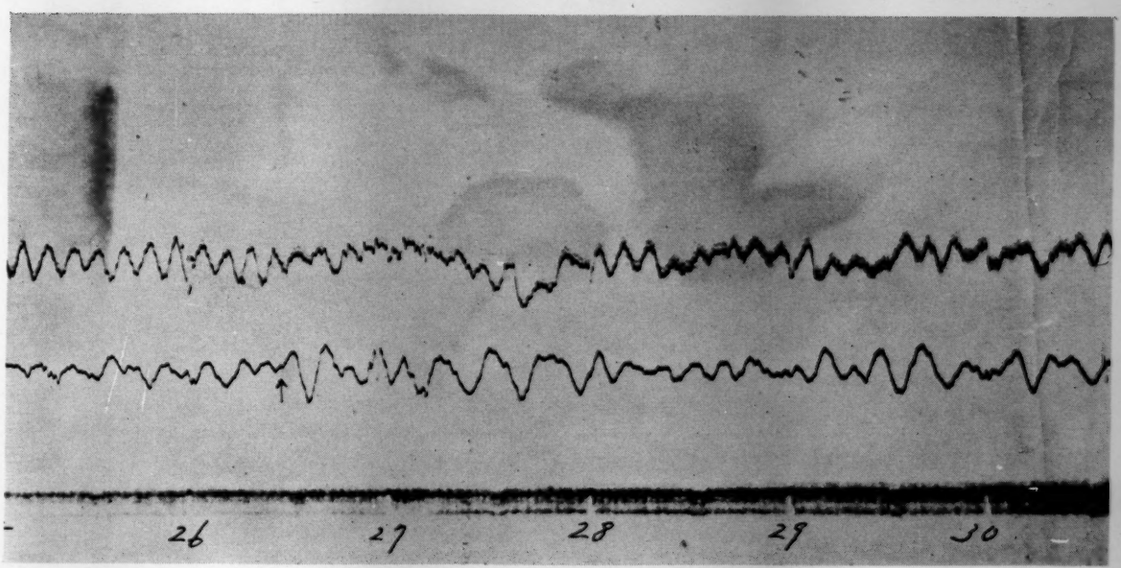


(2)

(3)

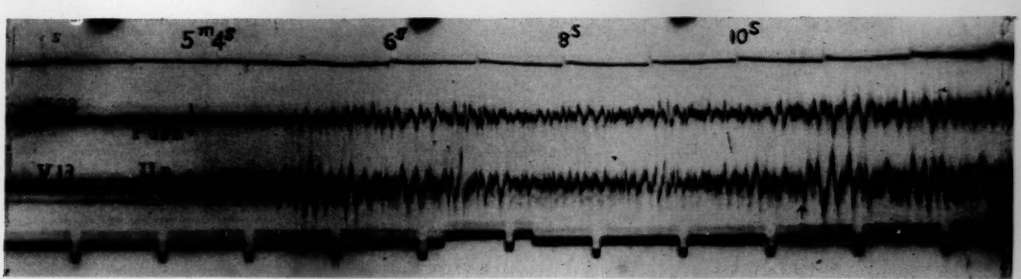


Fig. 7. Examples of records with class $a_2$.

(1) Seismogram at Motegi in I–III ($\Delta$=290.7 km).
(2) Seismogram at Nenosiroisi in I–III ($\Delta$=87.8 km).
(3) Seismogram at Kesenuma in K–II ($\Delta$=45.04 km).

(4)

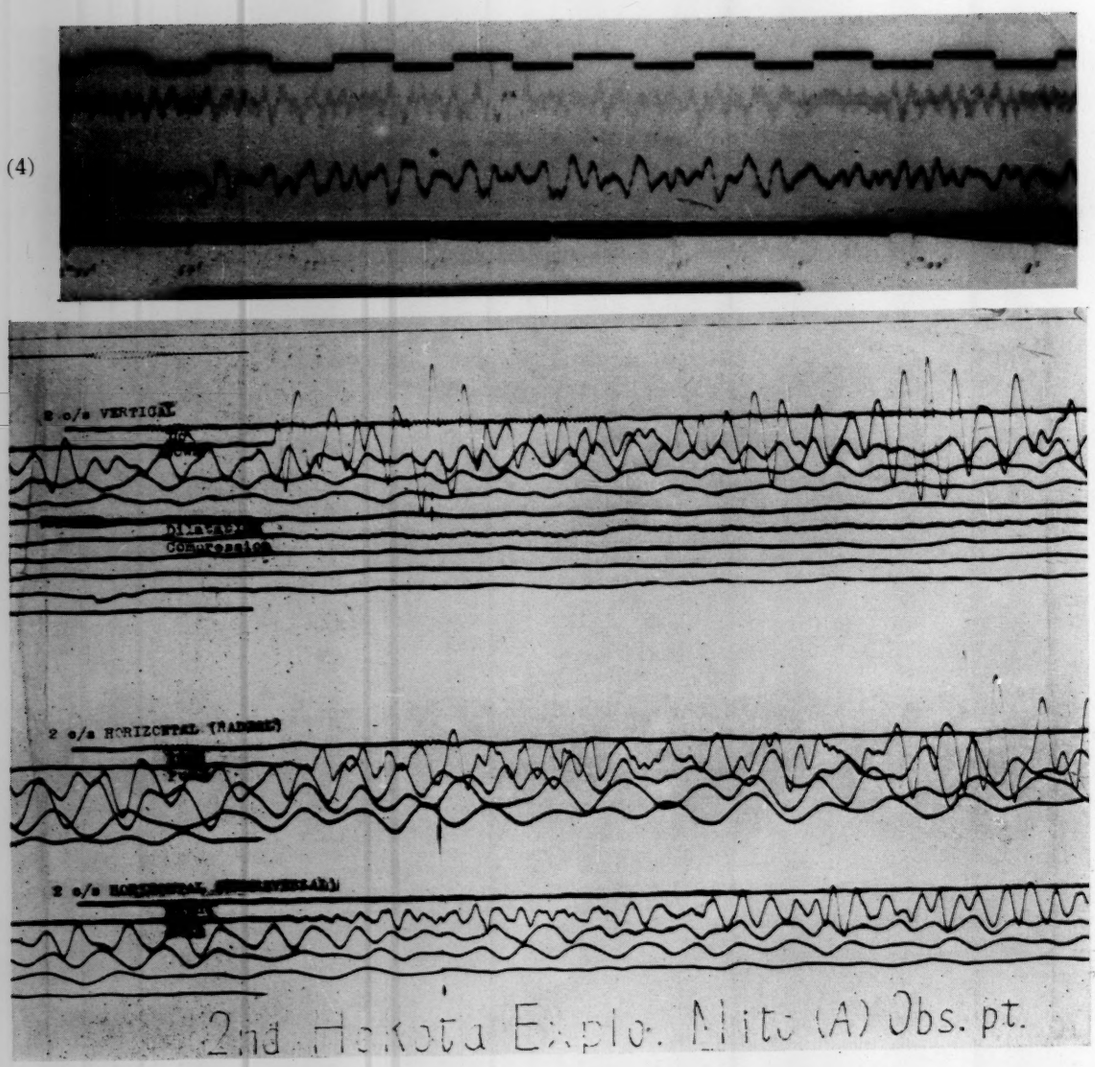


(5)

(6)

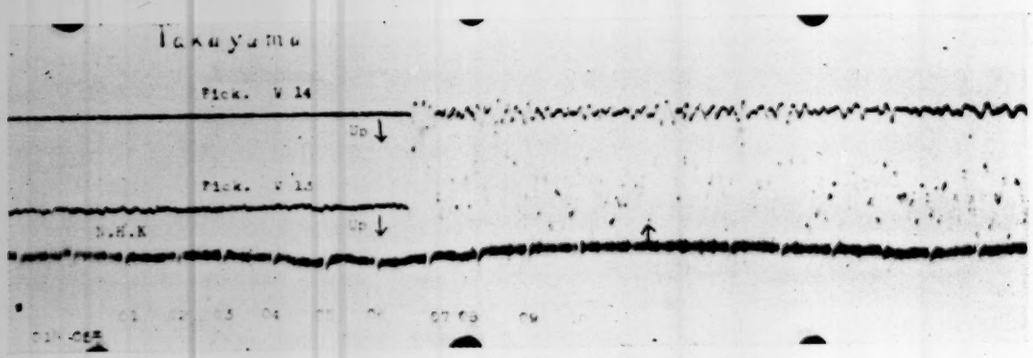


(4) Seismogram at Kawamata in K–II ($\Delta$=202.5 km).
(5) Seismogram at Mito (A) in H–II ($\Delta$=21.8 km).
(6) Seismogram at Takayama in N–I ($\Delta$=30.2 km).

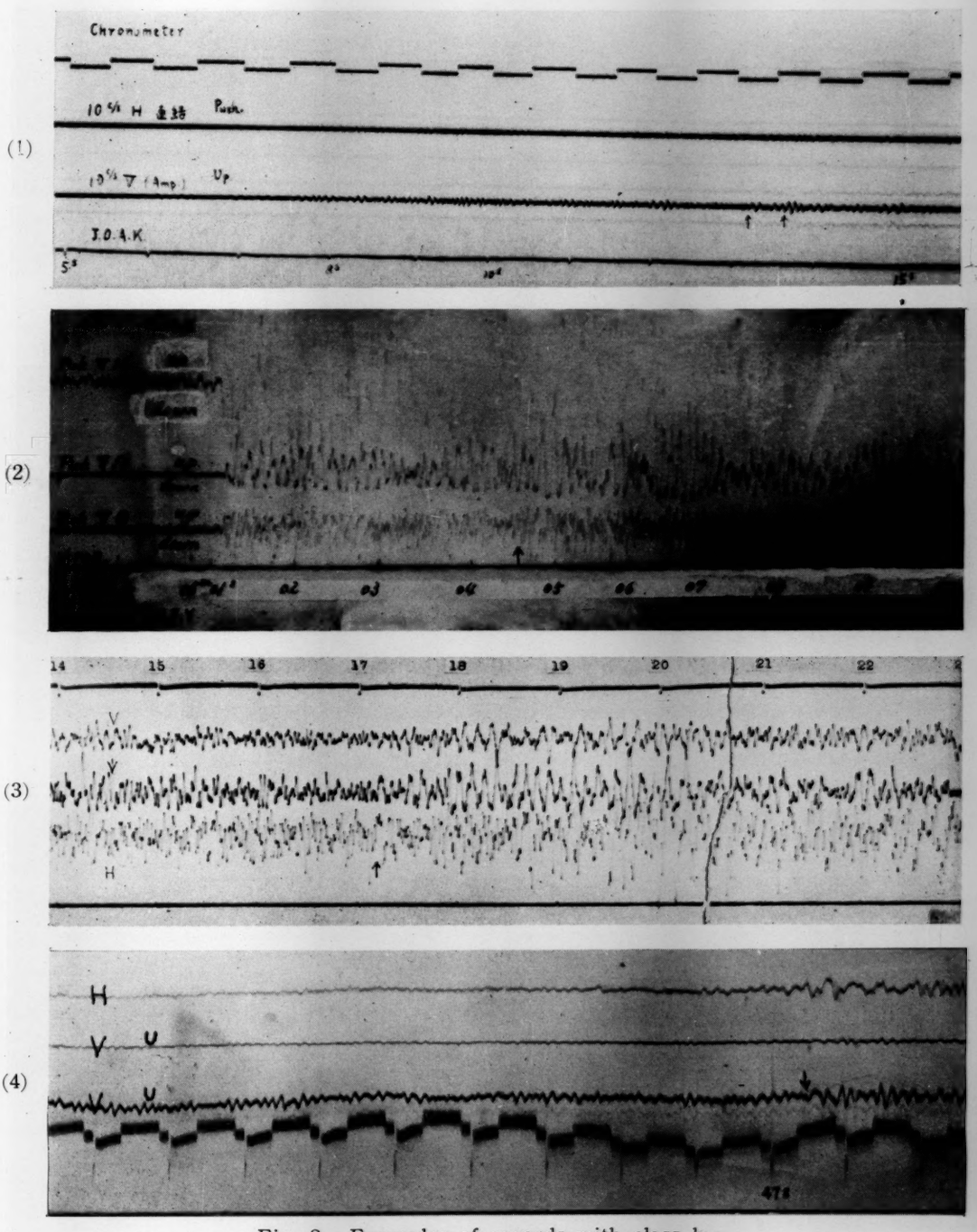


Fig. 8. Examples of records with class b.

(1) Seismogram at Kesennuma in K–I ($\Delta$=45.5 km).
(2) Seismogram at Sakari in K–II ($\Delta$=23.9 km).
(3) Seismogram at Sizugawa in K–II ($\Delta$=72.3 km).
(4) Seismogram at Kaneyama in K–II ($\Delta$=173.7 km).

(1)

(2)

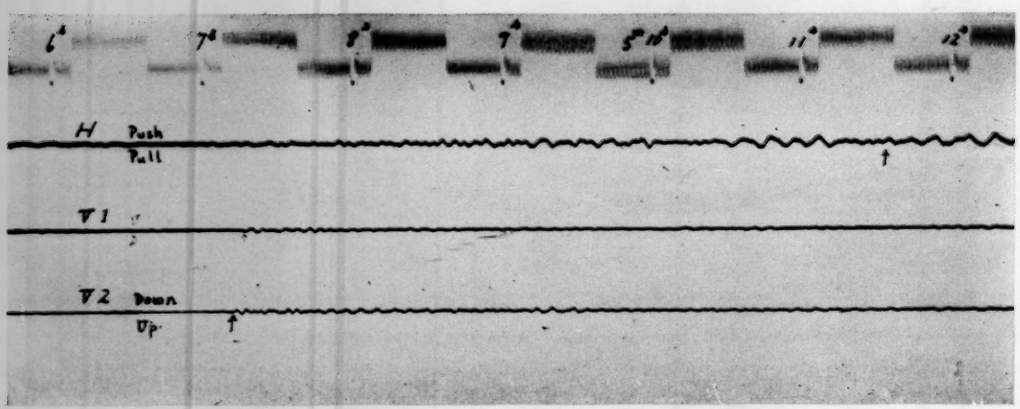


(3)

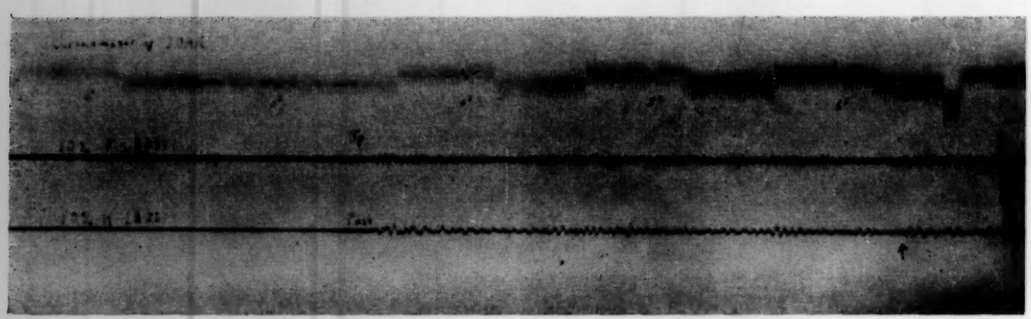

Fig. 9. Examples of records with class c.

(1) Seismogram at Mamurogawa in I–III ($\Delta$=58.7 km).
(2) Seismogram at Kawatabi in I–III ($\Delta$=41.9 km).
(3) Seismogram at Setamae in K–I ($\Delta$=20.4 km).

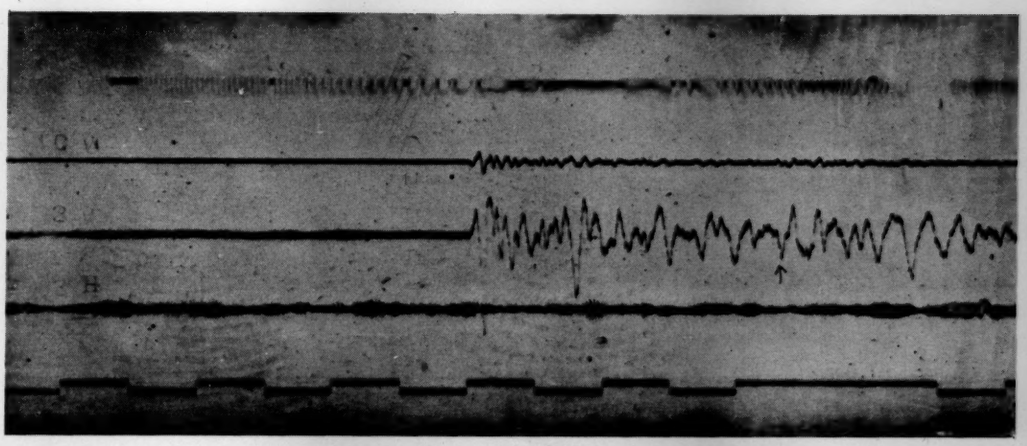

Fig. 10. Example of record with class d.
Seismogram at Hondera in I-III ($\Delta$=15.3 km).

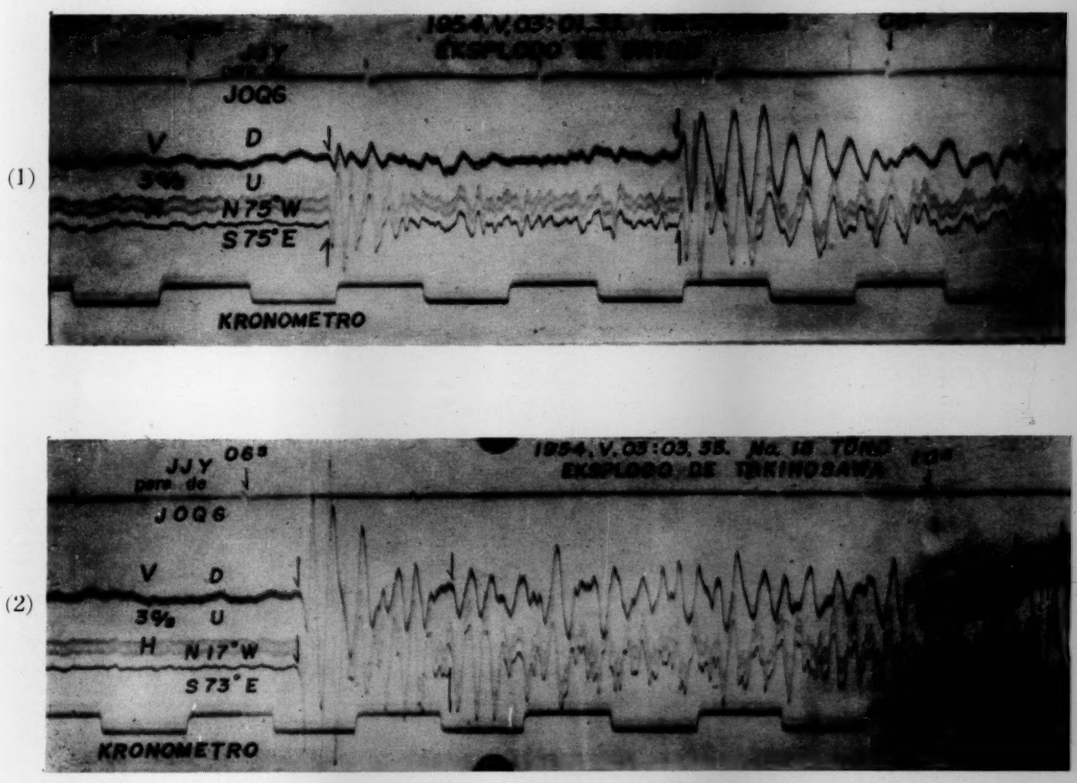


Fig. 11. Examples of records with class p.
(1) Seismogram at Tōno in Daidō Explosion ($\Delta$=14.64 km).
(2) Seismogram at Tōno in Takinosawa Explosion ($\Delta$=32.72 km).

(3)

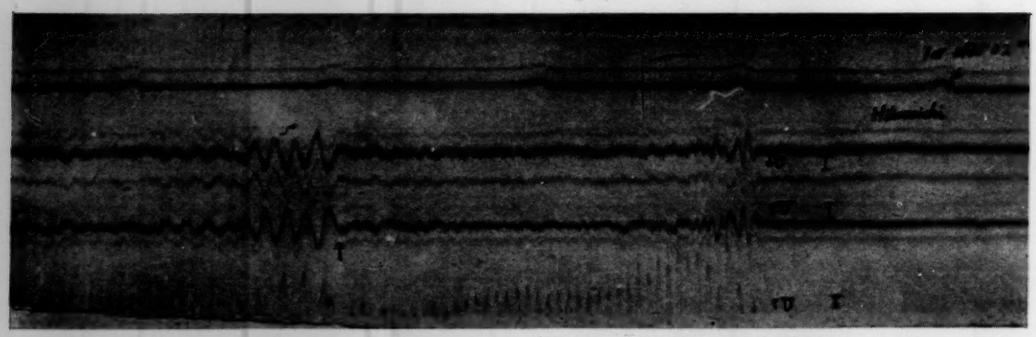

(4)

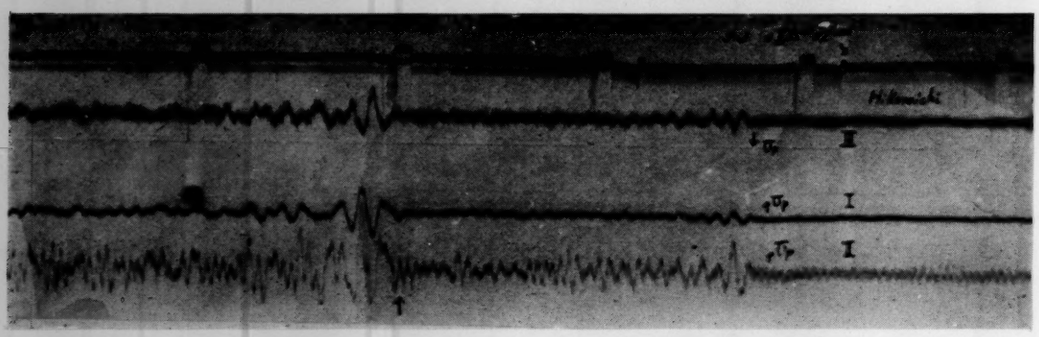

(5)

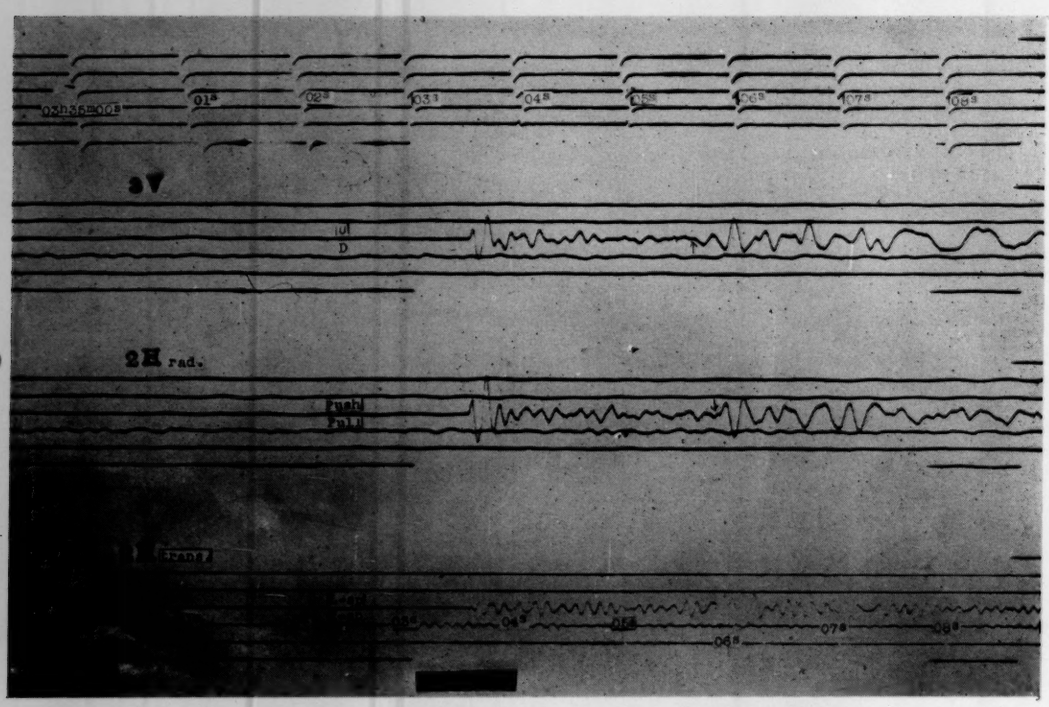

(3) Seismogram at Hikoroiti in Dōsen Explosion ($\Delta$=15.11 km).
(4) Seismogram at Hikoroiti in Daidō Explosion ($\Delta$=13.24 km).
(5) Seismogram at Ōhasi in Takinosawa Explosion ($\Delta$=16.73 km).

(6)

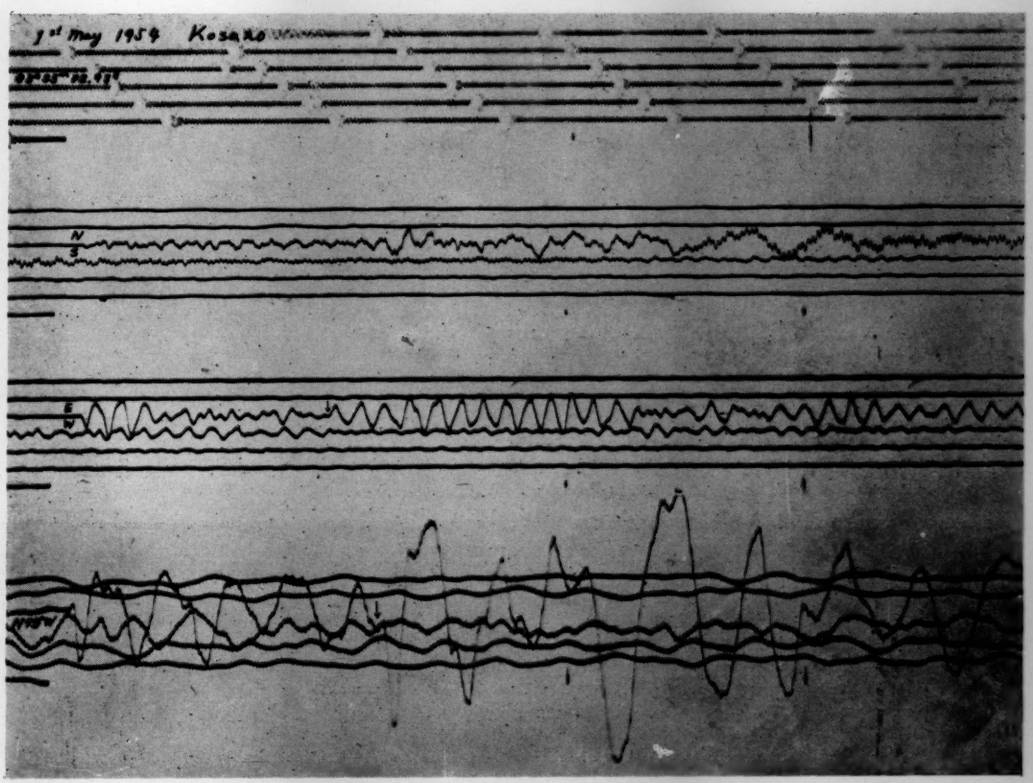

(6) Seismogram at Kosano in Sin'yama Explosion ($\Delta$=13.25 km).

(1)

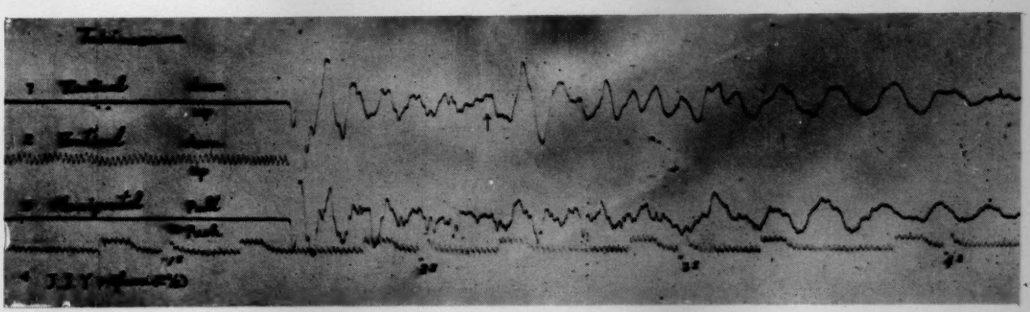

(2)

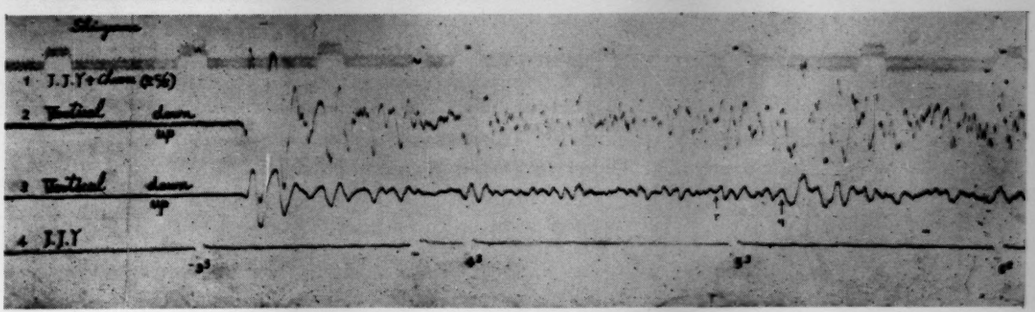

Fig. 12. Examples of records with class q.
(1) Seismogram at Nakatuma in Takinosawa Explosion ($\Delta$=4.89 km).
(2) Seismogram at Nakatuma in Sin'yama Explosion ($\Delta$=14.59 km).

(3)

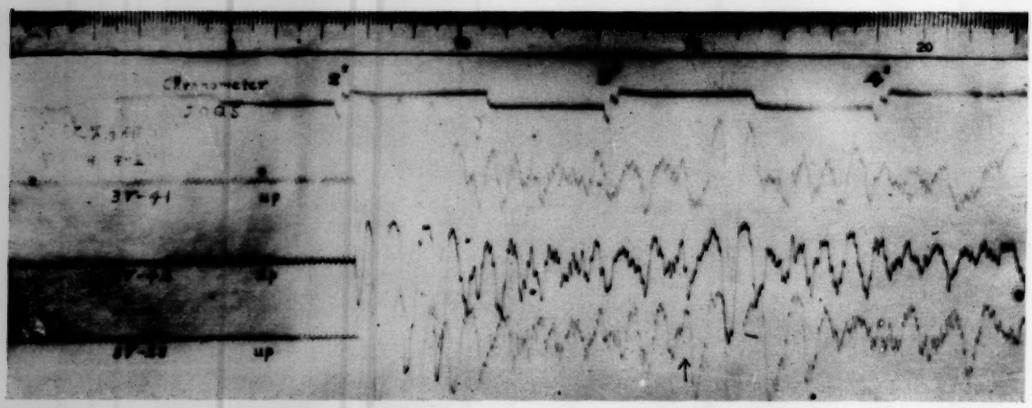

(4)

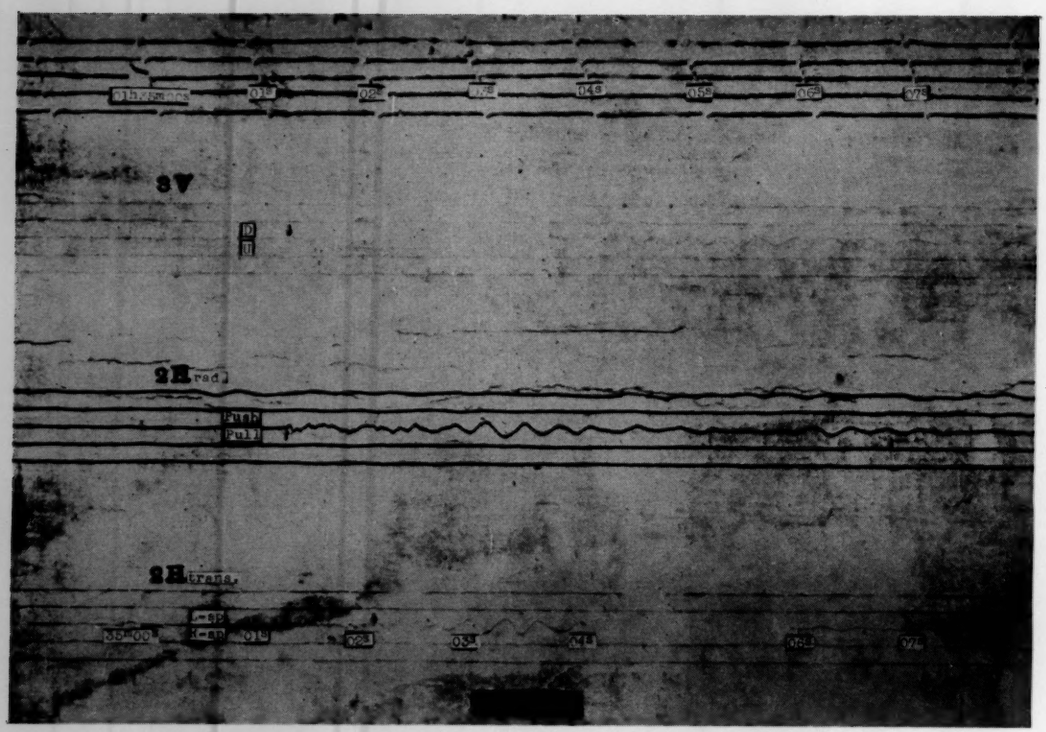

(3) Seismogram at Noda in Takinosawa Explosion ($\Delta$=8.15 km).
(4) Seismogram at Ōhasi in Dōsen Explosion ($\Delta$=5.62 km).

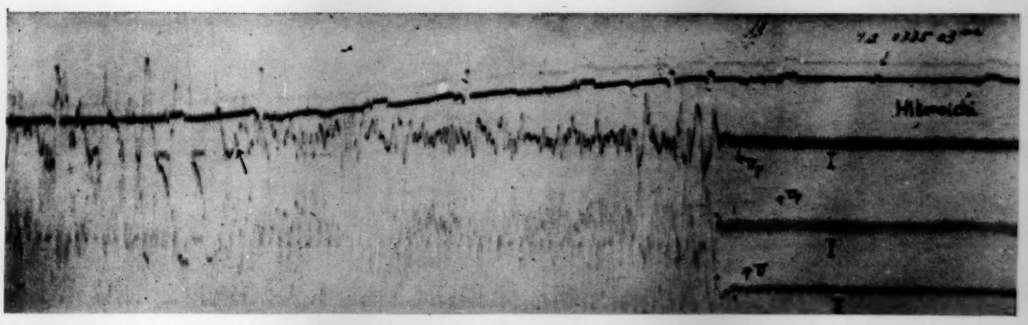

Fig. 13. An example of record with class r.
Seismogram at Hikoroiti in Sin'yama Explosion ($\Delta$=18.97 km).

(1)

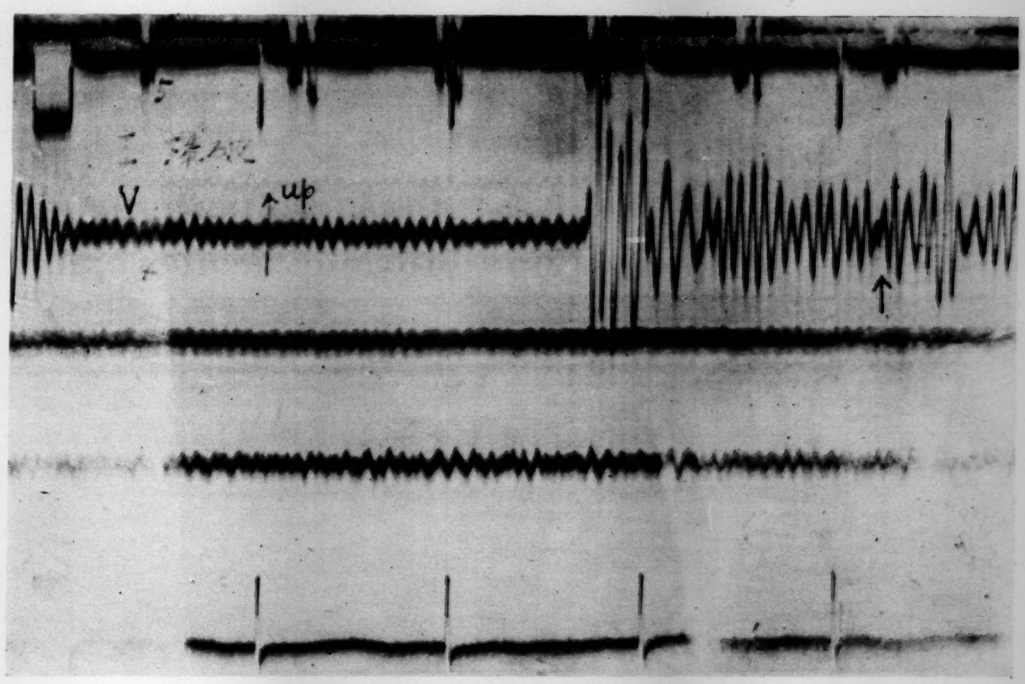


Fig. 14. Examples of records with class s.
(1) Seismogram at Takinosawa in Dōsen Explosion ($\Delta$=12.90 km).

(2)

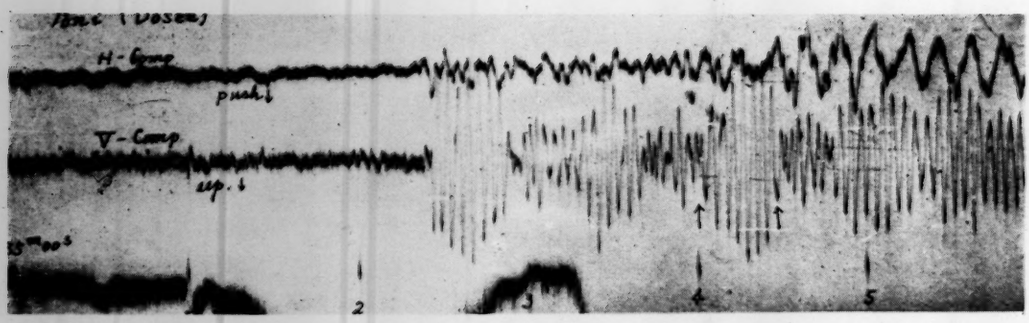


(2) Seismogram at Tōni in Dōsen Explosion ($\Delta$=11.41 km).

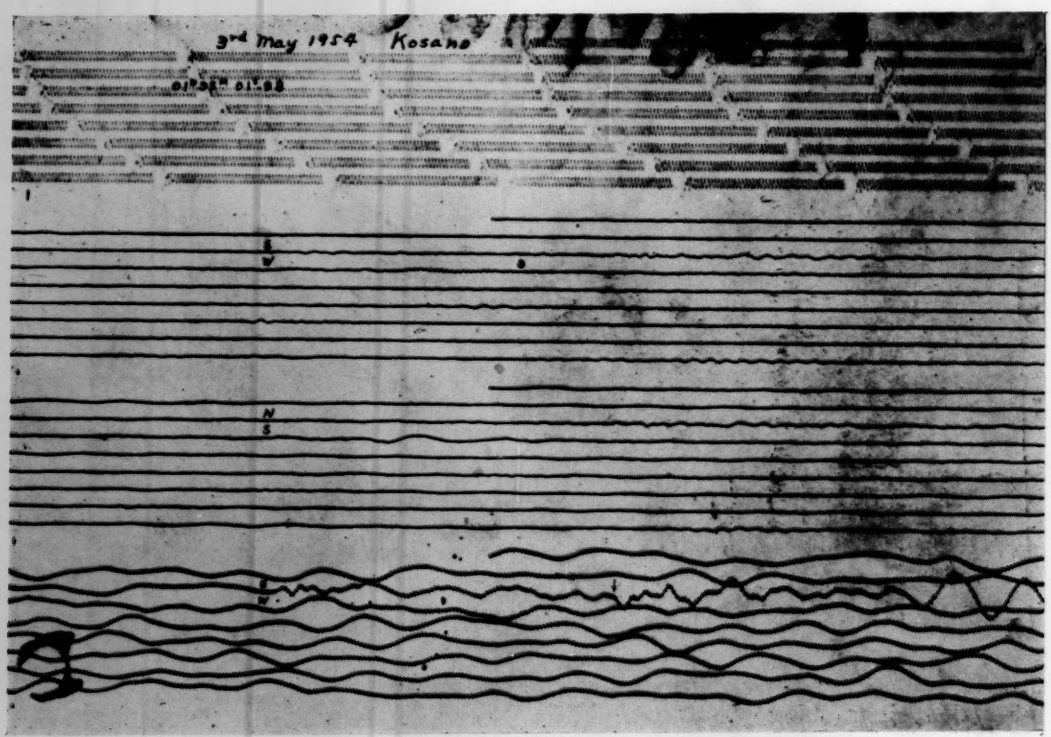


Fig. 15. An example of record with class t.
Seismogram at Kosano in Daidō Explosion ($\Delta$=13.11 km).

Table 4.

| | $P_n$ | $S_n$ | $P_n/S_n$ | $P_2$ | $S_2$ | $P_2/S_2$ | $P_1$ | $S_1$ | $P_1/S_1$ |
|---|---|---|---|---|---|---|---|---|---|
| Western Transvaal[10] | 8.27 | 4.83 | 1.72 | 6.09 | 3.68 | 1.66 | 5.65 | 3.37 | 1.68 |
| Canadian Shield[11] | 8.18 | 4.85 | 1.69 | 6.25 | 3.54 | 1.77 | — | — | — |
| Western Australia[12] | 8.21 | 4.75 | 1.73 | 6.03 | 3.55 | 1.70 | — | — | — |
| Japan Kwantô[13] | — | — | — | 6.10 | 3.63 | 1.68 | — | — | — |
| Japan Tôhoku | — | — | — | 6.15 | 3.57 | 1.72 | 5.80 | 3.36 | 1.73 |

The values of $V_P/V_S$ were also calculated, and tabulated in Table 4. The values of the Kwantō area are a little smaller. But in general their values are reasonable.

At the end of the discussion we must refer to the high sensitive seismometers used in most of our observations. These seismometers were designed by Den[14]. But they are designed to get a sharp break of initial motions, so the natural frequency of the seismometer is rather high, and characteristics are insufficient to get clear *S*-phases. Because, in general, periods of *S*-waves are rather longer than those of *P*-waves, so we had better reconstruct the seismometer and change the characteristics for the better study of the travel-times of *S*-waves.

## 5. Concluding remarks

From the observations of thirteen blasts in Tōhoku and Kwantō areas, we derived the velocities 3.04 km/sec and 3.36 km/sec near the Kamaisi Mine, 3.06 km/sec and 3.57 km/sec in Tōhoku area, and 3.63 km/sec in Kwantō area respectively. We take these velocities as those of *S*-waves.

The depths of the discontinuities from the surface calculated from these velocities are not so inconsistent with those of the depths calculated from *P*-waves, although these *S* velocities were those of mean values determined by the process explained in the text.

We could not get sufficient informations about $S_n$, because of the scanty data of the distant observations.

10) P. L. WILLMORE, A. L. HALES and P. G. GANE, *Bull. Seism. Soc. Amer.*, **42** (1952), 53.
11) J. H. HODGSON, *Publ. Dom. Obs. Ottawa*, **16** (1953), 113.
12) B. A. BOLT, H. A. DOYLE and D. J. SUTTON, *Gephys. Journ.*, **1** (1958), 135.
13) *loc. cit.*, 1), 2).
14) N. DEN, *Annual Meeting of the Seism. Soc. of Japan*, (Nov., 1954).

The values of $V_P/V_S$ were calculated, and these values are reasonable in general.

In conclusion, authors express their hearty thanks to Professor T. Matuzawa and to all other members of the Research Group for Explosion Seismology who gave them facilities for using the valuable seismograms.

---

## 18. 爆破地震動観測によつて得られた $S$ 波の走時について

地震研究所 浅野周三
東京大学地球物理学教室 田望
京都大学地球物理学教室 三雲健
地震研究所 嶋悦三
気象庁 宇佐美竜夫

爆破地震動研究グループにおいては，現在までに，自力発破2回を含め13回の観測を行つた．グループの観測の主眼は地下構造の推定にあり，このため解析には原則として初動の走時のみをとりあつかつていた．この論文では，Late Phase の中で特に $S$ 波と思われるものをとりあげ，その速度を最小自乗法によつて求めた．式 (1), (2) は釜石鉱山附近で得られた値，(3), (4) は東北地方，(5) は関東地方における値である．なお $S_n$ に相当するものについては遠方の観測がたりないために得られなかつた．これ等の式を用いて平行層の仮定のもとに，intercept time から不連続面の深さをきめると，釜石附近で 0.67 km，東北地方で 4.72 km を得るが，この値は $P$ 波よりもとめたものとそう矛盾しない．

$V_P/V_S$ の値は，関東が少々小さいが，東北地方の値は妥当な値であると思われる。(Table 4) なお世界各地の，爆破により求められた $S$ 波の速度に似ているものがあるのは面白いことである．

---

BULLETIN OF THE EARTHQUAKE
RESEARCH INSTITUTE
Vol. 37 (1959), pp. 307-325

# 19. *Investigations into Microseisms Using the Observational Data of Many Stations in Japan. (Part I)*

## —On the Origin of Microseisms.—

By Tetsuo A. SANTÔ,

Earthquake Research Institute.

(Read November 25, 1958.—Received March 31, 1959.)

### § 1. Introduction

Numerous papers on microseisms with periods of 3~6 seconds have been written by many seismologists in various countries. In spite of their efforts, however, we cannot say that the true nature of microseisms have been fully described. Taking a general view of the past investigations, their observational results seem to depend upon the positions at which microseisms were recorded. That is to say, the character of microseisms seems to depend, to some extent, upon the regional characteristics of the observational stations. It means that a considerable number of unknown small factors are contained in the phenomena of microseisms.

Accordingly, it is rather appropriate to examine them by a synoptic method using the observational data at many stations over a wide area.

From July, 1957, continuous observations for microseisms have begun at about 15 stations throughout Japan as part of the I.G.Y. program. At these stations, the amplitudes, periods and characters of microseismic wave have been measured at least four times a day and have been reported.

Fortunately, these data were at the writer's disposal and he had an opportunity to make a synoptic study on microseisms, i.e. to investigate them from a macroscopic standpoint. The purpose of the present study is, at first, to see the relation between the occurrence of microseismic storms recorded by these stations and any of meteorological disturbances near Japan, and secondly, by using these observational results, to consider the mechanism of the occurrence of microseismic storm with the aid of some oceanographical data.

The data of microseisms used in this paper are those from Septem-

ber 1957 to May 1958.

## § 2. Observational facts

1) *General features of the occurrence of microseismic storms*

Fig. 1 shows some examples of the time variations of microseismic amplitude being recorded at eleven observational stations on the mainland of Japan. The locations of these stations are shown in the annexed maps of the following figures, for instance of Fig. 2.

In general, the occurrence of many microseismic storms at many stations seem to be correlated with each other. Examining the meteorological conditions which are considered to induce such microseismic storms, it was clearly noticed that these microseismic storms were caused by the existence of atmospheric low pressure centers, namely cyclones and typhoons, in the vicinity of Japan, or the passing of a strong cold front from west to east across the main island. Some of the storms, of cause, were induced by more than two causes, for instance, the co-existence of two or three cyclones on the sea, or the passing of a cold front accompanied by some other cyclones, etc.

In order to find the effect of these causes to microseisms separately, it is necessary to investigate the cases when only one of these three causes appeared on meteorologi-

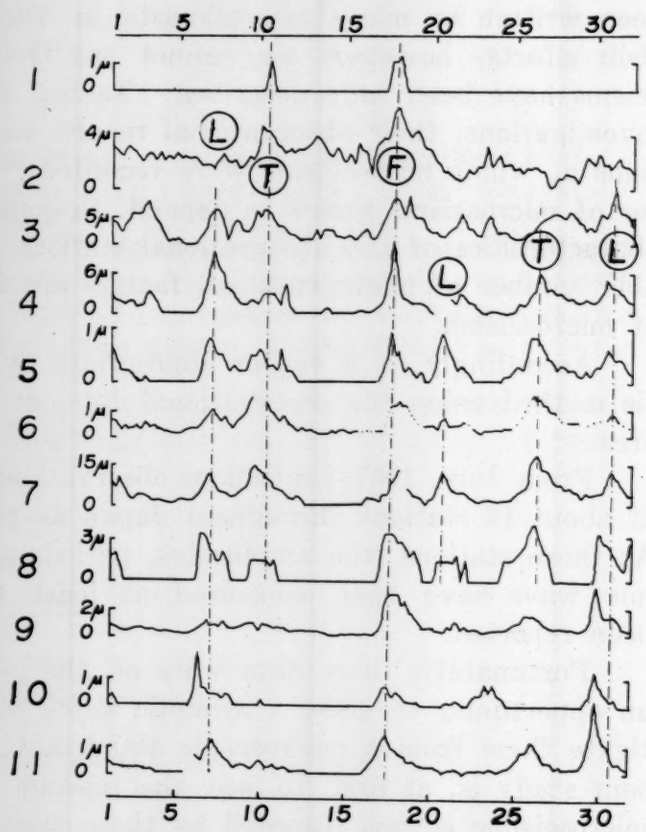


Fig. 1. Some examples of the variations of microseismic amplitudes with time at many stations. Dates are taken as abscissa. Numbers 1~11 correspond to the observational positions which are shown in the annexed map of Fig. 2.

cal maps. These cases are shown in Fig. 1 marked by T, L and F, which mean that the cause of microseismic storm is undoubtedly the passing of a single typhoon, a cyclone and that of a strong cold front passing across the island, respectively.

Fig. 1 shows us an interesting feature indicating the difference between two cases, the case of a strong cold front F and that of a cyclone L or typhoon T. In the case of a cyclone or a typhoon, the appearance of maximum amplitudes of a microseismic storm was regularly delayed for the northern stations or the microseismic storms appeared only at the stations in a rather restricted area. When a strong cold front was passing, on the other hand, the microseismic storms were not only recorded at most of the stations, but their maximum amplitudes appeared almost at the same time at every station.

Fig. 2(a).

Fig. 2(a)~(c). Shift of the maximum amplitudes of microseismic storms at every station due to the passing of cyclones. In order to make the fact clear, the times of maximum microseismic amplitudes at every station are marked by black triangles. Numerals and small dots along the path of each cyclone show the dates at every 0 o'clock and the positions at every 12 hours of their centers respectively.

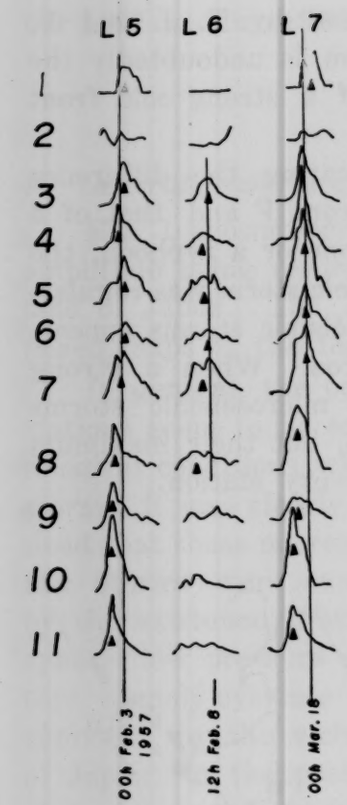
L 5
L 6
L 7
1
2
3
4
5
6
7
8
9
10
11
00h Feb. 3 1957
12h Feb. 8
00h Mar. 18

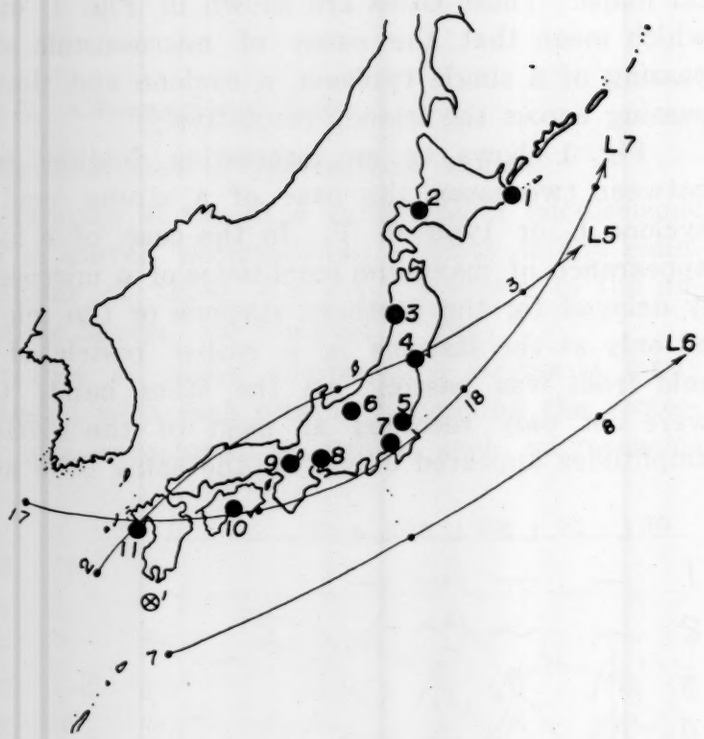
L7
L5
L6
1
2
3
4
5
6
7
8
9
10
11
12
15
16
17
18
20

Fig. 2(b).

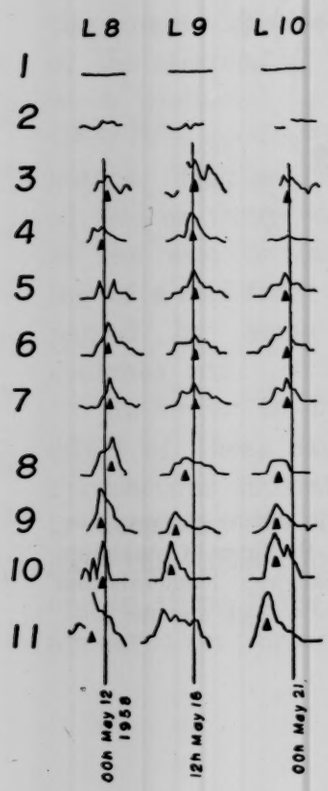
L 8
L 9
L 10
1
2
3
4
5
6
7
8
9
10
11
00h May 12 1958
12h May 16
00h May 21

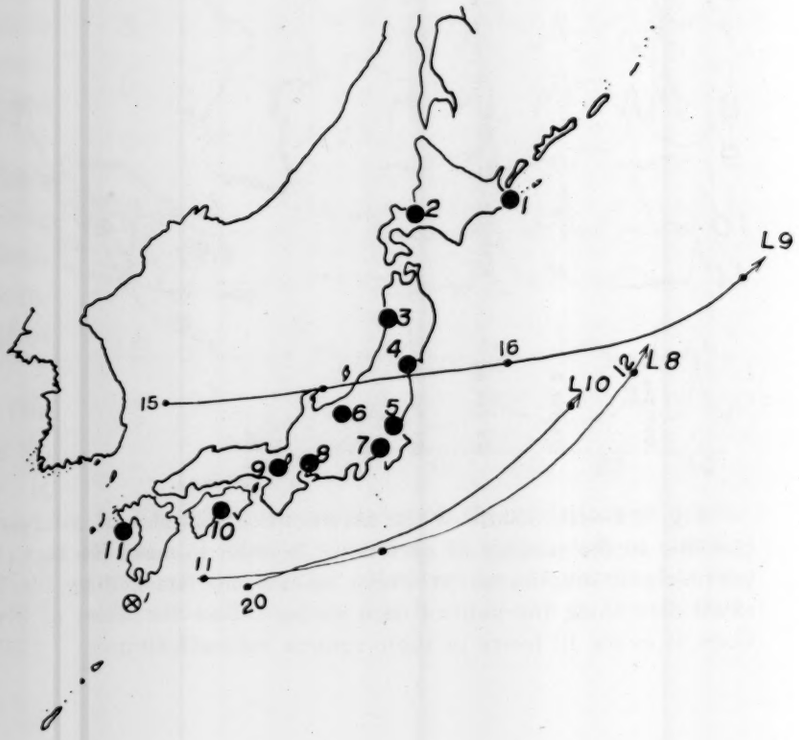
L9
L8
L10
1
2
3
4
5
6
7
8
9
10
11
12
15
16
20

Fig. 2(c).

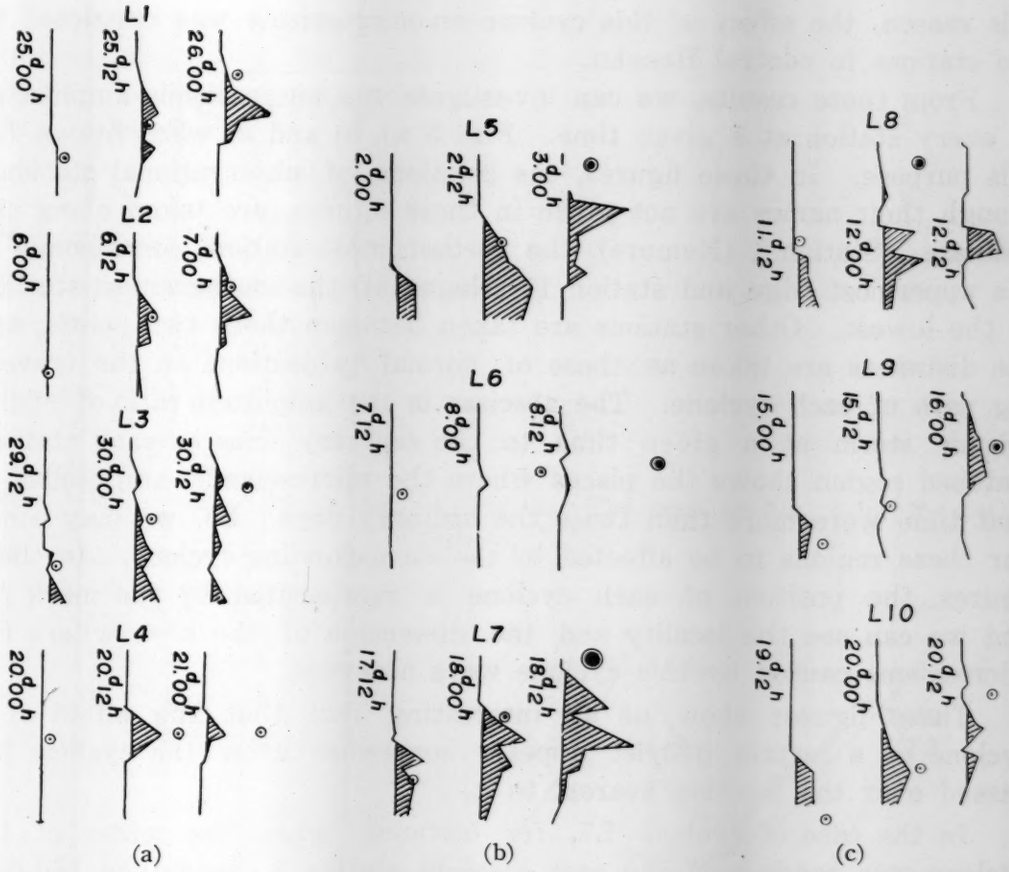


Fig. 3. Shift of the region of microseismic storms due to the passing of the cyclones correspond to those in Fig. 2. The relative positions of the corresponding cyclones are represented by the mark ⊙. The diameters of the inner black circles are inversely proportional to the central pressures of cyclones.

2) *Feature of microseismic storms due to cyclones and typhoons*

In the following figures, several examples of these features will be shown. Fig. 2 a), b) and c) show how the microseismic storms appeared at each station when a cyclone was passing near Japan along the path shown in the annexed maps. For instance, when cyclone L7 passed through the southern coast of Japan and went away towards northeast, the microseismic storm at first began at southern stations and then gradually shifted to the northern stations as the cyclone shifted to the north. This tendency can be clearly seen in all other cases in this figure, except L4. In this exceptional case, however, the reason can be well explained. In this case, the cyclone L4 appeared off the coast of central Honshu and turned to the east at once. For

this reason, the effect of this cyclone on microseisms was restricted to the stations in central Honshu.

From these results, we can investigate the microseismic amplitudes of every station at a given time. Fig. 3 a), b) and c) were drawn for this purpose. In these figures, the positions of observational stations, though their names are not given in these figures, are taken along the ordinate. Station 1 (Nemuro), the northernmost station, corresponds to the uppermost edge and station 11 (Nagasaki) the southernmost station, to the lowest. Other stations are taken between these two points, and the distances are taken as those of normal projections on the travelling path of each cyclone. The abscissa is the amplitude ratio of microseismic storm at a given time to the ordinary ones at each station. Hatched region shows the places where the microseismic amplitudes at that time were more than twice the ordinary ones. So, we may consider these regions to be affected by the corresponding cyclone. In these figures, the position of each cyclone is represented by the mark ⊙, and we can see the locality and the dimension of the area where the microseisms caused by this cyclone were observed.

These figures show us an interesting fact that the effect of a cyclone on a certain district appears somewhat after the cyclone has passed over the position nearest to it.

In the case of cyclone L7, for instance, when the center of the cyclone was passing off the east coast of station 4 (Sendai) on 18d 00h, the microseismic amplitudes in this district were still not so large, but they became large when the center of the cyclone had gone away far from this region.

This tendency has been often noticed by several authors, and recentely, F. I. Monakhov reported that "the sources of microseisms lag behind the cyclonic center by approximately $10 \cdot V$ km," in which $V$ is the travelling speed of that cyclone in km per hour.[1]

In the cases of L4, L6 and L9, the tendency given above cannot be seen in this figure. The reason, however, can be very easily found in annexed map of Fig. 2 corresponding to these cyclones. For, these cyclones were all running off towards the east.

When a typhoon passes near Japan, the relation between the occurrence of microseismic storms at each station and the running path

1) F. I. MONAKHOV, "Developement of Microseismic Method of Tracing Storms at Sea," *Abstracts of the Reports at the XI General Assembly of the International Union of Geodesy and Geophysics* (1957), 76.

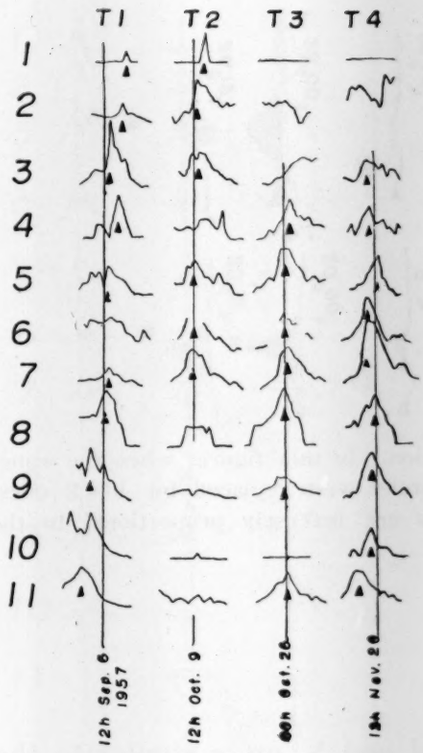


Fig. 4. The same as Fig. 2 for the case of typhoon.

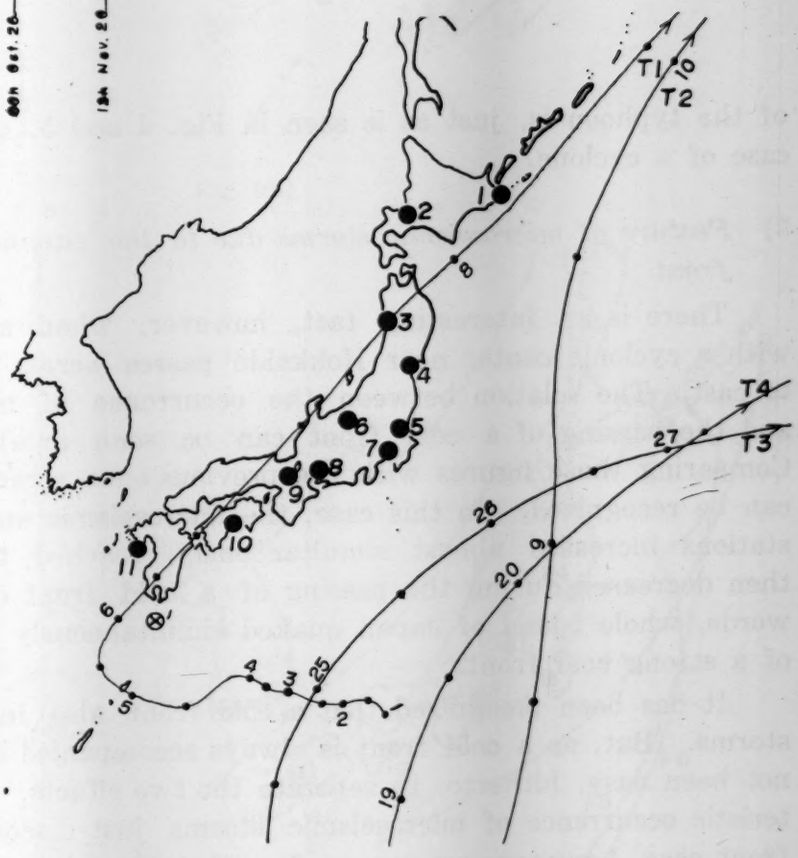

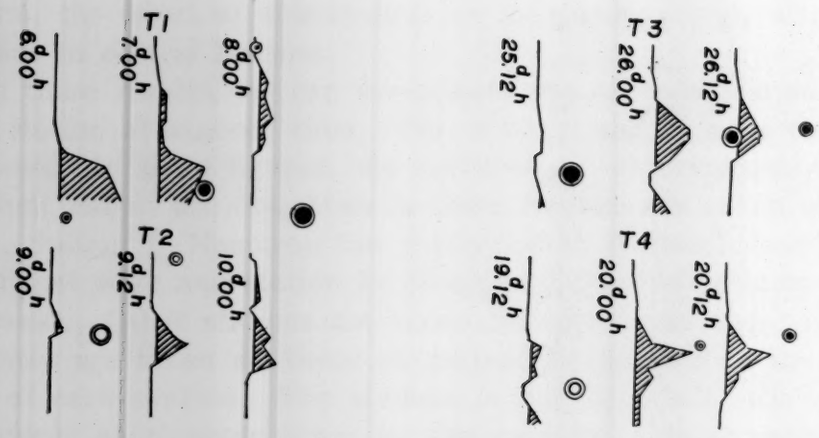


Fig. 5. The same as Fig. 3 for the case of typhoon. In this figure, when the atmospheric pressure was lower than 960 mb., the white circles were replaced for black ones. In this case, the diameters of the inner white circles are inversely proportional to the central pressures of typhoons.

of the typhoon is, just as is seen in Fig. 4 and 5, quite similar to the case of a cyclone.

3) *Feature of microseismic storms due to the passing of a strong cold front*

There is an interesting fact, however, when a strong cold front with a cyclonic center near Hokkaido passes across Japan from west to east. The relation between the occurrence of microseismic storms and the passing of a cold front can be seen in a) and b) of Fig. 6. Comparing these figures with the previous ones, a remarkable difference can be recognized. In this case, the microseismic amplitudes of all the stations increased almost simultaneously, reached the maximum and then decreased during the passing of a cold front (Fig. 7). In other words, whole island of Japan quaked simultaneously due to the passing of a strong cold front.

It has been recognized that a cold front also induces microseismic storms. But, as a cold front is always accompanied by a cyclone, it has not been easy, hitherto, to separate the two effects. Using the characteristic occurrence of microseismic storms just discovered for the cold front case, however, we can confirm that these storms were undoubted-

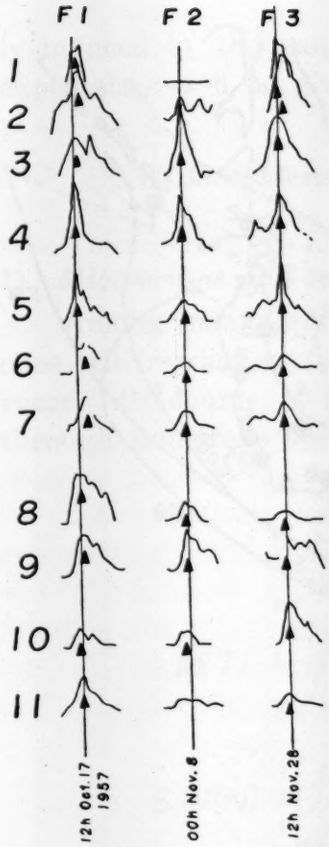
F1
F2
F3
1
2
3
4
5
6
7
8
9
10
11
12h Oct.17 1957
00h Nov.8
12h Nov.28

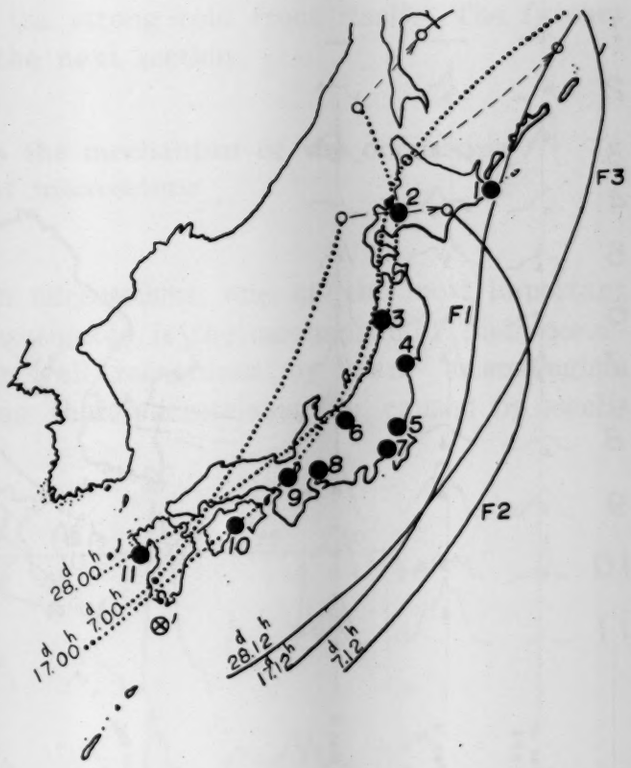
F3
F1
F2
1
2
3
4
5
6
7
8
9
10
11
28d 00h
17d 00h
7d 00h
28d 12h
17d 12h
7d 12h

Fig. 6(a).

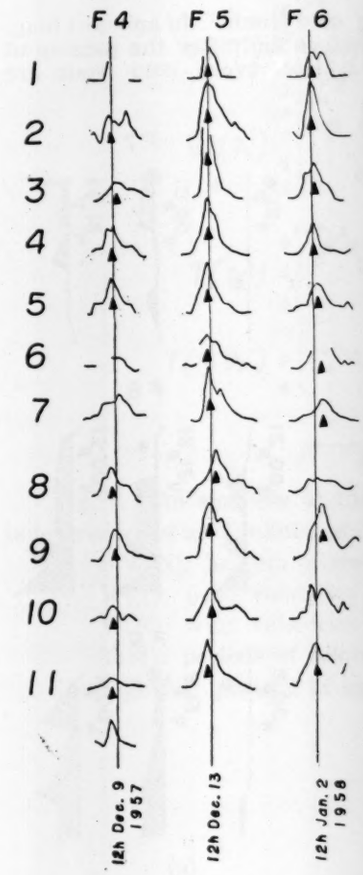
F4
F5
F6
1
2
3
4
5
6
7
8
9
10
11
12h Dec. 9 1957
12h Dec. 13
12h Jan. 2 1958

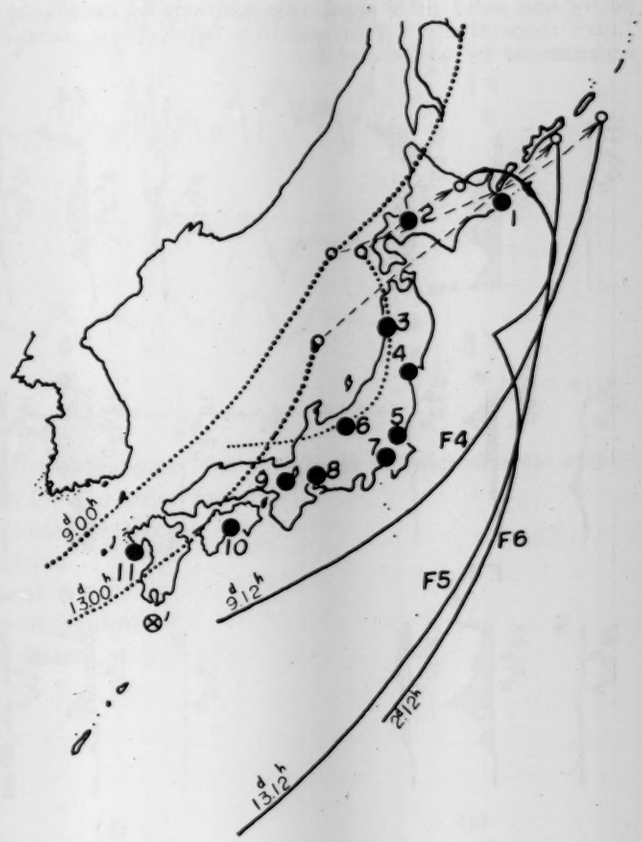
F4
F6
F5
1
2
3
4
5
6
7
8
9
10
11
9d 00h
13d 00h
9d 12h
2d 12h
13d 12h

Fig. 6(b).

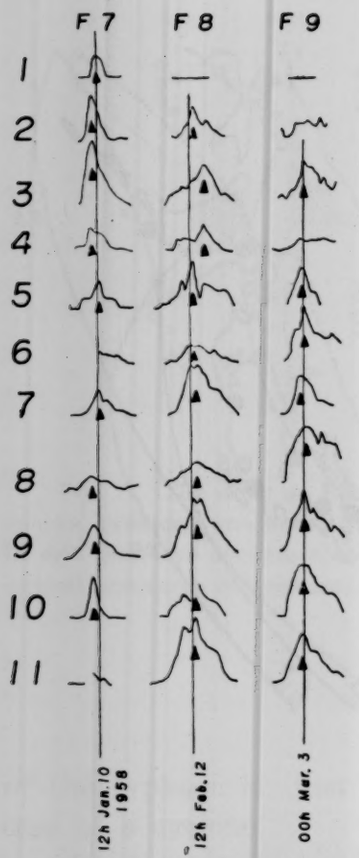


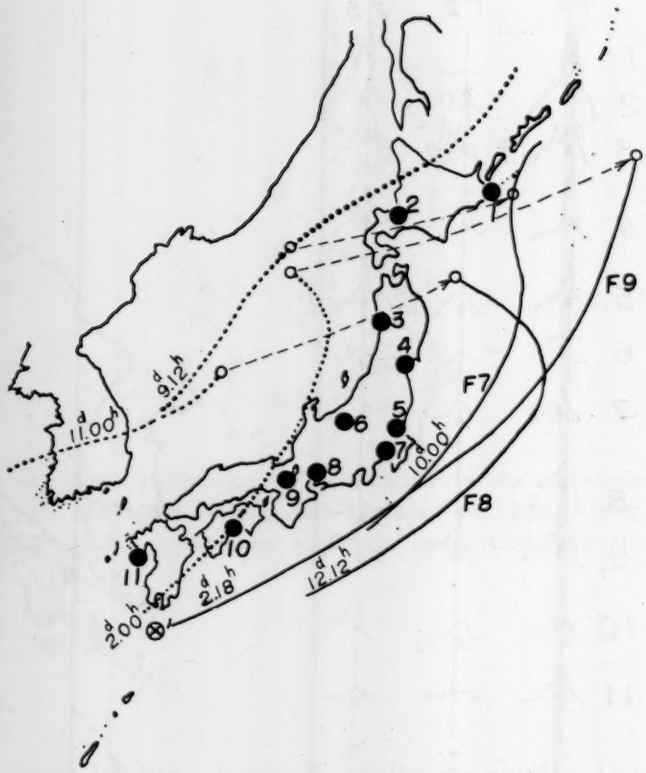


Fig. 6(c).

Fig. 6(a)~(c). The same as Fig. 2 for the case of strong cold fronts. In annexed map, dotted and solid lines show the positions of each cold front before and after the passing of Japan respectively. The positions of cyclonic centers which lead every cold front are represented by white circles.

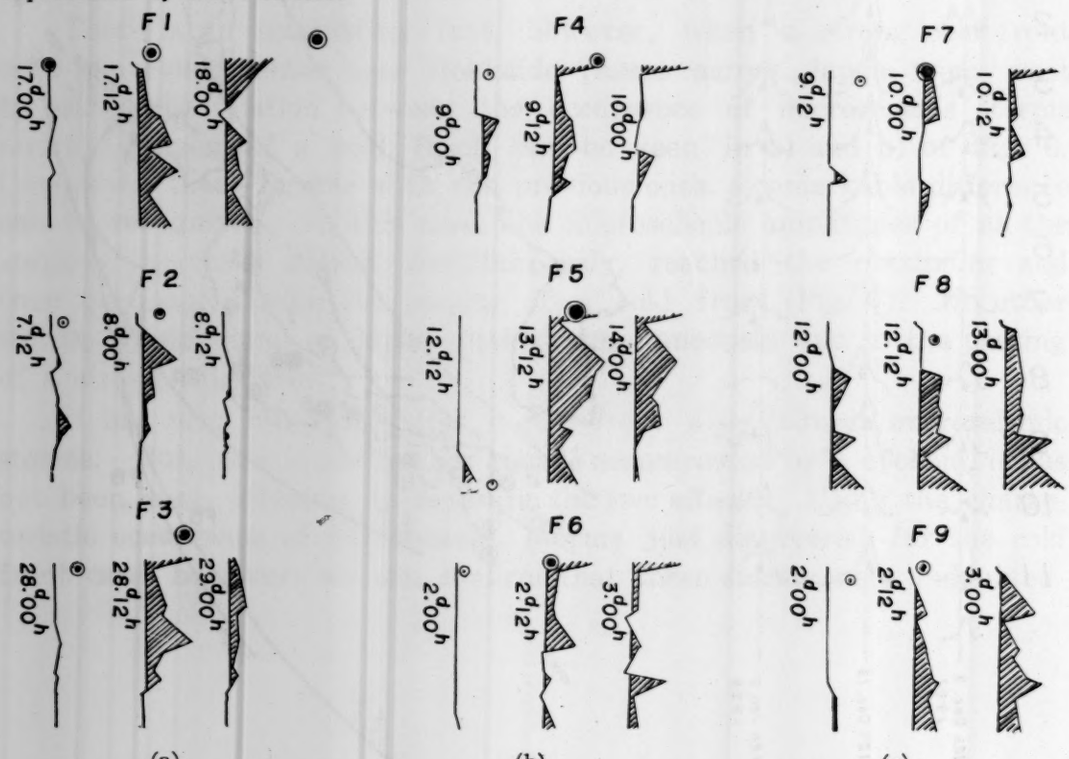


Fig. 7. The same as Fig. 3 for the case of strong cold fronts.

ly induced by the passing of the strong cold front itself. The further explanation will be given in the next section.

## § 3. Considerations on the mechanism of the occurrence of microseisms

1) *Microseisms and swells*

Among many problems on microseisms, one of the most important ones still remaining to be investigated is the mechanism of their occurrence. Of course, it has been well recognized by many seismologists through numerous observations that microseisms are caused by swells

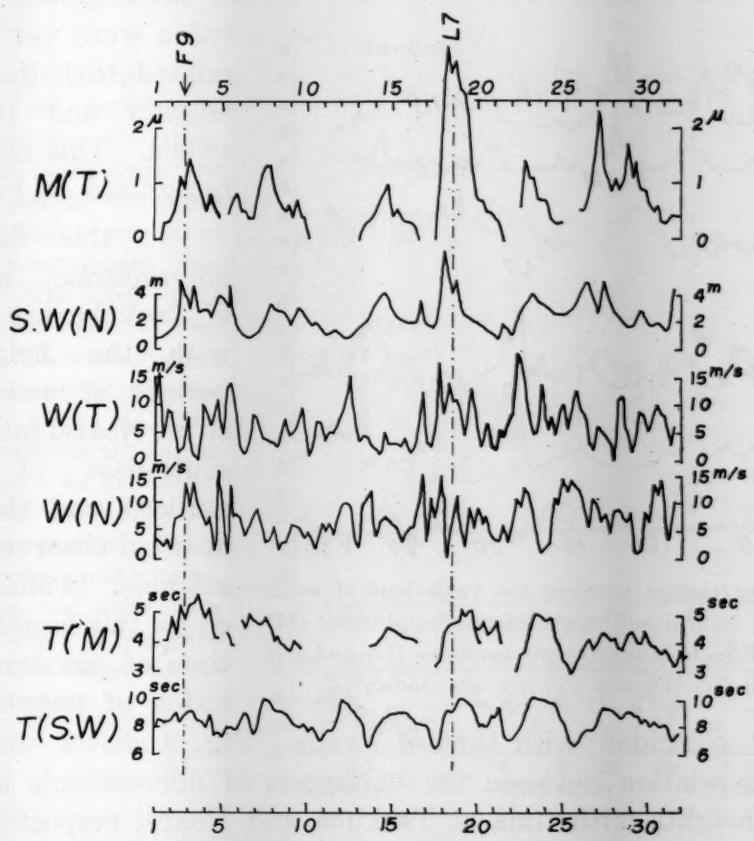


Fig. 8. An example of the correlations between the variations of microseismic amplitudes recorded at Tsukuba station (M(T)) and other factors.
S.W(N): heights of swells recorded at Naarai.
W(T): wind velocities at Tsukuba.
W(N): wind velocities at Naarai.
T(M): periods of microseisms at Tsukuba.
T(S.W.): periods of swells at Naarai.

due to some disturbances on the sea surface.

This conclusion was checked in the present investigations. The writer examined the relation of the amplitudes of microseismic storms with other reasonable factors, for example, with the heights and periods of swells or the strengths of wind recorded at a neighbouring station. As the result, it was quite clearly seen that the variations of the microseismic amplitudes were very well correlated with those of the heights and periods of swells. This can be well recognized in Fig. 8.

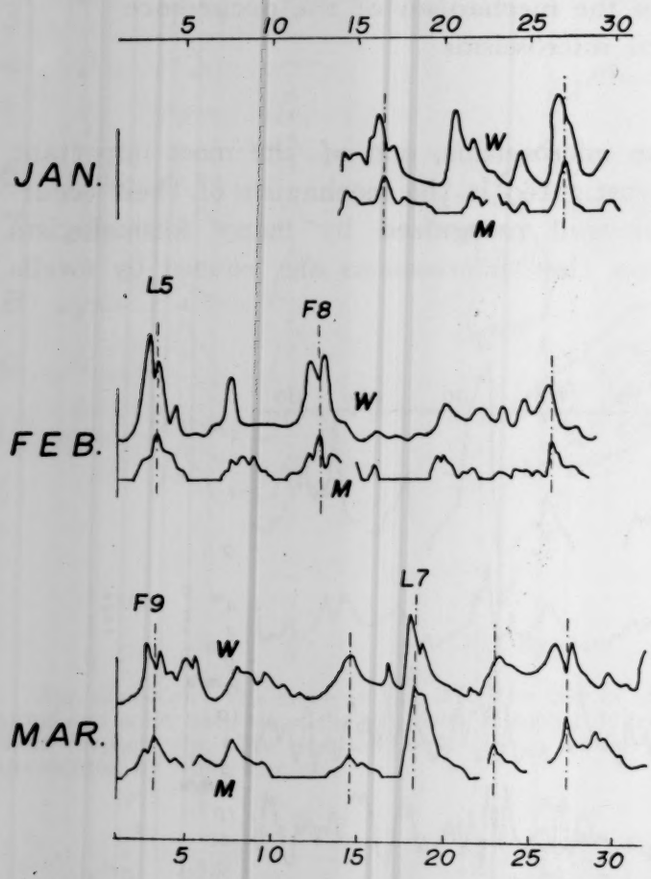


Fig. 9. Correlation between the variations of swell heights (W) at Naarai and microseismic amplitudes (M) at Tsukuba. Effects due to two cyclones (L5 and L7) and two cold fronts (F8 and F9) are also indicated.

In this figure, the microseismic amplitudes at Tsukuba are compared with the heights and periods of swells recorded at Naarai (about 80 km south-east of Tsukuba station) and the velocity of wind observed at both stations. It must be noticed in this figure, that the time of maximum amplitudes of microseisms approximately coincided with that of swells. Fig. 9 shows some examples of this relation between the variations of microseismic amplitudes and swell heights with time at Tsukuba and Naarai respectively.

Examining the time difference, by this figure, between the occurrence of the largest microseismic storms (Tsukuba) and the arriving of the highest swells (Naarai), several cases can be seen in which the above coincidence is not so good, but the phases of swell heights occur several hours before those of microseismic amplitudes. Considering that the velocity of microseismic waves is much higher than that of

swells, this phenomenon seems to be strange and the reason cannot be explained at present. It is important, however, that the maximum amplitude of microseisms never occurs before that of swells. Later, this feature will be utilized for considering the origin of microseisms.

2) *Relation between the periods of microseisms and swells*

Inspite of numerous investigations into microseisms, there still remain two points to be cleared up; that is, how and where the motion of the sea water (swells) turns into propagating elastic waves in the earth.

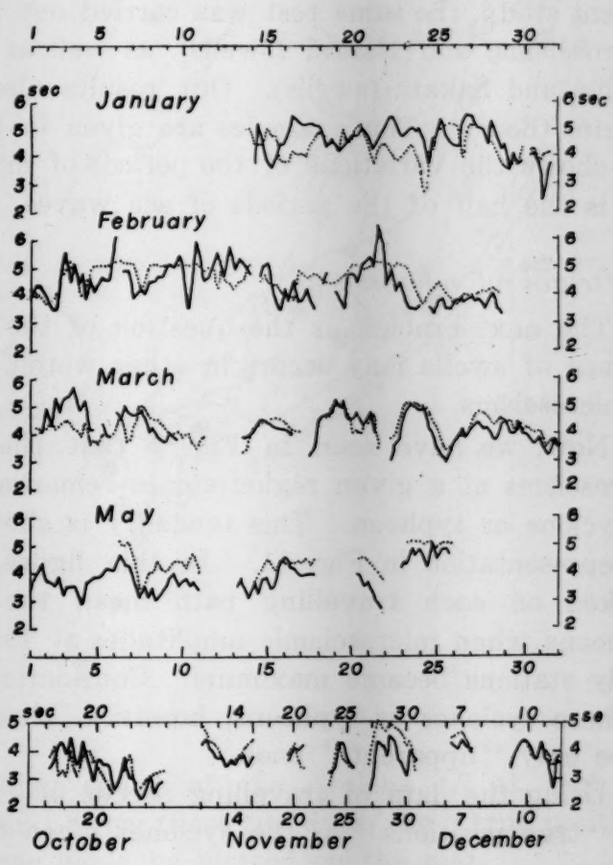


Fig. 10. Relation between the variation of the periods of microseisms (solid line) and half periods of swells (dotted line) recorded at two neighbouring stations. The upper figure indicates those of Tsukuba (microseisms) and Naarai (swells) and the lower those of Akita (microseisms) and Sakata (swells). As the observations of swells at Sakata especially were very scanty and not continuous, the writer was only able to compare these two variations intermittentely.

On the first point just mentioned, that is the mechanism of energy transformation from swells to microseisms, Longuet-Higgins has suggested a well-known and powerful theoretical conclusion. He concluded that this energy transformation can be done only when the standing waves occur owing to the interference of two swells with approximately the same periods travelling in opposite directions to each

other.[2] His theoretical suggestion was also experimentally verified by the same author and Cooper.[3] In order to confirm his theory by observations, the simplest method is to compare the periods of both microseisms and swells, for if microseisms are induced by the standing waves due to the interference of two trains of swells, the periods of microseisms must become half of the periods of a single train of swells.

Not a few observational studies concerning the relation between microseisms and swells have been published, and they seems to satisfy this relation between periods of these two kinds of waves.[4] In the present study, the same test was carried out using the data of Tsukuba (microseisms) and Naarai (swells), as well as the data of Akita (microseisms) and Sakata (swells). Our results also seem to fit the Longuet-Higgins theory. The examples are given in Fig. 10, in which the solid line shows the variations of the periods of microseisms, while the dotted line is the half of the periods of sea waves.

3) *Origin of microseisms*

The next broblem is the question of the position on which interference of swells may occur, in other words, the problem of the origin of microseisms.

Now, we have seen in Fig. 3 that the maximum amplitudes of microseisms at a given region comes remarkably later than the passage of cyclone or typhoon. This tendency is shown again in another way of representation in Fig. 11. In this figure, semi-circles and triangles marked on each travelling path mean the positions of cyclones and typhoons when microseismic amplitudes at Tsukuba and Nemuro respectively stations became maximum. Considering the travelling velocities of these cyclones or typhoons, however, these positions are considered to be only "apparent" ones.

Using the data of travelling speeds of cyclonic centers and swells, the "true positions" of the cyclones when they sent the swells which

2) M. S., LONGUET-HIGGINS, "A Theory of the Origin of Microseisms," *Phil. Trans Roy. Soc. London, A*, **243** (1950), 1.

3) R. I. B. COOPER and M. S., LONGUET-HIGGINS "An Experimental Study of the Pressure Variations in Standing Water Waves," *Proc. Roy. Soc. A*, **206** (1951), 424.

4) W. INOUYE, T. HIRONO and G. MURAI, "Microseisms and Surf," *Geophysical Magazine*, **25**, **Nos. 3~4** (1954).

J. E. DINGER, "Microseisms and Ocean Wave Studies on Guam," *Trans. Amer. Geophys. Union*, **36** (1955).

caused microseismic storms at a given district can be easily found.

For instance, let us consider the case of L7 in Fig. 11. The observed period of microseisms measured at Tsukuba station was approximately 5 seconds at its maximum amplitude. Therefore the period of swell which reached the coast near Tsukuba might be about 10 seconds. The velocity of swell for this period is approximately 25 km/hr.[5] On

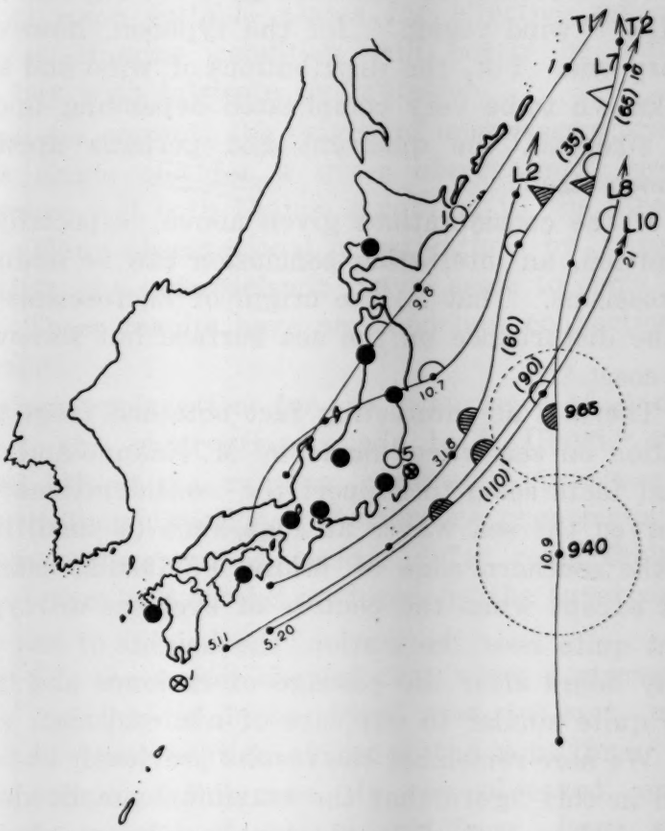


Fig. 11. Apparent and true positions of cyclones and typhoons when they induced the highest microseismic amplitudes at Tsukuba and Nemuro stations. Numerals in the bracket beside the travelling baths of cyclones or typhoons show the travelling speed of them about that time. Dotted circles around the centers of typhoons represent the region where atmospheric pressures were lower than 990 mb. at the corresponding times.

the other hand, the travelling speed of the cyclone L7 at that time was approximately 60 km/hr. From these two data, the "true position" of the center of this cyclone could be plotted on the map.

These "true positions" are also shown in the same figure by hatched semi-circles and triangles for Tsukuba and Nemuro stations respectively. They are distributed, as is seen in this figure, near the respective stations, which fact seems to be reasonable.

5) S. UNOKI, "On the Speed, Travel Time and Direction of Ocean Waves due to Tropical Cyclones," *Journal of the Meteo. Soc. Japan*, [ii], **34** (1956), No. 6, 354.

However, in the case of typhoons having a considerably large scale of wind region, a large swell would be sent even from the circumference of a somewhat large region around the center. Assuming this "wind region" as the area in which the atmospheric pressure is lower than, say, 990 mb., and further, using the travelling time of the swells from this fringe to the coast near Tsukuba, the "true positions" of the typhoons become the positions given in Fig. 11. This simple assumption of the "wind region" for the typhoon, however, is of course a temporary one. For, the distributions of wind and swells in the wind region are known to be very complicated depending upon the travelling speed, the strength, the quadrant and perhaps upon the structure of the typhoon itself.

If the considerations given above, especially for the cyclones, are permitted, an interesting conclusion can be deduced about the origin of microseisms. That is, the origin of microseisms exists not in the center of the disturbance on the sea surface but somewhere in the vicinity of the coast.

There is an interesting fact obtained from the observational investigation on sea waves made by M. Nakano and others.[6] Their observational facts seem to support the considerations just mentioned. They observed the sea waves at Jogashima (a small island several kilometers off the southern edge of Miura Peninsula, central Honshu) and found that except when the centers of cyclones or typhoons went through a point quite near the station, the heights of sea waves became maximum many hours after the passage of cyclones and typhoons. This tendency was quite similar to our case of microseisms.

We here remember the results previously shown in Fig. 9. We have seen in this figure that the maximum amplitudes of microseisms never occur before that of the highest swells recorded in one district. If the energy transformation from sea waves to microseismic waves occurs at the vicinity of the cyclonic center, the microseismic waves must be observed remarkably earlier than the swells at one station. Therefore, combining this result with the oceanographical study given above, our theory about the origin of microseisms will be greatly emphasized.

The next problem is how the interference phenomena of the swells occur at the vicinity of a coast after they were sent from around the center of cyclone or typhoon.

6) M. NAKANO, S. UNOKI and Y. KUGA, "On the Result of Wave Observations at Jogashima Island and Its Application to Wave Forecasting (I)," *Papers in Met. and Geophys.*, **40** (1953), Nos. 3-4, 115.

Unfortunately, we are lacking in the observation of interference phenomena on swells near the coast, therefore we cannot give any decisive answer to this question at present. But, if it is permitted to make some suggestions, a few conditions may be considered for the occurrence of interference phenomena near the coast. First, is the interference which takes place between the refracted swells behind an island. Second, is the interference caused between the reflected swells and the incident ones at some suitable places for effective reflection. Further to say, Longuet-Higgins condition will nearly be satisfied somewhere inside of a bay with intricate configuration.

If these suggestions are correct, the origins of microseisms are neither fixed points nor a single one for a given observational station. Their locations and number will both change according to the direction of the incident swells. Many observational investigations by tripartite method have shown that the microseismic wave seem to come from diversified directions.[7] These results have an important connections to the assumption just made.

There may be another explanation for the occurrence of standing sea waves. According to the observations made by S. Unoki,[8] swells and sea waves remained behind the running cyclones. As these two waves have different travelling directions, interference phenomena may also occur between them. However, as periods differ remarkably between them, stationary waves will not be produced by the superposition of these two waves.

In the last part of § 2, the writer showed that when a strong cold front passed across the mainland of Japan from west to east, microseismic storms occurred at every station almost at the same time. This is a characteristic phenomenon of this case. It was observed, on the other hand, that with the passing of such a cold front, large swells also arrived at an observational station. (See the cases of F8 and F9 in Fig. 9.) This fact was also confirmed by oceanographical reports.[9] Therefore, it is obvious that the microseismic storm which occurred in this case is undoubtedly due to the passing of the cold front and not to the centers of cyclones which were running near Hokkaido.

---

7) R. IKEGAMI and F. KISHINOUYE, "A Study on the Propagation of Microseismic Waves. III," *Bull. Earthq. Res. Inst.*, **29** (1951).

8) *loc. cit.* (5).

9) S. UNOKI and M. NAKANO, "On the Ocean Waves at Hachijo Island," *Papers in Met. and Geophy.*, (1955), No. 1, 63.

## § 4. Conclusions

What the writer wishes to say in the present paper can be summarized as follows:

1) When a cyclone or a typhoon is travelling towards the northeast over the ocean, the microseismic storm at a given station on the mainland of Japan occurs considerably later than the passing of the center of the cyclone or typhoon. In this case, the microseismic storm shifts from one region to another as if running after the cyclonic center.

2) Microseismic storms also occur when a strong cold front passes across Japan from west to east. In this case, it occurs almost at the same time at every station throughout Japan.

3) The direct cause of microseisms is undoubtedly swells. Maximum amplitudes of microseisms at a station never occur before the arrivings of the highest swells near this station.

4) Periods of microseisms are nearly equal to half the periods of swells, which fact satisfies the condition of the Longuet-Higgins theory.

5) Assuming that microseisms were induced by the condition of the Longuet-higgins theory, it seems that the region where interference takes place between two trains of swells is rather at the vicinity of the coast than around the center of the cyclone or typhoon. In other words, these disturbances on the ocean are undoubtedly the energy sources of microseisms, but they are not the origins of microseisms.

## § 5. Acknowledgment

At the conclusion of this paper, the writer wishes to express his sincere thanks to Dr. K. Wadati and to Mr. S. Miyamura who encouraged him during the course of his investigations. The writer's hearty thanks are also due to Mr. T. Kizawa who gave him much help in collecting the data on swells.

# 19. 多くの観測点の資料による脈動の研究 (其の一)
## —脈動源について—

地震研究所　三　東　哲　夫

I·G·Y の日本国内の脈動観測資料を用いて，各地の脈動嵐が何の影響でどんな起り方をするか，また各地の脈動嵐相互間の時間的な関係はどのようになつているかを，天気図と対照しつつ調べた．その結果，

1) 低気圧や台風が日本の東方海上を東北進する場合には，脈動嵐はそれを追いかけるようにして西南日本から東北日本へと移つてゆく．そしてこの場合，ある地区に脈動嵐が一番ひどくなる時期は，低気圧や台風の中心がかなり行きすぎてしまつてからである．この傾向は，低気圧の場合に特に著しい．

2) 脈動嵐は，顕著な寒冷前線が日本海側から太平洋側に日本列島を横切る時にも起る．そしてこの場合の特徴は，寒冷前線が太平洋側に抜ける時刻に日本列島全体が一斉に脈動嵐を起すことである．

ことが分つた．また，波浪や風などとの関係を調べて見た結果，

3) 脈動の直接の原因はやはり波浪であつて，しかも最も大きな波浪がある観測点で記録される時刻は，その附近の脈動振幅が最大になる時刻よりおくれることはない．

4) 脈動の周期は波浪の周期の約半分になつていて，ヒギンスのいうように，二つの同周期の波浪の干渉による定常波が脈動を起していると考えられる．

ということが認められた．

一般に，波浪と脈動波の伝ぱん速度の大きな相異を考え，且つ，以上の 4 つの観測事実をすべて説明するためには，どうしても脈動源を陸地のすぐそばに考えなくてはならなくなる．つまり，台風や低気圧によつて生じた風浪が沿岸近くで何等かの機構で定常波をつくる．その場所こそ脈動源だと考えられる．もしそうだとすると，脈動源は観測点附近に点在することが考えられ，風浪の来る方向によつてはその数も変つても差支えないが，今迄の多くの三点観測による脈動波の到来方向についての研究結果も，以上の推論を裏がきしているように思える．

BULLETIN OF THE EARTHQUAKE
RESEARCH INSTITUTE
Vol. 37 (1959), pp. 327-335

# 20. An Electromagnetic Horizontal Seismograph for Recording Microseisms.

By Fuyuhiko KISHINOUYE and Yoshio WATANABE,

Earthquake Research Institute.

(Read Sept. 24, 1957.—Received March 25, 1959.)

An electromagnetic seismograph of self-vibration period 10 sec was newly made by the writers to record the horizontal component of microseisms for investigation of microseisms. The senior writer had previously designed a mechano-optical seismograph[1] for the same purpose. In this case electromagneto-optical recording was adopted, because it has the following merits in comparison with the former method: (i) practically no friction, (ii) high magnification can be obtained easily, (iii) hardly affected from slow tilting of the ground which is apt to cause, in the case of the mechano-optical method, the image of the earth motion to run off the recording paper, (iv) simultaneous observation at many places can be recorded at one place, and (v) recording can be managed by a few men.

The instrument consists of a horizontal pendulum, or transducer, a galvanometer and an optical recording camera. The galvanometer was bought from a maker, and pendulum and recorder were designed by the writers.

## Horizontal Pendulum Transducer

A pair of horse-shoe magnets were put as a bob of the pendulum, with unequal poles facing each other. A spool made of bakelite wound with copper wire was stood on the table of the pendulum between the poles of the magnets. The spool was wound with two coils: the inner coil was for an electromagnetic damper of the pendulum, and the outer coil for transducer or generation of electromotive force by earth motion. The magnets were made of "MK magnet Steel No. 5" (similar to "Alnico"), remnant magnetism about 12000 gauss. With these strong magnets we could design the seismograph (Figs. 1 and 2).

1) F. KISHINOUYE, *Bull. Earthq. Res. Inst.*, **20** (1942), 215-219.

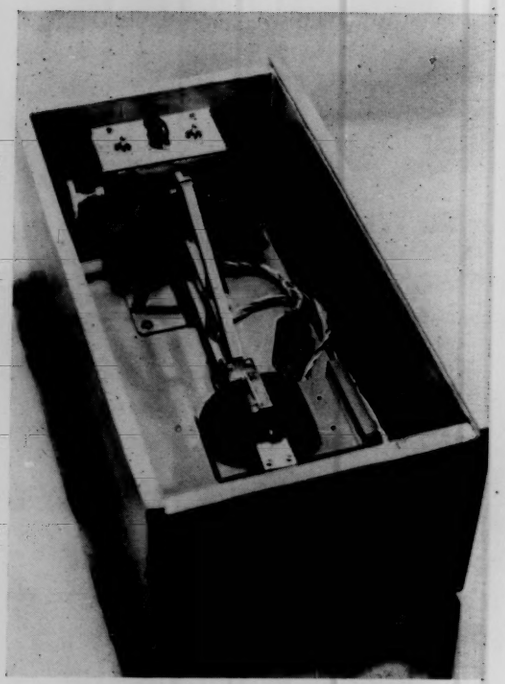

Fig. 1. Pendulum in a wooden cover. The upper box in the photograph is resistor box to make critical damping for the galvanometer and the pendulum.

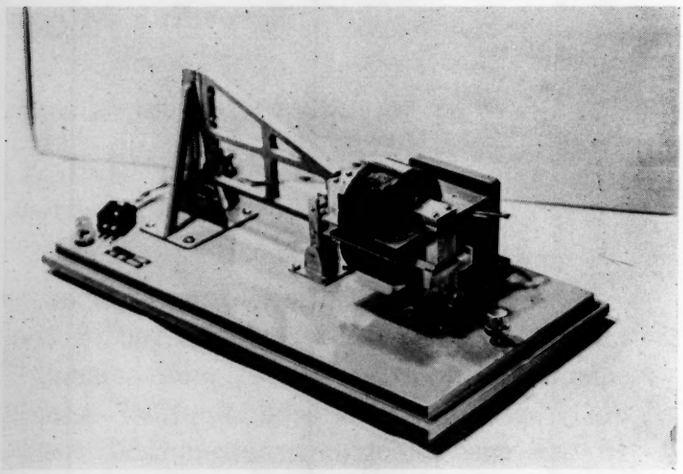

Fig. 2. The Pendulum.

## Theory of the Seismograph[2)]

Suppose a rectangular electric circuit $ABCD$ and $AD$, the length of which is $l$, moves with a velocity $v$ in the direction perpendicular to it in a magnetic field $H$. Then in an elementary time interval $dt$ magnetic flux $\Delta\phi$ in the rectangle $ABCD$ increases as

$$\Delta\phi = Hlvdt$$

and an electromotive force $e$ is induced in the circuit

$$e = \frac{d\phi}{dt} = Hlv \ .$$

If the number of turns of the coil is increased to $n$, the force becomes

$$e_n = n\frac{d\phi}{dt} = Hlnv \ .$$

2) Notations of the theory was described after Wenner's well-known paper, F. Wenner, Bur. Stand. Journ. Res. **2** (1929), 962-999.

On a frame of the horizontal pendulum two horse-shoe shaped magnets were fixed. When they moved by earth movements, in coils interposed between the magnets induced electromotive force (EMF) generated as the magnets moved. The electric current generated in the pendulum flows to a galvanometer as shown in Fig. 3. In the diagram $R$ denotes electric resistance of the pendulum coil, $R_g$ that of the moving coil of the galvanometer, and $r$ resistance of inserted resistor and wire.

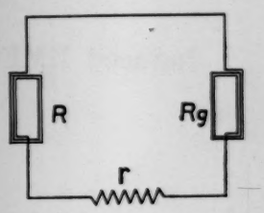

Fig. 3.

The electromotive force caused by angular displacement $\phi$ of the pendulum motion is

$$E_1=G\frac{d\phi}{dt} \qquad (1)$$

where

$$G=nHlL\,,$$

and $L$ is the distance from the axis of rotation to the centre of the pendulum coil.

When the electromotive force goes to the galvanometer, opposite electromotive force $E_2$ generated,

$$E_2=-g\frac{d\phi}{dt} \qquad (2)$$

where g is a constant of the galvanometer

$$g=N'A'H'$$

and $N'$ is number of turns of coil,

$A'$ is area of the coil,

$H'$ is intensity of magnetic field,

and electric current $i_1$ is excited in the galvanometer

$$i_1=G\frac{d\theta}{dt}\frac{1}{R_g+r+R}\,, \quad \text{or} \quad i_1=\frac{G}{Q}\frac{d\theta}{dt}\,. \qquad (3)$$

where $\theta$ is angular displacement of the galvanometer coil,

$$Q=R_g+r+R\,,$$

$Q$ is total resistance of the circuit,

$R_g$ is resistance of the galvanometer coil,

$R$ is resistance of the pendulum coil,

$r$ is resistance of wires connecting the coils and inserted resistor.

Next, electric current $i$ created by the movement of the galvanometer coil is obtained.

$$i=-g\frac{d\phi}{dt}\frac{1}{R_g+r+R}, \quad \text{or} \quad i=-\frac{g}{Q}\frac{d\phi}{dt}. \tag{4}$$

Induced EMF due to current in the transducer coil is expressed as

$$E_3=-\Lambda\frac{di_d}{dt} \tag{5}$$

where $\Lambda$ is mutual inductance between the pendulum coil and the galvanometer coil.

$i_d$ is current in the damper coil.

Induced EMF in the damper coil by the motion of the pendulum is

$$E_4=G'\frac{d\theta}{dt}$$

and then the current in the damper coil is expressed by the formula

$$i_d=\frac{E_4}{R_d}=\frac{G'}{R_d}\frac{d\theta}{dt} \tag{6}$$

where $R_d$ is resistance of the damper coil, and $G'=n_dHlL$ ($n_d$ number of turns of the damper coil).

Putting (6) in (5), current in the transducer coil $i_3$ is obtained,

$$i_3=\frac{E_3}{Q}=-\frac{\Lambda G'}{QR_d}\frac{d^2\theta}{dt^2}. \tag{7}$$

Total current $I$ flowing in the transducer coil in the condition of free vibration is

$$I=i_1+i_2+i_3=\frac{G}{Q}\frac{d\theta}{dt}-\frac{gd\phi}{Qdt}-\frac{\Lambda G'd^2\theta}{QR_ddt^2}. \tag{8}$$

When current $i_3$ flows in the damper coil, the pendulum is influenced by force $G'i_3$. But the force due to EMF in the transducer coil and force acted on by the current in the transducer may be neglected because these are very small.

The pendulum is acted on by force due to the current in the damper coil

$$-G'i_d \tag{9}$$

and the galvanometer is acted on by force $gI$.

Consequently the equations of motion of pendulum and galvanometer are given by

$$K\frac{d^2\theta}{dt^2}+D\frac{d\theta}{dt}+U\theta=-ML\frac{d^2x}{dt^2}-G'i_a \tag{10}$$

and

$$k\frac{d^2\phi}{dt^2}+d\frac{d\phi}{dt}+\mu\phi=gI \tag{11}$$

where $x$ is earth motion,

$K$ is moment of inertia of the pendulum,

$D$ is liquid damping of the pendulum,

$U$ is restitutive force of the pendulum for deflexion angle $\theta$,

$L$ is the pendulum length,

$k$ is moment of inertia of the galvanometer coil,

$d$ is liquid damping of the galvanometer coil,

$\mu$ is restitutive force of the galvanometer coil.

Put (6) and (8) in (10) and (11), the equations of motion become

$$K\frac{d^2\theta}{dt^2}+\left(D+\frac{G'^2}{R_a}\right)\frac{d\theta}{dt}+U\theta=-ML\frac{d^2x}{dt^2} \tag{12}$$

and

$$k\frac{d^2\phi}{dt^2}+\left(d+\frac{g}{Q}\right)\frac{d\phi}{dt}+\mu\phi=\frac{Gg}{Q}\frac{d\theta}{dt}-\frac{gG'\Lambda}{QR_a}\frac{d^2\theta}{dt^2}\,. \tag{13}$$

To solve these equations, we assume earth motion to be harmonic

$$x=x_m\cos(\omega t+\alpha)\,,\qquad \text{or}\qquad x=x_me^{j\alpha}e^{j\omega t}=Xe^{j\omega t}\,, \tag{14}$$

where

$$j=\sqrt{-1}\,.$$

Deflexion angle of the pendulum is expressed also in complex form

$$\theta=\theta_me^{j\beta}e^{j\omega t}=\Theta e^{j\omega t} \tag{15}$$

and deflexion angle of the galvanometer mirror

$$\phi=\phi_me^{j\gamma}e^{j\omega t}=\Phi e^{j\omega t} \tag{16}$$

Putting the above relations in the equations of motion, relations between $X$, $\theta$ and $\Phi$ are obtained,

$$\frac{\theta}{X}=\frac{\omega^2 ML}{U-\omega^2 K+j\omega(D+G'^2/R_a)} \tag{18}$$

and

$$\frac{\Phi}{\theta}=\frac{\omega^2 gG'\Lambda/R_aQ+j\omega Gg/Q}{\mu-\omega^2 k+j\omega(d+g^2/Q)} \tag{18}$$

The above relations give the relation between deflexion of the galvanometer mirror and earth motion as follows:

$$\begin{aligned}\frac{\Phi}{X}&=\frac{\omega^2 ML(\omega^2 G'\Lambda/R_aQ+j\omega Gg/Q)}{\{U-\omega^2 K+j\omega(D+G'^2/R_a)\}\{(u-\omega^2 k)+j\omega(d+g^2/Q)\}}\\&=\frac{\omega^2 H(\omega K+jN)}{(\omega^3 A-\omega B+C/\omega)+j(E-\omega^2 F)}\end{aligned}$$

where

$$\begin{aligned}A&=Kk\\B&=kU=Ku+Dd+Dg^2/Q+dG^2/R_a+g^2G'^2/(QR_a)\\C&=Uu\\E&=dU+Ug^2/Q+Du+G'^2u/R_a\\F&=Kd+Kg^2/Q+kD+kG'^2/R_a\\H&=ML\\K&=gG'\Lambda/(R_aQ)\\N&=Gg/Q\end{aligned}$$

The deflexion of the galvanometer mirror is drawn on photographic paper which is $s$ cm distant from the mirror. Then the magnification $V$ of the seismograph is

$$V=2s\frac{\Phi}{X}\ .$$

The magnification for this instrument can be changed by increasing or decreasing the number of turns of the transducer coil. In Fig. 4 variation of $\Phi/X$ with period of earth motion for the number of coil turn 300, and when increasing of magnification is necessary coil taps or 600, 900 and 1200 turns can be used. In such case magnification becomes large in proportion to the ratio of numbers of coil turns.

Phase lag of the motion of galvanometer mirror from that of earth motion is an important factor in seismometry. It is computed by the following formula.

$$(\alpha-\gamma)=\tan^{-1}\frac{\omega^4(NA+KF)-\omega^2(NB+KE)+NC}{\omega\{\omega^4KA-\omega^2(KB+NF)+KC+NE\}}$$

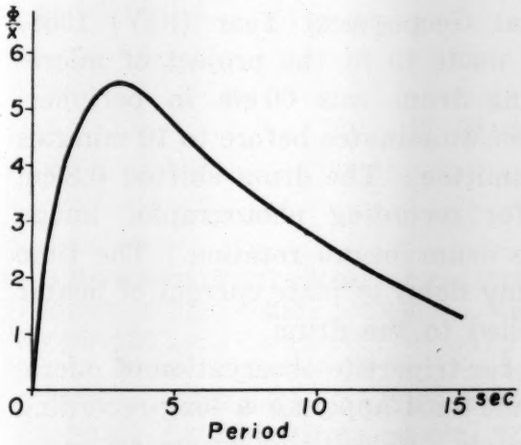


Fig. 4. Magnification curve.

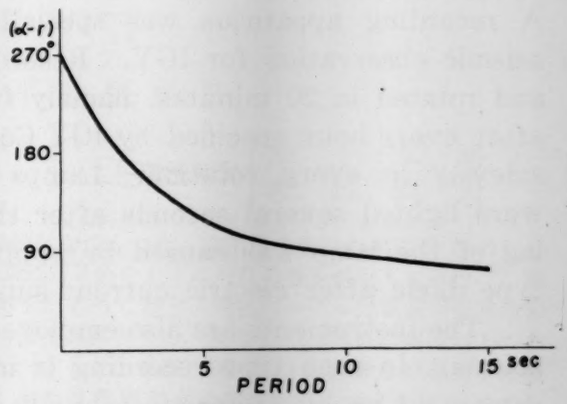


Fig. 5. Phase lag.

In Fig. 5 variation of phase lag with period of earch motion is shown.

## Construction of the Seismograph

The diagrams in Figs. 4 and 5 were calculated from following values of the pendulum.

| | | |
|---|---|---|
| $M$: | $1.35\times10^3$ | g |
| $L$ : | $2.2\times10$ | cm |
| $K$ : | $6.53\times10^5$ | g cm$^2$ |
| $U$ (10 sec): | $1.19\times10^4$ | g cm/sec$^2$ |
| $G$ : | $1.0\times10^8$ | dyne cm/e.m.u. |
| $G'$: | $5.0\times10^8$ | dyne cm/e.m.u. |
| $Q$ : | $1.0\times10^{12}$ | c.g.s. e.m.u. (1000 Ω) |
| $R$ : | $1.2\times10^{11}$ | 〃 (120 Ω) |
| $A$ : | $1.5\times10^7$ | 〃 ($6.8\times10^{-2}$h) |
| $D$ : | 0 | g cm$^2$/sec |

Constants of the galvanometer published were period of vibration 9 sec, sensitivity $7\times10^{-10}$ A or $0.8\times10^{-6}$ V and the critical damping resist-

ance 1100 Ω. The writers were kindly told by the maker about constructional data of the galvanometer, but they were not permitted to describe here the data for certain reasons of him.

Calibration of the seismograph was carried out by comparison of records of microseisms registered with this instrument and those with the mechano-optical seismograph mentioned above. The result of the calibration was satisfactory to the writers, and they were taken to record microseisms in the International Geophysical Year (IGY) 1958. A recording apparatus was specially made to fit the project of microseismic observation for IGY. Recording drum was 60 cm in peripheri and rotated in 20 minutes, namely from 10 minutes before to 10 minutes after every hour specified by IGY Committee. The drum shifted 0.8 cm sideway in every rotation. Lamps for recording photographic image were lighted several seconds after the drum began rotation. The time lag of the lamp was caused by applying delay of plate current of heater type diode after electric current supplied to the drum.

The instruments are also employed for tripartite observation of microseisms. In such time recording is made with applying a long-recording camera of an electromagnetic oscillograph. Velocity of recording paper for microseisms is usually set at about 6.5 mm/sec.

## Appendix. An electronic circuit to change duration of timing

Time marks on seismogram play an important part in seismometry. Timing is usually made by electric contact clock or by wireless time signals. To increase reading accuracy of time on seismogram, shortening or sometime lengthening of duration of electric action on timing

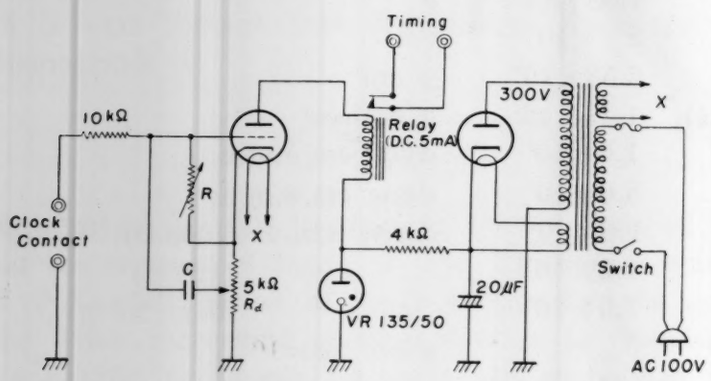


Fig. 6.

apparatus is required. But it is difficult to change the duration of ordinary timing clocks. Then the writers divised an electronic circuit to change length of timing. Fig. 6 shows the circuit. The maximum duration is fixed by time constant, or product of capacity **C** and resistance of the circuit **R**, and the duration can be changed with variable resistance $R_a$. Using power voltage regulator, error of the duration of timing may be less than 1%.

---

## 20. 電磁水平動脈動計

地震研究所 岸上冬彦 渡辺義夫

土地の脈動の水平成分を記録するために電磁脈動計をつくつた，精密級検流計の周期 9 秒のものに組合せ，水平振子の重錘として馬蹄形の MK 鋼磁石 2 個を上下に異なる極を相対して取付け，磁極の間に固定したコイルをおいた．コイルは 2 個をかさねて巻き．内側のコイルは電磁制振器の回路とし，外側のコイルはその起電力によつて検流計を偏れさせる．鏡の偏れは写真印画紙の上に光学的に拡大して記録させる．この器械と前に岸上のつくつた器械-光学的の微動計とで脈動の比較記録をした．その結果は良好であつたので，1958 年の国際観測年の東京本郷における観測につかい，脈動の三点観測にもつかい，脈動の研究を進めるのに用いる．

なお刻時時間を長くし，または短かくする装置を考案し実用したものについて記した．

---

地震研究所彙報
第37号(1959)337-345頁

# 21. 震源決定の精度について（第3報）

地震研究所　浅野周三

(昭和34年2月24日発表——昭和34年3月31日受理)

## §1. 序

著者は前報[1]において，震源決定の精度に対する目安を得る一方法として，実際の震源の位置及び発震時が判つている火薬爆発による地震動の観測資料を用い，それらを未知として実際既知の爆発時刻，震源の位置を定め比較する事を行なつた．その結果によると，震央の位置及び速度は比較的よく決定されるが，発震時と深さは精確に定め得ない事などが判つた．しかして，今まで用いた資料は特別にその地震動を観測する準備をされた非常に精度のよいものであり，これは自然地震の常時観測，特に気象庁によりなされているものに比してかなりの相違があり，直ちに気象庁の資料を用いたものに対する目安を得ることは出来ない．この意味において，大量の火薬を爆発させてその地震動が気象庁の観測網により記録されれば，その結果より，常時観測の精度の見当をつけ得，従つて従来の資料の利用価値に対する目安が得られる筈である．偶々1958年6月15日正午，岐阜県大野郡白川村御母衣ダム建設工事において，156 屯の火薬の大爆発が実施され，その地震動が約10 ケ所の測候所で記録されたものの報告が気象庁地震課へ集まつた．地震課の御好意により，その資料を使わせていただき，震源決定を試みたので報告する．

## §2. 資料の性質

先ず資料の性質について考えてみる．$P$の報告があつたのが，次の 13 ケ所である．

高山，富山，松本，岐阜，伊吹山，飯田，名古屋，福井，彦根，松代，長野，亀山，甲府

これらの位置は Fig. 1 に示されている．このうち，underline された7ケ所には Wiechert 地震計が据付けてあり，他の5ケ所には普通地震計がある．松代のみは特別で Benioff の地震計を始め，種々の地震計がある．

156 屯のダイナマイトによる energy は 1g～1000 cal. として概算すると $0.7\times10^{19}$ erg. であるが，この何%が地震波になるか知るのは，発破の種々の条件によるので，むずかしい．従つて如何程の energy の地震に相当するかは，はつきりしないが，爆破点付近で有感であつた事から，局発地震程度と考えてよいであろう．

実際にとれた記録の例として，岐阜 ($\Delta = 81.50$ km)，名古屋 ($\Delta = 106.30$ km)，松代

1) S. Asano, *Bull. Earthq. Res. Inst.*, **32** (1954), 371; **33** (1955), 199.

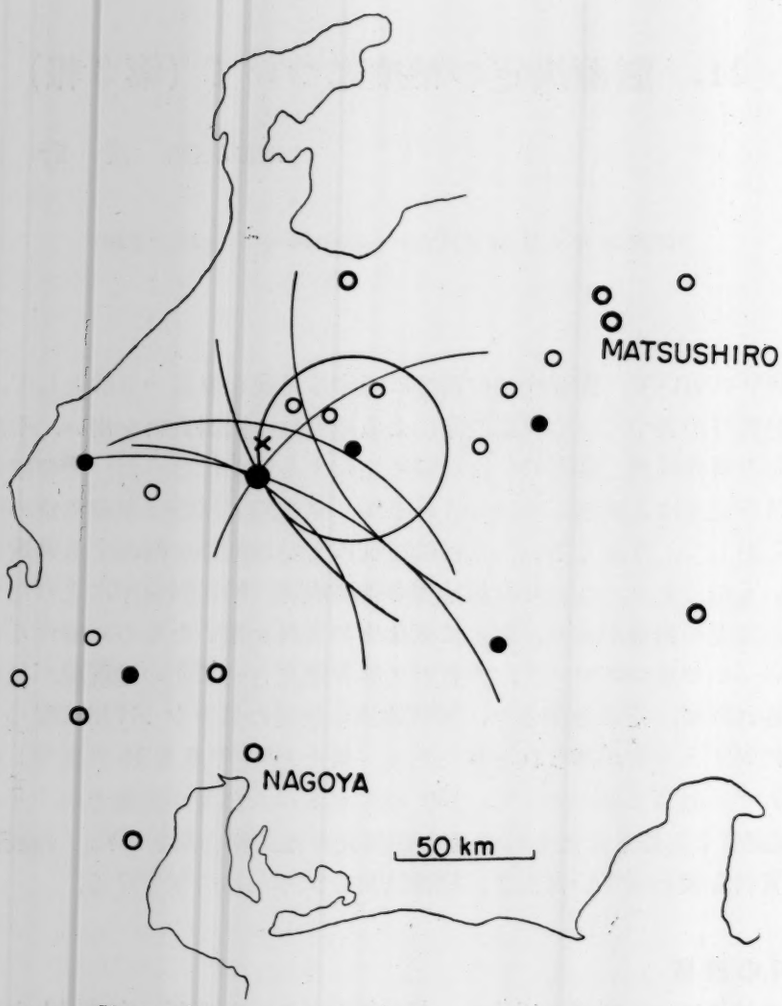


×: Shot point
●: I
○: Observatory of J. M. A. with Wiechert seismographs
●: Observatory of J. M. A. with portable seismographs
○: Observation station by R. G. E. S.

Fig. 1. Shot point, epicenter of first approximation and observing stations.

($\Delta = 125.74$km) の記録を Fig. 2～5 に示す．この程度でも，各測候所ではよみとりが行われるとの事であるが，地震としては小さすぎ，初動の判定は極めてむつかしく（特に岐阜の場合），気象庁の資料としては，わるい方であろう．但し，松代のみは極めてよい記録である．本報告では，Table 1 に示された各測候所よりの報告値をそのまま用い，議論してみる．この報告値の精度をみる意味で，実際の走時図をかいてみると，Fig. 6 の如くなる．Fig. 6 には，比較のために，爆破地震動研究グループ（以下 R. G. E. S. と略

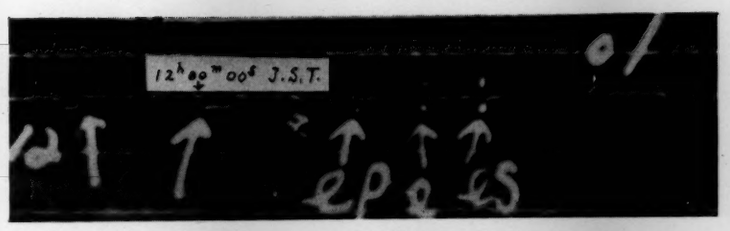


Fig. 2. Seismogram of NS component at Gifu

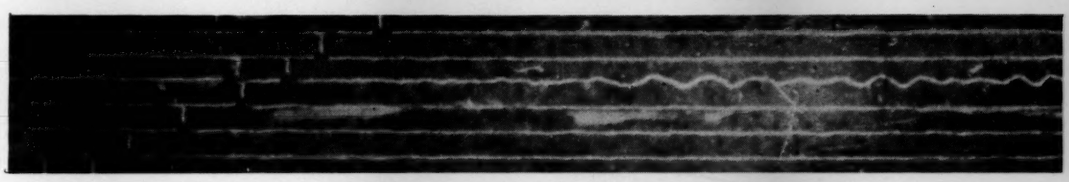

Fig. 3. Seismogram of NS component at Nagoya

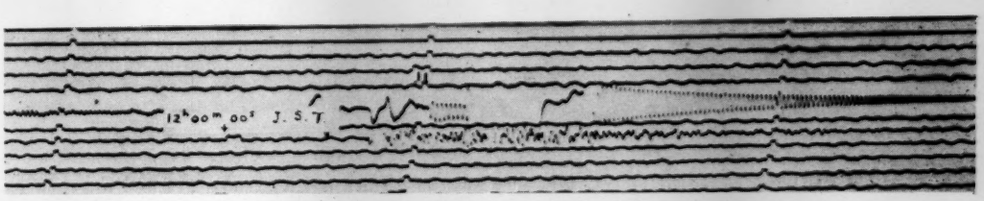


Fig. 4. Seismogram of Vertical component by Short Period Electromagnetic Seismograph at Matsushiro.

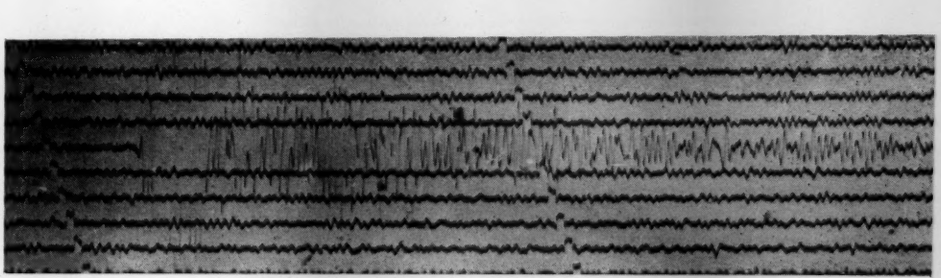

Fig. 5. Seismogram of EW-component by Benioff Seismograph with Short Period at Matsushiro.

記する）の好意により，同グループが同じ爆破地震動を Fig. 1 に示した観測点で観測した値[2)]が記入してあり，常時観測網による観測が大体において 1～2 秒近くおくれている．また，Fig. 6 には，気象庁で使用されている和達，益田の $P$ 波の走時曲線及び，鷺坂，竹花の $S$ 波走時曲線が記入されている．Fig. 6 をみると，大体の発破点の位置は新聞で報道されたので，大体の震央距離が判り，走時表を基にして読みとりを行なつた所が，2，3 ケ所あるのではないかとの恐れがある．併し，一応，報告値を信用して話を進める．

2) 爆破地震動研究グループ　日本地震学会秋季講演会（昭和 33 年 10 月）

Table 1.

| Station | $\Delta$ (km) | $t_P$(sec) | $t_S$(sec) | $t_S-t_P$ (sec) | $t_P-t_0$ (sec) | $t_S-t_0$ (sec) | $(O-C)_S$ sec |
|---|---|---|---|---|---|---|---|
| 1. Takayama | 32.48 | 12 h 00 m 1.9 | 12 h 00 m 12.3 | 4.4 | 6.1 | 10.5 | −0.9 |
| 2. Toyama | 70.15 | 14.0 | — | — | 12.2 | — | — |
| 3. Matsumoto | 96.80 | 14.7 | — | — | 12.9 | — | — |
| 4. Gifu | 81.50 | 18.3 | 30.2 | 11.9 | 16.5 | 28.4 | 2.3 |
| 5. Mt. Ibuki | 90.22 | 19.2 | 30.1 | 10.9 | 17.4 | 28.3 | −0.4 |
| 6. I-ida | 107.96 | 21.4 | 35.5 | 14.1 | 19.6 | 33.7 | −0.3 |
| 7. Nagoya | 106.30 | 21.4 | — | — | 19.6 | — | — |
| 8. Fukui | 61.88 | 21.9 | — | — | 20.1 | — | −0.1 |
| 9. Hikone | 111.58 | 22.4 | — | — | 20.6 | — | — |
| 10. Matsushiro | 125.74 | 23.3 | 38.3 | 15.0 | 21.5 | 36.5 | −2.8 |
| 11. Nagano | 130.24 | 27.0 | 45.3 | 18.3 | 25.2 | 43.5 | 2.9 |
| 12. Kameyama | 146.19 | 28.1 | 46.5 | 18.4 | 26.3 | 44.7 | −0.7 |
| 13. Kôfu | 157.45 | 28.3 | — | — | 26.5 | — | — |

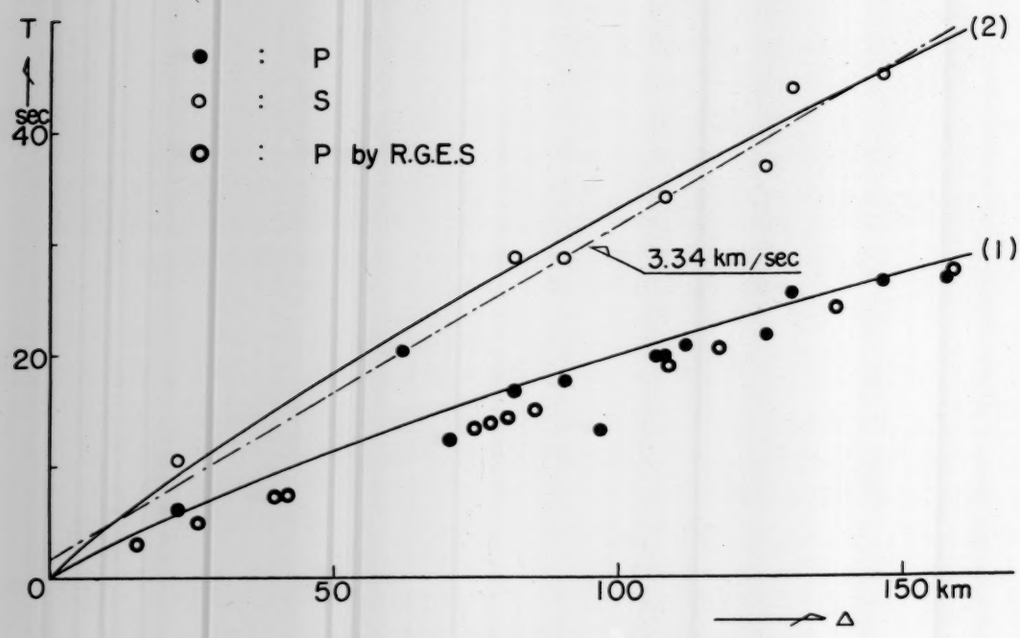


Fig. 6. Travel time graph for actual epicenter

## §3. 震源決定

震源を定めるために，先ず，第一近似の量を求める．震央を定めるために，$S$ の報告があつた7ケ所を用い，大森係数を 7.5 と仮定して $7.5\tau$ km ($\tau$ は $P$–$S$ 時間) の円をかくと Fig. 1 に示される如く，高山，伊吹山，長野，亀山，飯田の円が比較的よく交るので，大体の交点をとると，$\lambda = 136°54.2'\mathrm{E}$，$\varphi = 36°2.5'\mathrm{N}$ となり，実際の Shot point を原点にとつた直角座標で $x = -0.44\,\mathrm{km}$, $y = -8.90\,\mathrm{km}$ となる（この計算及び震央距離の計算は Richter の表[3]を用いて行なつた）．実際の震央との距離は 8.91 km である．円が殆んど一点で交わるので，深さは殆んど 0km と考えてよく，深さの考察は行なわない[4]．

次に，発震時を求めるために，よくやるように，縦軸に $P$–$S$ 時間，横軸に $P$ の発震時をとつて，$P$–$S$ の観測のある7ケ所の値を用いて図をかくと，Fig. 7 の如くなり，よく直線にのり origin time は $12^h00^m1.6^s$ となる．

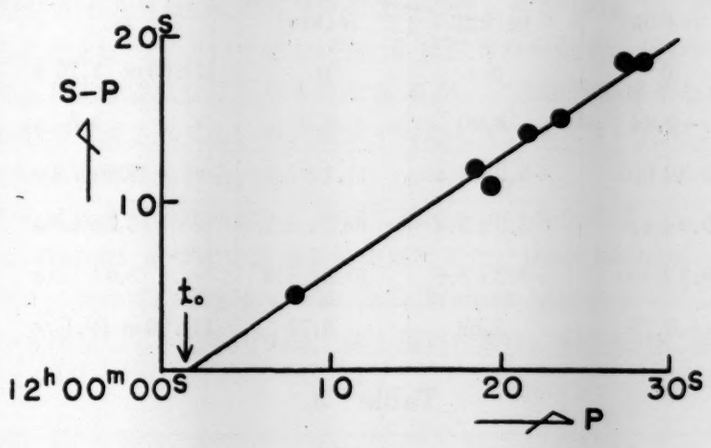


Fig. 7.

この origin time 及び震央を用いて走時図をかくと，Fig. 8 の如くなる．適当に線をひくと，Fig. 8 の白丸によつて示される如く，5.2km/sec の速度が得られる．Fig. 8 には

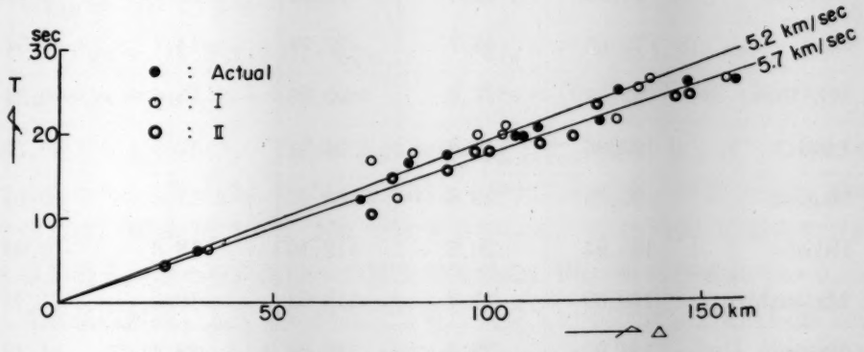


Fig. 8. Travel time curves of the first and the second approximations.

3) C. F. RICHTER, *Bull. Seism. Soc. Am.*, **33** (1943), 243.

4) 震源の深さも未知として，第一近似の量は深さ 0km 以外は以下で用いたのと同じ値を用いてやつてみたが，よく定められなかつた．

又，比較のために，Fig. 6 に示された実際の走時（黒丸）を重ねて示してある．

以上の第一近似の量を用い

$$(x_0-x_i)\delta x_0+(y_0-y_i)\delta y_0+v_0^2(t_i-t_0)\delta t_0-v_0(t_i-t_0)^2\delta v_0=v_0^2(t_i-t_0)\delta t_i$$

なる式により，最小2乗法で補正量を求めると．

$$\delta x_0=(9.8\pm6.0)\ \text{km} \qquad \delta y_0=(2.7\pm4.4)\ \text{km}$$

$$\delta t_0=(2.0\pm1.8)\ \text{sec} \qquad \delta v_0=(0.49\pm0.43)\ \text{km/sec}$$

になる．但し，松本は deviation が大きいため，又福井は恐らく，$S$ を $P$ と混同しているため，計算からは除いた．補正をほどこした結果は，Table 2 に実際の量及び第一近似の量 I と共に II の行に与えられている．第2近似の諸量を用いた走時表は Table 3

Table 2.

| | $x_0$ (km) | $y_0$ (km) | $R$ (km) | $t_0$ | $v_0$ km/sec |
|---|---|---|---|---|---|
| Actual | 0 | 0 | 0 | 12h00m 1.75 s | 5.9 |
| I | −0.44 | −8.90 | 8.9 | 〃 〃 1.6 s | 5.20 |
| II | 9.3±6.0 | −6.0±4.4 | 11.1±7.5 | 〃 〃 (3.6±1.8)s | 5.69±0.43 |
| II′ | 9.9±4.0 | −3.9±3.4 | 10.7±5.2 | 〃 〃 (3.2±1.7)s | 5.68±0.45 |
| II″ | 10.1±4.0 | −3.2±3.6 | 10.6±5.4 | 〃 〃 (3.0±1.9)s | 5.67±0.46 |
| J. M. A. | −0.75 | 8.69 | 8.72 | 11h59m 59.5 s | |

Table 3.

| Station | $\Delta_1$ (km) | $t_P-t_{01}$ (sec) | $\Delta_2$ (km) | $t_P-t_{02}$ (sec) | $(O-C)_P$ sec |
|---|---|---|---|---|---|
| 1. Takayama | 34.99 | 6.3 | 24.82 | 4.3 | −0.06 |
| 2. Toyama | 78.60 | 12.4 | 72.96 | 10.4 | −2.42 |
| 4. Gifu | 72.65 | 16.7 | 77.74 | 14.7 | 1.04 |
| 5. Mt. Ibuki | 82.39 | 17.6 | 90.36 | 15.6 | −0.28 |
| 6. I-ida | 102.96 | 19.8 | 96.94 | 17.8 | 0.77 |
| 7. Nagoya | 97.45 | 19.8 | 100.25 | 17.8 | 0.19 |
| 9. Hikone | 103.94 | 20.8 | 112.10 | 18.8 | −0.90 |
| 10. Matsushiro | 129.69 | 21.7 | 119.62 | 19.7 | −1.32 |
| 11. Nagano | 134.93 | 25.4 | 125.05 | 23.4 | 1.43 |
| 12. Kameyama | 137.54 | 26.5 | 143.41 | 24.5 | −0.70 |
| 13. Kôfu | 155.24 | 26.7 | 146.70 | 24.7 | −1.08 |

に，走時図は Fig. 8 に重ねて示されており，$P$ 波に対する走時の観測値Oと計算値 $C$ の差 $(O-C)_P$ は，Table 3 に与えられている．更に近似を進めれば，よりよく求められるであろうが，この程度でも実際の震央との距離は 11.1km で 0.1° 以内に収まつていて，震央はよく求められたといつてよい．R. G. E. S. の石淵第 2, 3 回の資料を用いた前報の結果では，2, 3 の試みにより求められた震央と実際の爆破点との距離は 1.5～1.9km の範囲であつた．地殻構造，地震計の配置などの相違があるので，完全な比較は出来ないが，観測の精度は 10 倍以上，R. G. E. S. の資料の方がよい事を考えると，観測精度の向上による震源決定の精度の向上の目安を，或る程度得る事が出来ると考えられる．また前報に述べた如く，この場合も実際の震央が，第2近似の震央を中心とし Probable Error を半径とした円に含まれない．origin time は表土層に敏感であるので，よく求められていない．この付近の地殻構造は R. G. E. S. により求められている[5]が，同グループの観測による走時図上では 5.9 km/s の見掛けの速度が得られる (Fig. 6)．従つて，速度もかなりよく求められたといつてよい．なお Fig. 6 に示された如く，用いた報告値は R. G. E. S. の観測値より1秒前後おくれたものであるが，この程度に求められたという事は，概して小さい初動が見落されても，各測候所で対応している大きい波をよみとつている事によるのではないかと考えられる．

次に，松代のみは他の測候所に比し，特別に精度がよい事を考慮して，松代のみ，仮に 10 及び 100 の Weight をつけて震源を決定してみた．time keeping だけでなく，倍率も遥かに大きく，従つて記録もよく，10 位の Weight では小さすぎるかも知れないので，100 の場合も行なつてみたのである．第1近似の量は，前に定めた値をそのまま用いた．補正量は

Weight 10 の場合

$\delta x_0 = (10.4 \pm 4.0)$ km　　$\delta t_0 = (1.6 \pm 1.7)$ sec

$\delta y_0 = (5.0 \pm 3.4)$ km　　$\delta v_0 = (0.48 \pm 0.45)$ km/sec

Weight 100 の場合

$\delta x_0 = (10.6 \pm 4.0)$ km　　$\delta t_0 = (1.4 \pm 1.9)$ sec

$\delta y_0 = (5.7 \pm 3.6)$ km　　$\delta v_0 = (0.47 \pm 0.46)$ km/sec

と求まる．補正した結果は，Table 2 に他の量と共に，夫々 II′, II″ の行に与えられている．この表から，Weight をつけた方がよく求められた事，特に origin time $t_0$ がよくなつている事，Weight 10 と 100 では大差ないが，$t_0$ は 100 の場合の方がよく求まつている事が判る．求められた種々の震央の関係は，Fig. 9 に示されている．

一方，地震課にお願いして特に同課で日常行なつている方法で orgin に関する量を求めてもらつた所，Table 2 の J. M. A. の行に示す如くであり，origin time は和達 et al の表にあうように求められたので，早くなつている．この震央も，Table 2 に示される

5) 爆破地震動研究グループ　*loc. cit.*, 2)

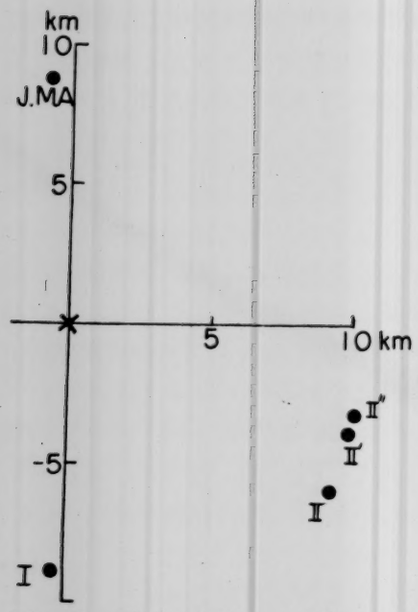


Fig. 9. The relative positions of determined epicenters to the actual one.
×: Actual epicenter
I, II, II′, II″ and J.M.A. are given in Table 2.

如く，実際の震央と 8.72km 離れ，最小2乗法で求めたものとは 20km も離れている．併し，異なつた方法で求めた震央が，実際のものと 10km 程度しかちがわない事は，注意してよい事である．

最後に本題から離れるが，$S$ と報告のあつた位相は，$P$ の怪しい測候所でも或る程度信頼出来ると推察されるので，この速度を最小2乗法で求めてみた．その結果，

$$t = (1.65 \pm 1.35) + \Delta/(3.34 \pm 0.15)$$

と求められ，この線は Fig. 6 に示されている．また $(O-C)_S$ は Table 1 に与えられている．但しこの計算においては，$P$ と報告のあつた福井は，丁度 $S$ の線にのるので，$P$ を見落して $S$ を $P$ とよんだものと考え計算に入れた．$V_P = 5.90$ km/sec を用いると，$V_P/V_S = 1.76$ となり，妥当な値である．爆破地震動の観測資料より，この程度の震央距離では，東北地方で 3.57 km/sec，関東地方で 3.63 km/sec の値が得られており[6]，今回の値は少し小さいが，釜石付近の中発破の観測資料では 3.36 km/sec の値が得られている[7]．自然地震からは，$S$ 波の速度として，この程度の値がしばしば求められている[8]．

## §4. 結 語

少くとも局発地震に相当する 156 屯の火薬爆発による地震動が，気象庁の約 10 ケ所の測候所に記録された．記象は，振幅が小さく不十分であるが，一応，気象庁のよみとりの侭を使い，既知の震源に関する諸量を最小2乗法で定めてみた．その結果，震央は 11.1 km 離れた所に求まり，かなりよく定められた．気象庁地震課で採用されている方法でも 8.7km 離れた所に求まり，震央に関しては，方法によらず，よく決定されるといつてよい．速度も Table 2 に示される如く，よく定められ，origin time は，余りよく求められなかつた．但し，低速表面層の存在がこれに関係しているかも知れない．この事は，前報までの結果とよくあい．この程度の資料でも確かめられた．また，松代のみは，time keeping もよく地震計の倍率も大きく，実際に得られた記象もよい事を考慮して 10，100

6) S. ASANO, N. DEN, T. MIKUMO, E. SHIMA and T. USAMI, *Bull. Earthq. Res. Inst.*, **37** (1959).
7) 同 上.
8) 例えば岸本兆方・神月彰 地震 [ii] **9** (1957), 200.
Y. KOSHIKAWA, *Bull. Utsunomiya Univ.*, No. **6**, Section **2** (1956), 31.

の Weight をかけて定めてみた結果，Weight をかけた場合の方が特に origin time に関して，よく定まる事，今回の資料では，10 と 100 の Weight では，その差ははつきりしない事が判つた．なお，前報において述べた如く，以上は一定の地震計の配置，地殻構造等の下に得られたものである．

副産物として，$S$ 波の速度を定めた結果，3.34 km/sec の値が得られた．

§2 でも断つた如く，今回の資料は気象庁のものとしても余りよいものとはいえず，大地震の資料を用いて行う走時曲線等の議論では，今回の資料に比べれば初動が明瞭であるので，かなり精度が上記のものよりよいものと推測される．従つて，本報の結果を以つて，直ちに全観測の精度の目安とする事は勿論出来ない．今後，機会があれば，更に検討する積りであるが，この程度の観測でも 0.1° 以内に実際の震央との距離が収まる事は 10～50 km の範囲の地震活動の統計に局発地震を用いてもよいことを示すという事が出来よう．

また，精度のよい R. G. E. S. の資料を用いて震源決定を試みると，観測精度の向上による震源決定の精度向上の程度の目安が得られる筈であるが，近い将来試みる予定である．

終りに御指導頂いた河角広教授，資料をお貸し下さり，いろいろ御協力下さつた気象庁地震課の方々及び，資料の使用を許可下さつた爆破地震動研究グループに深く感謝する次第である．

---

## 21. *On the Accuracy of Hypocentre Determination III.*

By Shûzô ASANO,
Earthquake Research Institute.

At 12h 00m, June 15, 1958, 156 tons of explosives were fired in Gifu Prefecture, central part of Japan, in order to obtain rocks for the construction of Mihoro dam. The seismic waves generated by this blast were recorded at about 10 observatories under the Japan Meteorological Agency. Although the recorded amplitude was rather small and the onset of initial motion was not clear except at Matsushiro, the attempt to determine the quantities concerning hypocentre was done by the method of least squares. The results which are given in Table 2 confirmed my previous conclusions. In the present calculation the position of epicentre was determined within 0.1 degree, the velocity was determined rather well, but the determination of the origin time is not good. Giving weight to the observation at Matsushiro we could obtain better results, especially with respect to the origin time. The velocity of $S$ wave was also obtained as 3.34 km/sec.

地震研究所彙報
第37号(1959) 347-358頁

# 22. 紀伊半島の局地地震(第1報)

## ——和歌山県御坊における小地震の観測——

地震研究所　宮村攝三

(昭和27年5月20日発表——昭和34年3月28日受理)

1949年後半よりふたたび活動期にはいつた和歌山地方の局地地震活動に関して，電子式地震計をもちいた小3点観測法による偵察的観測をおこない，将来の観測計画のための基礎資料としてえた若干の結果を報告する．

### 1. 序　　論

1920年ごろから和歌山地方に頻発した局地的地震活動は今村明恒その他[1]によつて研究され，いわゆる名草地震群として注目されていた．そののち，この地方の地震活動は1923年ごろを頂点として次第におとろえ，同時に田口克敏，渡辺正之ら和歌山測候所関係者[2]のしらべによれば，その活動中心は名草山に代表される和歌浦湾方面より，順次，有田郡から日高郡へと南方にうつつていつた．

今村明恒は，これらの地震群に対し，将来予想される第2の安政地震(南海道地震)との関連において，紀伊半島の水準再測等による地殻運動の研究と併行して，その調査をすすめていたが，不幸にして戦争のため次第に観測事業を縮少，ついに中絶のやむなきにいたつた．そして1944年12月7日東海道地震，ついで1946年12月21日南海道地震とあいついで，この予想された大地震はおこつたが，今村の構想による観測は最後の成果をあげることができなかつた．南海地震後，海南市において今村久らによる地震観測がおこなわれ，岸上冬彦[3]により報告されたが，余震活動は約10ヶ月後にほとんど終止しており，局地的地震群の活動はむしろこの前後には，もつとも低調であつたといえる．

こうした地震活動の状況の一端をうかがうため，Fig. 1 に和歌山測候所における毎年の有感地震回数を図示した．この図でもあきらかなように，1949年後半にいたつてふた

1) A. IMAMURA, T. KODAIRA and H. IMAMURA, "The Earthquake Swarms of Nagusa and Vicinity," *Bull. Earthq. Res. Inst.*, **10** (1932), 636–648.

2) 渡辺正之「和歌山地震について」和風(和歌山気象同好会) **25** (1952), 9月号 1–4.
和歌山測候所「紀伊半島の地震について」紀淡海峡頻発地震調査報告(大阪管区気象台, 1953年3月) pp. 35–43.

3) F. KISHINOUYE, "Monthly Numbers of Earthquakes at Kainan City, Wakayama Prefecture in 1947," *Bull. Earthq. Res. Inst.*, **26** (1948), 81–82.

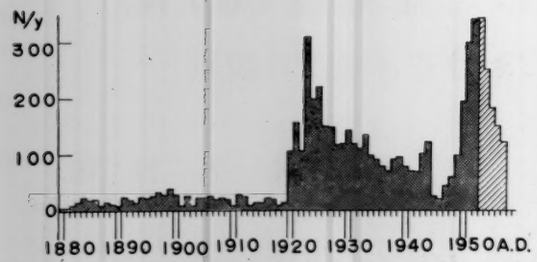


Fig. 1. Annual number of earthquakes felt at Wakayama Meteorological Observatory since 1880. (Data for 1953—1957 were added during the preparation of the manuscript.)

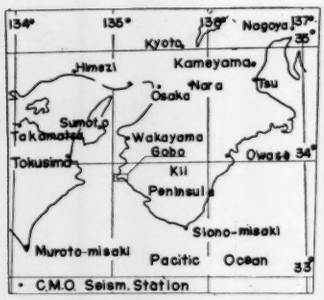


Fig. 2. Index map, showing the temporary station, Gobo, and C. M. O. seismological stations in and near Kii Peninsula, Central Japan.

たび急激に地震回数がふえている．つまり，ひさしく一般の注意をひくことのなかつた和歌山地震群の第2の活動期がここにはじまつたのである．

再開された和歌山地方の局地的地震活動が 1920 年代のような和歌浦湾中心のものか，1930年代のようにやや南方にその中心をもつものをふくむかは，有感地震の報告や，測候所の観測だけではかならずしも，充分はつきりしたことはわからなかつた．われわれはまず今後の観測実施の計画をいかにたてるべきかを決定するひとつの方法として，ほぼ和歌山県の中部に位置する御坊町 (Fig. 2 参照) において，高感度の電子式地震計による偵察的観測を実施することにした．

自然地震の確認のため，(実際には記象型だけで自然地震として容易に確認できたが,) 約100m の辺長をもつ3点観測をおこない，あわせて，これによつて震央方位をだすことができれば，*S–P* 時間とくみあわせて，地震活動の中心の移よその見当をつけうることも期待した．

地震計の周波数特性として低周波 (10 c/s 以下) およびやや高周波 (10 c/s 以上) に中心をもつ2種類のものをもちい，どのような特性の地震計を採用すべきかの資料がえられるようにした．

将来の精密観測の準備として，短波標準電波分秒報時 (JJY) のこの地方の受信状況をしらべておくために，これを記録に直接刻時する方法を採用した．

記録装置はオッシログラフをもちいたので比較的のろい記録紙速度で 2～10 時間程度毎晩観測することで満足しなくてはならなかつた．しかし，これによつて一応発生の頻度についての概略の情報をうることができた．

最後に，もしできうれば，種々の位相のみかけの速度を3点観測法からもとめ，地殻成層についての知識をうることも企図したが，これは記録紙速度がおそいので，よい結果を期待することは無理であつた．

## 2. 計　　器

爆破地震学のために開発された換振器，増幅器[4]，記録装置よりなる電子式地震計を利用した．すでにのべたように，換振器として自己振動数 10 c/s, 3 c/s の 2 種類のものをもちいたが，それぞれのばあいの地震計全体の周波数特性はほぼ Fig. 3 にしめしたようなものである．実際にもちいた利得は土地の雑振動のため，ほぼ最高感度数万倍程度であつた．

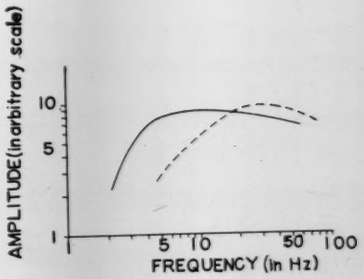


Fig. 3. Frequency characters of two electronic seismographs adopted for the reconnaissance observation of minor shocks at Gobo, in Jan.～Feb., 1952.

## 3. 観　　測

1952 年 1 月 13 日より 2 月 23 日まで，和歌山県日高郡御坊町県立日高高等学校（旧日高中学校）の地震計室を利用して観測をおこなつた．Fig. 4 a にみるように同校は日高川の沖積原にあり，道路，鉄道にちかく，市街地もとおくないので，土地の雑振動水準はかなりたかい．南海道地震の余震を利用した御坊附近の地盤の振動性能比較観測[5]の結果によれば，中生層岩盤の露出している観測点にくらべ，ほぼ 1.4 倍の振幅増幅度をもつことがわかつている．したがつて，高感度の観測をおこなうにはあまりよくない地点であるが，

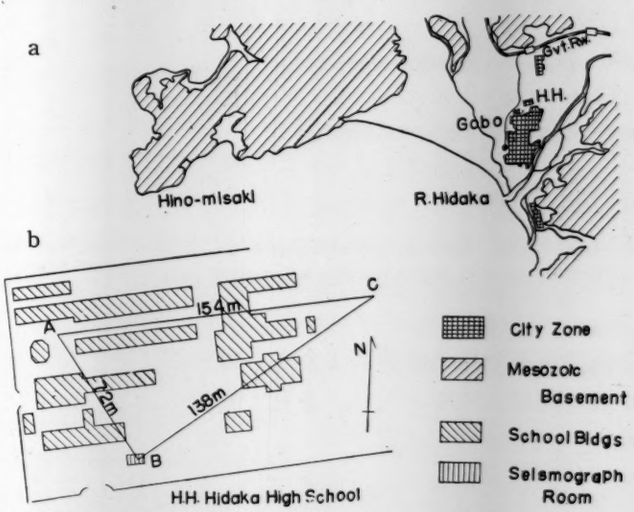


Fig. 4. Location of Hidaka High School (a), and tripartite stations A,B,C in the campus (b).

4) 田望「爆破地震動観測用増幅器」地震 **[ii]**, **6** (1953), 33–40.

5) S. MIYAMURA, "Tertrema movado kaj kvalito de grundo ĉirkaŭ la urbeto de Gōbō, Wakayama Prefectejo," *Bull. Earthq. Res. Inst.*, **26** (1948), 101–104.

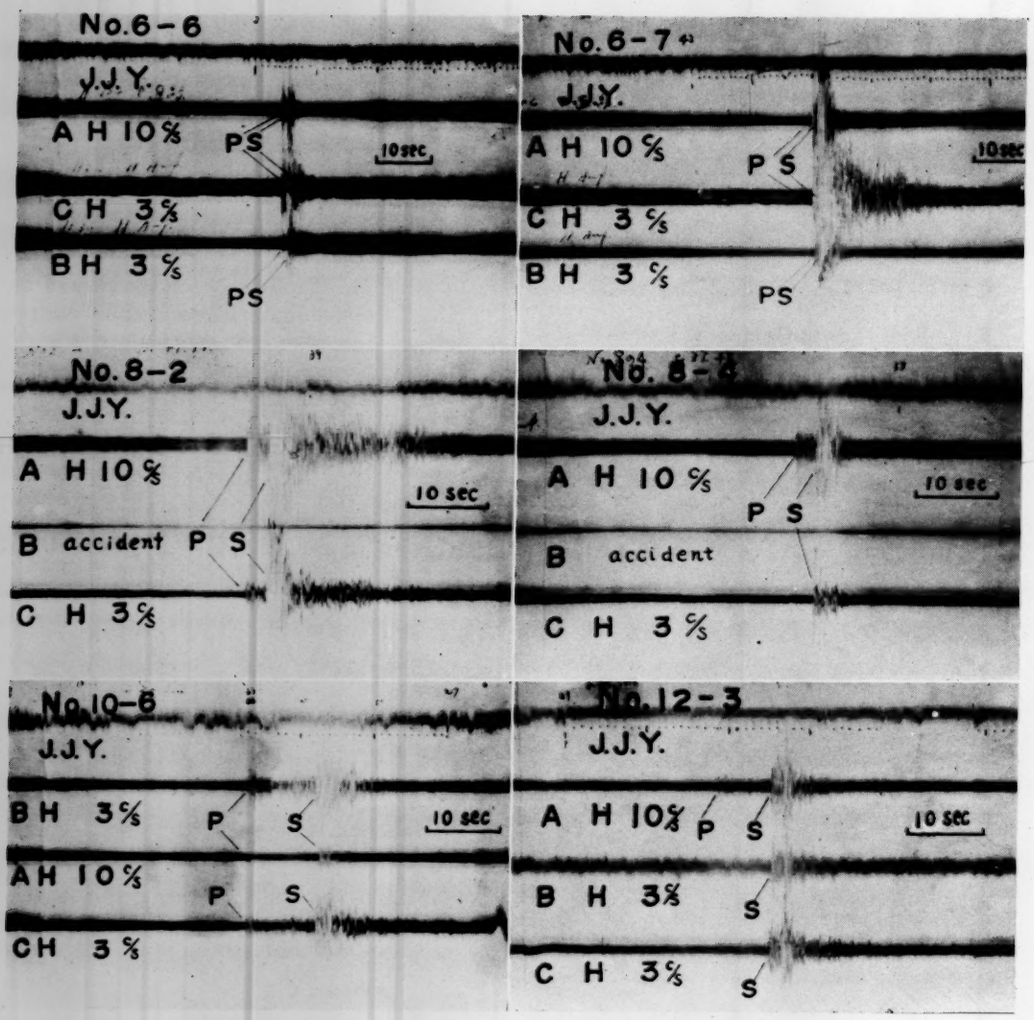


Fig. 5. Examples of typical seismograms of minor shocks obtained by the reconnaissance observation at Gobo, Jan.～Feb. 1952.

3点観測をおこなう便宜その他の事情によりえらばれた．そして，雑振動水準のひくい，天気のよい，しずかな夜半のみをえらび，観測を実施し，Table 1 にしめすような 12 回の観測をおこなうことができた．

最初の5回は3台の換振器を同一点（観測室内，Fig. 4b の B 点）において観測し，あとは Fig. 4b にしめすような A, B, C の3点で，いわゆる3点観測法 (Tripartite Method) による観測をおこなつた．

えられた記録の代表的な実例を Fig. 5 にしめす．

Table 1. Items of the reconnaissance observation of minor shocks at Hidaka High School, Gobo, Wakayama Prefecture, Central Japan.

Period: Jan.～Feb. 1952. Instruments: Electronic seismographs for explosion seismology. Two lower and one higher frequency characteristics. Observation: 3 NS in one place (Nos. 1～5) or in tripartite points (Nos. 6～12). On selected calm midnights.

| No. | Date | Time | | Paper speed cm/min. | Number of shocks recorded | | Number of shocks observed by C. M. O. seism. net |
|---|---|---|---|---|---|---|---|
| | | h m h m | hour | | Total | Per hour | |
| 1 | I 13～14 | 22.00～02.07 | 4.12 | 8.5 | 16 | 3.9 | 2 |
| 2 | 15～16 | 20.20～06.40 | 10.30 | 2.8 | 12 | 1.1 | 3 |
| 3 | 17～18 | 23.23～03.12 | 3.82 | 8.5 | 6 | 1.6 | 0 |
| 4 | 21 | 00.00～05.00 | 5.00 | 8.5 | 10 | 2.0 | 1 |
| 5 | 28 | 00.02～00.20 | 1.97 | 21.0 | 1 | 0.5 | 0 |
| 6 | 28～29 | 23.37～03.29 | 3.85 | 8.5 | 7 | 1.8 | 1 |
| 7 | II 4 | 00.44～02.38 | 3.37 | 12.0 | 2 | 0.6 | 0 |
| 8 | 6～ 7 | 23.30～02.53 | 3.38 | 12.0 | 9 | 2.7 | 0 |
| 9 | 9～10 | 22.20～00.34 | 2.23 | 12.0 | 3 | 1.3 | 0 |
| 10 | 11～12 | 23.30～02.38 | 3.13 | 12.0 | 6 | 1.9 | 0 |
| 11 | 20～21 | 22.20～00.30 | 2.17 | 8.5 | 6 | 2.8 | 0 |
| 12 | 22～23 | 23.00～02.02 | 3.03 | 12.0 | 4 | 1.3 | 0 |
| Total | | | 46.37 | | 82 | 1.8 | 7 |

## 4. 考　　察

**4・1. 地震発生の時間的状況**　Table 1 からあきらかなように，12 回の通算観測時間 46 時間余で合計 82 の地震がよみとられた．頻度は平均 1.8 回毎時乃至 4.3 回毎日で，Fig. 6 にしめすように約 40 日間の全観測期間中において，特にいちじるしい消長はみられない．ただ Fig. 6 にあわせてしめした和歌山および潮岬両測候所の毎日の地震記録回数と有感地震回数とを参照すると，1月すえより2月はじめと，2月 10 日前後などに，地震活動のややよわいときがあつて，御坊における小地震の記録回数も，感度をかえて観測したばあいもあり，多少正確さをかく点もあるが，ほぼこれと並行しているようにみえる．したがつて，高感度観測でもある程度以下の短期間観測では真の地震活動度をつかむことはできない．岸上冬彦[3]によれば南海地震の余震の海南市の観測において，震度のつよい地震の発生と小地震の回数とのあいだに相関がみられたのであるが，御坊でのぬきとり的観測による小地震の回数もまた測候所で記録されるようなやや震度のつよい地震の発生と相関をもつようにみえるが非常に明瞭ではない

毎回の観測中における地震の時間間隔についても特に顕著な性質を推定することはでき

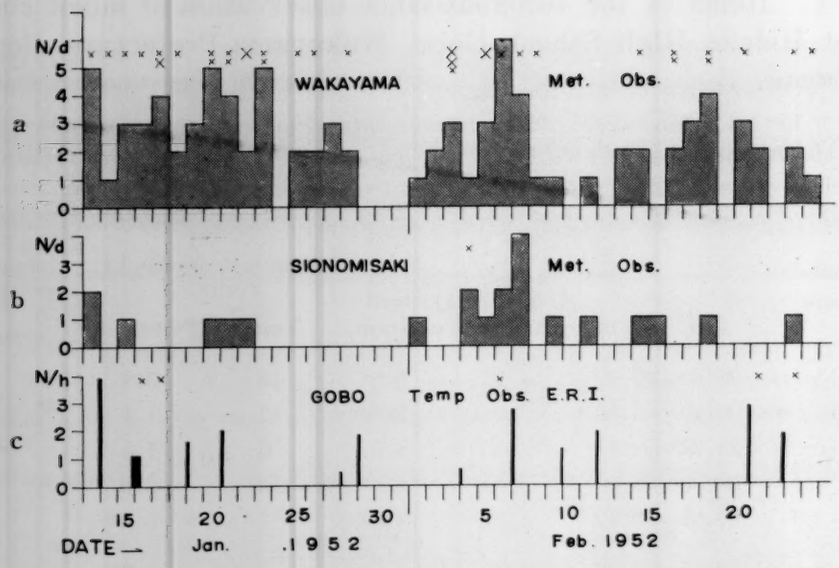


Fig. 6. Number of shocks observed by the sporadic observation at Gobo, from 14. Jan. through 23. Feb., 1952 (c), together with the daily numbers of shocks recorded at Wakayama and Sionomisaki Met. Obs. during the same period. (a, b) Asterisks indicate felt shocks; small ones are for intensity I, and large ones for intensity II.

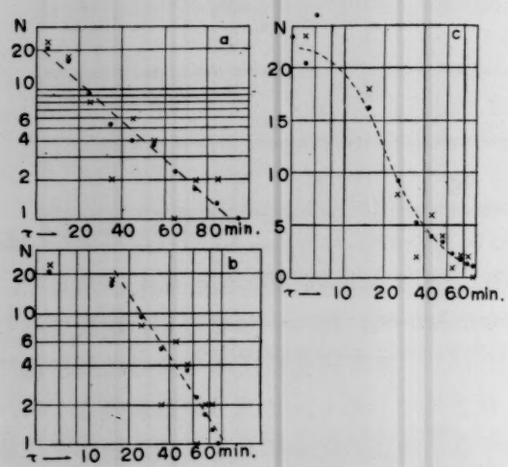


Fig. 7. Frequency distribution of time intervals between successive earthquakes identified in the temporary observation at Gobo, 1952.

ない．Fig. 7 の時間間隔頻度分布をみると，ほぼ指数分布をなしているようにみえ (Fig. 7a)，世界全体，または日本附近をとつた有感地震などがそうであると同様，この紀伊半島の局地的小地震の発生は 1 時間程度以内の発生間隔について，第一近似としては偶発的であるとしてよさそうである[6]．そして，これは Fig. 7b でみられるように，火山地震や大地震の余震など時間間隔のみじかい系列になりたつといわれている $k\tau^{-p}$ ($k$, $p$ 常数) 型分布ではないらしい．しかし Fig. 7c をみれば $\log\tau$ が正規分布をするという推定もできそうである．要するに全体の標本数がすくないのであるから，いずれとも確定的なことはいえないというのがただしいかもしれない．統計的議論により，いずれの分布がより適合しているかを順位づけることは可能であるが，地球物理学的にはこれだけの資料で結

6) 友田好文「地震の時間間隔の分布，及びこれと地震動の最大振幅との関係に関する統計的記述」地震 **[ii]**, **7** (1954), 155–169.

論をいそいでもあまり意味がない．今後さらに観測的研究をすすめるべきものとおもわれる．

**4・2．初期微動時間 $t_{S-P}$ の頻度分布**　記録された地震 82 個のうち 37 個（45%）について初期微動継続時間 $t_{S-P}$ をよみとることができた，その頻度分布は Fig. 8a にしめすとおりであり，$t_{S-P}=1$～3sec. のものが大部分(72%)をしめる．上下動のみの記録から $t_{S-P}$ をよみとることはやや無理があるが，後述のごとく低周波と高周波の2種類の振動特性をもつ2種の地震計で記録したことがよみとりを容易にしたばあいのおおいことに注意したい．Fig. 8 b, c にらなべてかかげた 1952 年における和歌山測候所，潮岬測候所の有感地震の $S$–$P$ 時間の頻度分布とくらべてみると，和歌山では 0～2 秒が大多数であり，潮岬では全体の地震数もすくなく，はつきりしたやまはないが，2秒以下のものはごくすくない．したがつて局地地震のおおくは，御坊よりも北方，和歌山よりに発生していると推定してよい．無論御坊にも潮岬にも $S$–$P$ の1秒ちかいものがあるので，御坊から南方にも全然局地地震がないわけではないことも，一応注意しておきたい．

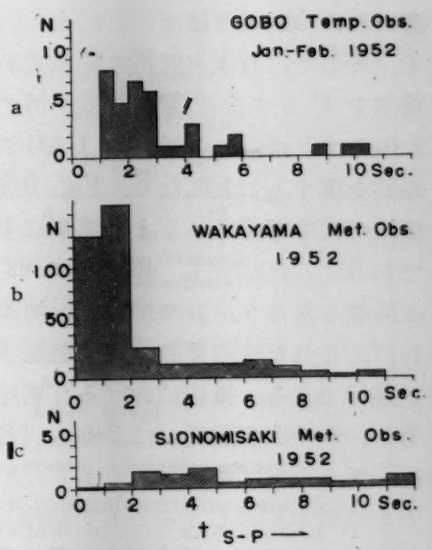


Fig. 8. Frequency distributions of $S$–$P$ times. a) For the reconnaissance observation at Gobo in Jan.～Feb., 1952. b) For the earthquakes felt at Wakayama Meteorological Observatory through 1952. c) For the earthquakes felt at Siono-misaki Meteorological Observatory through 1952.

**4・3．最大振幅 $A_m$ の頻度分布**　増幅器の利得をかえて観測をおこなつたときを除外して，記録振幅の最大値 $A_m$ の頻度分布をしらべた．最大振幅は大体 $S$ 波につづく波群中にふくまれるので $A_m(S)$ としるした．Fig. 9 には振幅のわりかたを $\delta A=5$mm ごとにとつてしめした．石本・飯田の式 $N=kA^{-m}$ の関係がなりたつとすると $N\geq 1$ の範囲で最小，最大の振幅区割を除外する常用の計算法によれば直線 a のごとく，$m=2.37\pm0.36$, $\log k=3.81\pm0.58$ となり，$N>1$ の部分にかぎるなら直線 b のように，$m=2.02\pm0.55$, $\log k=3.43\pm0.67$ なる関係式がえられる．標本数がすくないため確実性をかくが，いずれにしても，ここで観測された小地震の発生頻度の性質は，普通の地震や余震でえられている $m=1.8$ 程度の値と有意の差があるとはかんがえられない．

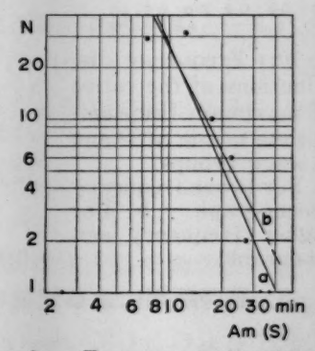


Fig. 9. Frequency distribution of maximum trace amplitudes of minor shocks observed at Gobo, which is approximately expressed by the ISHIMOTO-IIDA formula, $N=kA^{-m}$. a: $m=2.4\pm0.36$, b: $m=2.0\pm0.55$.

石本式加速度計（$V=200$, $T_0=0.1$ sec）を変位計とかんがえれば 10 c/s 以上の地震

高周波についてはほぼここにもちいられた電子式地震計の 1/400 の倍率のものとみなせる．そこで，石本・飯田の関係式がなりたつとき，1点で観測される地震の数は地震計の倍率を $V$ とすると $V^{m-1}$ に比例するので[7]，この石本式加速度計で観測した場合は $m=2.0$ とすれば，この場合の 1/400 になる．したがつて同数の地震を観測するに 400 倍の期間を要することになる．Fig. 9 からわかるように $A_m < 5$ mm の観測地震数は石本・飯田の式で期待されるより極端にすくないが，これはちいさい地震をみおとしているからである．したがつて，46 時間に 82 という数は実際の 1/5 程度の倍率でえられたものとほぼ同等であろう．したがつて，加速度計による観測で 80 倍の期間，約 150 日の観測をすれば，これだけの数の地震が記録できるとかんがえられる．すなわち 1 ケ月で約 15 程度が期待できる．御坊における有感地震は 1952 年において 53 回[8]（月平均約 4.5 回）であるが，和歌山測候所では 340 回（月平均約 28 回）であるから，御坊より北方に局発の中心があることはあきらかであり，紀北では加速度計による 1〜2 月程度の観測で 100 あまりの地震を記録しうることを期待してよいであろう．

**4・4. $P$ 波群，$S$ 波群中の最大振幅の比 $A_m(P)/A_m(S)$**　ひとつの地震について，$P$ 波群と $S$ 波群の振幅の比較をすることは，計器の絶対感度を必要としないから，振幅自体をとりあつかうより精度がたかいといえる．$P$ 波群の最大振幅 $A_m(P)$，$S$ 波群の最大振幅 $A_m(S)$ をよみとり，その比 $A_m(P)/A_m(S)$ をつくる．3 c/s および 10 c/s の換振器をもちいた地震計（周波数特性 Fig. 3 参照）について別々に $A_m(P)/A_m(S)$ の頻度分布をつくると Fig. 10 a, b がえられる．前者 (a) における頻度のやまが 0.2〜0.4 にあり，後者 (b) ではその比は 0.5〜0.6，0.8〜0.9 に集中していて，おたがいにずれていることは，(a) 低周波(10 c/s〜3 c/s) において $A_m(P)$ が $A_m(S)$ にくらべ小で，(b) 高周波(10 c/s 以上) で $A_m(P)$ が $A_m(S)$ に比して相対的におおきくでていることをしめしている．すなわち，$P$ 波群が $S$ 波群より，より高周波分にとんでいることがわかる．

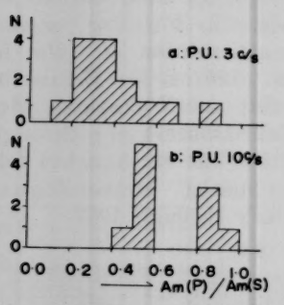


Fig. 10. Frequency distributions of the ratios of maximum trace amplitude in mm of $P$ and $S$ wave groups.
a) For lower frequency seismograph. b) For higher frequency seismograph.

**4・5. 震源距離による記象の全体的かたちのくずれていきかた**　記象の全体のかたちを代表するものとして $A_m/t_{F-S}$ ($t_{F-S}$ は $S$ から振動がおわるとき $t_F$ までの時間) をつくる．任意の単位をとつた数でこの頻度は Fig. 11 にしめすように(a) P. U. 3 c/s のものは 0〜1 にやまがあり，(6) P. U. 10c/s の方は 2〜3 にやまがくる．つまり，後者の方が全体の振動が最大動をおなじとすると比較的みじかく，前者の方がながくつづき，$S$波以後の部分に高周波分のすくないことをしめしている．

$A_m(S)/t_{F-S}$ と $t_{S-P}$ との関係をしめした図が Fig. 12 である．$t_{S-P}$ は震源距離を代表

7) 浅田 敏「地震のマグニチュードの頻度分布，サイズミシティとそれらに関連した諸問題」地震 **[ii]**, **10** (1957), 28.
8) 大阪管区気象台 地震月報 (1952), Jan.〜Dec.

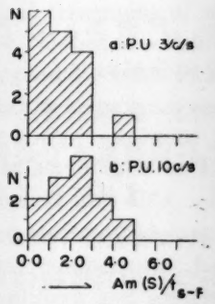


Fig. 11. Frequency distributions of the ratios of maximum trace amplitude in mm and the duration time in sec after $S$, $t_{F-S}$.
a) For lower frequency seismograph. b) For higher frequency seismograph.

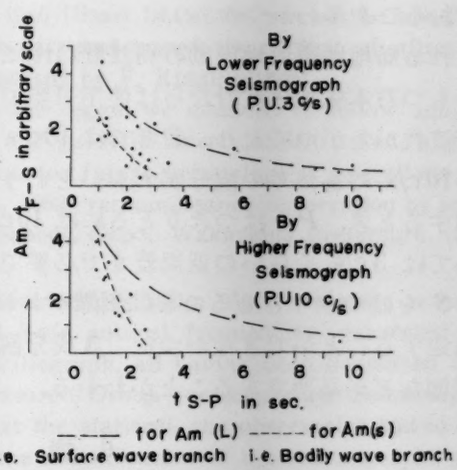


Fig. 12. Ratio of maximum trace amplitude $A_m$ to duration time after $S$, $t_{S-F}$ versus $S$-$P$ times. Points around the dotted lines are supposed to be the case, that $A_m$ is measured at $S$ and those around the broken lines at $L$ phase.

するから，震源がとおいほど振動が $A_m$ に対し相対的にながくつづくことをしめしている．さて $A_m$ としてとつたものが実体波（$S$）のばあいと表面波（$L$）のばあいとがありうる．そして主として近距離では前者，遠距離では後者のばあいとなりうるので，一応図のように分類をして，それぞれ2つの線上にのるとかんがえることもできる．点線を実体波のばあいとし，破線を表面波のばあいとし，それぞれこれは振動時間が距離とともにのびる状況のちかいをあらわしている．さらに実体波の方で P. U. 10 c/s の方が P. U. 3 c/s の方より減少が急であることは，高周波分の方が震源距離による減衰の大であることをしめすものとかんがえられる．

## 5. 結　　論

御坊における上記観測の結果，和歌山地方の今回の頻発地震は主として御坊より北方和歌山市にちかい方面でおこつていることが判明した．御坊において $S$-$P$ 時間1秒（震源距離 5～10 km）くらいのものもないわけではないが，大部分は紀北方面とかんがえられる．今後の観測は第一目標をこの地域にむけることがよいとおもわれる．

発生の消長をみると，ときにかなりすくない日がつづくことがあるので，たとえ高感度で連続的に観測できても，1ケ月程度の期間は観測をつづけないと，非常に活動の不活溌なときにであうおそれがある．もし，1ケ月程度連続して臨時的観測をおこなうなら，御坊附近で約 15，和歌山よりであればその数倍の地震が 200 倍の石本式加速度計でも記録できよう．より高感度の観測をおこないうるよい場所がえられれば，それはのぞましいが勿論連続記録の装置等を工夫する必要がある．

JJY 報時を刻時として直接もちいることは長期間連続では多少疑問があるが，ある程度

は可能であることがわかつた.

観測される局地地震の地震動の周波数特性はかなりはやいものであるが，10 c/s の自己振動数をもつ石本式加速度計ならば使用可能であろう．なお，$P$ 波群と $S$ 波群とにおいて多少周波数がちがつており，前者では 10c/s 以上の高周波成分がおおくふくまれ，後者では 3～10 c/s のあたりの成分がおおいということがわかつた．高感度でこのような小地震を観測するとき，$P$をはつきりとるには 10c/s よりさらに高周波数まで必要とするし，$S$については 3c/s くらいの低周波まで必要であるといえる．いずれにしても，1成分観測で $P$, $S$ をはつきりさせることは困難がおおく，記録された地震の半分あまりは $S$-$P$ 時間を判定することができなかつた．3成分観測およびちがつた周波数特性をもつ地震計による観測などが必要であることがわかる.

## 6. 謝　　辞

今回の観測において深夜の作業を遂行された同僚辻浦賢技官にこころから感謝の意を表する．観測上種々の御協力をえた日高高等学校の野田三郎先生はじめ生徒有志諸君にもあつくお礼もうしあげたい．また爆破地震観測用計器の流用をゆるされた爆破地震動研究グループの各位に感謝する.

---

## *22. Local Earthquakes in Kii Peninsula, Central Japan. Part I. Reconnaissance Observation of Minor Shocks at Gobo, Wakayama Prefecture.*

By Setumi MIYAMURA,
Earthquake Research Institute.

Renewal of the local shock activity in Wakayama Prefecture began again in the second half of 1949. Annual numbers of earthquakes felt at Wakayama from 1880 through 1956 are shown in Fig. 1 which represent the general tendency of seismicity in the region. For the last culmination of the activity some thirty years ago A. IMAMURA[1] executed comprehensive investigations, among which we cannot pass unnoticed his seismological net-work operations and precise level surveys. Although he anticipated the re-occurrence of great Nankaido earthquake like that of 1854, and tried to continue his observation and survey programmes, intending to catch any forerunning phaenomena, eventually should occur before the comming great earthquake. But, various difficulties during the War hindered him from developing his investigations, and at last compelled him to give up his whole plan, when the anticipated great earthquakes attacked the Tokaido and Nankaido regions, adjoining in the Kii Peninsula, successively in December 7th 1944 and December 21st 1946. On the other hand, however, local shock seismicity in Wakayama Prefecture had gradually lowered its activity after 1925, shifting or diverging its center from north to south[2], and before the Tokaido Earthquake in 1944 number of felt shocks at Wakayama Meteorological Observatory reached a minimum of about 70 per year. After-shock activities of the two great earthquakes, of course, affected the region, but they had ceased in a year or

two. After the Nankaido Earthquake of 1946 Hisasi IMAMURA, son of the late Prof. A. IMAMURA, re-opened his station at Kainan City and traced the decline of after-shocks, the statistical treatment of which was reported by F. KISHINOUYE[3].

For the re-opened seismic activity in the region we intended to follow again IMAMURA's programme both in seismometric and geodetic investigations. And, at first, in order to obtain some necessary information for future seismological operations in the region, the author executed in Jan.～Feb., 1952, reconnaissance observation by sensitive electronic seismographs at Hidaka High School, Gobo, Wakayama Prefecture. (See the maps in Figs. 2 and 4.)

Instruments used are two kinds of inverted pendulum electrodynamic transducers of horizontal components, having 10 and 3 c/s natural frequencies, connected to the E. L. F. amplifiers and electromagnetic oscillograph, all having been developed for explosion seismolgy by the R. G. E. S. (Research Group for Explosion Seismology)[4]. Owing to the high level of ground noise at the station[5], the observation had to be performed only on calm mid-nights to keep the magnification of the seismographs as high as 50,000～80,000 at 10 c/s. Relative amplitude-frequency characteristics are shown in Fig. 3. Some items of the observation are given in Table 1. There was a total of 82 shocks during the effective 46 hours observation, or more strictly we could identify this number of shocks as natural earthquakes on the 12 night oscillograms. Typical examples of seismograms are illustrated in Fig. 5.

The numbers of earthquakes recorded by our sporadic high gain observation at Gobo are given in Fig. 6, togather with those recorded daily at Wakayama and Sionomisaki Meteorological Observatories during the same period. Felt shocks at the three stations are also inserted in the figure as asterisks of large and small size, following the intensities. The figure suggests to us that the seismic activities around the three stations, which are situated in the northern, central and southern parts of the Prefecture are parallel in general tendency, though their degrees of activeness are fairly different. It was also pointed out by F. KISHINOUYE in the after shock statistics mentioned before[3].

The frequency distribution of time intervals between successive earthquakes at Gobo indicates no distinctive nature other than ordinary tectonic earthquakes, of which the time intervals are empirically expressed by an exponential law, implying a random occurrence of the events[6]. Following Y. TOMODA[6], time intervals of after shocks and volcanic swarms are expressed by other formula, and we may conclude that the minor shocks around Gobo are not similar to the above cited sorts of activities in their occurrence. (cf. Fig. 7)

Among the recorded 82 earthquakes only 37 shocks gave us clear $S$–$P$ times, frequency mode of which lies between 1～3 seconds as shown in Fig. 8a. Comparing it to the histograms of $S$–$P$ time frequencies of felt earthquakes at Wakayama and Sionomisaki Meteorological Observatories in Figs. 8b and 8c respectively, we can easily conclude that the center of seismicity lies to the north of Gobo, rather nearer to Wakayama City, as was the case in the first period of the former activity in the region. Moreover, numbers of felt shocks in 1952 at the three stations, Wakayama, Gobo and Siono-misaki were about three hundreds, fifty and five respectively, which further convinces us of the last mentioned northerly biased distribution of seismic activity.

Tripartite observations were tried in vain to add some information in locating the center of seismicity as eventual direction of approach of any phase. The size of the tripartite stations was too small and the recording paper speed was also somewhat slow.

Frequency distribution of maximum trace amplitude was examined, taking the class interval dA=5mm. As is shown in Fig. 9, it can be expressed by ISHIMOTO-IIDA's formula (I–I formula) with $m \fallingdotseq 2$. Minor shocks with maximum amplitudes smaller than several millimeters might be missed owing to the difficulty of identifying natural earthquakes from other oscillations of artificial or unknown origins. Thus the number of identified shocks must be taken to correspond to that recorded by several times lesser magnification seismograph. And, if we extend the above obtained I–I formula to rather larger shocks, considering the effective magnification as about ten thousands instead of fifty to eighty thousands, we can guess a possible time of temporary observation using a seismograph with lower magnification. Number of shocks recorded by a seismograph with magnification $V$ is proportional to $V^{m-1}$, where $m$ is the constant in I–I formula (T. ASADA[7]. 1957). Thus, if we use ISHIMOTO's accelerograph ($V = 200$), the time of observation enough to record as much shocks as the present sporadic one, becomes fifty times longer, i. e. about three months. If we make our future observation by the accelerographs in the northern area near Wakayama, we may expect to catch more shocks and shorten the period to a month or so. But, as was seen in Fig. 2, the earthquake occurrence has a rather sporadic nature, and if we take too short a period for observation, we will miss the general nature of seismic activity, however we can logically shorten the time by selecting calm stations and raising instrument sensitivity.

Comparison of seismograms obtained by higher and lower frequency characteristics indicates clearly the difference of spectral natures existed in the principal wave groups, $P$- and $S$- groups. Fig. 10 illustrates it well, as the mode of frequency of $A_m(P)/A_m(S)$ by lower frequency seismograph (3c/s P.U.) lies in 0.2~0.3, while that of by higher frequency instrument (10c/s P.U.) lies in rather higher values.

It is well known that the seismogram changes its shape according to its epicentral distance. Ratio between maximum trace amplitude in mm and total duration in second is taken as a measure of seismogram degeneration. As seen in Fig. 11, mode of frequency distribution of the above proposed ratio obtained by lower frequency seismograph lies between 0~1, while that of by higher frequency instrument between 2~3. It means that, for the same maximum amplitude lower frequency oscillation continues longer than shorter frequency ones. If we take $S$–$P$ time as a substitute of epicentral distance, it is illustrated in Fig. 12 that the above ratio gradually decreases with epicentral distance. Dotted lines and broken lines in the figure separate the plots for the shocks, whose maxima were measured in $S$ and $L$ phases respectively. Declinations of the curves with $S$–$P$ times or epicentral distances are steeper for higher frequency seismograph than for lower frequency instrument both in $S$ and $L$ phase maximum cases.

In conclusion, the main active area of the present local earthquake swarms in Kii Peninsula lies in the northern half of Wakayama Prefecture and our future expedition should be first focussed in that area. The instruments with fairly low magnification like ISHIMOTO accelerographs will probably be useful if we observe for a month or so. Direct use of JJY standard radio time signals as seismographic time marks was tested and gave some hope in future practice. Identification of $P$ and $S$ phases by one component observation was very difficult and 3-component observation and/or observation with different frequency character seismographs must be recommended in future observation.

地震研究所彙報
第37号(1959) 359-374頁

# 23. 近地地震初動の到来方向とみかけの速度

地震研究所 宮村攝三
辻浦賢

(昭和33年9月16日，12月23日発表——昭和34年3月31日受理)

辺長数百米の3点観測により，筑波山支所附近に到達する近地地震波動の解析をこころみ，50あまりの地震について，初動の到来方向とみかけの速度(表面速度)とを決定した．これにより推定される筑波を中心とする関東地方の震央分布は長期の通常の観測網によりえられた地震活動状況と大体一致している．また解析された地震の震源距離の代用としてとつた初期微動時間と初動のみかけの速度との関係は，爆破地震学によりえられたこの地方の地下速度分布とほぼ矛盾しない．なお，この3点観測による到来方向とみかけの速度決定の誤差を吟味し，あわせてこの方法の将来の発展についても論じた．

## 1. 序　　言

かぎられた範囲内の地点におかれた多数の地震計の記録を処理して地震波動の性質についての各種の情報をひきだす方法は，ひろい地域に分布する独立した観測所からの計測資料にもとずく方法にくらべて，比較的小区域の地下の状態をよりくわしくしらべることができ，あるいはまた記録処理の迅速化を発展させる可能性がおおきいなどの点に特徴がある．さらにまた独立した多数の観測所を高度に精密化した水準に整備するのにくらべれば多点集中観測をおこないうる高水準の観測所の小数を維持することは種々の点でより容易である．独立観測所において最初の験測報告をだすのに，たとえ成分，感度，周波数特性等のちがういくつかの地震計の記録を対比しつつ位相の同定をおこなうにしても，その観測所附近の多点観測があつて，局所的伝播の性質が決定できているならば，震央からつたわつてきたただしい位相と，散乱的な妨害波とを区別することができ，その験測はより信頼性をますことはいうまでもない．

このような見地から，すでに地震学においても地下探査法における発展にならつて，このような多点観測法が次第に採用されてきている．ソビエットでおこなわれている対比法地震観測 КМИЗ[1] はそのもつともよい例であろう．

しかし，このような方法の原型はすでにふるく震災予防調査会の事業のなかで「電線を

1) Г. А. Гамбурцев, ДАН. **87**, No. 1, 1952. ДАН. **92**, No. 4, 1953.
Г. А. Гамбурцев и Е. И. Гальперин, Изв. АН СССР, сер. геофиз., No. 1, No. 2, 1954.
(КМИЗ は Корреляционные Методы Изучения Землетрясений の略)

使用して地震波伝達速度を測定するの件」として関谷清景，大森房吉により立案され，今村明恒[2]により，本郷，一ツ橋，麻布，小松川の4点観測として実施されたものにはじまつている．

そののち，この3点観測法は土地の脈動の研究において岸上冬彦[3]により採用され，以後その方面ではかなりさかんにもちいられていたが，自然地震の観測では，有効な観測のための，観測点距離の増大の困難などによりあまり発展しなかつた．1948年にいたり浅田敏，鈴木次郎[4]は電磁地震計による微小地震の研究においてこの方法をとりあげ，有意義な観測をおこなつた．これ以後，わがくにでは爆破地震学のさかんになるのにつれて発達した電気的地震計の普及にともない，この3点観測法がいろいろの機会にこころみられるようになつた[5]．

これら自然地震における3点観測法は記録装置として普通電磁オッシログラフの長時間記録カメラをもちいたので，10～30 cm/min の記録紙速度で1～4時間の記録ができる程度であつたから，一般に地震活動がかなり活潑なばあいのみおこなわれたし，そのばあいにも位相時間差の決定精度が1/500秒に達することは困難であつたから，200m 前後の点間距離では精度の点であまり充分なものとはいえなかつた．

われわれの開発した超短波多重遠隔記録地震計 RTS-II[6]においては，周波数変調された3回線の副搬送波が1軌道の磁気テープに記録できるので，2軌道の磁気録音機で2台の RTS-II をもちい6回線の記録が可能であり，磁気録音機に無終端まきわくをもちいるならば，自然地震の観測において，磁気テープによる高速度の多点観測をおこなうことができ，その再生によつてきわめて精度のたかい験測をなしうるのである．

この方法により，三浦半島においてえられた記録を相関計算機で処理した結果は安芸敬一，その他[7]により発表されており，ひきつづいて同種の研究をおこなう目的をもつて，筑波山支所附近において6点観測をおこない，RTS-II による近地地震波動の磁気テープ記録をえた．相関的処理については安芸敬一，辻浦賢[8]により別に報告されるので，ここでは初動の時間差による普通の3点観測法的処理による結果だけをまとめ，若干の議論をつけくわえて報告する．

---

2) 大森房吉 震災予防調査会報告 **21** (1898), 21-30.
今村明恒 震災予防調査会報告 **21** (1898), 31-43. 同前, **32** (1900), 121-126.

3) F. KISHINOUYE, *Bull. Earthq. Res. Inst.*, **13** (1935), 146-154.

4) H. TSUYA, *The Fukui Earthquake of June* 28, 1948. Chapter III, Section 4, 58-64, 1950. (Studies of T. ASADA and Z. SUZUKI compiled by S. OMOTE)

5) T. ASADA and Z. SUZUKI, *Bull. Earthq. Res. Inst.*, **28** (1950), 415-420.
S. MIYAMURA and M. TSUJIURA, *Bull. Earthq. Res. Inst.*, **37** (1959), 347-358.
松本利松・田望・浅田 敏「高倍率電磁式微動計による十勝沖地震の余震観測結果について」地震研究所第290回談話会 (1952, VI, 17).

6) S. MIYAMURA and M. TSUJIURA, *Bull. Earthq. Res. Inst.*, **35** (1957) 381-394. *ibid.*, **37** (1959), 193-206.

7) K. AKI, M. TSUJIURA, M. HORI and K. GOTO, *Bull. Earthq. Res. Inst.*, **36** (1958), 71-98.

8) K. AKI and M. TSUJIURA, *Bull. Earthq. Res. Inst.*, **37** (1959), 207-232.

## 2. 観　　測

第1図にしめすような構成で，6台の上下動地震計の出力を，RTS-II の超短波伝送路を通じて筑波より本郷におくり，受信端において，2軌道の無終端磁気テープにおさめ，別に説明する時間装置により，適当な地震動が記録されたとき停止させ，適宜テープをとりかえ，解析のために保存する．テープの停止時刻は時計によつてしめされるが，モニー

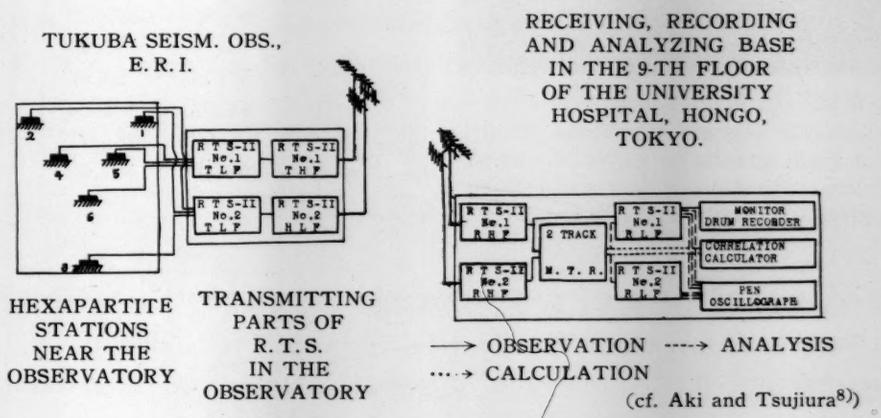


第1図　観測方法概要
Scheme of observation.

ターとして1成分はインクがき電流計で大型記録円筒に分刻時とともに連続記録される．

**観測点**　は筑波山支所ののる花崗岩の新鮮な露出をえらび，第2図に示すような 1～5 の5点に，第3図にみるようなコンクリートの小箱を固定設置した．第2図にしめした位置は技術部岡田惇教官により三角測量でもとめられたものである．坐標数値は Table 1 のごとくであり，第2図に記入した辺長は斜平面上のながさである．第6点は支所の地震計室である．各観測点より送信端局のある支所事務室までは遮蔽ビニール線を架設した．

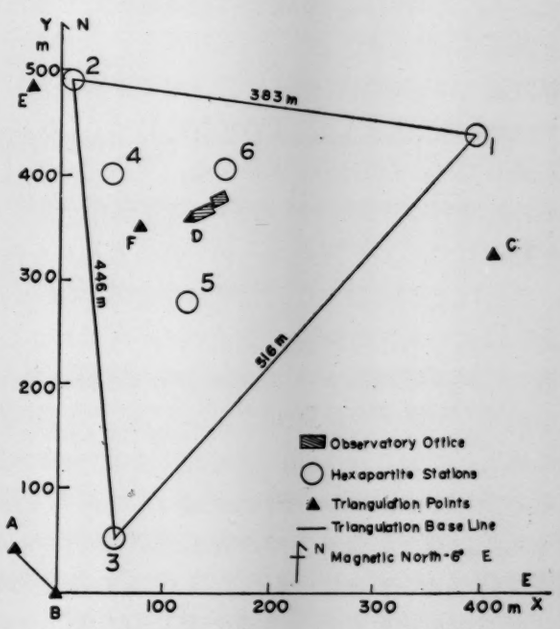


第2図　観測点位置
Map of seismometer location.

第3図 地震計収容箱外観
Small concrete seismometer house, firmly built on a fresh granite base. No. 3 station of the hexapartite stations near the Tukuba Seismological Observatory, E. R. I.

Table 1. Relative coordinates of the hexapartite stations near the Tukuba Seismological Observatory, E.R.I. (Triangulation survey was executed by A. OKADA, Techn. Div., E.R.I.)

| Station No. | $X(+E)$ | $Y(+N)$ | $h$(above sea level) |
|---|---|---|---|
| | m | m | m |
| 1 | 392.58 | 439.59 | 301.33 |
| 2 | 12.79 | 492.03 | 299.11 |
| 3 | 57.30 | 50.97 | 250.25 |
| 4 | 51.92 | 402.82 | 287.37 |
| 5 | 125.98 | 281.77 | 274.04 |
| 6 | 155.10 | 403.60 | 292.50 |

**地震計** は RTS–II 用に製作した上下成分動線輪型動電換振器であり，自己周期 3.0 c/s，制振分枝抵抗 60 kilo–ohms としてもちい，出力は約 3 volts/kine である．

**地震波送受信装置** RTS–II は F9 電波，周波数 417.7 Mc/s，送信出力 20 watts，端局として副搬送波3回線 800，2670，8900 c/s をふくみ，超低周波地震動入力がこれを周波数変調する FM–FM 方式である．この装置を2台（ただし電波の偏波面は水平垂直たがいに直交する）を利用し，6成分の観測をおこなう．装置の詳細についてはすでに発表した報告を参照されたい[6]．

**記録方法** は受信端で検波出力（副搬送波混合）を商用の2軌道テープ・レコーダー (Stereocorder, Sony Co., Type ST–1) に，無終端まきわくを附加して運転し，常時これに記録しては，数分後に消去する．テープ速度は 7.5 inches/sec. (19 cm/sec.) である．停止用時間装置は安芸敬一の製作したもので，0.5 volt 以上の振動入力が 6 sec 以上つづくと動作して，テープレコーダーのまきわくを停止する．このとき電気時計の電源がきれて，時計はその時刻をしめして停止する．モニターとして普通の観測を 2～5 mm/sec. の記録紙速度で大型円筒によりインクがきでおこなう．

**解析** は無終端磁気テープにおさめた地震記録を RTS–II 受信低周波部の沪波回路検波回路を利用して再生し随時おこないうる．スペクトク的研究のための相関計算もここで相関器に導入しておこなうが，位相対比法のためには，インキがきオッシログラフに種々の記録紙速度 (30 mm/sec., 50 mm/sec.) で再生記録をつくり，秒刻時を併記せしめ，ペンさきのずれを補正したうえで，対応位相の時刻差をよみとる．

**観測準備** としてまず 1958 年4月筑波山支所附近を踏査して，上記観測点を選定し，5月に観測台を設置した．7月に RTS–II 2台の調整をおえて，送信部を筑波山支所廊下に設置，観測点までの架線工事をおこなつた．受信室は本郷の東大附属病院新館9階の一部を借用し，その塔上を利用して地上 35m，海抜約 50m ちかい空中線をえたので，きわ

めて良好な受信状況を保持しえた.

**観測実施**　は第1期—VII月22日～VIII月30日，第2期—X月1日～X月21日，第3期—XI月10日～XI月17日で，期間中主として昼間は受信を中止して，解析のために装置をもちい，夜間のみ観測した．ときには昼間観測したばあいもあり，そのとき，タイマーによらず，手動でまきわくを停止し，テープのとりかえをしたこともある.

各期間中とも筑波からは連続に送信していたので，本観測のために特に支所員をわずらわすことはなかつた．第2期以後は 1, 2, 3 の3点のみの記録をおこなつた.

**観測結果**　第4図に磁気記録の大小の記録紙速度での再生記象の一例をしめす．1, 2, 3 点の初動（矢印）を，ペンさきのずれをしめす位置線からはかつて，時刻差をもとめることになる.

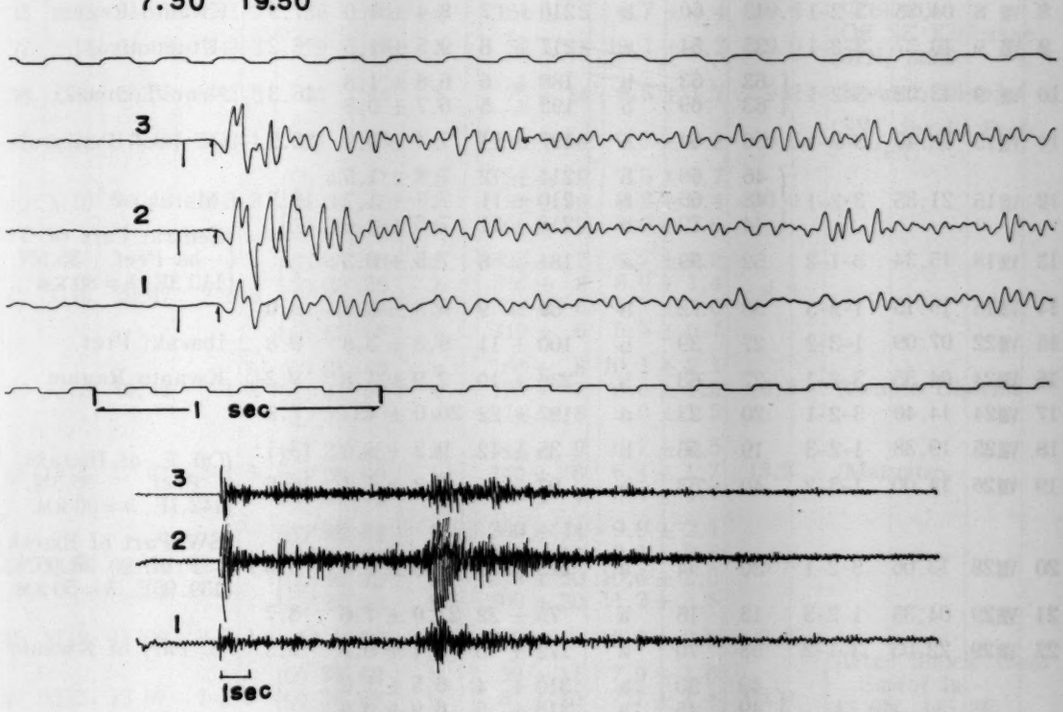


第 4 図　地震記象の実例（記録紙速度 10cm/sec., 1cm/sec.) No. 5.
Example of seismogram (with paper speed of 10cm/sec. and 1cm/sec.)
(Earthquake No. 5)

このようにした磁気テープ記録の再生による 1, 2, 3 の3点の初動またはそれにつづく対応波動の到達時刻差 $t'$, $t''$，そのよみとりの良否，それからもとめられた波動到来方向の方位 $\Theta$，およびみかけの速度 $v$ の数値は Table 2 にしめす．Table 2 には次節の議論にもとずく到来方向とみかけの速度の誤差も記入してある.

第 5～9 図には，再生記録とそれからえられた初動部対応波動の到来方向およびみかけの速度（矢印の方向とながさ）をならべたものを若干の地震についてかかげた.

## Table 2. Results of Observations.

| Earthquake No. | Date | Time (h m) | Arrival order of stations | Difference of onset $t'$ (ms) | $t''$ (ms) | Quality of onset * | Direction of approach $\Theta \pm \delta\Theta$ | Apparent velocity $v \pm \delta v$ (km/s) | $S$–$P$ at Tukuba (s) | Published Data by J. M. A. |
|---|---|---|---|---|---|---|---|---|---|---|
| 1 | VII22 | 15.43 | 3–1–2 | 58 | 58 | a | 184° ± 7° | 7.6 ± 0.7 | 7.6 | (Kakioka)** |
| 2 | VII29 | 02.30 | 2–1–3 | 32 | 63 | b | 334 ± 7 | 6.7 ± 1.6 | 6.7 | |
| 3 | VII29 | 13.53 | 2–1–3 | 58 | 58 | a | 313 ± 3 | 5.4 ± 0.4 | 9.7 | On the border of Gumma and Totigi |
| | | | | 48 | 58 | a | 319 ± 4 | 6.1 ± 0.5 | | |
| 4 | VII30 | 00.05 | 3–2–1 | 55 | 65 | a | 198 ± 7 | 7.2 ± 0.5 | 8.6 | Near (Tokyo) |
| 5 | VII30 | 19.50 | 3–2–1 | 26 | 39 | a | 206 ± 1 | 12.7 ± 2.1 | 7.2 | |
| 6 | VIII 6 | 23.22 | 3–2–1 | 13 | 36 | a | 249 ± 4 | 25.8 ± 3.1 | 9.0 | (Kakioka) |
| 7 | VIII 7 | 14.43 | 1–3–2 | 46 | 50 | a | 89 ± 5 | 7.6 ± 0.9 | 23.0 | Off E. of Kwanto |
| 8 | VIII 8 | 04.35 | 3–2–1 | 43 | 60 | b | 210 ± 7 | 8.4 ± 1.0 | 7.9 | Kwanto Region |
| 9 | VIII 9 | 10.37 | 3–2–1 | 35 | 54 | a | 217 ± 8 | 9.5 ± 1.5 | 6.2 | (Utunomiya) |
| 10 | VIII 9 | 13.02 | 3–2–1 | 63 | 63 | b | 188 ± 6 | 6.8 ± 1.8 | 16.3 | Near Tomisaki |
| | | | | 63 | 69 | b | 193 ± 5 | 6.7 ± 0.5 | | |
| 11 | VIII15 | 18.49 | 3–2–1 | 56 | 64 | b | 197 ± 11 | 7.4 ± 0.9 | 22.5 | Off Bôsô Peninsula |
| 12 | VIII15 | 21.35 | 3–2–1 | 46 | 66 | b | 211 ± 12 | 7.8 ± 1.5 | 16.5 | (Matusiro) |
| | | | | 48 | 66 | b | 210 ± 11 | 7.7 ± 1.7 | | |
| | | | | 44 | 70 | b | 218 ± 11 | 7.5 ± 1.6 | | |
| 13 | VIII18 | 15.34 | 3–1–2 | 52 | 59 | a | 181 ± 6 | 7.5 ± 0.3 | | Central Part of Tiba Pref. 35.5N, 140.3E, $h$=80 KM |
| 14 | VIII18 | 19.15 | 1–2–3 | 53 | 72 | b | 69 ± 9 | 6.3 ± 0.8 | 9.0 | |
| 15 | VIII22 | 07.09 | 1–3–2 | 27 | 39 | b | 100 ± 11 | 9.8 ± 3.6 | 9.8 | Ibaraki Pref. |
| 16 | VIII24 | 04.55 | 3–2–1 | 27 | 63 | b | 236 ± 10 | 7.9 ± 1.8 | 9.2 | Kwanto Region |
| 17 | VIII24 | 14.40 | 3–2–1 | 20 | 23 | a | 197 ± 22 | 20.0 ± 43. | 7.9 | |
| 18 | VIII25 | 19.38 | 1–2–3 | 19 | 56 | b | 35 ± 12 | 9.2 ± 4.5 | 13.1 | |
| 19 | VIII26 | 14.00 | 1–3–2 | 40 | 53 | a | 97 ± 5 | 7.2 ± 1.1 | 16.6 | Off E. of Ibaraki Pref. 36.3N, 142.1E, $h$=30 KM |
| 20 | VIII28 | 13.06 | 3–2–1 | 30 | 54 | a | 223 ± 9 | 9.8 ± 2.0 | 5.3 | SW Part of Ibaraki Pref. 36.05N, 139.95E, $h$=50 KM |
| 21 | VIII29 | 04.35 | 1–2–3 | 13 | 16 | a | 75 ± 22 | 27.0 ± 7.6 | 8.7 | |
| 22 | VIII29 | 22.03 | 3–1–2 | 53 | 70 | a | 172 ± 5 | 6.4 ± 0.7 | 5.3 | S. Part of Kwanto |
| 23 | X 1 | 13.40 | 2–3–1 | 49 | 50 | a | 310 ± 4 | 6.5 ± 1.6 | 6.2 | |
| | | | | 49 | 45 | a | 313 ± 5 | 6.9 ± 0.6 | | |
| | | | | 51 | 51 | a | 310 ± 4 | 6.4 ± 0.5 | | |
| | | | | 47 | 43 | a | 313 ± 5 | 7.2 ± 0.7 | | |
| | | | | 36 | 38 | a | 309 ± 4 | 8.8 ± 2.2 | | |
| 24 | X 2 | 19.57 | 1–2–3 | 22 | 48 | a | 46 ± 9 | 10.7 ± 2.6 | 13.5 | SE. Part of Hukusima Pref. 37.1N, 140.7E, $h$=90 KM |
| | | | | 21 | 45 | a | 45 ± 8 | 11.4 ± 2.7 | | |
| | | | | 21 | 49 | a | 42 ± 8 | 10.7 ± 2.7 | | |
| 25 | X 3 | 10.50 | 1–3–2 | 35 | 38 | a | 88 ± 7 | 10.1 ± 1.7 | 9.0 | |
| 26 | X 4 | 23.17 | 3–1–2 | 44 | 48 | b | 189 ± 16 | 9.3 ± 1.9 | 36.0 | NE. Off Hatizyo Is. 33.4N, 140.5E, $h$=160 KM |
| 27 | X 6 | 08.29 | 3–1–2 | 27 | 30 | a | 185 ± 10 | 15.0 ± 1.9 | 7.3 | Kwanto Region |
| 28 | X 7 | 20.00 | 3–1–2 | 52 | 55 | b | 189 ± 5 | 8.0 ± 0.9 | 8.4 | SW. Part of Ibaraki Pref. |

(to be continued)

(continued)

| Earthquake No. | Date | Time | Arrival order of stations | Difference of onset $t'$ | $t''$ | Quality of onset | Direction of approach $\Theta \pm \delta\Theta$ | Apparent velocity $v \pm \delta v$ | $S$-$P$ at Tukuba | Published Data by J. M. A. |
|---|---|---|---|---|---|---|---|---|---|---|
| | | h m | | ms | ms | | ° | km/s | s | |
| 29 | X 11 | 04.49 | 3–1–2 | 41 | 57 | a | 170 ± 8 | 8.0 ± 1.4 | 9.2 | S. Part of Kwanto |
| 30 | X 11 | 16.17 | 1–2–3 | 15 | 43 | b | 36 ± 15 | 12.0 ± 0.6 | 51.0 | E. off Aomori Pref. 40.7N, 142.4E, $h$=60 KM |
| 31 | X 11 | 20.56 | 3–2–1 | 46 | 58 | b | 204 ± 21 | 8.4 ± 1.8 | 55.0 | |
| 32 | X 13 | 05.37 | 3–1–2 | 21 | 41 | a | 156 ± 5 | 10.4 ± 2.5 | 5.4 | SE. Part of Saitama Pref. 35.9N, 139.7E, $h$=80 KM |
| 33 | X 13 | 17.29 | 1–3–2 | 26 | 54 | a | 111 ± 28 | 6.9 ± 1.2 | 8.5 | Off E of Ibaraki Pref. |
| 34 | X 13 | 17.40 | 1–3–2 | 18 | 29 | a | 105 ± 10 | 13.4 ± 5.4 | 6.5 | (Kakioka) |
| 35 | X 13 | 18.15 | 1–2–3 | 31 | 43 | a | 69 ± 12 | 11.0 ±13. | | Ibaraki Pref. (felt) |
| 36 | X 15 | 01.45 | 3–1–2 | 38 | 68 | b | 161 ± 5 | 6.7 ± 1.4 | 9.6 | (Tokyo) |
| 37 | X 16 | 04.02 | 1–2–3 | 29 | 49 | b | 57 ± 18 | 10.1 ± 3.2 | 29.0 | Off SE Kinkazan 37N, 142E |
| 38 | X 20 | 17.38 | 1–2–3 | 36 | 44 | b | 75 ± 14 | 9.8 ± 1.7 | 9.2 | Kwanto District |
| 39 | X 21 | 17.15 | 3–2–1 | 36 | 53 | a | 213 ± 6 | 9.7 ± 1.2 | 5.6 | SW. Ibraki Pref. (felt) |
| 40 | XI 10 | 21.18 | 1–3–2 | ② 45 | 51 | b | 91 ± 9 | 7.5 ± 1.7 | | |
| | | | | ② 34 | 48 | b | 98 ± 10 | 8.2 ± 2.4 | 30.0 | |
| | | | | ③ 31 | 48 | b | 102 ± 9 | 8.0 ± 2.6 | | |
| 41 | XI 10 | 20.47 | 2–1–3 | ① 41 | 58 | b | 323 ± 7 | 6.7 ± 1.2 | | |
| | | | | ② 38 | 38 | b | 316 ± 8 | 8.0 ± 1.4 | 8.7 | |
| | | | | ③ 45 | 72 | b | 328 ± 6 | 5.7 ± 1.0 | | |
| | | | | ④ 55 | 68 | b | 319 ± 6 | 5.5 ± 0.7 | | |
| 42 | XI 12 | 10.44 | 3–1–2 | ① 31 | 43 | a | 168 ± 8 | 10.1 ± 2.1 | | |
| | | | | ① 41 | 50 | a | 176 ± 7 | 9.0 ± 1.3 | 6.3 | Kwanto District |
| | | | | ①′39 | 50 | a | 174 ± 8 | 9.0 ± 1.5 | | |
| 43 | XI 12 | 17.01 | 2–1–3 | ① 24 | 65 | b | 343 ± 9 | 6.7 ± 2.5 | | |
| | | | | ①′28 | 69 | b | 340 ± 6 | 6.4 ± 1.7 | 13.3 | (Matusiro) |
| | | | | ② 31 | 72 | b | 338 ± 7 | 6.1 ± 1.7 | | |
| 44 | XI 13 | 02.01 | 3–2–1 | ①′38 | 51 | b | 209 ± 14 | 9.9 ± 2.1 | | |
| | | | | ②′30 | 49 | b | 220 ± 14 | 9.1 ± 2.8 | 5.5 | |
| | | | | ③′36 | 43 | b | 218 ± 10 | 10.6 ± 2.3 | | |
| | | | | ④′27 | 53 | b | 200 ± 30 | 11.2 ± 3.5 | | |
| 45 | XI 13 | 11.09 | 3–2–1 | 14 | 39 | a | 242 ± 9 | 12.2 ± 2.9 | 6.3 | |
| 46 | XI 13 | 13.07 | 1–2–3 | ② 38 | 62 | b | 59 ± 11 | 7.9 ± 1.6 | | After Shock from Etorof Is. 43.6N, 145.2E $h$=80 KM |
| | | | | ③ 39 | 63 | b | 61 ± 10 | 7.7 ± 1.4 | 105.0 | |
| | | | | ④ 36 | 56 | b | 62 ± 12 | 8.6 ± 1.8 | | |
| 47 | XI 13 | 17.03 | 3–2–1 | ① 10 | 38 | a | 243 ± 14 | 12.2 ± 1.4 | | |
| | | | | ①′16 | 43 | a | 250 ± 5 | 10.7 ± 2.0 | 5.6 | Central Kwanto |
| 48 | XI 13 | 23.19 | 3–2–1 | ① 41 | 48 | a | 199 ± 10 | 10.0 ± 1.1 | | |
| | | | | ① 41 | 51 | a | 203 ± 14 | 9.6 ± 1.5 | | |
| | | | | ② 48 | 51 | a | 194 ± 8 | 8.9 ± 0.7 | 9.4 | Southern Kwanto |
| | | | | ③ 48 | 51 | a | 194 ± 8 | 8.9 ± 0.7 | | |
| | | | | ④ 45 | 48 | a | 193 ± 8 | 9.6 ± 0.8 | | |
| 49 | XI 14 | 16.09 | 3–2–1 | ① 26 | 34 | a | 207 ± 13 | 14.4 ± 2.6 | | |
| | | | | ①′26 | 35 | a | 209 ± 13 | 14.1 ± 2.7 | | |
| | | | | ②′30 | 35 | a | 198 ± 13 | 13.5 ± 1.9 | 5.7 | |
| | | | | ③′30 | 35 | a | 198 ± 13 | 13.5 ± 1.9 | | |
| | | | | ④′28 | 40 | a | 209 ± 12 | 12.9 ± 3.1 | | |

(to be continued)

(continued)

| Earthquake No. | Date | Time | Arrival order of stations | Difference of onset $t'$ | $t''$ | Quality of onset | Direction of approach $\Theta \pm \delta\Theta$ | Apparent velocity $v \pm \delta v$ | $S$–$P$ at Tukuba | Published Data by J. M. A. |
|---|---|---|---|---|---|---|---|---|---|---|
| | | h m | | ms | ms | | ° | km/s | s | |
| 50 | XI16 | 10.51 | 3–1–2 | ① 0.7 | 49.5 | a | 131 ± 15 | 76. ± 68. | 9.8 | |
| | | | | ② 0.3 | 44.5 | a | 131 ± 201 | 172. ± 258. | | |
| | | | | ③ 0.7 | 51.0 | a | 131 ± 182 | 76. ± 91. | | |
| | | | | ①′ 0.4 | 47.6 | a | 131 ± 38 | 129. ± 1550. | | |
| 51 | XI15 | 18.03 | 1–2–3 | 51 | 68 | b | 70 ± 9 | 6.6 ± 6.7 | 108.0 | 44N, 149E $h$=70 KM |
| | | | | 27 | 58 | b | 48 ± 12 | 8.8 ± 2.8 | | |
| | | | | 21 | 58 | b | 32 ± 7 | 7.5 ± 3.2 | | |
| | | | | 41 | 58 | b | 66 ± 12 | 8.0 ± 1.4 | | |
| 52 | XI16 | 02.40 | 3–1–2 | 10 | 22 | a | 153 ± 1 | 18.6 ± 2.0 | 7.5 | Kwanto District |
| 53 | XI16 | 14.30 | 2–1–3 | ① 53 | 63 | b | 318 ± 6 | 5.6 ± 0.7 | 9.0 | |
| | | | | ② 45 | 62 | b | 323 ± 7 | 6.1 ± 1.0 | | |
| | | | | ③ 45 | 58 | b | 321 ± 8 | 6.2 ± 1.0 | | |
| | | | | ④ 34 | 55 | b | 328 ± 7 | 7.2 ± 1.5 | | |
| 54 | XI16 | 16.20 | 3–2–1 | 58 | 58 | a | 188 ± 4 | 7.5 ± 1.2 | 9.2 | Central Part of Tiba Pref. 35.3N, 140.2E $h$=60 KM (felt) |
| | | | | 58 | 61 | a | 192 ± 7 | 7.4 ± 0.8 | | |
| 55 | XI17 | 02.16 | 3–2–1 | 22 | 34 | a | 220 ± 13 | 15.0 ± 3.9 | 5.8 | (Kakioka) |
| | | | | 20 | 31 | a | 215 ± 15 | 16.6 ± 4.4 | | |
| | | | | 19 | 27 | a | 212 ± 17 | 18.6 ± 5.0 | | |

* Quality a: $\delta t = \pm$ 3 ms; b: $\delta t = \pm$ 5 ms.

** (Kakioka) means "only recorded at Kakioka".

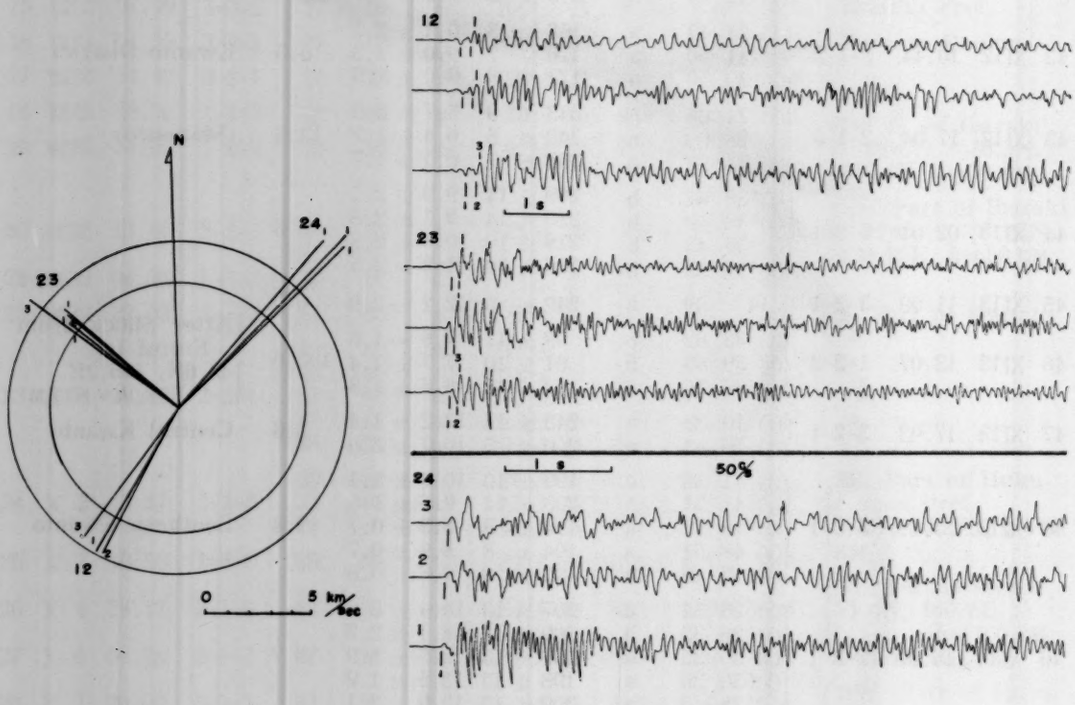


第 5 図 (Original × 1/4)

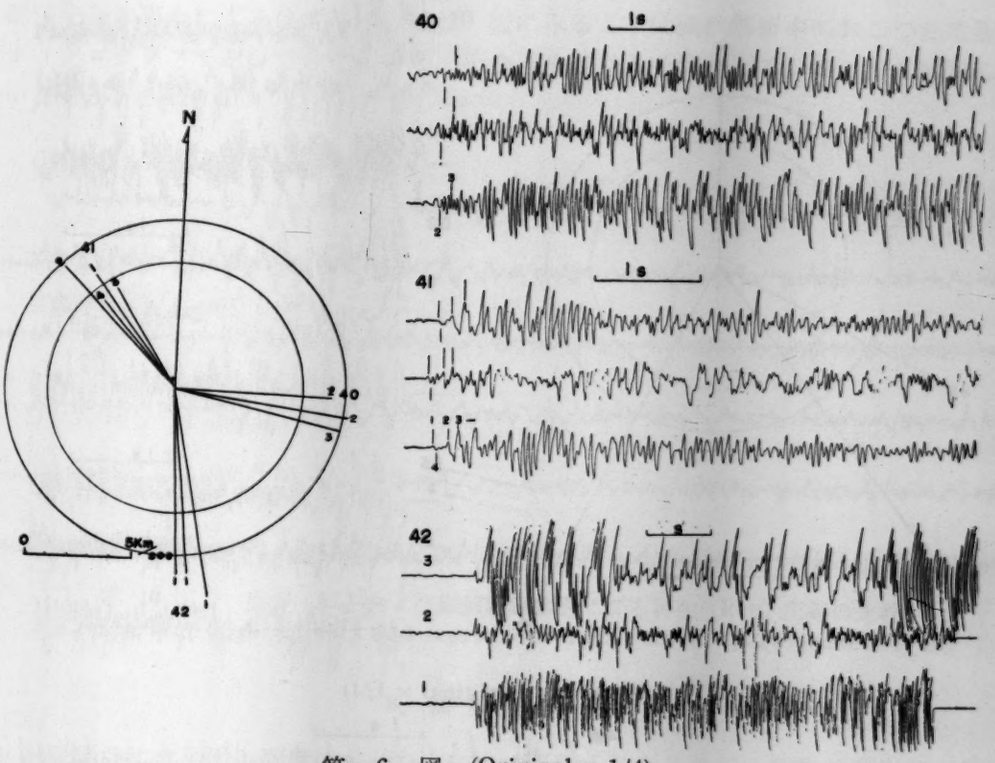


第　6　図　(Original × 1/4)

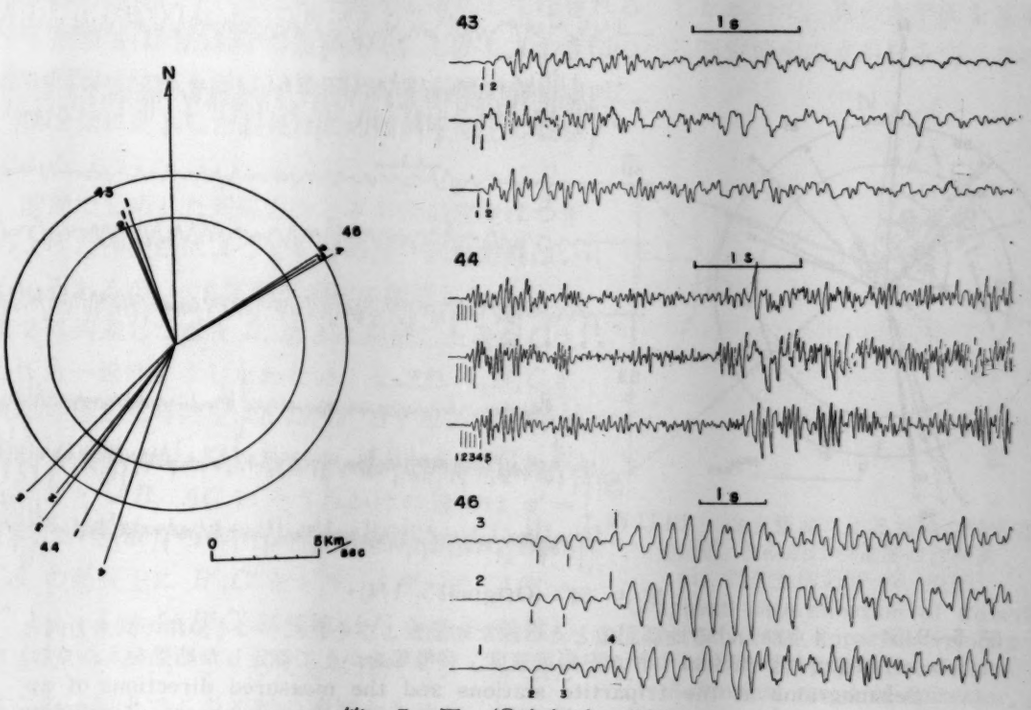


第　7　図　(Original × 1/4)

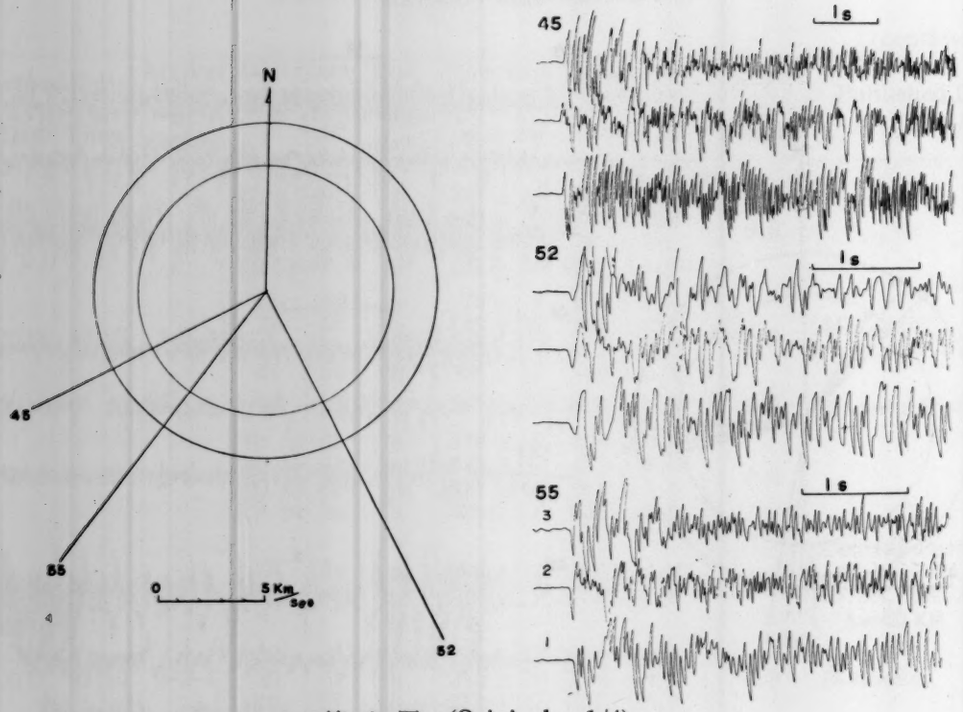


第 8 図 (Original × 1/4)

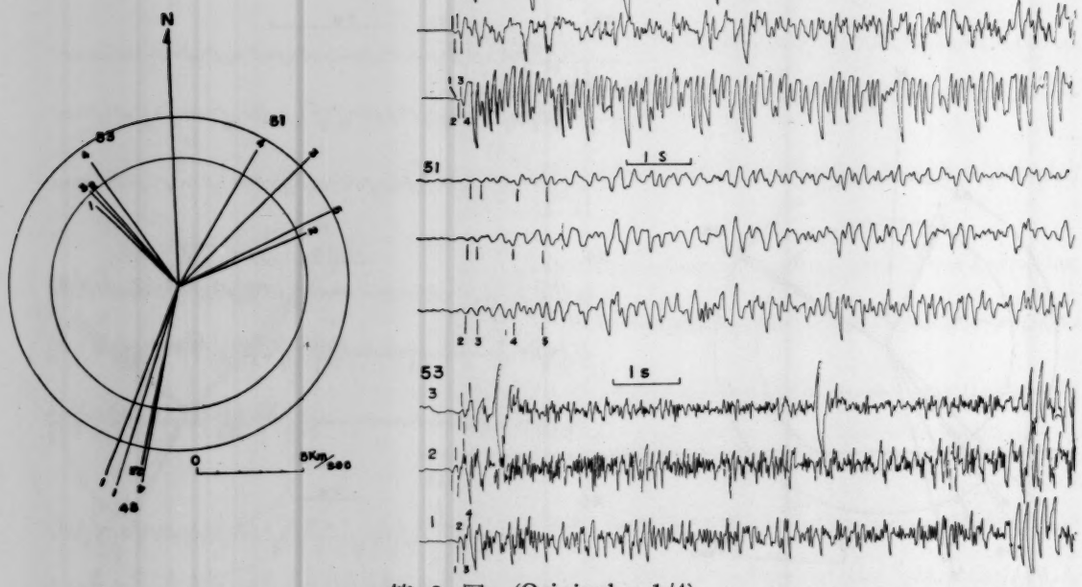


第 9 図 (Original × 1/4)

第 5～9 図　3点における地震記象とえられた初動およびそれにつづく位相の到来方向とみかけの速度(同一位相につき，記録紙速度，利得等をかえて測定した結果をもふくむ)

Seismograms at the tripartite stations and the measured directions of approach and apparent velocities of inital and a few following phases. (including those of a phase measured with different reproducing paper speeds and/or gains.) Earthquake Nos. should be referred to Table 1.

磁気記録の再生によるひずみは，第 10 図にみるように偶然解析中におこつた地震を直接オッシログラフで記録できたものと，その再生記録とを比較して，ほとんど問題にならないことがわかる．

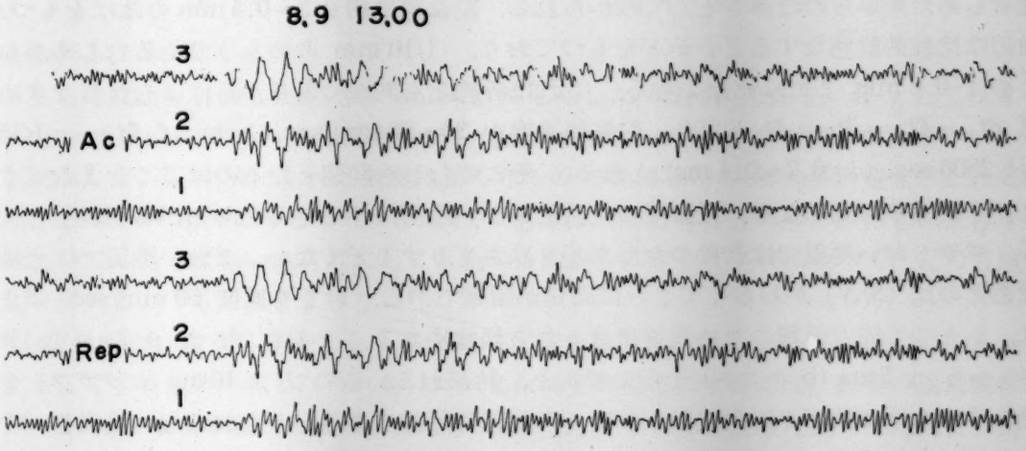


第 10 図　直接 (Ac) および磁気記録装置による再生 (Rep) 記録の比較
Comparison of direct (Ac) and reproduced (Rep) record. (Earthquake No. 10)

## 3. 結果の精度

3 観測点は水平面と数度のかたむきをもつ平面上にあるので，初動の到来方向およびみかけの速度はすべてこの平面をもとにしてなされる．したがつて，真の水平面を基準とする数値とは当然若干の差がある．しかし，つきにのべる測定精度の点からみて，この相違を問題にすることはいまのところ必要でない．

第 2 図に記入した辺長はこの傾斜平面上の数値である．

前節でしめした到来方向とみかけの速度はつぎのような作図法によつてもとめた．到来方向はいろいろあるが，いま波動が最初に到達した点を $A$，第 2 に到達した点を $B$，第 3 に到達した点を $C$ としても一般性をうしなわない．そこで $A,B,C$ に波動の達した時刻を $t_A, t_B, t_C$ とすると到達時刻差は $t'=t_B-t_A$, $t''=t_C-t_A$. $\overline{AB}=d'$, $\overline{AC}=d'$, とすると $AB$, $AC$ にそうみかけの速度は $v'=d'/t'$, $v''=d''/t''$. そこで第 11 図のように $BA$, $CA$ の延長上に $B',C'$ をとり，$AB'=v'$, $AC',=v''$ とし，$A$ から $B'C'$ に垂線 $AE$ をひき，垂線の足を $E$ とする．こうしてえられたベクトル $\overrightarrow{AE}$ はこの平面上でこの波動の速度をしめす．つまり

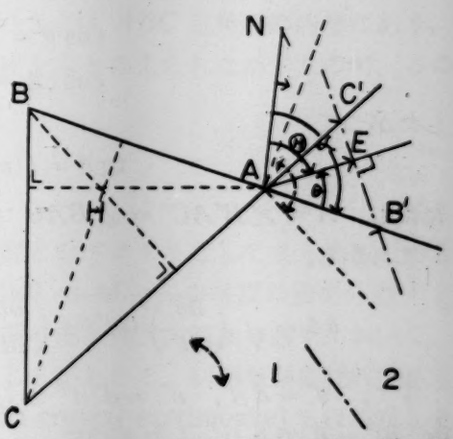


第 11 図　3 点観測による初動の到来方向（波面）とみかけの速度の作図法
（1. 到来方向範囲　2. 波面）
Graphical determination of direction of approach and apparent velocity of initial motion by tripartite stations.
(1. Azimuthal range of epicenter, 2. Plane wave front.)

$AE$ の延長上に震央があり，$AE=v$ がこの平面にそうみかけの速度ということになる．

到達時刻差 $t'$, $t''$ の測定誤差 $\delta t'$, $\delta t''$ はそれぞれ $t_A$, $t_B$, $t_C$ の測定誤差 $\delta t_A$, $\delta t_B$, $\delta t_C$ に依存する．後者はすでにのべたように記録紙上で同時刻の点，たとえばペンのずれを記録せしめた点からのながさとしてはかられる．記録線は約 0.3～0.4 mm のはばをもつが，縁辺は比較的鮮明なするどいかどをもつており，1/10 mm のめもりのあるむしめがねでよめば 0.2 mm までは充分よめる．これは各線とも同様であるから，よむ位置をきめれば $\delta t_A=\delta t_B=\delta t_C=\delta t$ となり，記録紙速度を 30～50 mm/sec. とすれば $\delta t=\pm 1/1500$ ～1/2500 sec. ($\fallingdotseq 0.7$～0.4 ms) となる．そこでむしろ問題となるのはどこをよむべきかという位相の同定になる．近距離の比較的ふかい地震はするどくたちあがる初動をしめすが，ややとおい地震では初動のたちあがりはあまりするどくない．よわい地震では土地の微動との比 ($S/N$) がわるくてさらに同定が困難である．おくり速度 50 mm/sec. 以上では，かえつて同定困難のため誤差は大となる傾向にある．一般に $\delta t$ は $\pm 3$ ms (a クラス) から $\pm 5$ ms (b クラス) くらいであり，特にわるいもので $\pm 10$ ms (c クラス) までである．これは数回の再生記録から別々に位相時間差のよみとりをおこない見当をつけることができた．

さて，$t'=t_B-t_A$, $t''=t_C-t_A$ であるから $\delta t'=\sqrt{(\delta t_B)^2+(\delta t_A)^2}$, $\delta t''=\sqrt{(\delta t_C)^2+(\delta t_A)^2}$ であり，$\delta t_A=\delta t_B=\delta t_C=\delta t$ とすると，$\delta t'=\delta t''=\sqrt{2}\,\delta t$ となる．

つぎに第 11 図の作図法によると到来方向乃至震央方位を $\Theta$ とし，$\overrightarrow{AB'}$ の方位を $\alpha$ (常数) とすると，$\angle B'AE=\theta$ とおくとき，$\theta=\Theta-\alpha$ となるから，$\Theta$ の誤差は $\theta$ の誤差にひとしい．方位は北から時計まわりにはかり，角度はすべて時計まわりを正とする

さて，図からあきらかに

$$\cos\theta=\overline{AE}/\overline{AB'}=v/v',$$
$$\cos(A-\theta)=\overline{AE}/\overline{AC'}=v/v''.$$

したがつて

$$\operatorname{tg}\theta=\{(v'/v'')-\cos A\}/\sin A.$$

ただし $A=\angle B'AC'=\angle BAC$ である．

これから，

$$\delta\theta=\sqrt{\left(\frac{\partial\theta}{\partial t'}\right)^2(\delta t')^2+\left(\frac{\partial\theta}{\partial t''}\right)^2(\delta t'')^2}=\sqrt{2}\sqrt{\left(\frac{\partial\theta}{\partial t'}\right)^2+\left(\frac{\partial\theta}{\partial t''}\right)^2}\,\delta t.$$

さて，$v'=d'/t'$, $v''=d''/t''$ から，$\partial v'/\partial t'=-v'/t'$, $\partial v''/\partial t''=-d''/t''$, $\partial v'/\partial t''=\partial v''/\partial t'=0$ であり，したがつて

$$\frac{\partial\theta}{\partial t'}=-\frac{\cos^2\theta}{\sin A}\cdot\frac{v'}{v''}\cdot\frac{1}{t'},\quad \frac{\partial\theta}{\partial t''}=\frac{\cos^2\theta}{\sin A}\cdot\frac{v'}{v''}\cdot\frac{1}{t''}$$

となるから，

$$\delta\theta=\sqrt{2}\,\frac{\cos^2\theta}{\sin A}\cdot\frac{v'}{v''}\sqrt{\frac{1}{t'^2}+\frac{1}{t''^2}}\,\delta t$$

となる.

さらに　$v = v' \cos\theta$　から

$$\frac{\delta v}{v} = \sqrt{\frac{1}{t'^2} + (f \cdot \mathrm{tg}\,\theta)^2}\,\delta t, \quad f = \sqrt{2} \cdot \frac{\cos^2\theta}{\sin A} \cdot \frac{v'}{v''}\sqrt{\frac{1}{t'^2} + \frac{1}{t''^2}}$$

がえられる.

これらの式から計算した誤差が Table 1 にしめした $\delta\theta, \delta v$ であり，$\delta t$ としてはaクラスで ±3ms, bクラスで ±5ms としておいた.（cクラスのものはすてた.）

上式から $t', t''$ が大であれば精度はよくなるのであるが，入射角が一定ならこれには点間距離 $d', d''$ を大にするよりほかない．あとは到来方向と三角形のかたちに依存する量であつて，あるばあいに有利にしても他の方向からに対して不利になつて，どの方向にもよい形状というものはきまらない*.

$\delta t$ 自体を小にするには，よみとり位置の同定の精度をあげるために記録のたちあがりをするどくする必要がある．これを 1ms またはそれ以下にするには，計器の周波数帯域を 50～100 c/s までひろげる必要があろう．しかし，ややとおい近地地震では地震波のかたちがすでにこうした高周波成分をふくまない公算がおおい．こうした高周波観測については浅田敏が研究をすすめているので期待される．しかし，もし初動の波形自体が高周波分をふくまない，ゆるやかなものであれば，計器の特性をかえてもしかたないので，点間距離を増大するほかない．このばあい，わがくにでは地質，地形上均一性が保証されないおそれがおおいので，これには地中ふかくに地震計をいれることが必要となる．3点以上の観測点をもうけて $B', C'$ 以外に $D', E'$, etc. の点をえて，これらの点で決定される，波面の観測点平面とのきりくちの直線を最小自乗法的に決定することにより，精度をあげうることは当然である．われわれのばあい $D, E, F$ の3点は $ABC$ 三角形の内部にあり，辺長が小となり，その時間差から充分よい精度の速度をもとめえられなかつたので，この方法を採用することはできなかつた.

## 4. 議　　論

第 12 図に，えられた初動到来方向とみかけの速度とをベクトルとしてまとめてしめした．これを第 13 図にかかげた関東地方の 1914～1940 の $M \geq 5$ の地震の震央分布[9]とくらべると，筑波を中心とする地震活動はこの短期間の標本抽出的観測の結果において，長期間の常設観測網による結果とほぼ一致していることがわかる．初期微動継続時間からみると，観測された小地震はすべて地殻内地震 (Intra-crustal earthquake) とはみなしえないものである．長期観測による結果は地殻内地震もふくむといえ，やはり大部分は地殻下地震 (Sub-crustal earthquake) とかんがえられるので，この地方の地殻下地震の発生

---

*　3点観測法の誤差については浅野周三が脈動観測に関連して論じたことがある.（震研談話会，昭 28. 5月，昭 28. 6月）

9)　T. Asada, *Journ. Phys. of the Earth.*, **5** (1957), 83–113.

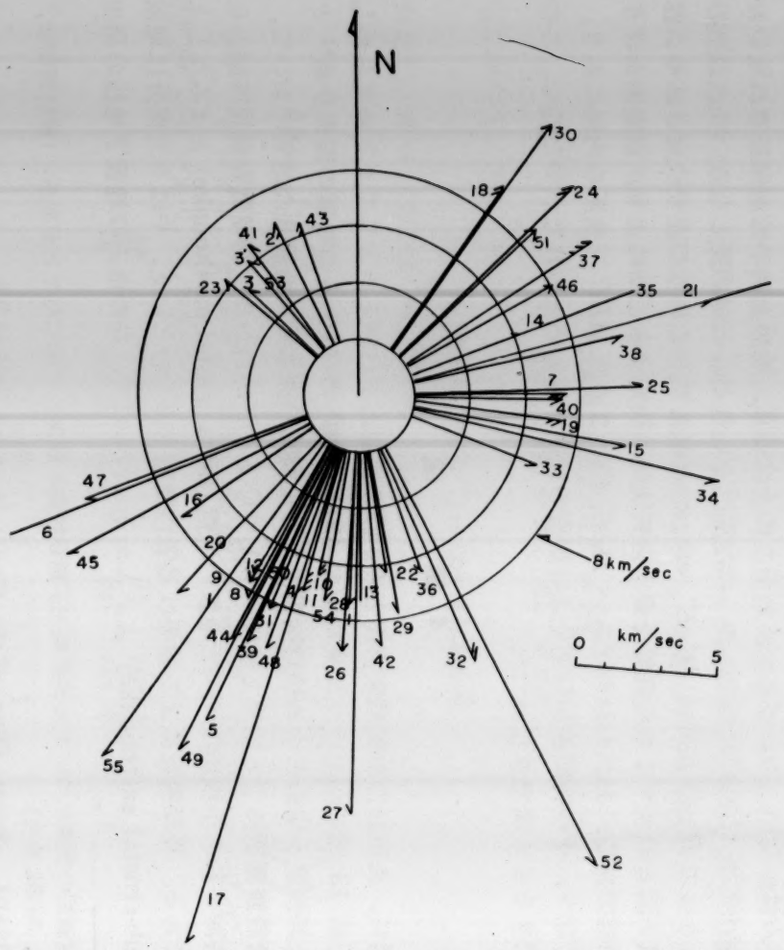


第 12 図　筑波において 3 点観測で記録された近地地震の初動到来方向とみかけの速度
Directions of approach and apparent velocities of intial motions of near earthquakes recorded by the tripartite stations at Tukuba, Japan. Nos. of earthquakes are referred to those in Table 2.

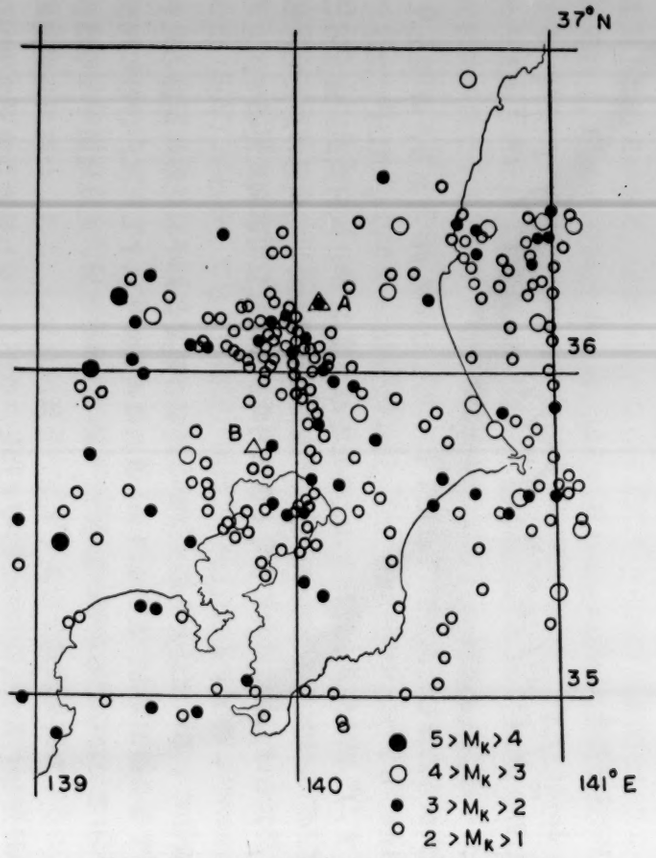


第 13 図　関東地方の震央分布
Distribution of epicenters in Kwanto district during 1914～1940. $M = 4.85 + 0.5\,M_K$
A : Tukuba, B : Tokyo. (After T. Asada[9])

は地震の規模のひろい範囲にわたつて，時間的に定常であるということが推定できる．

到来方向を観測した地震のうち気象庁で震源位置を発表したものはすくないが，それらはほぼ誤差の範囲内でその方向は一致している．しかし，筑波における初動方向のずれがしらべられているのに対応するような到来方向のずれがあるかどうかは残念ながら精度の点からまだはつきりいえなかつた．相関計算法による初動部波群の平均的到来方向等については安芸敬一，辻浦賢[10]により別にくわしく論じられているので省略する．

震源未決定のものがおおいので，震源距離の代用として初期微動時間 $t_{P-S}$ をとり，これとみかけの速度の関係を図示したものが第 14 図である．浅田敏，鈴木次郎[11]がすでにのべているように，各震源距離における最小のみかけの速度が地下の速度をしめす数値として意味がある．Table 2 にみるように，われわれのえた速度はかなりの誤差をもつもので，なおきわめて不充分なものであるが，爆破地震動研究グループ[12]によりえられた関東地方の地下速度をしめす線を図にしめすと，ほぼこれが各距離のみかけの速度の最小値をなしており，筑波において 5.4 km/sec の層が欠除しているということもふくめて，矛盾がないことがわかる．

速度の精度をたかめて，$P_n$ の速度の精確な数値をもとめることをのぞんだが，これではそこまでは到達できなかつた．

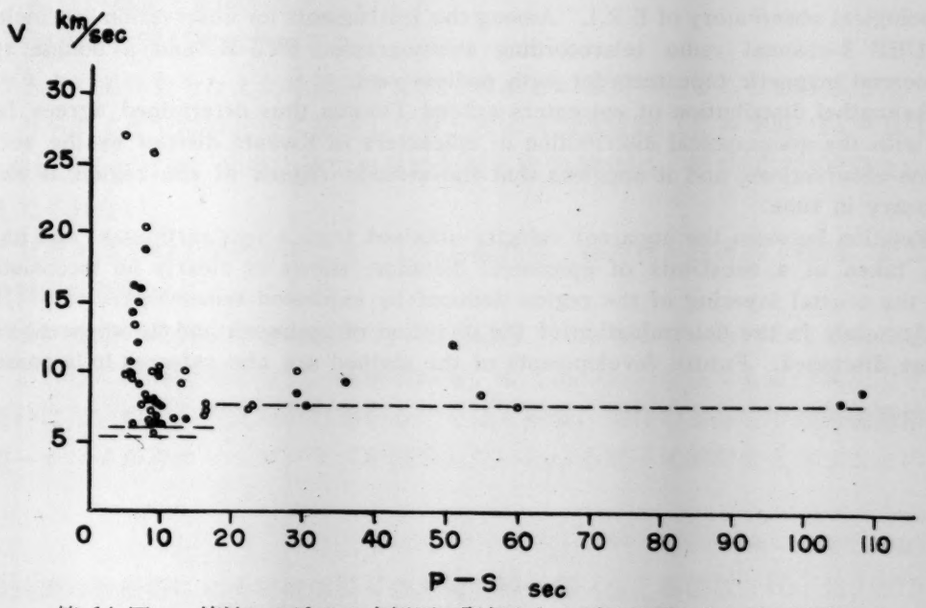


第 14 図　筑波における 3 点観測で記録された近地地震のみかけの速度とその $P$-$S$ 時間との関係
Apparent velocities of near earthquakes recorded by the tripartite stations at Tukuba and their $P$-$S$ times.

10) K. AKI and M. TSUJIURA, *loc. cit.*, 8)
11) T. ASADA and Z. SUZUKI, *loc. cit.*, 4).
12) 爆破地震動研究グループ (R. G. E. S.), 地震 (*Zisin*), [ii], **11** (1958), 102–113.

## 5. 謝　　辞

本郷における受信記録室を貸与された東大附属病院，筑波における地震計設置点および架線地域の利用をゆるされた筑波神社にふかく感謝する．観測の準備および実施には堀実，松本英照，安芸敬一，岡田惇，後藤健一，鈴木喜吉，その他技術部，事務部の諸氏，および筑波山支所渡辺正雄氏の御協力をえた．また安芸敬一氏には本研究中種々討議に参加していただいた．特に謝意を表したい．なおこの研究計画の全般について御支援をえた那須所長，萩原観測部主任，実川技術部主任に感謝する．

---

## 23. *Direction of Approach and Apparent Velocity of Near Earthquake Initial Motion.*

By Setumi MIYAMURA and Masaru TSUJIURA,
Earthquake Research Institute.

Directions of approach and apparent velocities of the initial motions of more than fifty near earthquakes* arrived at Mt. Tukuba were determined by tripartite stations separated by about several hundred meters from each other in the vicinity of the seismological observatory of E.R.I. Among the instruments for observation are included two UHF 3-channel radio telerecording seismographs, RTS-II, and a double track commercial magnetic tape recorder with endless reel.

Azimuthal distribution of epicenters around Tukuba thus determined agrees fairly well with the geographical distribution of epicenters in Kwanto district by the secular routine observations, and it suggests that the seismic regime of the region is rather stationary in time.

Relation between the apparent velocity obtained from a near earthquake and its S-P time, taken as a substitute of epicentral distance, shows us clearly no inconsistency with the crustal layering of the region deduced by explosion seismology.

Accuracy in the determination of the direction of approach and the apparent velocity are discussed. Future developments of the method are also referred to in passing.

---

* About twenty of them observed in the earlier period were treated by AKI, K. and TSUJIURA, M. (1959) from the spectral point of view using a correlation calculator. (cf. *loc. cit.*, 8)

地震研究所彙報
第37号(1959)375-380頁

# 24. 全商用交流電源簡易電子地震計

地震研究所　松本英照

(昭和31年12月18日発表——昭和34年3月27日受理)

## §1.

微小地震を局地的に観測してその発震時や初期微動継続時間等を正確に記録し，その資料の解析をするならばわれわれは地震について未知の複雑な問題をとくいとぐちをうることができるとかんがえられる.

この目的でわれわれは 1952 年来和歌山地方で 10 数点の臨時観測点や7点の委託常時観測点をもうけ観測を実施してきた.

この経験により，よい地震記象を有効にかつかずおおくうるためには,

i) 感度が適当にたかいこと.

ii) 取扱が簡単で故障がすくないこと.

iii) 周波数範囲が適当であること.

この3点の条件をそなえた地震計を使用することが必要であることを痛感した.

ところがいままでに委託用に使用してきた石本式加速度計（$V=200$, $T_0=0.^s1$）では ii) を満足するだけで，和歌山地方の局地的微小地震観測に，短期間では充分よい資料をあたえてくれない.

そこで筆者はこの3条件をそなえ，しかも製作費，維持費が経済的で輸送，設置にも便利な地震計を設計することにした.

i), iii) の条件を満足する地震計は，光学記録方式のものでいろいろな型式のものがあるが，これらには委託用として，経済的にも，とりあつかいの点でも充分満足できるような地震計はないので，設置場所の制約もすくなく設置，操作の容易な可動線輪型換振器—増幅器—インクがきオッシログラフを結合したいわゆる電子地震計をえらぶことにした.

## §2.

この装置の換振器は本所技術部製可動線輪型換振器（自己振動数3 Hz，出力約3 Volts/kine）を利用し，ペンがきオッシログラフは三栄測器社製のペンがき検流器をもちい，これらに適合した増幅器を設計することにした.

この増幅器は ii) の条件を満足させるために，電源を全部商用交流で供給することを設計の第1方針とした.

このために安定度，感度，球数におのずから限度ができたが，これらの点については，いろいろ実験をして最良の条件をもとめた.

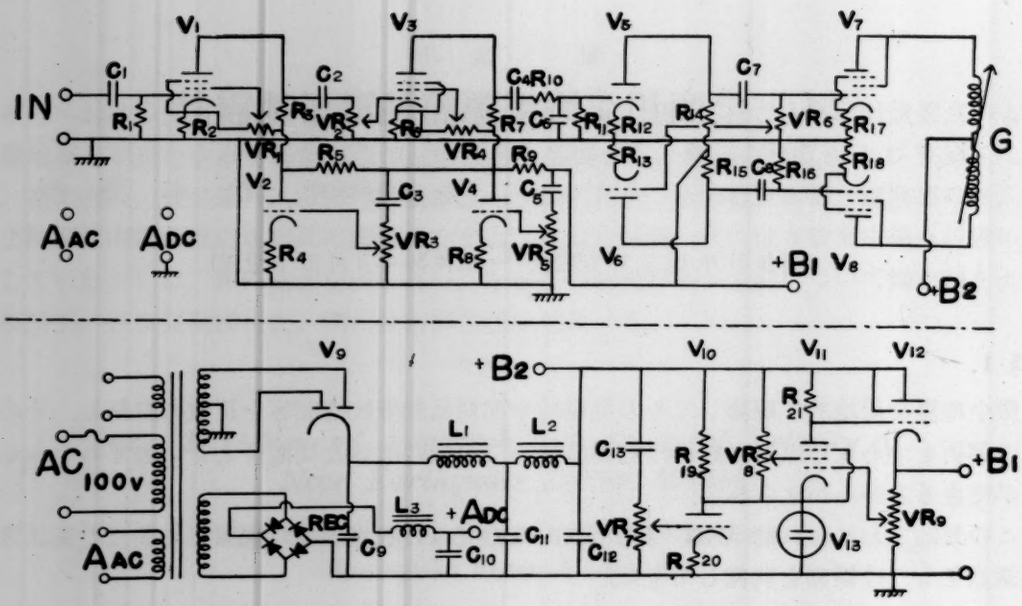


| | | | |
|---|---|---|---|
| $V_1$. $V_3$. $V_{11}$. | 6 SJ 7 | $R_{17}$. $R_{18}$. | 420 Ω. |
| $V_2$. $V_4$. $V_5$. $V_6$. | $\frac{1}{2}$6 SN 7 | $R_{19}$. | 30 KΩ. |
| $V_7$. $V_8$. | 6F6. | $R_{21}$. | 1 MΩ. |
| $V_9$. | 5Z3. | $VR_1$. $VR_4$. $VR_8$. | 50 KΩ. |
| $V_{10}$. | 6J5. | $VR_2$. $VR_3$. $VR_5$. $VR_6$. $VR_7$. | 500 KΩ. |
| $V_{12}$. | 6L6. | $VR_9$. | 100 KΩ. |
| $V_{13}$. | VRA 65/80 | $C_1$. $C_2$. $C_4$. $C_7$. $C_8$. | 1 μF. |
| $R_1$. $R_{11}$. $R_{16}$. | 500 KΩ | $C_3$. $C_5$. $C_{13}$. | 2 μF. |
| $R_2$. $R_6$. | 1 KΩ. | $C_6$. | 0.2 μF. |
| $R_3$. $R_7$. | 250 KΩ. | $C_9$. $C_{11}$. | 20 μF. |
| $R_4$. $R_8$. $R_{12}$. $R_{13}$. $R_{20}$. | 2 KΩ. | $C_{12}$. | 40 μF. |
| $R_5$. $R_9$. | 3 KΩ. | $C_{10}$. | 1000 μF. |
| $R_{10}$. | 300 KΩ. | $L_1$. $L_2$. | 20 H. |
| $R_{14}$. $R_{15}$. | 100 KΩ. | $L_3$. | 0.5 H. |

Fig. 1 Circuit of HFSA (M-1).

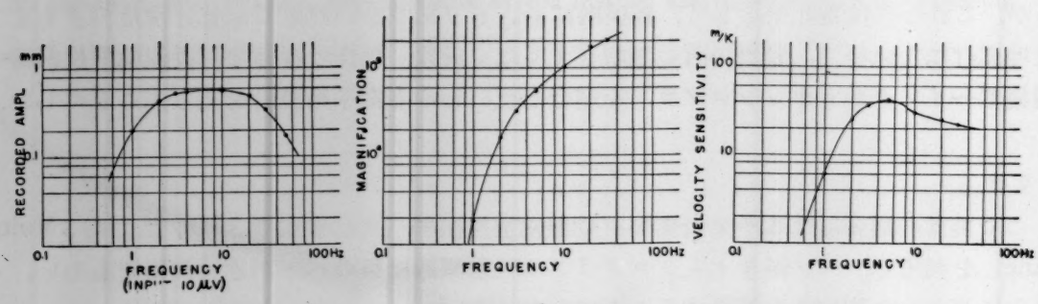


a b c

Fig. 2 a Frequency Characteristic of HFSA (M-1).
b Frequency Characteristic of a Seismograph with HFSA (M-1) (Displacement).
c Frequency Characteristic of a Seismograph with HFSA (M-1) (Velocity).

設計した増幅器はひとつは高周波用，他は中間周波用であつて，前者を HFSA (M-1)，後者を MFSA (M-2) となづけた*.

HFSA (M-1) は地震活動の中心部附近とおもわれる観測点用につくつた増幅器で，ヒラメントを交流加熱する増幅器としては，この感度が安定にはたらく最高限度で，重量は比較的かるく輸送に便利な点と，球数がすくないため保守面で経済的であるばかりでなく故障がすくない利点はあるが，周波数特性は範囲がせまく，そのために使用範囲も限定される．なお第1図にしめす配線図のように，整流平滑した電源でヒラメントを加熱すれば交流電圧変動のはげしい地域でも増幅器は安定に動作するが，交流直接加熱では若干安定度が低下するので条件がゆるすならばヒラメント用整流平滑装置はくみこむことがのぞましい．この増幅器の配線図および特性を第1図と第2図にしめす.

MFSA (M-2) は地震活動の中心部から数十粁以上はなれた観測点用につくつた増幅器でヒラメントは整流平滑した直流で加熱している.

この増幅器の配線図および特性を第 3，4，5 図と第6図にしめす.

なお，このばあいには換振器は出力を平坦化して使用周波数範囲をひろげるために出力端子に $1\mu F$ のコンデンサーを並列につないで使用している.

MFSA (M-2) は HFSA (M-1) にくらべ使用真空管数も使用電力もおおいので感度・安定度・周波数特性は良好であるが，実際使用の経験では使用条件の難点として使用電力のおおいことによる経済的制約および真空管の消耗による故障が (M-1) より増加したことが判明している.

§ 3.

以上これら2種の増幅器は既存の換振器・検流器を利用し地震計を構成するように設計したので特性は換振器・検流器の特性に左右され要求を充分満足することができなかつたが，製作してから現在まで約3年間紀伊半島各地の高等学校乃至発電所堰堤事務所数箇所にて委託観測をおこない，一応連続使用にたえ有効な記録を観測できることが判明したのでこの装置を報告する.

この装置を使用してえられた記録の実例を第7図にしめす.

今後これら増幅器に対する課題としてはより一層の安定度，耐久度の増加があるが，真空管自体に寿命や安定度，耐久度の問題があるので，この点を真空管寿命の統計的算出にもとずく真空管の早期交換あるいは真空管劣化の表示回路の採用による故障の早期発見ならびに防止の方法をこうずるか，または高信頼度のトランジスターが実用されるようになればこれを使用することによりこの課題を解決するつもりである.

しかし，現在わがくにでは真空管を使用した正規の連続観測はなく，真空管回路を採用

---

* 高周波用 HFSA (M-1) は High Frequency Type Seismic Amplifier (Matumoto's No. 1)，中間周波用 MFSA (M-2) は Medium Frequency Type Seismic Amplifier (Matumoto's No. 2) の意味で地震周波数 (Seismic Frequency) においては 0.03～0.3 c/s を Low Frequency, 0.3～3 c/s を Medium Frequency, 3.0～30 c/s (ELF) を High Frequency とよぶことにした.

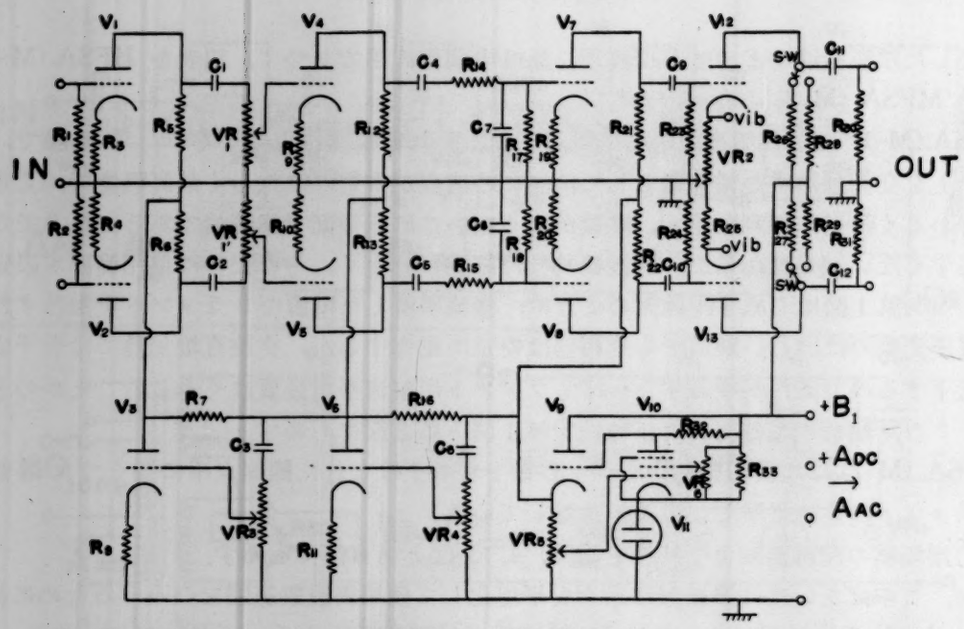


| | | | |
|---|---|---|---|
| $V_1$. $V_2$. $V_4$. $V_5$. $V_7$. $V_8$. | $\frac{1}{2}$6SL7. | $R_{28}$. $R_{29}$. | 1 K Ω. |
| $V_3$. $V_6$. $V_{12}$. $V_{13}$. | $\frac{1}{2}$6SN7. | $R_{32}$. | 1 M Ω. |
| $V_9$. | 6J5 | $R_{33}$. | 30 K Ω. |
| $V_{10}$. | 6SJ7. | $C_1$. $C_2$. $C_3$. $C_4$. $C_5$. $C_6$. | |
| $V_{11}$. | VRA 65/80 | $C_9$. $C_{10}$. $C_{11}$. $C_{12}$. | 2 μF. |
| $R_1$. $R_2$. $R_{17}$. $R_{18}$. $R_{23}$. $R_{24}$. | | $C_7$. $C_8$. | 0.5 μF. |
| $R_{30}$. $R_{31}$. | 500 K Ω. | $VR_1$. $VR_3$ $VR_4$. | 500 K Ω. |
| $R_3$. $R_4$. $R_9$. $R_{10}$. $R_{19}$. $R_{20}$. | 5 K Ω. | $VR_2$. | 3 K Ω. |
| $R_5$. $R_6$. $R_{12}$. $R_{13}$. $R_{21}$. $R_{22}$. | 250 K Ω. | $VR_5$. | 100 K Ω. |
| $R_7$. $R_{16}$. | 3 K Ω. | $VR_6$. | 50 K Ω. |
| $R_8$. $R_{11}$. $R_{25}$. | 2 K Ω. | vib. | Vibrator Out put. |
| $R_{14}$. $R_{15}$. | 300 K Ω. | S. W. | Vib-Galva Switch. |
| $R_{26}$. $R_{27}$. | 100 K Ω. | | |

Fig. 3 Circuit of MFSA (M-2), Main Amplifier Part.

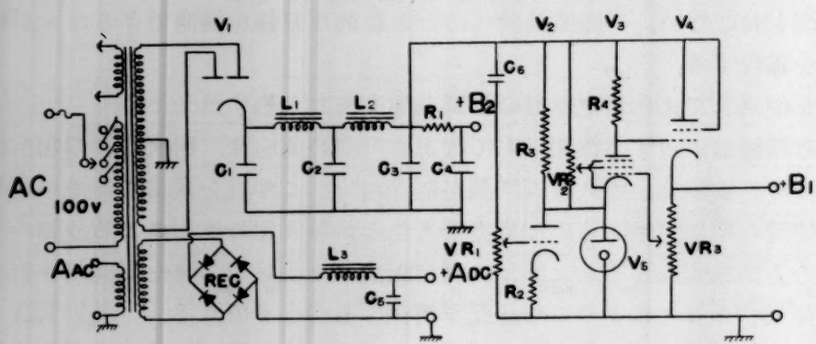


| | | | | | |
|---|---|---|---|---|---|
| $V_1$ | 5Z3. | $R_2$ | 2 K Ω. | $C_1$. $C_2$. $C_3$. $C_4$. | 20 μF. |
| $V_2$ | 6J5. | $R_3$ | 30 K Ω. | $C_5$. | 1000 μF. |
| $V_3$ | 6SJ7. | $R_4$ | 1 M Ω. | $C_6$. | 2 μF. |
| $V_4$ | 6L6. | $VR_1$. | 500 K Ω. | $L_1$. $L_2$. | 20 H. |
| $V_5$ | VRA 65/80. | $VR_2$. | 50 K Ω. | $L_3$. | 0.5 H. |
| $R_1$ | 1 K Ω. | $VR_3$. | 100 K Ω. | | |

Fig. 4 Circuit of MFSA (M-2), Power Source Part.

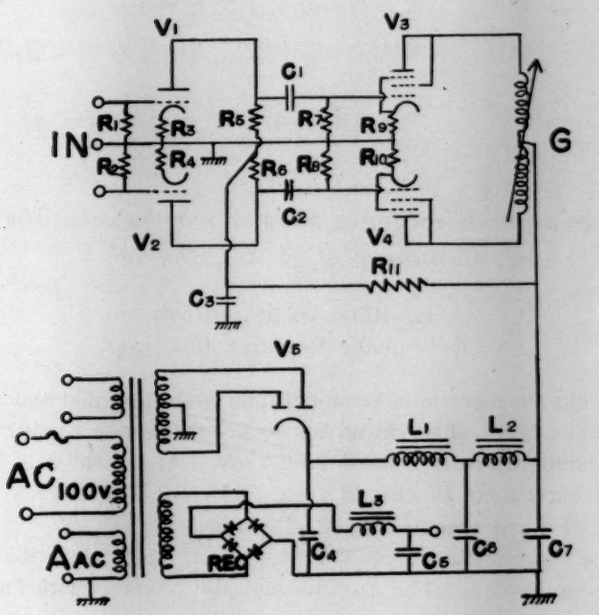


| | | | |
|---|---|---|---|
| $V_1$. $V_2$. | 1/2 6SN7. | $R_{11}$. | 50 K Ω. |
| $V_3$. $V_4$. | 6F6. | $C_1$. $C_2$. | 2 μF. |
| $V_5$. | 5Z3. | $C_3$. $C_4$. | 10 μF. |
| $R_1$. $R_2$. $R_7$. $R_8$. | 500 K Ω. | $C_5$. | 1000 μF. |
| $R_3$. $R_4$. | 2 K Ω. | $C_6$. $C_7$. | 20 μF. |
| $R_5$. $R_6$. | 100 K Ω. | $L_1$. $L_2$. | 20 H. |
| $R_9$. $R_{10}$. | 420 Ω. | $L_3$. | 0.5 H. |

Fig. 5 Circuit of MFSA (M-2), Recorder Part.

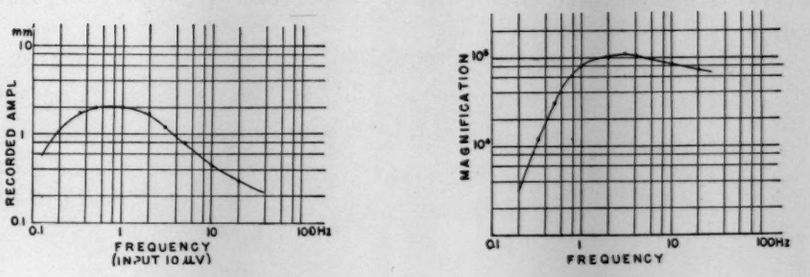


a　　b

Fig. 6 a Frequency Characteristic of MFSA (M-2).
b Frequency Characteristic of a Seimograph with MFSA (M-2), (Displacement).

して長期間観測が有効に実施できるかどうかという点に疑問がもたれていたが，この装置といままでの観測結果はこの問題に一応の回答をあたえることができたのではなかろうかとおもう．

おわりに種々御指導をえた宮村研究室主任，観測を担当された三重県立飯南高等学校教

諭朝倉一昭氏はじめ生徒諸氏，地震研究所和歌山観測所今村久氏，和歌山県古座町和歌山県営七川堰堤事務所原敏勝氏，和歌山県竜神村関西電力甲斐の川堰堤山口竜次郎氏に感謝する．

---

## 24. *Simple Electronic Seismographs supplied only with Commercial A. C. Source.*

By Hideteru MATUMOTO,
Earthquake Research Institute.

Two types of simple electronic seismographs were designed and constructed in order to increase the efficiency of observation for local earthquake study.

One of the seismographs is named HFSA (M-1)*, which will be utilized for the observation of extremly near shocks ($\Delta < ca.$ 20 Km). The circuit is shown in Fig. 1, and the characteristics are seen in Fig. 2.

The other one is named MFSA (M-2)*, which must be utilized for the observation of ordinary near shocks. The circuits and the characteristics are shown in Fig. 3, 4, 5, and Fig. 6.

The circuits were designed so as to keep the seismograph in stable condition by non-specialist observers.

Since 1955, they have been used to record the small earthquakes at a few stations in Kii Peninsula. i.e. Kayumi, Waka-ura, Kainokawa and Sitikawa.

Examples of seismograms including several kinds of small earthquakes which can be recorded only by a high sensitive seismograph are reproduced in Fig. 7.

They have been operated continuously without trouble by high school pupils or electric power station staff, and thus we conclude that such electronic seismographs having several stages of valve circuit fed by commercial A.C. only, are usable in routine operation.

---

* cf. footnote on p. 377.

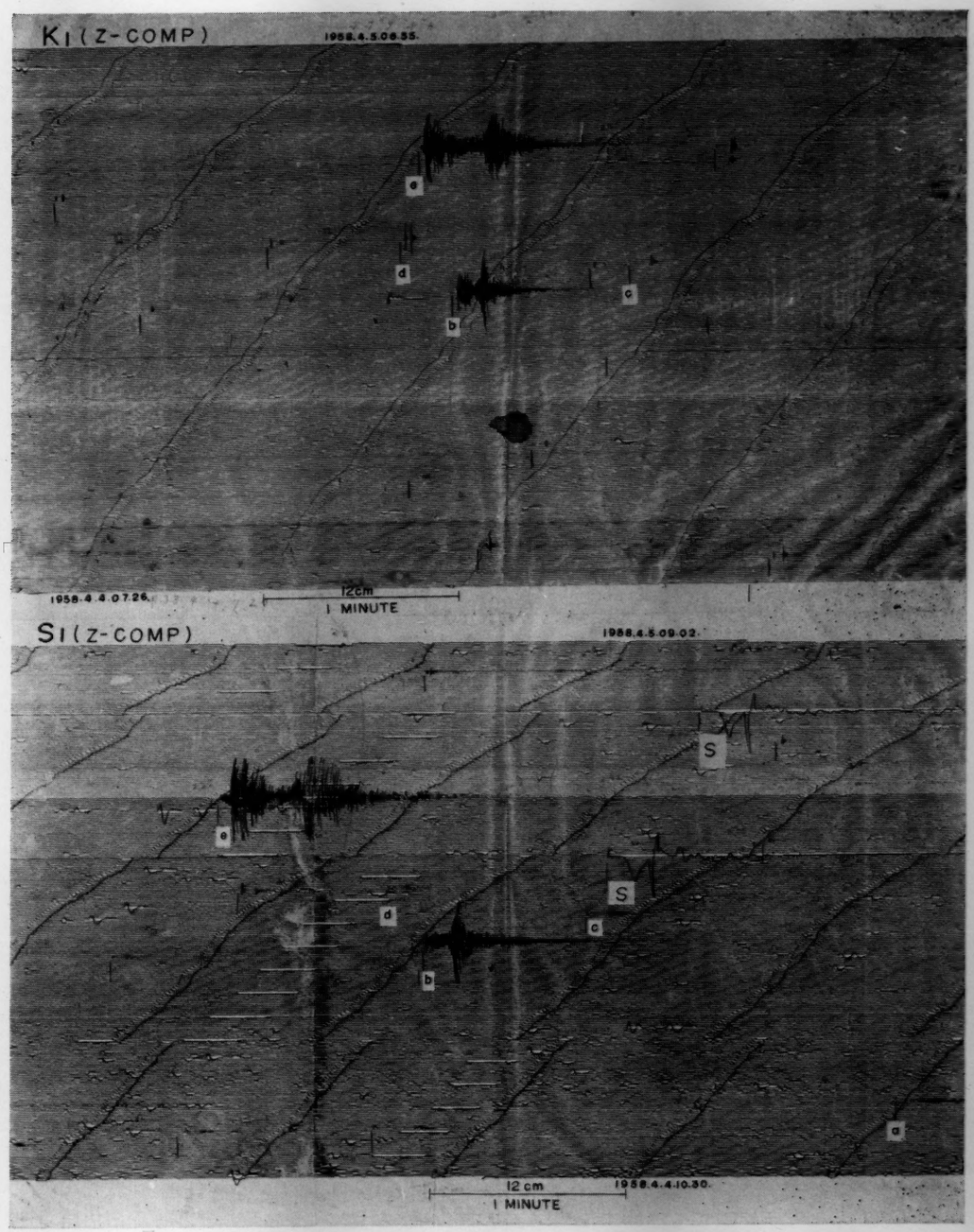


Fig. 7a Example of seismograms at Kainokawa (K 1) and Sitikawa* (S 1). recorded by HFSA (M-1) and MFSA (M-2) respectively on April 4–5, 1958.

Earthquakes are indicated by arrows, of which followings are identified at both stations. (a at Kainokawa is trace)

| | | | |
|---|---|---|---|
| a | Intensity. (0) | 4d13h13m (JST) | |
| b | 〃 (0) | 4d20h11m ( 〃 ) | Local shocks not recorded by J. M. A. station |
| c | 〃 (0) | 4d21h22m ( 〃 ) | |
| d | 〃 (0) | 4d22h30m ( 〃 ) | |
| e | 〃 (1) | 5d02h25m ( 〃 ) | From Western Part of Kanagawa. |

Disturbances by A.C. source break are shown by S. Fluctuations on the lines are due to rapid disturbances in A. C. main source.

* Also spelled as Shichikawa.

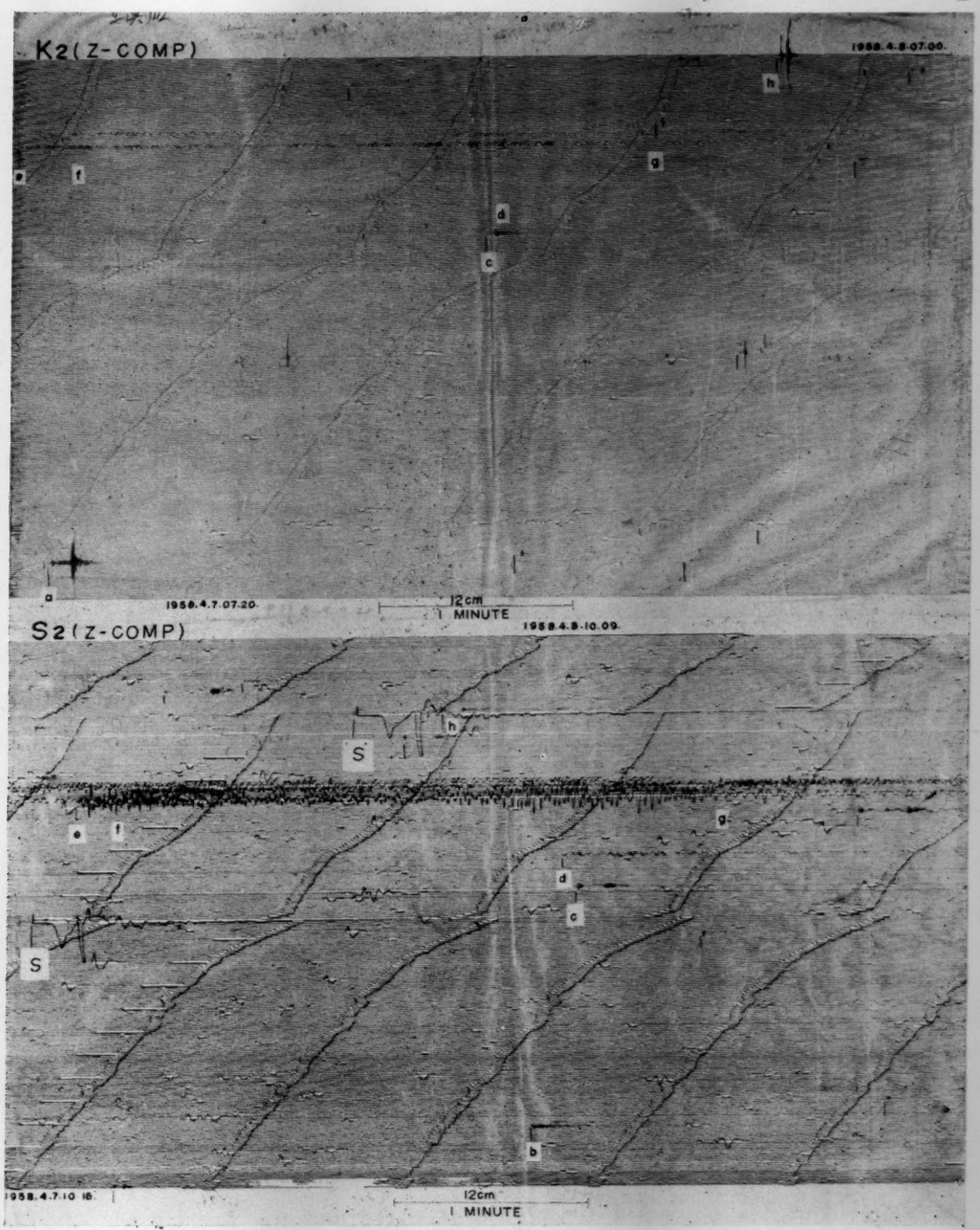


Fig. 7b Example of seismograms at Kainokawa (K 2) and Sitikawa (S 2) recorded by HFSA (M-1) and MFSA (M-2) respectively on April 7–8, 1958.

Earthquakes are indicated by arrows, of which followings are identified at both stations. (a at Sitikawa is on the other sheet.)

| | | | |
|---|---|---|---|
| a | Intensity | (0) 7d08h53 m (JST) | Local shocks not recorded by J. M. A. station. |
| b | 〃 | (0) 7d12h44 m ( 〃 ) | |
| c | 〃 | (0) 7d23h14 m ( 〃 ) | |
| d | 〃 | (0) 8d00h39 m ( 〃 ) | From Alaska. 66 1/2 N. 197 W. |
| e | 〃 | (0) 8d03h07 m ( 〃 ) | From Off E Coast of NE Honsyu 38 1/4 N, 143 3/4 E, h=20km. |
| f | 〃 | (0) 8d03h40 m ( 〃 ) | |
| g | 〃 | (0) 8d03h40 m ( 〃 ) | From Off E Coast of NE Honsyu 38 1/4 N, 143 1/2 E, Shallow. |
| h | 〃 | (0) 8d06h59 m ( 〃 ) | Local shocks not recorded by J. M. A. station. |

Disturbances by A.C. source break are shown by S. Fluctuations on the lines are due to rapid disturbances in A. C. main source.

地震研究所彙報
第37号(1959)381-388頁

# 25. 対数特性広振幅範囲電子地震計

地震研究所　松本英照

(昭和 34 年1月 27 日発表——昭和 34 年3月 27 日受理)

## §1

我々が地震とよんでいるものは規模の点で相当ひろい範囲をもち，現在までに観測からえられた結果によると，$10^{1}$ から $10^{25\sim6}$erg におよぶエネルギーをもつさまざまな地震が存在することがわかつている．そしてその地表にあたえる地震動についても，これもまた加速度にして $10^{-6}$ から $8\sim9\times10^{2}$ gal の範囲，速度，変位にしても同様のひろい範囲にわたるのである．

これらの地震動を，記録上でふりきらせることなく完全な形で記録するためには，感度のちがう数種あるいはそれ以上の地震計を併用して観測しなければならない．そして実際に，現在の地震観測所でも何種類かの地震計を併用してはいるが，これらは感度とともにその周波数特性もまたことなつているのが普通である．

もちろん，これら数種の地震計の感度だけをちがえて周波数特性は同一にしたものを使用することも不可能ではないが，現実には感度のちがう地震計相互では周波数特性もおのずからちがつてくることがおおく，地震を統計的に処理する場合には感度の換算が繁雑で手数がかかり，しかも誤差を生じやすい．

そこで，もしひとつの地震計が数種の地震計に対応する感度を全部そなえているならば，前述の不便さがさけられ，ことがらは非常に簡単になり，設置や保守の点でも大変有利で経済的である．特に余震観測等のような強弱さまざまの地震動を記録する臨時観測にはいろいろな利点を発揮するものとおもわれる．

それで筆者はひとつの記録中にできるだけひろい範囲の強弱の地震動を記録できる地震計をかんがえることにした．

ひとつのきまつた記録振幅範囲のなかに広範囲の感度をおさめるのは，振幅のレベル特性に圧縮特性をもたせるということであるが，その圧縮特性になにか意義のある関係をもたせたいため，マグニチュードやその他いろいろ地震の大きさをかんがえるときに記録振幅の対数がおおくもちいられているので，対数特性をもたせることにした．

この結果，普通の地震計ではよみとり上 1～30 mm，約 30 倍の振幅範囲しかもてないものが，$1\sim10^{4}$ mm 相当，約1万倍の振幅範囲を記録できることになつた．

この程度の範囲がとれれば，この装置を余震観測等に使用して微小地震から震度 IV 程度までの地震動をひとつの地震記象中に同一の特性で記録することができるので，地震の活動状況をしらべるために大変便利であるとおもわれる．

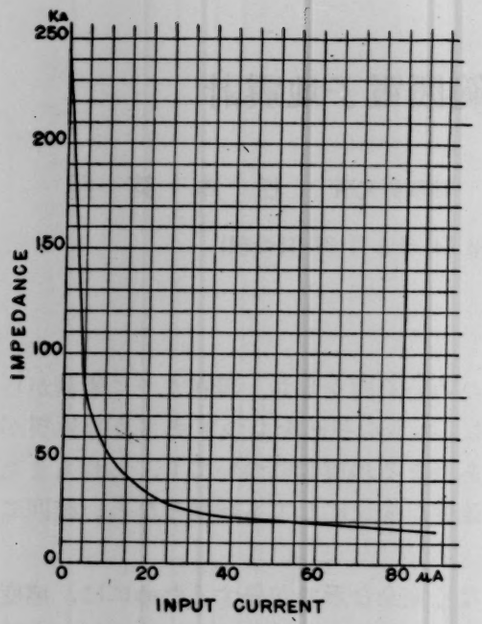


Fig. 1 Static characteristic of counter resistor which was used in the amplifier as N1, N2, N3.

1959 年 1 月この装置を使用し，筑波山支所において観測をこころみたが，一応初期の目的を満足することがわかつたので，簡単に報告する．

§ 2

この装置は電磁型換振器，増幅器，ペンがき検流器から構成されている．

増幅器は本装置の特性の主体をなすもので，5 段の容量抵抗結合増幅器である．圧縮特性をもたせるために第 1，第 2，第 3 段間に抵抗とくみあわせた亜酸化銅整流器網をもつている．

亜酸化銅整流器には Fig. 1 のような逆抵抗の性質があり，本器はその抵抗変化の顕著な部分の性質を固定抵抗と結合した分圧器として利用し，圧縮特性をもたせたものである．かかる圧縮器網は極超低周波用に筆者が特に考案したもので，1 段あたりの圧縮率がたかくとれない

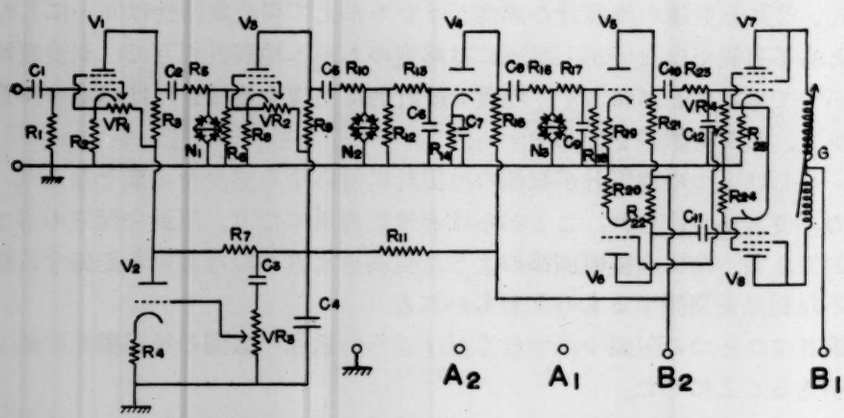


| | | | |
|---|---|---|---|
| $V_1$. $V_3$. | 6SJ7. | $R_{25}$. | 210 Ω. |
| $V_2$. $V_4$. $V_5$. $V_6$. | 1/2 6SN7. | $VR_1$. $VR_2$. | 50 KΩ. |
| $V_7$. $V_8$. | 6F6. | $VR_3$. $VR_4$. | 500 KΩ. |
| $R_1$. $R_6$. $R_{12}$. $R_{18}$. $R_{24}$. | 500 KΩ. | $C_1$. $C_2$. $C_5$. $C_8$. $C_{10}$. $C_{11}$. | 1 μF. |
| $R_2$. $R_8$. | 1 KΩ. | $C_3$. | 2 μF. |
| $R_3$. $R_9$. | 250 KΩ. | $C_4$. | 20 μF. |
| $R_4$. $R_{14}$. $R_{19}$. $R_{20}$. | 2 KΩ. | $C_6$. $C_9$. | 0.25 μF. |
| $R_5$. $R_{10}$. $R_{15}$. $R_{16}$. | | $C_7$. | 10 μF. |
| $R_{21}$. $R_{22}$. $R_{23}$. | 100 KΩ. | $C_{12}$. | 0.1 μF |
| $R_7$. $R_{11}$. | 3 KΩ. | $N_1$. $N_2$. $N_3$. | Oxide copper rectifier network. |
| $R_{13}$. $R_{17}$. | 300 KΩ. | | |

Fig. 2 Circuit of the amplifier, for logarithmic wide amplitude range seismograph.

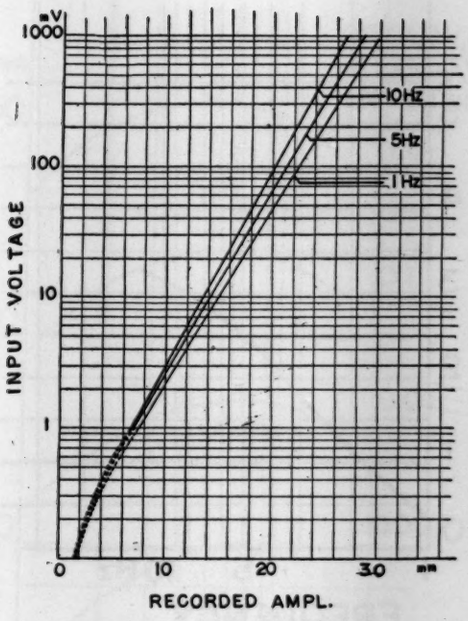


Fig. 3 Suppression character of the amplifier.

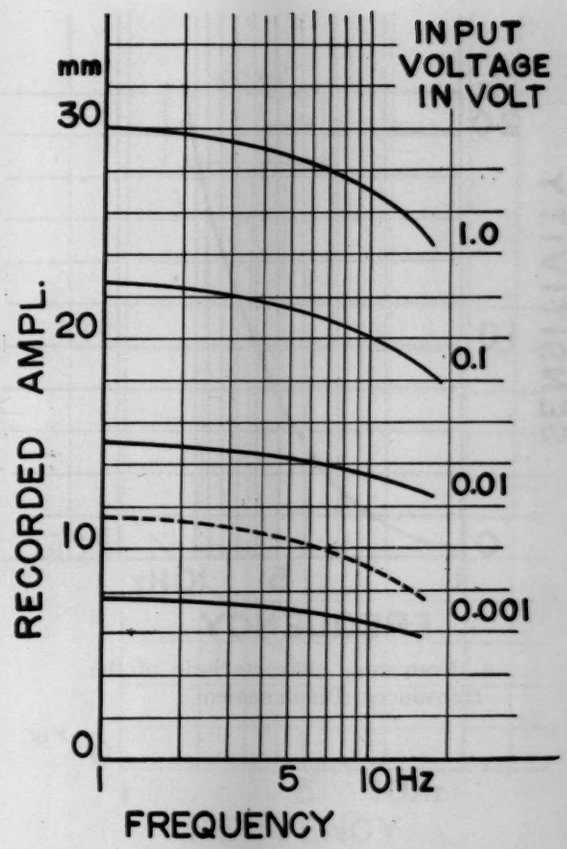


Fig. 4 Frequency characteristic of the amplifier. (Voltage level-amplitude) Solid lines indicate characteristic of the logarithmic amplifier and dotted line indicates characteristic of ordinary one, used for comparison.

ので3段に挿入することになつた．増幅器の配線図および圧縮特性を Fig. 2,3, 4 にしめす．

換振器は地震研究所技術部製可動線輪型換振器で，検流器は三栄測器製のものを使用した．これらの特性を Fig. 5, 6 図にしめす．

以上，個々の特性についてのべてきたが，これらを綜合して地震計としてのはたらきをみると，Fig. 7 にしめすように周波数特性が平坦でない．

おそい記録紙速度の記録では，周期がよみとれないので，振幅の大小がいかなる周波数に対応する地動を表現するかわからず，補正がきかないから地震計の機能として不満足である．かかる不都合は増幅器の特性を改善すればよいのではあるが，換振器をとりかえて使用することもあるので換振器の特性を平坦化して増幅器にあたえることにした．対象とする地震動の周波数を 1～10 c/s として，この範囲を平坦化することにしたが，完全に平坦化するには相当感度をさげることになる．適当な感度を保持するために，周波数特性の起伏を若干は許容することにして， Fig. 8 のような特性をもつ等化器を換振器の出力に挿入したが，その結果増幅器入力として Fig. 9 のようなものがえられた．

この等化器により平坦化された入力を増幅器にみちびき，地動の速度を変化させると，Fig. 10 のような速度に対するレベル特性がえられる．一応速度の対数と記録振幅とのあ

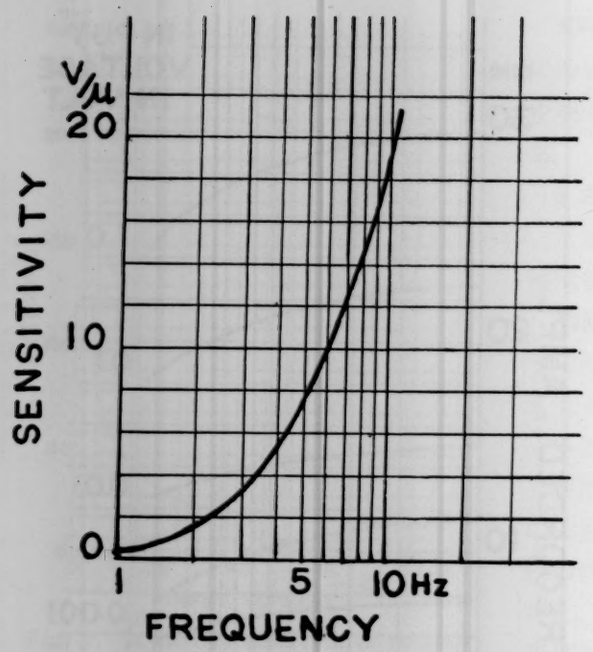


a Frequency characteristic of the transducer (Displacement).

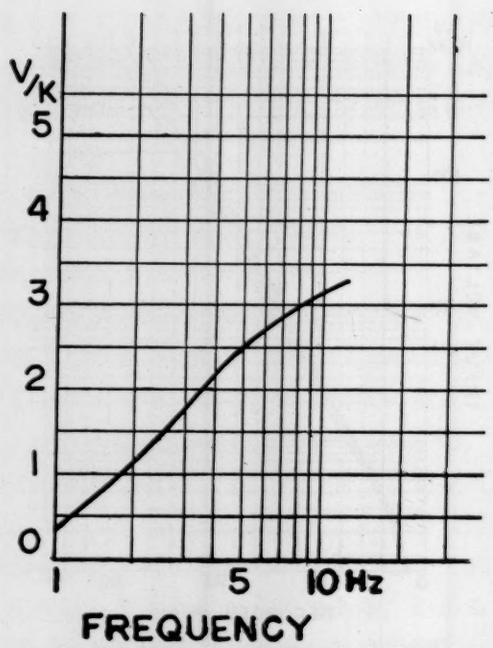


b Frequency characteristic of the transducer (Velocity).

Fig. 5

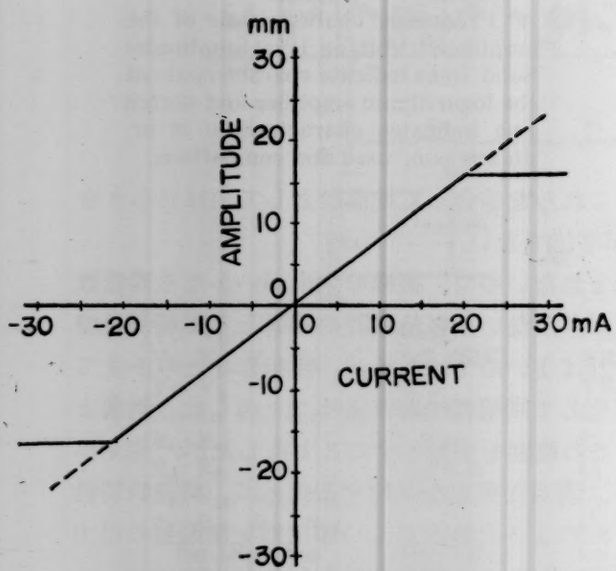


a Sensitivity characteristic of the galvanometer.

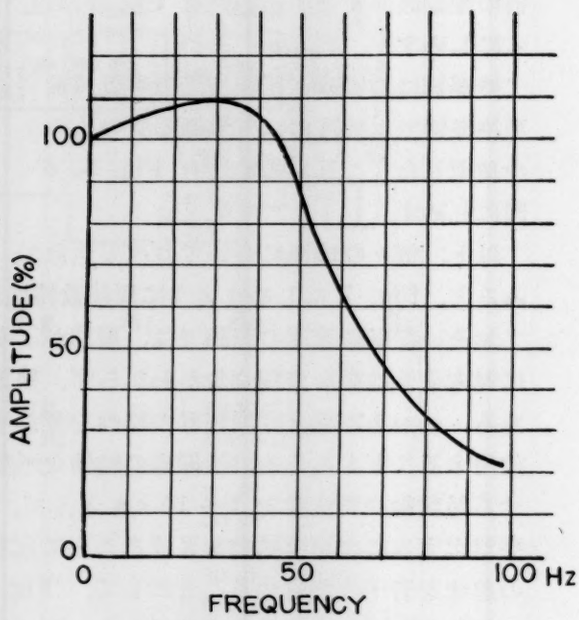


b Frequency characteristic of the galvanometer.

Fig. 6

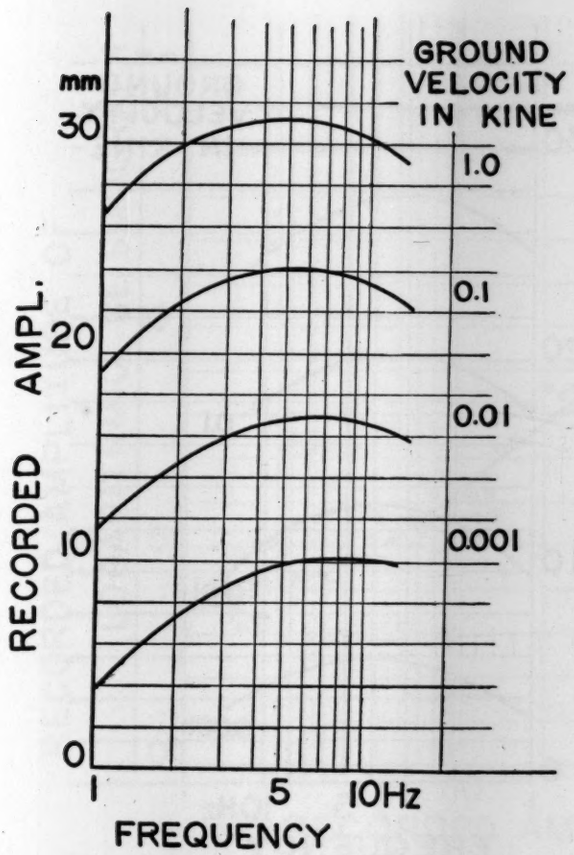


Fig. 7 Frequency characteristic of unequalized seismograph.

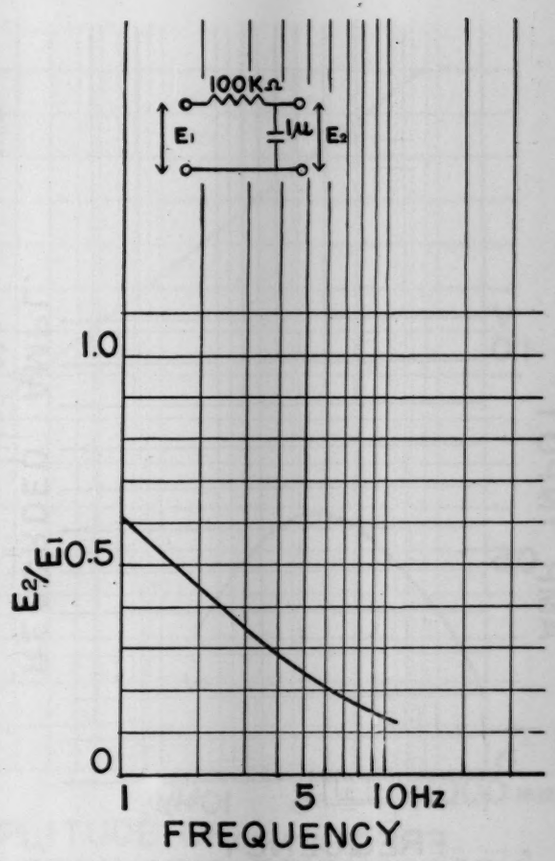


Fig. 8 Frequency characteristic of the equalizer.

いだには比例関係が成立している.

装置の特性を実際の地震観測でしらべるために 1959 年 1 月筑波山支所で観測を実施した結果, Fig. 11 の整理結果がえられた. 記録の実例を Fig. 12, Fig. 13 にしめした.

比較に使用した増幅器とこの装置の増幅器の周波数特性は 1 mV 入力時には Fig. 6 破線と直下の実線の特性をもつものでほとんど同一のものである. これら増幅器の周波数特性が同一で Fig. 11 の結果をえたということはこの装置が対数振幅特性をもつていることを意味し, 較正曲線からのずれはおそい記録紙速度による位相の対応誤差, あるいは較正曲線の周波数偏差等から説明できる範囲にあるので問題はない. 比較にもちいた増幅器の感度範囲の制限のため, 破線の部分では当然点はえられないわけであるが, 実際には観測期間中にそのようなつよい地震動をあたえる地震はなかつた.

**§ 3**

この装置を試作した最初の目的は

i) 記録できる振幅の範囲をひろげること.

ii) 振幅に対数特性をもたせること.

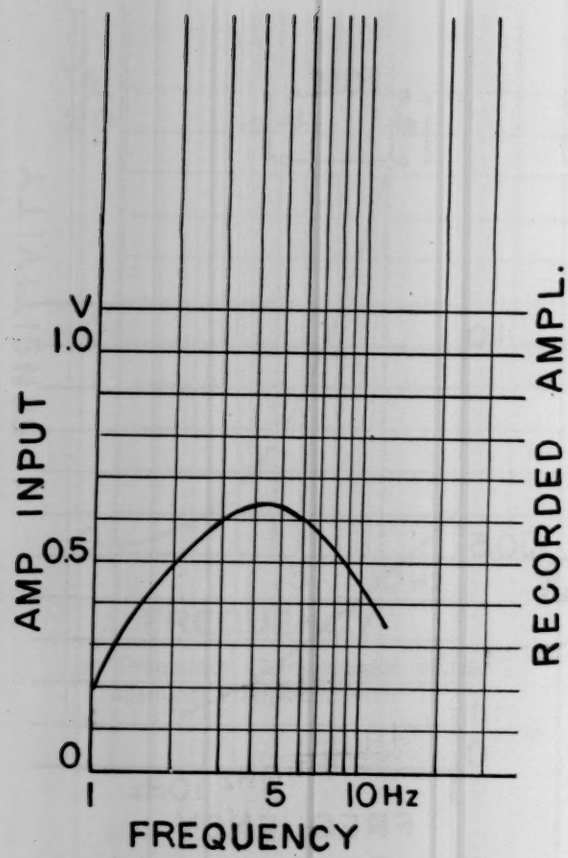


(Ground velocity 1 milli-kine constant.)

Fig. 9 Frequency characteristic of equalized transducer output.

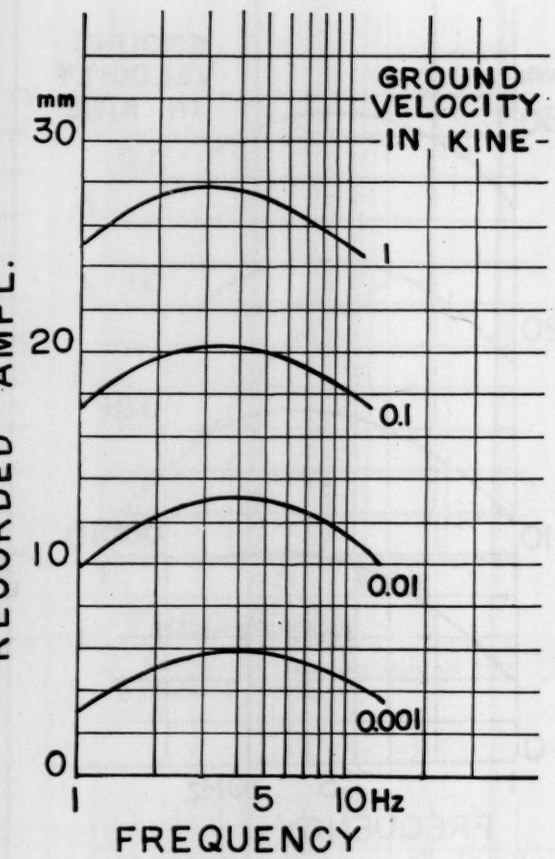


Fig. 10 Frequency characteristic of equalized seismograph.

この2点にあつたが，以上の結果からほぼこの目的は達成した．しかしながら，この装置でさらに厳密な定量的な測定をすることも希望されるので，周波数特性が，さらに平坦化されることがのぞましい．このことは換振器と増幅器両方で，今後の課題とすべき事項であるが，ちかい将来には任意の周波数帯を任意の振幅範囲，任意の感度で観測できるような完成されたものにしたいとおもつている．

この研究に関し宮村研究室主任の御援助と御指導をふかく感謝する．また観測にあたり種々御協力をえた筑波山支所渡辺正雄技官に感謝する．

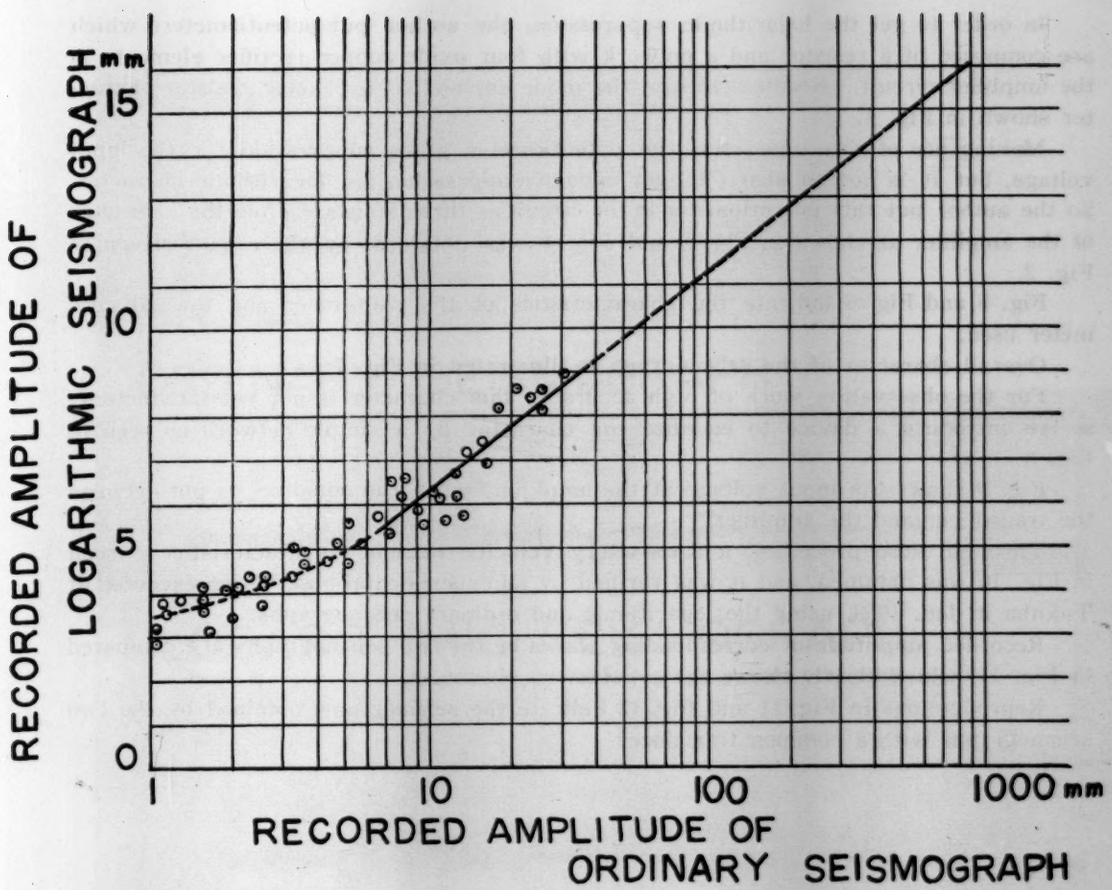


Fig. 11 Comparison of amplitudes recorded by the logarithmic and ordinary amplifiers.

## *25. Logarithmic Wide Amplitude Range Electronic Seismograph.*

By Hideteru MATUMOTO,
Earthquake Research Institute.

A logarithmic wide amplitude range seismograph was designed and constructed, in order to remove a defect of the ordinary seismograph which can record only earthquake motion of very limited intensity range. Namely, the ordinary seismograph of high sensitivity too often reaches its limited full amplitude range in the seismic observation.

But we can extend the amplitude range by making use of a suppression character in the amplifier circuit. For this pupose the author adopted the logarithmic character which is very often utilized in the analysis of seismic observation. And the recording amplitude range was extended 300 times to that of the ordinary seismograph in the same limited amplitude of 30 mm.

In order to get the logarithmic suppression, the author put potentiometers which are composed of a resistor and a network with four oxide copper rectifier elements in the amplifier circuit. Needless to say, the oxide copper has a counter resister character shown in Fig. 1.

Making use of this character, the potentiometer gives suppression for the input voltage, but it is not so sharp to get enough suppression for logarithmic character. So the author put this potentiometer in the circuit at three stages. Thus the character of the amplifier as shown in Fig. 3 and Fig. 4 was obtained by the circuit shown in Fig. 2.

Fig. 5 and Fig. 6 indicate the characteristics of the transducer and the galvanometer used.

Overall character of the seismograph is illustrated in Fig. 7.

For the observation work of high accuracy, this character is not yet satisfactory, so we introduce a device to equalize the character by a simple network as seen in Fig. 8.

Fig. 9 shows the input voltage of the amplifier, when the equalizer is put between the transducer and the amplifier.

Through these processes, a satisfactory velocity-frequency characteristic as seen in Fig. 10 was obtained, and it was verified by an experimental observation executed at Tukuba in Jan. 1959, using the logarithmic and ordinary seismographs.

Recorded amplitude of corresponding waves by the two seismographs are compared in Fig. 11, which clearly shows the satisfactory character.

Reproductions in Fig. 11 and Fig. 12 indicate the seismograms obtained by the two seismographs with a common transducer.

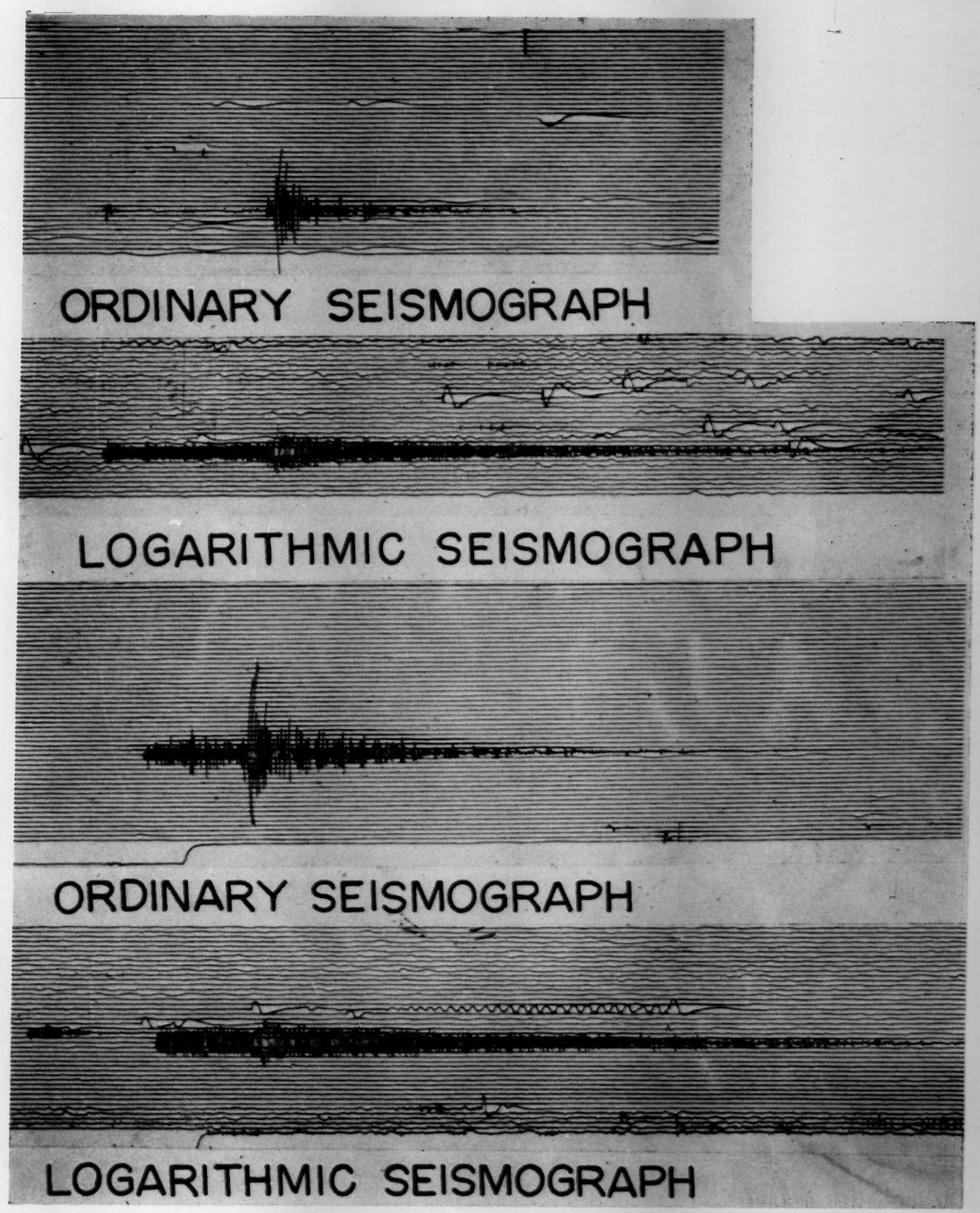


Fig. 12 Example of seismograms recorded at Tukuba by logarithmic amplifier and ordinary amplifier having characters as seen in Fig. 4.

（震研彙報 第三十七号 図版 松本）

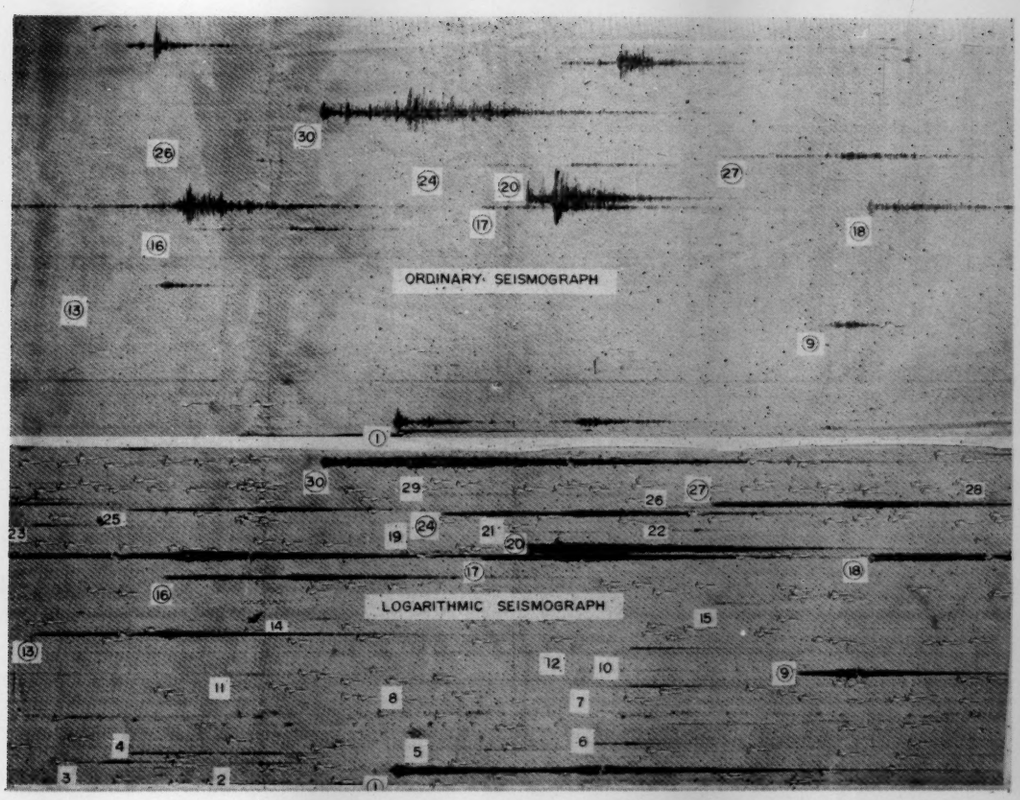


Fig. 13 Example of seismograms recorded at Tukuba by logarithmic amplifier and ordinary amplifier with characters shown in Fig. 4.

# 所　報

## ◎談話会記事

### 第 361 回談話会 (昭和 33 年 12 月 23 日)

1. 筑波における近地地震初動の到来方向とみかけの速度 — 宮村摂三・辻浦賢
2. 大地震に伴う地殻変動の研究 (第 5 報) (地震断層の dip を考慮した場合) — 笠原慶一
3. 地下における地震動の研究 (第 9 報) (地盤の粘性係数) — 金井清・吉沢静代
4. 庄内平野における常時微動の測定 (第 2 報) (振幅分布の問題) — 金井清・田中貞二・長田甲斐男
5. 爆破地震動観測による東北地方の地下構造 — 松沢武雄
6. 釜石鉱山附近 4 回の爆破地震動の観測 — 爆破地震動研究グループ 代表者 松沢武雄
7. 爆破地震観測によつて得られたS波の走時について — 浅野周三・田三望健・雲悦三・嶋宇佐美竜夫
8. S波に関する実験的研究 (1) — 小牧昭三吉・中島直
9. 昭和 33 年 11 月 10 日の浅間山大噴火に関する被害調査報告 — 佐山守
10. 浅間山産火山岩の化学成分 (1) いわゆる「迅速法」による岩石主成分の化学分析について — 南英一人・松井義人
11. 浅間火山の活動と同火山に発生する地震の研究 (続報) 特に最近の噴火に関連して — 水上武夫・茂木清夫・平賀士郎・内堀貞雄・宮崎務子・伊東喜久

### 第 362 回談話会 (昭和 34 年 1 月 27 日)

1. 常時微動による地盤種別の判定に関する第 2 試案 — 金井清
2. 福井平野における常時微動の測定 — 金井清・那須信治・岸上冬彦・河角広・中川恭次・中田貞二
3. 地球熱学 (第 2 報) 岩漿貫入と地表の熱の流れ — 武者力・常次一
4. 浅間山における最近の活動とガスの変化 — 南英一・野口喜三雄・神山宏・中谷弘

5. 浅間山の最近の噴火と抛出物　津屋弘達・村井勇

6. 対数特性をもつた広振幅範囲電子式地震計　松本英照

7. イランの地震調査報告　萩原尊礼

## 第 363 回談話会 (昭和 34 年 2 月 24 日)

1. 震源決定の精度について　第 3 報　浅野周三

2. 地磁気ダイナモの強制振動　力武常次

3. 日本各地の観測点の資料にもとずく脈動の研究 (其の 2)
脈動と台風　三東哲夫

4. 高層気象台構内における土地の脈動三点観測　岸上冬彦

## 第 364 回談話会 (昭和 34 年 3 月 24 日)

1. コンプレッサーによる地盤震動　金井清・田中貞二・長田甲斐男

2. 臨時精密観測網による和歌山附近局地地震の震源決定
特に初期微動時間法におけるその精度　宮村摂三

3. 三原山 1950 年～1951 年の噴火 (補遺)
昇華物，変朽物その他　森本良平・小坂丈予

4. 焼岳火山の最近の状況
特に 2, 3 の地球化学的調査　森本良平・小坂丈予

5. 浅間山産火山岩の化学成分 (2)
仏岩火山体の岩石の化学組成　南英一・松井義人

6. 霧島火山の活動について 1, 2 の調査　水上武・平賀士郎

7. 蔵王火山の地質学的研究　第 5 報
熊野火山　市村毅 (津屋所員紹介)

8. 米沢市関根地方に於ける花崗閃緑岩中の捕獲岩　市村毅

9. 浅間山噴火口附近における火山灰の分布とその浸出水の
化学成分について　南英一・野口喜三雄・神谷宏・中山弘

10. Geotectonic Position of Gango-Brahamputra
by R. S. Mithal and L. S. Srivastava,
University of Roorkee, India.　津屋弘達 (代読)

## 第 365 回談話会 (昭和 34 年 4 月 28 日)

1. 弟子屈地震余震調査報告　松本利松・唐鎌郁夫

2. 地震計用トランジスター前置増幅器　松本英照・後藤健一

3. 最大振幅と震央距離との関係について (補遺)　吉山良一

4. 地中の震動測定結果
(常時微動その他の場合)　金井清・田中貞二・吉沢静代

## 第 366 回談話会 (昭和 34 年 5 月 26 日)

1. 菊川流域の地盤調査 (第 1 報)　河角広・金井清・岸上冬彦・高橋龍太郎
2. 地盤の震動増幅度を求める一方法 (補遺)　金井清・吉沢静代
3. 最大振幅と震央距離との関係について<br>吸収係数の推定　吉山良一
4. 浅間火山湧水中の白色沈澱物について　南英一・小坂丈予

## 第 367 回談話会 (昭和 34 年 6 月 23 日)

1. 大地震前後の平均海水面変化について　山口生知
2. 地球核内の熱電磁流体振動　力武常次
3. 20 度不連続と電気的性質　力武常次
4. 振動周期頻度計算機の試作　田中貞二・金井清
5. 筑波山における HES 型地震計の常時観測結果について (序報)<br>局地的な小地震群の存在について　萩原尊礼・松本利松
6. 南極オングル島附近のパドルとその水質について　南英一・松本利松・小坂丈予

追加　表面波の波面の拡がりと吸収係数に就いて (序報)　吉山良一

昭和34年8月20日印刷
昭和34年8月25日発行

東京都文京区本富士町一番地
東京大学構内
編纂兼
発行者　東京大学地震研究所

東京都新宿区山吹町一八四番地
印刷者　笠井康頼

東京都新宿区山吹町一八四番地
印刷所　株式会社国際文献印刷社

売捌所
東京都中央区日本橋通二丁目六番地
丸善株式会社

Sold by Maruzen Co., Ltd., Nihonbashi-dôri, Chûô-ku, Tôkyô.
Price of this copy: 562 Yen. (Postage exclusive.)